2F

PNL-4819
UC-70

Off-Gas Characteristics of Defense Waste Vitrification Using Liquid-Fed Joule-Heated Ceramic Melters

R. W. Goles
G. J. Sevigny

September 1983

Prepared for the U.S. Department of Energy
under Contract DE-AC06-76RLO 1830

Pacific Northwest Laboratory
Operated for the U.S. Department of Energy
by Battelle Memorial Institute

PNL-4819

Battelle

(215 pgs)

DISCLAIMER

PACIFIC NORTHWEST LABORATORY
operated by
BATTELLE
for the
UNITED STATES DEPARTMENT OF ENERGY
under Contract DE-AC06-76RLO 1830

Printed in the United States of America
Available from
National Technical Information Service
United States Department of Commerce
5285 Port Royal Road
Springfield, Virginia 22161

NTIS Price Codes
Microfiche A01

Printed Copy

Pages	Price Codes
001-025	A02
026-050	A03
051-075	A04
076-100	A05
101-125	
126-150	A07
151-175	A08
176-200	A09
201-225	A010
226-250	A011
251-275	A012
276-300	A013

PNL-4819
UC-70

OFF-GAS CHARACTERISTICS OF DEFENSE WASTE VITRIFICATION USING LIQUID-FED JOULE-HEATED CERAMIC MELTERS

R. W. Goles
G. J. Sevigny

September 1983

Prepared for
the U.S. Department of Energy
under Contract DE-AC06-76RLO 1830

Pacific Northwest Laboratory
Richland, Washington 99352

SUMMARY

Off-gas and effluent characterization studies have been established as part of a PNL Liquid-Fed Ceramic Melter development program supporting the Savannah River Laboratory Defense Waste Processing Facility (SRL-DWPF). The objectives of these studies were to characterize the gaseous and airborne emission properties of liquid-fed joule-heated melters as a function of melter operational parameters and feed composition.

All areas of off-gas interest and concern including effluent characterization, emission control, flow rate behavior and corrosion effects have been studied using alkaline and formic-acid based feed compositions. In addition, the behavioral patterns of gaseous emissions, the characteristics of melter-generated aerosols and the nature and magnitude of melter effluent losses have been established under a variety of feeding conditions with and without the use of auxiliary plenum heaters.

The results of these studies have shown that particulate emissions are responsible for most radiologically important melter effluent losses. Melter-generated gases have been found to be potentially flammable as well as corrosive. Hydrogen and carbon monoxide present the greatest flammability hazard of the combustibles produced. Melter emissions of acidic volatile compounds of sulfur and the halogens have been responsible for extensive corrosion observed in melter plenums and in associated off-gas lines and processing equipment. The use of auxiliary plenum heating has had little effect upon melter off-gas characteristics other than reducing the concentrations of combustibles.

CONTENTS

ABSTRACT 1

INTRODUCTIUN 1

LIQUID-FED MELTER PROCESSING SYSTEM 1

MELTER 1

MELTER OFF-GAS SYSTEM 5

FEED COMPOSITION 6

EFFLUENT CHARACTERIZATION 8

OFF-GAS SAMPLING NETWORK 8

EXHAUST COMPOSITION 11

NATURE OF MELTER FEED COMPONENT LOSSES 20

CHARACTERISTICS OF MELTER AEROSOLS 21

MELTER EMISSION PERFORMANCE 23

MELTEK IDLING TEST 28

MELTER SLAG FORMATION 32

MOLTEN SALT ACCUMULATION 32

CLOSE-COUPLED SCRUBBER PERFORMANCE 32

MELTER FLOW RATES 35

CORROSION 37

CONCLUSIONS 38

REFERENCES 40

APPENDIX - OFF-GAS DATA COMPILATION FOR LIQUID FEEDING OF CERAMIC MELTERS .... A.l

INTRODUCTION .... A.l

EFFLUENT CHARACTERIZATION A.2

LFCM-2 - SEPTEMBER 1980 .... A.2

LFCM-3 - NOVEMBER 1980 .... A.9

PSCM-1 - DECEMBER 1980 .... A.10

LFCM-4 - JANUARY 1981 .... A.16

PSCM-2 - MARCH 1981 .... A.23

LFCM-6 - JUNE 1981 .... A.32

PSCM-3 - JULY 1981 .... A.38

LFCM-7 - AUGUST 1981 .... A.49

PSCM-4 - DECEMBER 1981 .... A.60

PSCM-5 - FEBRUARY 1982 .... A.69

PSCM-6 - MARCH 1982 .... A.75

PSCM-7 - MAY 1982 .... A.86

PSCM-8 - JUNE 1982 .... A.92

OFF-GAS FLOW RATES A.108

LFCM-4 - JANUARY 1981 .... A.108

LFCM-6 - JUNE 1981 .... A.110

PSCM-3 - JULY 1981 .... A.111

LFCM-7 - AUGUST 1981 .... A.111

PSCM-4 - DECEMBER 1981 .... A.112

PSCM-5 - JANUARY 1982 .... A.113

PSCM-6 - MARCH 1982 .... A.113

PSCM-7 - MAY 1982 .... A.115

PSCM-8 - JUNE 1982 .... A.116

MELTER IDLING TESTS A.119

CORROSION A.122

LFCM A.122

PSCM A.144

OFF-GAS SYSTEM A.151

OFF-GAS SYSTEM PERFORMANCE A.153

MATERIAL BALANCE Te, Se and Ru A.156

FIGURES

1 Liquid-Fed, Joule-Heated Ceramic Melter System 4

2 Melter Off-Gas Sampling Network 7

3 Composition of Combustion Boosted Melter Exhaust 11

4 Melter Exhaust Gas Composition of a 100-h Boosted. 20-h Unboosted Test 12

5 Compositional Behavior of Noncondensible Melter Exhaust Gases Accompanying a Flow Surge 14

6 Melter Off-Gas Compositional Behavior Associated with Feed Termination 15

7 Melter SO_2 Emission Characteristics Accompanying a 240-h Test 17

8 Melter Idling Emission Rates of Semivolatile Elements 28

9 Typical Off-Gas Flow Rate Behavioral Patterns Associated with Liquid-Fed Melters 34

APPENDIX

A.l Off-Gas Treatment System A4

A.2 LFCM-2 Off-Gas Line Schematic A5

A.3 LFCM-2 #1 .... A.5

A.4 LFCM-2 #2 .... A.6

A.5 LFCM-2 #3 .... A6

A6 LFCM-2 Mass-Size Particle Distribution A9

A7 PSCM-1 Off-Gas-Line Schematic .... A.ll

A.8 PSCM-1 #1 .... A.12

A.9 PSCM-1 #2 .... A.12

A.10 PSCM-1 #3 .... A.12

A.11 PSCM-1 #4 .... A.12

A.12 PSCM-1 #5 .... A.13

A.13 PSCM-1 #6 .... A.13
A.14 PSCM-1 #8 .... A.13
A.15 PSCM-1 #9 .... A.13
A.16 PSCM-1 #10 .... A.14
A.17 PSCM-1 #11 .... A.14
A.18 PSCM-1 #12 .... A.14
A.19 PSCM-1 #13 .... A.14
A.20 PSCM-1 #14 .... A.15
A.21 PSCM-1 #15 .... A.15
A.22 LFCM-4 Off-Gas Line Schematic A.18
A.23 LFCM-4 #4 .... A.18
A.24 LFCM-4 #3 .... A.18
A.25 LFCM-4 #2 .... A.19
A.26 LFCM-4 #1 .... A.19
A.27 LFCM-4 #0 .... A.19
A.28 PSCM-2 Off-Gas Line Schematic A.25
A.29 PSCM-2 #1 .... A.26
A.30 PSCM-2 #2 .... A.26
A.31 PSCM-2 #3 .... A.26
A.32 PSCM-2 #4 .... A.26
A.33 PSCM-2 #5 .... A.27
A.34 PSCM-2 #6 .... A.27
A.35 PSCM-2 #7 .... A.27
A.36 PSCM-2 #8 .... A.27
A.37 PSCM-2 #9 .... A.28
A.38 PSCM-2 #10 .... A.28

A.39 PSCM-2 #11 .... A.28

A.40 PSCM-2 #12 .... A.28

A.41 PSCM-2 #13 .... A.29

A.42 PSCM-2 #14 .... A.29

A.43 PSCM-2 Plenum Off-Gas Composition A.33

A.44 LFCM-6 Off-Gas Line Configuration A.34

A.45 LFCM-6 Melter Lid A.35

A.46 LFCM-6 #4 .... A.35

A.47 LFCM-6 #3 .... A.35

A.48 LFCM-6 #2 .... A.35

A.49 LFCM-6 #1 .... A.36

A.50 LFCM-6 #0 .... A.36

A.51 PSCM-3 Off-Gas-Line Configuration A.42

A.52 PSCM-3 #1 .... A.43

A.53 PSCM-3 #2 .... A.43

A.54 PSCM-3 #3 .... A.43

A.55 PSCM-3 #4 .... A.43

A.56 PSCM-3 #5 .... A.44

A.57 PSCM-3 #6 .... A.44

A.58 PSCM-3 #7 .... A.44

A.59 PSCM-3 #8 .... A.44

A.60 PSCM-3 #9 .... A.45

A.61 PSCM-3 #10 .... A.45

A.62 PSCM-3 #11 .... A.45

A.63 PSCM-3 Noncondensible Off-Gas Composition A.50

A.64 H_2 Variation During PSCM-3 .... A.51

A.65 LFCM-7 Noncondensible Off-Gas Composition A.58

A.66 H_2 Variation During LFCM-7 .... A.59

A.67 PSCM Off-Gas-Line Confiyuration A.61

A.68 PSCM-4 Off-Gas-Line Horizontal Section A.62

A.69 PSCM-4 Off-Gas-Line Horizontal Section A.62

A.70 PSCM-4 Off-Gas-Line Vertical Section A.62

A.71 PSCM-4 Off-Gas Composition A.67

A.72 PSCM-5 Off-Gas Composition A.76

A.73 PSCM-5 Off-Gas Composition A.77

A.74 PSCM-6 Off-Gas Composition A.83

A.75 Melter Off-Gas Compositional Behavior Associated with Feed Termination A.85

A.76 PSCM-7 Off-Gas Composition A.94

A.77 Material Buildup in Melter Plenum Exhaust Port - Axial Hose was Where Spray Nozzle was Located A.96

A.78 Horizontal Off-Gas Line A.96

A.79 SEM Photographs of Particulate Samples Taken Downstream of the Close-Coupled Scrubber A.102

A.80 X-Ray Fluorescence Spectra of Individual Particles Called Out in Figure A.79 .... A.103

A.81 PSCM-8 Off-Gas Composition A.105

A.82 Compositional Behavior of Noncondensible Melter Exhaust Gases Accompanying a Flow Surge A.106

A.83 Melter SO_2 Emission Characteristics Accompanying a ~240-h Test A.107

A.84 LFCM-4 Off-Gas Flow Rate Behavior A.109

A.85 PSCM-5 Off-Gas Flow Characteristics A.114

A.86 Qualitative Index of Off-Gas Flow Rate Instabilities A.117

A.87 Melter Idling Emission Rates of Semivolatile Elements A.120

A.88 Underside of LFCM Lid North A.125

A.89 SEM Photograph of Ni-Cr Base Coat Under 100X Maynification - Control A.129

A.90 SEM Photograph of Ni-Cr Base Coat Showing Very Little Corrosion Under 100X Magnification A.129

A.91 SEM Photograph of Ni-Cr-6% Base Coat with a Cr_2O_3 Secondary Coat Under 100X Magnification - Control A.130

A.92 SEM Photograph of Ni-Cr-6% Base Coat with a Cr_2O_3 Secondary Coat and Some Cracking Under 100X Magnification A.130

A.93 SEM Photograph of ZrO-Coated Sample with a Ni-Cr Base Coat Under 100X Maynification - Control A.131

A.94 SEM Photograph of ZrO-Coated Sample with a Ni-Cr Base Coat Under 100X Magnification A.131

A.95 Inconel-625 Unexposed Sample Under 10X, 100X and 250X SEM Magnification A.134

A.96 Inconel-625 Sample Under 10X, 100X and 250X SEM Magnification A.135

A.97 Inconel-625 Sample Under 10X, 100X and 250X SEM Magnification A.136

A.98 Hastelloy Sample X Under 10X, 100X and 250X SEM Magnification A.137

A.99 Haynes 188 Sample #1 Under 10X SEM Magnification A.138

A.100 Haynes 188 Sample #1 Under 100X and 250X SEM Magnification A.139

A.101 Haynes 188 Sample #2 Under 10X, 100X and 25UX SEM Magnification A.140

A.102 Haynes 25 Sample Under 10X, 100X and 250X SEM Magnification A.141

A.103 Inconel-690 Sample Under 10X, 100X and 250X SEM Magnification A.142

A.104 PSCM Plenum Heater Thimbles A.145

A.105 Inconel-600 Thimble 8X SEM Cross Section with 50X and 250X Magnification A.146

A.106 Inconel-600 Thimble Cross Sections of Regions B and C Under 50X and 250X Magnifications A.147

A.107 Inconel-601 Thimble 8X. SEM Cross Section A.148

A.108 Inconel-601 Cross Section Under 100X and 250X SEM Magnification A.149

A.109 Inconel-690 Thimble Cross Section Under 8.3X, 100X and 250X SEM Magnification A.150

A.110 Off-Gas System A.154

A.111 Material Buildup in Melter Plenum Exhaust Port A.155

A.112 PSCM-8 Melter Floor Survey A.157

TABLES

1 Operational Parameters for Liquid-Fed Melter Tests

2 Simulated Waste Slurry and Glass Compositions 5

3 Concentration of Trace Additives in Melter Feed 6

4 Melter Noncondensible Off-Gas Composition 10

5 Melter-Generated Off-Gas Components 13

6 PSCM-6 Particulate and Total Feed Component DFs 18

7 Size Distribution of Melter Aerosols 19

8 Elemental Distribution Across the Cyclonic Sampling System 20

9 Composition of 16 µm Cyclonic Sample Fraction 21

10 Submicron Particulate Composition 22

11 Melter Effluent Emission Characteristics 23

12 Steady-State Aerosol Emission Characteristics 24

13 Melter Idling Deposits 26

14 Relative Melter Production and Loss Rates of Sulfur 30

15 Close-Coupled Scrubber Particulate DFs 32

16 Liquid-Fed Melter Flow Rates 35

17 Corrosion Sample Results 36

APPENDIX

A.1 Liquid-Fed Melter Operational Parameters A.3

A.2 LFCM-2 Plug Composition A.7

A.3 LFCM-2 Decontamination Factors A.8

A.4 LFCM-3 Decontamination Factors A.10

A.5 PSCM-1 Process Line Deposits A.16

A.6 PSCM-1 Decontamination Factors A.17

A.7 PSCM-1 Noncondensible Off-Gas Results A.17

A.8 LFCM-4 Pipe Deposition Composition A.20

A.9 LFCM-4 Decontamination Factors A.21

A.10 LFCM-4 Particulate Data A.22

A.11 LFCM-4 Noncondensible Off-Gas Composition A.23

A.12 LFCM-4 Idling Emissions A.24

A.13 PSCM-2 Pipe Deposits A.30

A.14 Compositional Comparison of Off-Gas-Line Deposits A.31

A.15 PSCM-2 Decontamination Factors A.32

A.16 LFCM-6 Off-Gas-Line Deposits A.37

A.17 Melter Pipe Deposition Composition A.38

A.18 LFCM-6 Decontamination Factors A.39

A.19 LFCM-6 Comparative DFs A.40

A.20 LFCM-6 Noncondensible Off-Gas Composition A.41

A.21 PSCM-3 Pipe Deposition Composition A.46

A.22 Melter Pipe Deposit Composition A.47

A.23 PSCM-3 Feed Component DFs A.48

A.24 PSCM-3 Comparative DFs A.49

A.25 PSCM-3 Off-Gas Composition A.51

A.26 Differential Particulate Data A.52

A.27 Elemental Distribution Across Cyclonic Sampling System A.53

A.28 HEPA Filtration Data A.54

A.29 Particulate Data from Off-Gas Sampling Train A.55

A.30 Particulate and Total Feed Component DFs A.55

A.31 LFCM-7 Comparative DFs A.56

A.32 Gross DF Values A.57

A.33 LFCM-7 Off-Gas Composition A.59

A.34 PSCM-4 Aerosol DFs A.63

A.35 Particulate and Total Elemental Melter DFs A.63

A.36 PSCM-4 Comparative DFs A.64

A.37 PSCM-4 Gross Aerosol DFs A.65

A.38 PSCM-4 Particulate Size Data A.65

A.39 PSCM-4 Submicron Particulate Composition A.66

A.40 PSCM-4 Noncondensible Off-Gas Composition A.68

A.41 PSCM-4 SO_2 Off-Gas Concentration A.68

A.42 Melter Decontamination Factors A.69

A.43 PSCM-5 Gross Melter Entrainment A.70

A.44 PSCM-5 Particulate and Total Feed Component DFs A.71

A.45 PSCM-5 Comparative DFs A.72

A.46 PSCM-5 Differential Particulate Data A.72

A.47 Elemental Distribution Across Cyclonic Aerosol Size Fractions A.74

A.48 PSCM-5 Gross Entrainment DFs A.75

A.49 PSCM-5 Noncondensible Off-Gas Composition A.78

A.50 PSCM-5 Off-Gas-Line Deposits A.78

A.51 PSCM-6 Gross Melter Entrainment A.79

A.52 PSCM-6 Particulate and Total Feed Component DFs A.80

A.53 PSCM-6 Comparative DFs A.81

A.54 PSCM-6 Differential Particle Size Data A.81

A.55 Feed Component Distribution Across Cyclonic Aerosol Size Fractions A.82

A.56 PSCM-6 Aerosol DFs A.83

A.57 PSCM-6 Off-Gas Composition A.84

A.58 Off-Gas-Line Deposits - PSCM-5 & -6 .... A.86

A.59 Gross Melter DF A.87

A.60 PSCM-7 Particulate and Total Feed Component DFs A.88

A.61 PSCM-7 Comparative DFs A.89

A.62 Cyclonic Melter Aerosol Size Analysis A.90

A.63 Elemental Distribution Across Cyclonic Size Fractions A.91

A.64 PSCM-7 Close-Coupled Scrubber Particulate DFs A.92

A.65 PSCM-7 Gross Aerosol DFs A.93

A.66 Melter Surface Samples After PSCM-7 .... A.95

A.67 Assumed Salt Compounds for PSCM-7, wt% A.95

A.68 Gross Melter Aerosol DF A.96

A.69 PSCM-8 Particulate and Total Melter Feed Component DFs A.97

A.70 PSCM-8 Comparative DFs A.98

A.71 PSCM-8 Particulate Analysis of Melter Generated Aerosols A.99

A.72 PSCM-8 Elemental Distribution Across Cyclonic Fractions A.100

A.73 Particulate Melter Scrubber DFs A.101

A.74 PSCM-8 Gross Aerosol DFs A.104

A.75 Flow Surging Characteristics During LFCM-4 .... A.110

A.76 Frequency. Duration and Extent of LFCM-4 Surges A.110

A.77 LFCM-6 Surging Flow Rate Behavior A.111
A.78 PSCM-3 Flow Rate Behavior A.111
A.79 LFCM-7 Flow Rate Behavior A.112
A.80 Off-Gas Surging Behavior A.112
A.81 PSCM-5 Off-Gas Flow Rate Behavior A.113
A.82 PSCM-6 Off-Gas Flow Characteristics A.115
A.83 Noncondensible Gas Flow A.116
A.84 PSCM-8 Flow Data A.118
A.85 Melter Operation Summary A.123
A.86 Composition of Material from Off-Gas Plug A.124
A.87 Metallic Corrosion Sample Results A.126
A.88 Protective Coating Off-Gas Samples A.127
A.89 Spray Powder Characteristics A.128
A.90 Corrosion Data A.133
A.91 Summary of Alloy Micrographs A.143
A.92 Plenum Thermowell Measurements A.151
A.93 Metal Found on Melter Floor A.158
A.94 Te, Se. and Ru Material Between PSCM-4 & PSCM-8 .... A.159

INTRODUCTION

Liquid-fed, joule-heated ceramic melters are to form the basis of the planned Defense Waste Processing Facility (DWPF) to be constructed at the Savannah River Plant (SRP). The purpose of the DWPF is to isolate and immobilize defense-related nuclear waste in a borosilicate glass. Pacific Northwest Laboratory (PNL) is assisting the Savannah River Laboratory (SRL) in establishing the design criteria for the DWPF by transferring existing melter technology and by providing all necessary liquid-fed ceramic melter research and development.

Off-gas characterization studies have been established as part of the SRL-DWPF melter development program being conducted at PNL. The objective of these studies is to determine the off-gas properties of liquid-fed, joule-heated melters as a function of melter operational parameters and feed composition.

The scope of these studies covers all aspects of off-gas concern including: 1) effluent characterization, 2) emission abatement, 3) flow rate behavior, and 4) corrosion effects. This paper will discuss the results obtained from studies of each of these areas of interest after a brief description of the liquid-fed melter process.

LIQUID-FED MELTER PROCESSING SYSTEM

The following is a brief description of the liquid-fed melter processing system which was developed at PNL in support of the SRP-DWPF. A much more detailed account of the liquid-fed melting process can be obtained from a report by Buelt and Chapman (1978).

MELTER

Several processes for solidifying and immobilizing high-level liquid waste (HLLW) in a stable borosilicate glass continues to be evaluated at PNL (Bonner 1979). The process being studied here utilizes a joule-heated ceramic-lined melter, which is directly fed a uniform slurry composed of glass formers and simulated liquid radioactive waste. Upon entry into the melter, the waste components of the slurry are oxidized and melted with the glass formers present in the feed to form a molten borosilicate glass.

The power required to maintain this continuous glass production process is supplied by resistive alternate current (ac) heating of the melter glass pool. In addition to the primary source of power, auxiliary radiant heaters located in the melter plenum above the glass melt surface have been employed to increase or "boost" feeding and glass production rates. Plasma and propane combustion torches have also been used to supply additional heating to the melter plenum. Figure 1 illustrates the liquid-fed melting process.

Two different joule-heated ceramic melters used in these developmental studies are referred to as the liquid-fed ceramic melter (LFCM), which has a melting surface area of 1.05 m^2, and the pilot-scale ceramic melter (PSCM), which possesses a 0.73 m^2 surface area. The maximum glass production rates associated with these melters are 40 kg/h-m^2 for unboosted operation, and 60 kg/h-m^2 when auxiliary plenum heaters are employed. Table 1 summarizes all important operational parameters associated with tests of the LFCM and PSCM. These melter tests, which are arranged chronoloyically in Table 1, form the bases of the off-gas studies which are discussed below.

MELTER OFF-GAS SYSTEM

Both the PSCM and LFCM share a common 0.1-m (4-in.) stainless steel off-gas system consisting of an ejector venturi scrubber, a downdraft condenser, a packed scrubbing tower, and a final absolute filter, physically arranged in the order listed. In addition to these common off-gas elements, both melters are equipped with a close-coupled HEPA filter receptacle and a total (condensible and noncondensible) off-gas flowmeter. Since the purpose of the DWPF off-gas support studies was to establish melter off-gas characteristics, the performance of the generic off-gas processing equipment present in the common melter off-gas system was of little programmatic interest and consequently will not be discussed here. However, the operating characteristics of a close-coupled scrubber, utilized during the last two pilot-scale melter tests, will be discussed since such a device will be required in support of full-scale production melters.

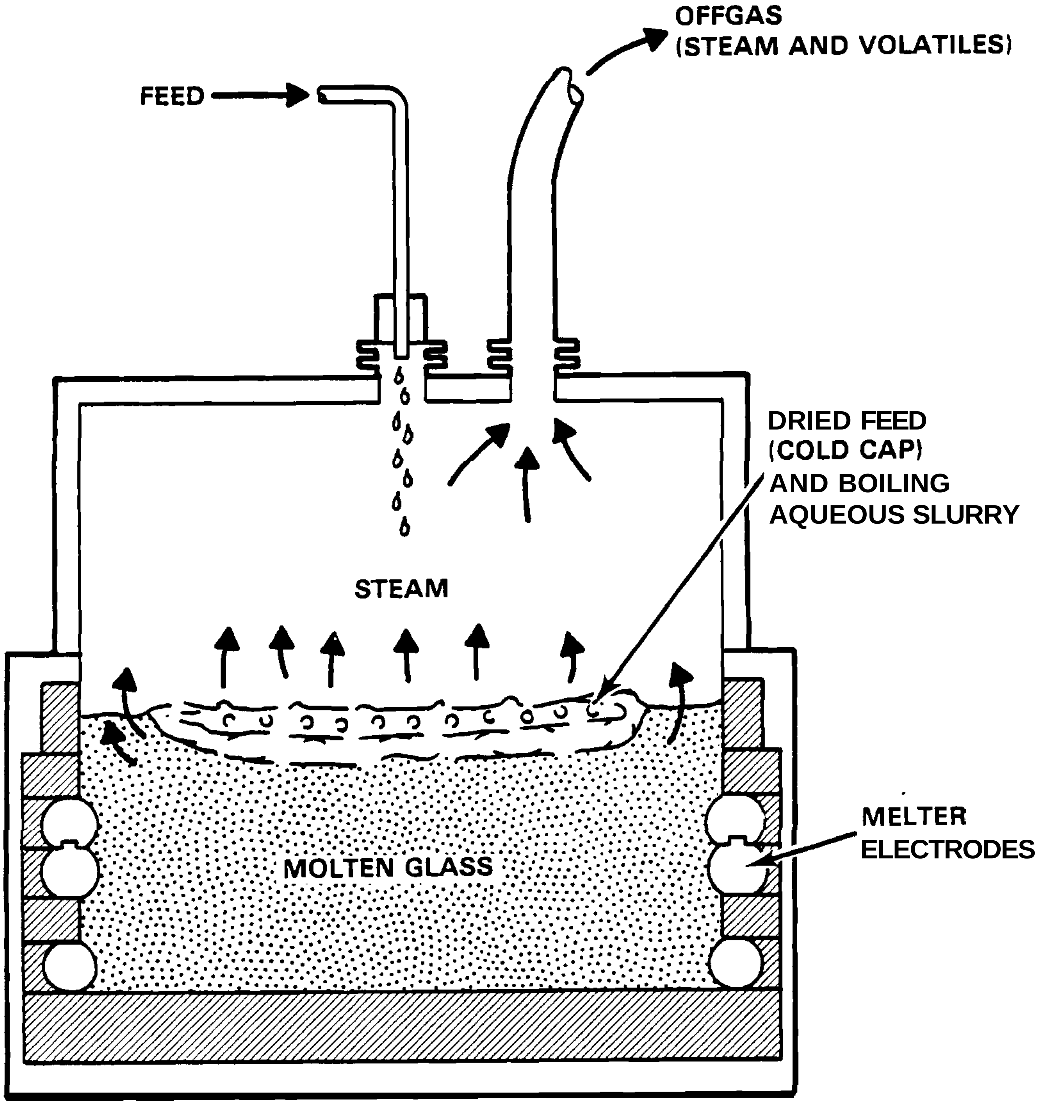

FIGURE 1. Liquid-Fed, Joule-Heated Ceramic Melter System

FEED COMPOSITION

The liquid slurry feed used in the SRL-DWPF melter development program was a uniform mixture of simulated defense waste sludge and glass formers (frit). The composition of this slurry as equivalent oxides is detailed in Table 2. The effective waste loading of the slurry is 29 wt% of the total oxides present in the feed. In addition to the major elements listed in Table 2, SRL simulated waste also contained stable elemental substitutes for all volatile and

TABLE 1. Operational Parameters for Liquid-Fed Melter Tests

Parameters	PSCM-1	LFCM-4	PSCM-2	LFCM-6	PSCM-3	LFCM-7	PSCM-4	PSCM-5	PSCM-6	PSCM-7	PSCM-8
Feed type	**Basic**	**Basic**	**Basic**	**Basic**	**Acidic**	**Acidic**	**Acidic**	**Acidic**	**Acidic**	**Acidic**	**Acidic**
Feed rate, Vh-m^2	45	90	110	100	62	121	83	100	122	68	103
Glass prod. rate, kg/h-m^2	22	41	50	45	28	57	39	50	60	43	49
Plenum temp., °C	400	600	400-800	600	300	500	400	520	850	300	700
Boosting type	None	Elect. Lid Heat	Propane Combustion	Elect. Lid Plasma Torch	None	Elect. Lid Heat	None	Elect. Lid Heat	Elect. Lid Heat	None	Elect. Lid Heat
Boosting power, kW	--	30	35	40	--	15	--	36	55	--	45
Off-gas temp., °C	375	375	375	400	250	300	275	375	400	270	360
Off-gas cooling, L/h	0	8	23	24	0	Variable	0	23	23	0	30
Experiment duration, h	120	120	120	120	125	111	107	99	138	115	232

semivolatile isotopes of radiological concern that are present in typical defense waste. The trace element composition of the SRL feed slurry is presented in Table 3.

Although the waste composition of the liquid feed remained essentially constant throughout the period of testing covered in this report (see Table 2), the rheology of the feed was dramatically affected by the addition of formic acid to the DWPF waste stream. Initial experiments were conducted with an alkaline (pH 11 to 12) slurry having the physical characteristics of a Bingham plastic fluid. Acidification (to pH 5 to 6) of the liquid waste stream with formic acid resulted in slurries which behaved more like an ideal Newtonian fluid. The presence of formic acid in melter feed slurries not only changed

TABLE 2. Simulated Waste Slurry and Glass Compositions

Waste Slurry Composition				Typical Slurry and Glass Oxide Composition[a]					
Alkaline Waste		Acidic Waste		Equivalent Oxide Concentration, g/L					Final Glass
Compound	Conc., g/L	Compound	Conc., g/L	Oxide	Waste Sludge	Frit-131[b]	Zeolite[c]	Total	Composition., Wt. %
Frit-131	338.0	Frit-131	341.3						
Zeolite	14.7	Zeolite	9.9						
Anth. Coal	3.30	$HCHO_2$	18.0						
$Fe(OH)_3$	90.9	$Fe(OH)_3$	81.2	Fe_2O_3	60.7			60.7	12.7
$Al(OH)_3$	21.0	$Al(OH)_3$	34.2	Al_2O_3	22.3		1.9	24.2	5.1
MnO_2	19.5	$Mn(CHO_2)_2$	28.2	MnO	13.8			13.8	2.9
$Ni(OH)_2$	10.4	$Ni(CHO_2)_2$	8.3	NiO	4.1			4.1	0.8
$CaCO_3$	8.90	$Ca(CHO_2)_2$	16.7	CaO	7.2		1.1	8.3	1.7
SiO_2	5.84	SiO_2	15.6	SiO_2	15.6	197.6	4.7	219.9	45.6
NaOH	4.93	$NaCHO_2$	8.42	Na_2O	4.6	60.4	0.2	65.2	13.6
$NaNO_3$	2.01	NaNO	2.01						
Na_2SO_4	0.73	Na_2SO_4	0.72	Na_2SO_4	0.7			0.7	0.1
				B_2O_3		50.2		50.2	10.5
				Li_2O		19.4		19.4	4.1
				MgO		6.8		6.8	1.4
				TiO_2		3.4		3.4	0.7
				La_2O_3		1.7		1.7	0.4
				ZrO_2		1.7		1.7	0.4
				TOTAL	129.0	341.2	7.9	480.1	100.0

(a) Feed slurry glass content = 0.48 kg/L.

(b) Frit-131 Composition (-200 mesh).

Oxide	Wt%
SiO_2	57.9
B_2O_3	14.7
Na_2O	17.7
Li_2O	5.7
MgO	2.0
TiO_2	1.0
La_2O_3	0.5
ZrO_2	0.5
TOTAL	100.0

(c) Zeolite Composition: Linde Ionsiv IE-95.

Component	Wt%
$CaAl_2Si_4O_{12}$ $6H_2O$	80
$Na_4Ca_{1.5}Al_3Si_8O_{24}8H_2O$	20
TOTAL	100
Assumed Oxide Forms	**Wt%**
CaO	10.6
Al_2O_3	19.2
SiO_2	47.7
Na_2O	2.5
H_2O	20.0
TOTAL	100.0

TABLE 3. Concentration of Trace Additives in Melter Feed

Additives	Concentration, g/L Oxides	Elemental
Cs_2O	0.25	0.24
SrO	0.098	0.083
Sb_2O_3	0.16	0.060
SeO_2	0.04	0.029
CdO	0.38	0.033
TeO_2	0.05	0.036
RuO_2	0.085	0.064

the fluidic properties of the feed; **it** also dramatically influenced the off-gas emission properties of the liquid-fed melter.

EFFLUENT CHARACTERIZATION

One of the major tasks involved in the DWPF off-gas studies was that of determining melter emission characteristics. The nature and extent of melter-generated effluents had to be established before off-gas system criteria could be finalized for the DWPF melters. Consequently, an off-gas sampling system was developed to provide this basic off-gas design data.

OFF-GAS SAMPLING NETWORK

The sampling network, which was developed in support of melter emission characterization studies, is schematically illustrated in Figure 2. The

---

NOTE: In the list of network components on page 8, effluents which could not be used directly appear in parentheses adjacent to chemical analogs which were used to simulate their behavior.

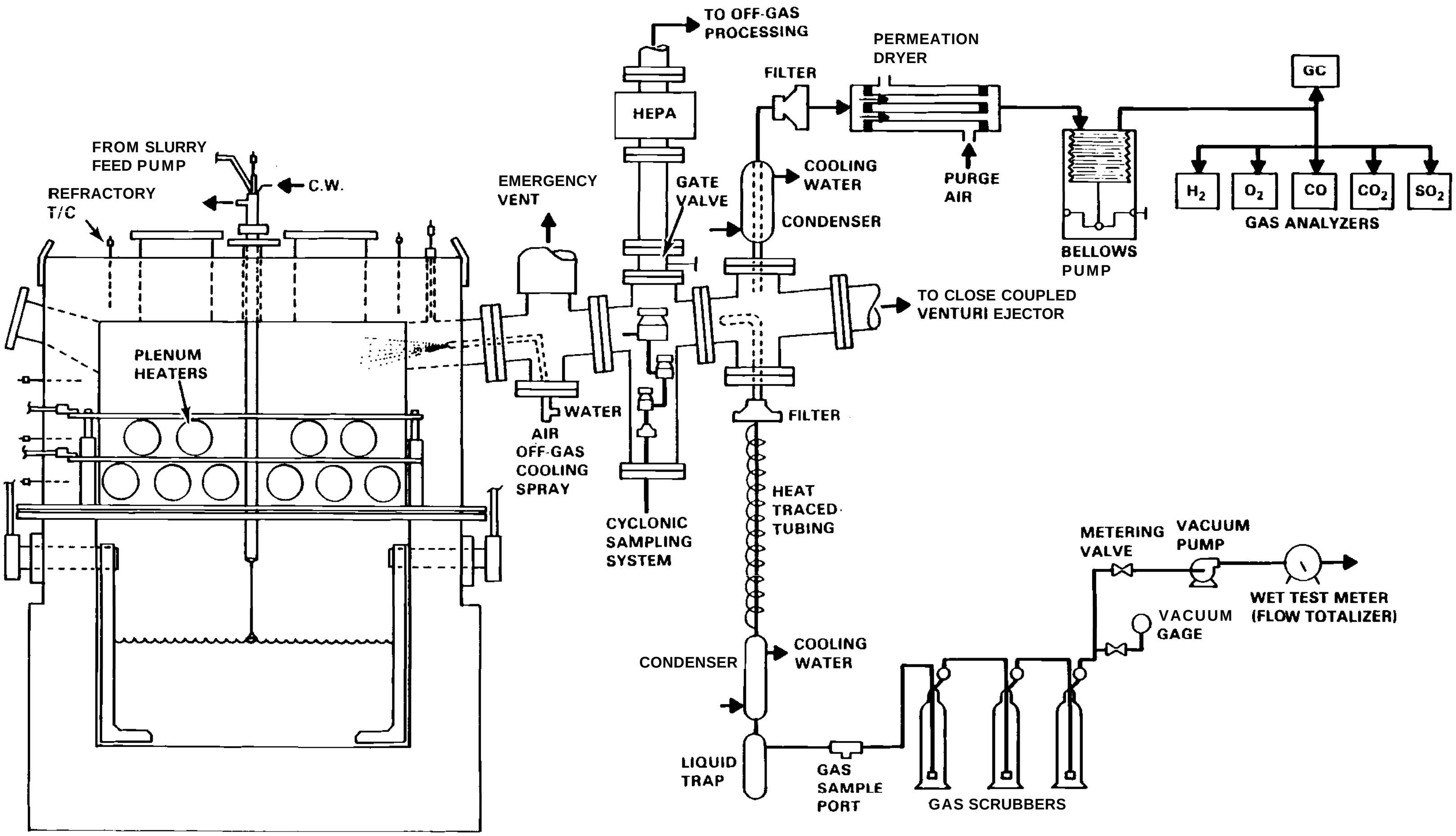

FIGURE 2. Melter Off-Gas Sampling Network

components making up this network were designed to determine the composition of melter exhaust with regard to the effluents listed below.

- Gases:
  - SO_2
  - N_2
  - O_2
  - CO
  - CO
  - SO_2
- Semivolatiles:
  - Halogens
  - Sb
  - Se
  - Te
  - Mn (Tc)
  - Ru
  - Cd (Hg)
  - Sr
  - Others
- Particulates

The gaseous composition of melter off-gas emissions was established using a gas chromatograph (GC) and real-time gas analyzers. The gas stream sampled was extracted prior to any off-gas processing. This hot, water-laden gas stream was first passed through a tube and shell condenser, which reduced the water loading of the gas, while minimizing the gaseous interactions with condensed-phase water. The quenched gas stream was then passed through a filter and a permeation dryer, and finally distributed to the individual gas analyzers using a stainless steel bellows pump.

The GC used in these studies is programmed to sample and analyze the composition of the continuously flowing gas stream every 30 min. The gaseous components routinely quantified by this instrument include O_2, N_2, CO, and CO_2. In addition, the GC provides semi-quantitative information with regard to gaseous concentrations of H_2 and SO_2.

Real-time measurements of melter noncondensible gas concentrations were initiated during the latter part of this study with five continuous gas monitors. These instruments have provided continuous off-gas data on the concentrations of H_2, O_2, CO, CO_2, and SO_2 for all melter tests following PSCM-4.

The pathways and magnitudes of melter-generated semivolatile emissions were assessed using a differential sampling system composed of a filter, a heat-traced sampling line, a condenser, and a series arrangement of three gas scrubbing units (Figure 2). The distribution of semivolatiles across the five discrete sample fractions generated by the system were determined using emission spectrometry (ICP), atomic absorption (AA), ion chromatography (IC), and X-ray fluorescence (XRF). All semivolatile studies have been exclusively concerned with characterizing the composition of the unquenched melter exhaust.

The concentration, size and composition of melter-generated aerosols were also characterized. Total off-gas particulate loading was established gravimetrically by HEPA filtration of the entire melter off-gas stream (Figure 2). Particle size information was obtained from a cyclonic sampling system consisting of a series arrangement of three cyclones and a final absolute filter. The cut points of the cyclones employed were 16 µm, 6 µm, and 1 µm at 18 actual L/min. The final absolute filter was designed to collect submicron fines which are able to pass through all three preceding cyclones. The elemental composition of the particulate matter collected by these sampling devices was established using ICP, AA, and IC.

EXHAUST COMPOSITION

The noncondensible (20°C) gases generated by liquid-fed melters are dependent upon slurry feed composition as well as melter operating conditions. The alkaline waste feed used during the initial stages of this study possessed very low concentrations of organic matter. Consequently, the gross off-gas composition was essentially CO_2-enriched inleakage. The emission rates of the combustible gas CO during all of the alkaline feed tests were always less than 1/10 the rate associated with CO_2. Table 4 summarizes the average gross compositional data associated with alkaline-feed melter exhausts.

The dramatic difference between the PSCM-2 data and the other experiments listed in Table 4 is due to the method of boosting used in that test. During PSCM-2, a propane torch supplied supplemental heat to the melter plenum to increase the feeding rates. Consequently, the major source of off-gas combustion products was the boosting torch and not the melter. Figure 3 illustrates the time-correlated behavior of the melter exhaust during PSCM-2. The relationships illustrated are consistent with the propane combustion process.

TABLE 4. Melter Noncondensible Off-Gas Composition (basic waste)

	Melter Inleakage,	Molar %											
		CO_2			CO			O_2			N_2		
Experiment	scfm	High	Avg	Low	High	Avg	Low	High	Avg	Low	High	Avg	Low
PSCM-1	5-10	6.4	3.4	1.8	0.01	—	--	20	14.0	7.1	89	81	73
LFCM-4	32	1.1	0.58	0.40	0.03	0.02	0.001	21	20.5	20.0	78	78	78
PSCM-2	45	8.6	4.6	0.20	3.0	0.50	0.001	21	14.0	8.0	82	80	79
LFCM-6	29	0.87	0.54	0.13	0.07	0.02	0.001	20	20.0	18.0	80	79	78

The composition of melter-generated, noncondensible gases was dramatically affected when formic acid was added to the simulated melter feed. This compositional alteration increased the organic loading in the melter feed by approximately an order of magnitude. Consequently, melter exhaust gases were of particular interest during these acidified feed tests due to the possibility of generating enough H_2 and CO (water gas) to present a flammability hazard after off-gas quenching.

Figure 4 illustrates the time-related behavior of gross melter exhaust gases during a 120-h melter test which employed 100 h of radiant lid heat boosting followed by 20 h of unboosted operation. The presence of plenum heaters during liquid feeding clearly reduced melter emissions of the combustible gases H_2 and CO. With the termination of lid heating, the melter plenum cooled, reducing the oxidation rates of these gases sufficiently to allow significant quantities of each gas to escape the plenum through the off-gas system. This result is quite reproducible; however, virtual elimination of combustible gas emissions during boosting,' as is illustrated in Figure 4, may not always be achievable.

Similarly, the concentrations of combustibles leaving an unboosted melter may be significantly higher than indicated in Figure 4 since these concentrations are slurry composition-, temperature-, feed-, and inleakage-rate-dependent variables. Indeed, dilution air was required during the unboosted PSCM-7 test to reduce H_2 in the quenched off-gas stream to below 70% of its lower inflammability limit (-4%). A summary of the gaseous concentrations of organic decomposition and reaction products generated during all formate feed testing is presented in Table 5, along with average melter inleakage rates.

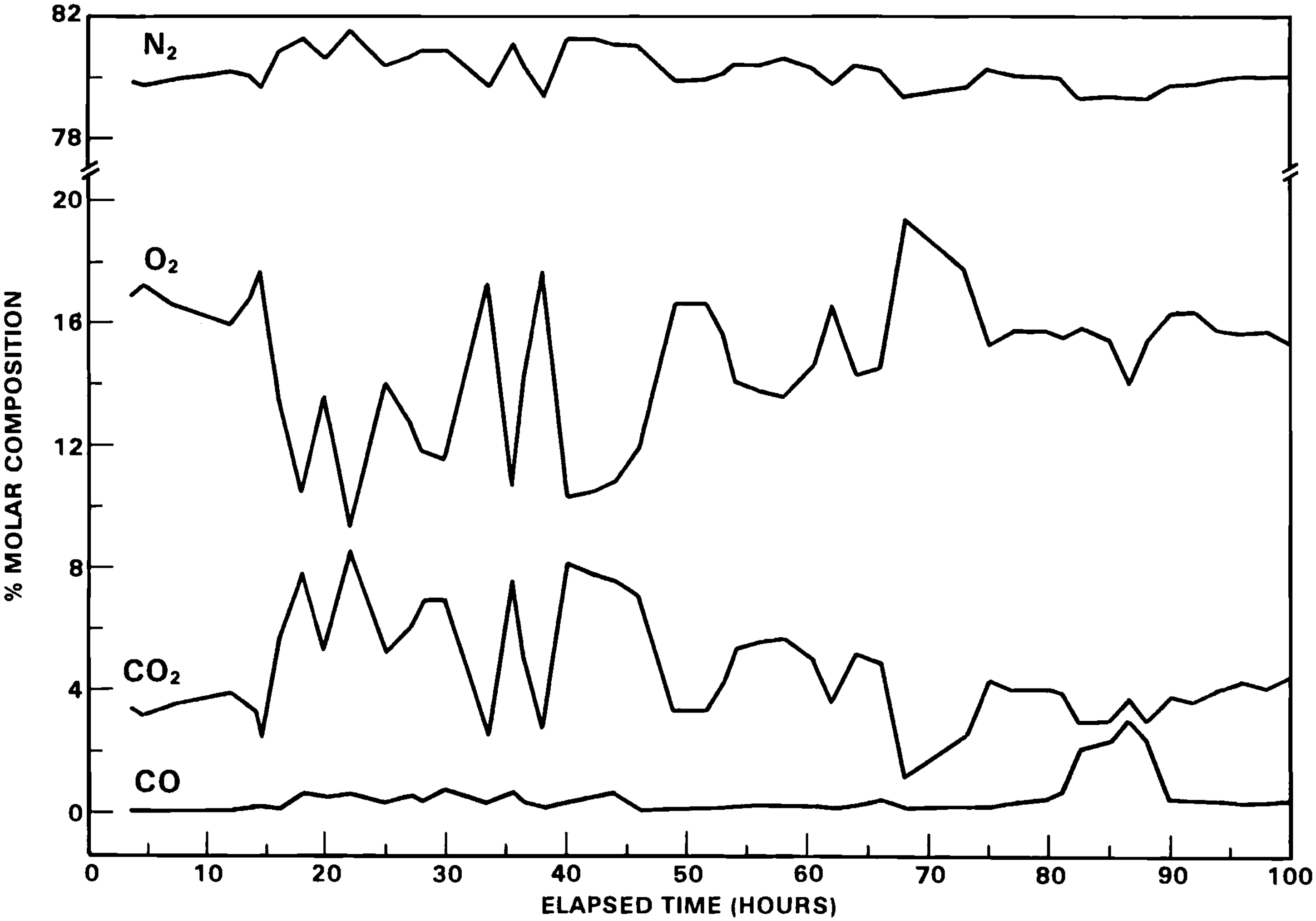

FIGURE 3. Composition of Combustion Boosted Melter Exhaust

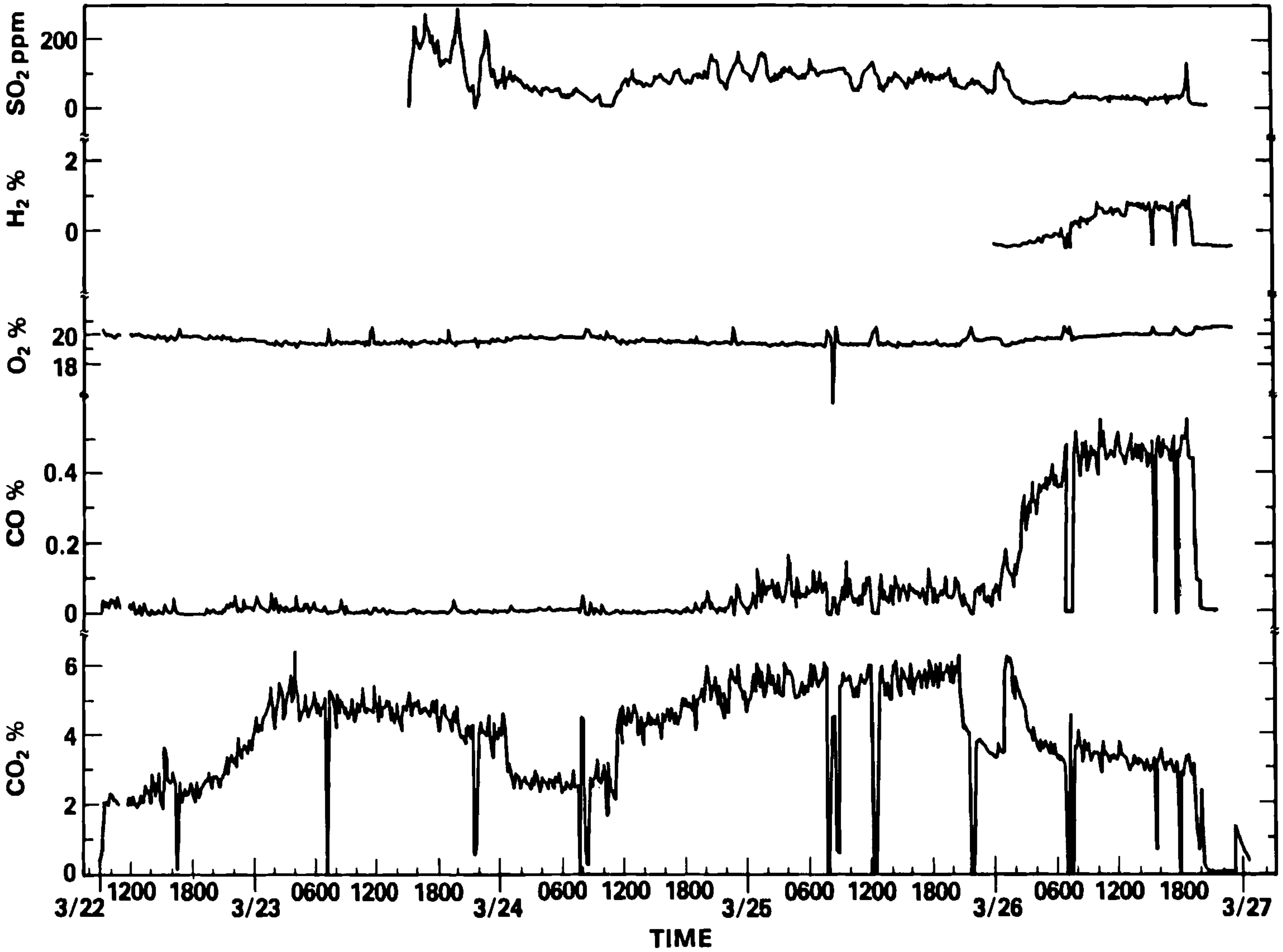

FIGURE 4. Melter Exhaust Gas Composition of a 100-h Boosted, 20-h Unboosted Test

TABLE 5. Melter-Generated Off-Gas Components (acid waste)

Experiment	Melter Inleakage, scfm	Molar %								
		CO_2			CO			H_2		
		High	Avg	Low	High	Avg	Low	High	Avg	Low
PSCM-3[a]	20	29	13	0.26	1.3	0.40	0.04	1.11	NA	0.17
LFCM-7	90	2.2	0.74	0.03	0.44	0.13	0.002	0.63	0.54	0.40
PSCM-4	20	4.4	2.9	1.5	0.75	0.44	0.20	1.3	1.1	0.94
PSCM-5	30	6.5	2.8	2.0	0.90	0.35	0.10	1.8	0.80	0.10
PSCM-6	30	6.5	4.1	2.0	0.60	0.09	0.005	1.2	NA	0.05
PSCM-7	12[b]	8.0	5.0	1.5	1.2	0.75	0.10	3.5	1.9	0.30
PSCM-8	14	9.3	6.1	1.2	0.8	0.16	<0.005	NA	NA	NA

(a) Sample stream diluted ~2.5 times.

(b) Off-gas dilution was used.

The off-gas data presented in Figure 4 illustrates that melter emissions are not generated smoothly or continuously even under the most controlled operational conditions. This behavior is due to the erratic, nonuniform way in which melter feed is dried, oxidized, and melted during the liquid feeding process. Large variations in gas generation rates usually occur when dammed-up liquid feed lying atop an insulating layer of dry feed (the cold cap) abruptly flows out upon a hot glass surface. The liquid quickly flashes off this hot surface, producing a flow pulse composed of steam and volatile organic reaction products.

Figure 5 illustrates the behavior of some of the more important melter-generated gases accompanying flow surges. The frequency and magnitude of these surges are positive indicators of melter system instabilities, which are most often associated with erratic or excessive feeding.

The correlation between the emission rates of noncondensible gases and steam flow surges suggests that the evolution of combustible gases from the cold cap is quite prompt. Figure 6 portrays the time-dependent compositional behavior of the melter exhaust stream upon feed interruption or termination. With the exception of SO_2, none of the melter-generated gases increased in concentration when feeding was terminated. This fact implies that volatile

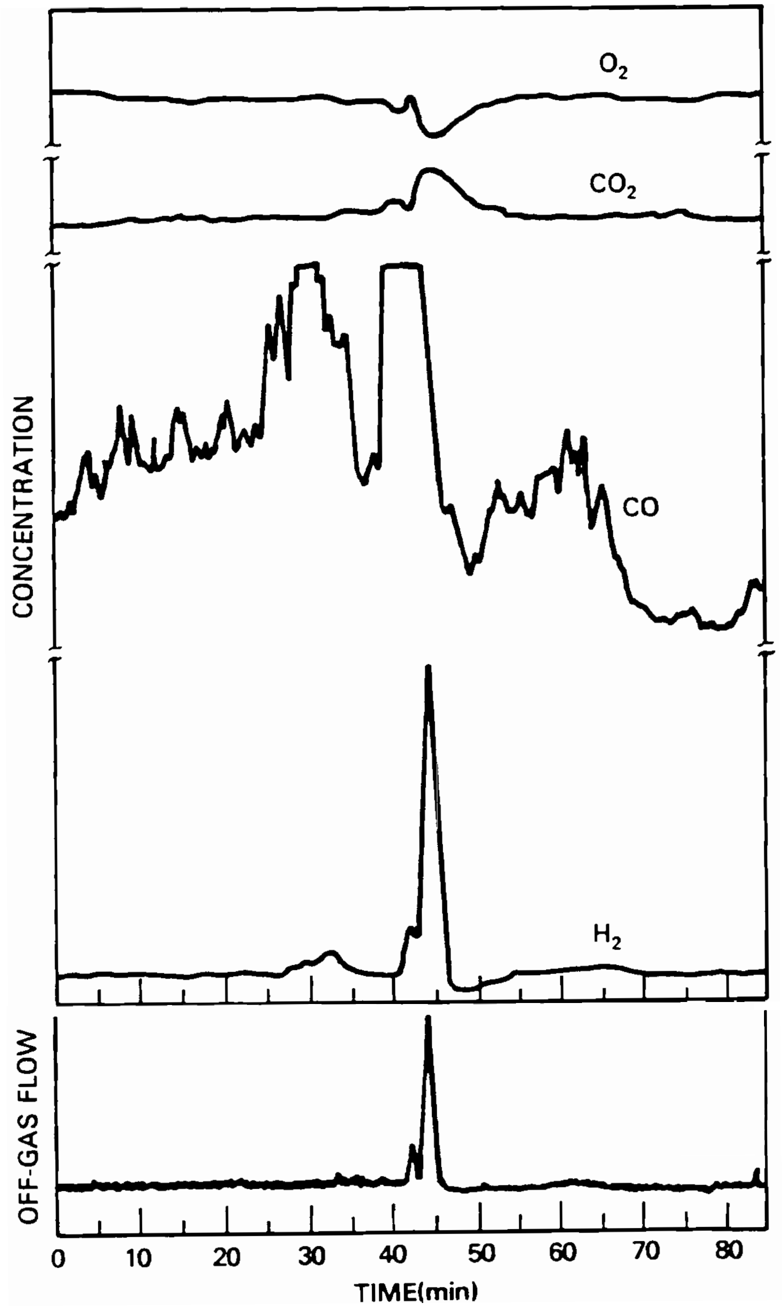

FIGURE 5. Compositional Behavior of Noncondensible Melter Exhaust Gases Acconipanyiny a Flow Surge. (Maximum extent of the surge event: flow-3X; H_2 <3.5%; CO >>0.5%; CO_2-15%; O_2-17%.)

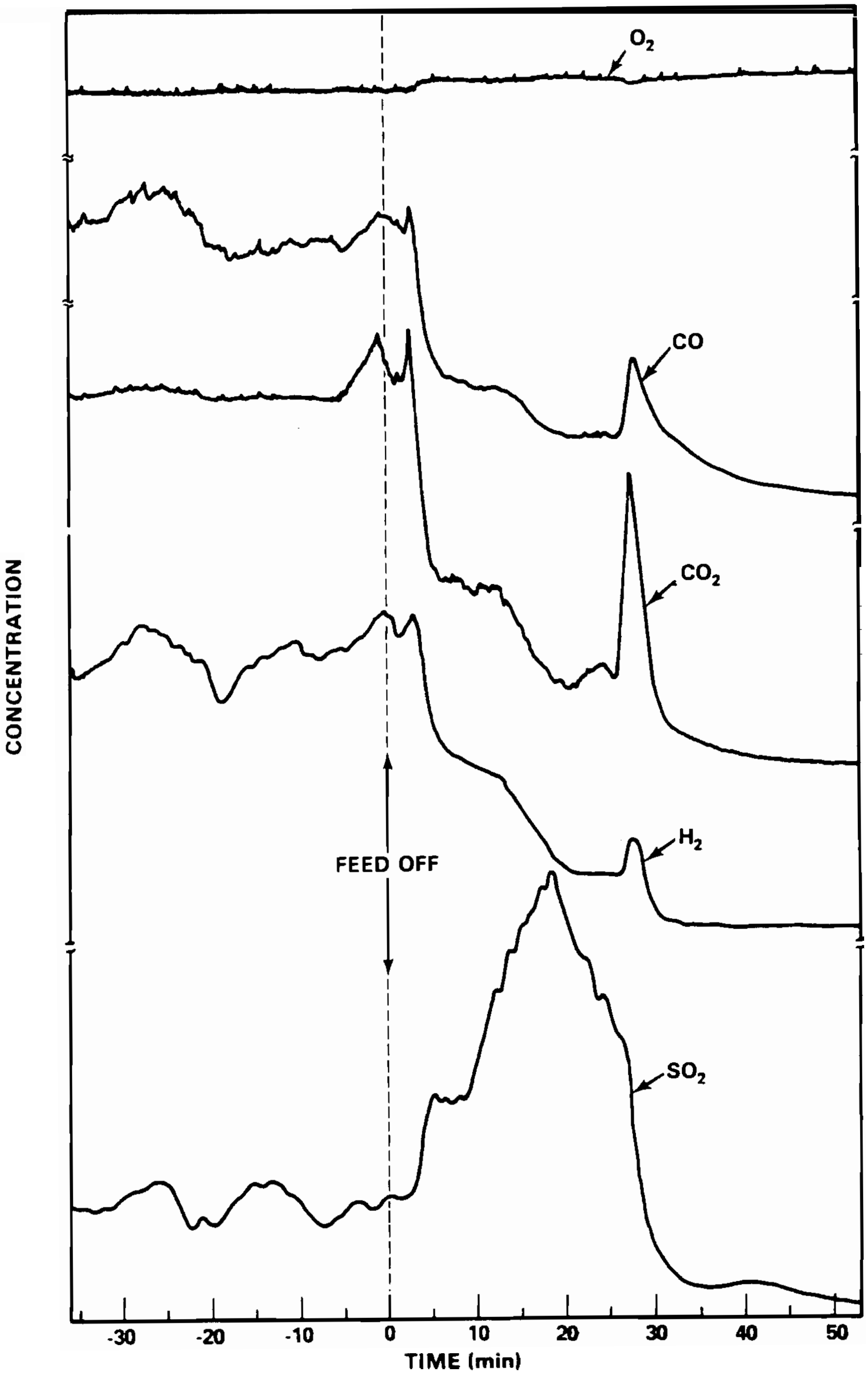

FIGURE 6. Melter Off-Gas Compositional Behavior Associated with Feed Termination. (The t = 30 min compositional spike is due to the injection of a small quantity of liquid feed.)

decomposition and reaction products generated from the melter feed are formed soon after introduction of the feed into the melter. Consequently, significant accumulations of chemically reactive, organic feed components within the melter cold cap apparently do not occur under steady-state feeding conditions.

On the other hand, the increase in terminal SO_2 exhaust concentration (illustrated in Figure 6) suggests that sulfur, as Na_2SO_4, may be accumulating within the melter as a molten salt. This was indeed the case, as post-run inspection of the idling melter glass surface later proved. This observation stimulated speculation that accumulations of Na_2SO_4 could be responsible for changes in the melting capacity of liquid-fed melters that occur during the initial 24 hours of liquid feeding (the startup phase).

Melter emission characteristics of SO_2 further support this notion, as is shown in Figure 7. During the initial startup phase, when the melter's ability to handle feed is limited, feed-rate-normalized SO_2 emission rates are uncharacteristically low, indicating that Na_2SO_4 is probably accumulating. As processing continues at a fixed feeding rate, SO_2 emission rates gradually increase along with the melting capacity of the liquid-fed melter. It is known (Conroy, Manning and Bauer 1966) that the presence of a molten Na_2SO_4 phase within a ceramic melter will increase the heat transfer rate between the molten glass and the feed, thereby boosting melting capacity. All of the above mentioned liquid-fed melter characteristics are consistent with this fact.

Although Figure 7 suggests that SO_2 evolution is an important mechanism responsible for sulfur melter feed losses, this is true only for boosted experiments where plenum temperatures are greater than 700°C. Emission rates of SO_2 during unboosted runs are at least an order of magnitude lower than when boosting techniques are employed. However, total melter losses of sulfur are independent of boosting, indicating the presence of other volatile chemical channels of escape (SO_3). Filtered gas-scrubbing techniques have further verified that significant concentrations of acidic volatile gases of sulfur, as well as the halogens, always exist in unquenched melter exhaust streams independent of melter operating conditions. This subject will be developed further in discussions that follow.

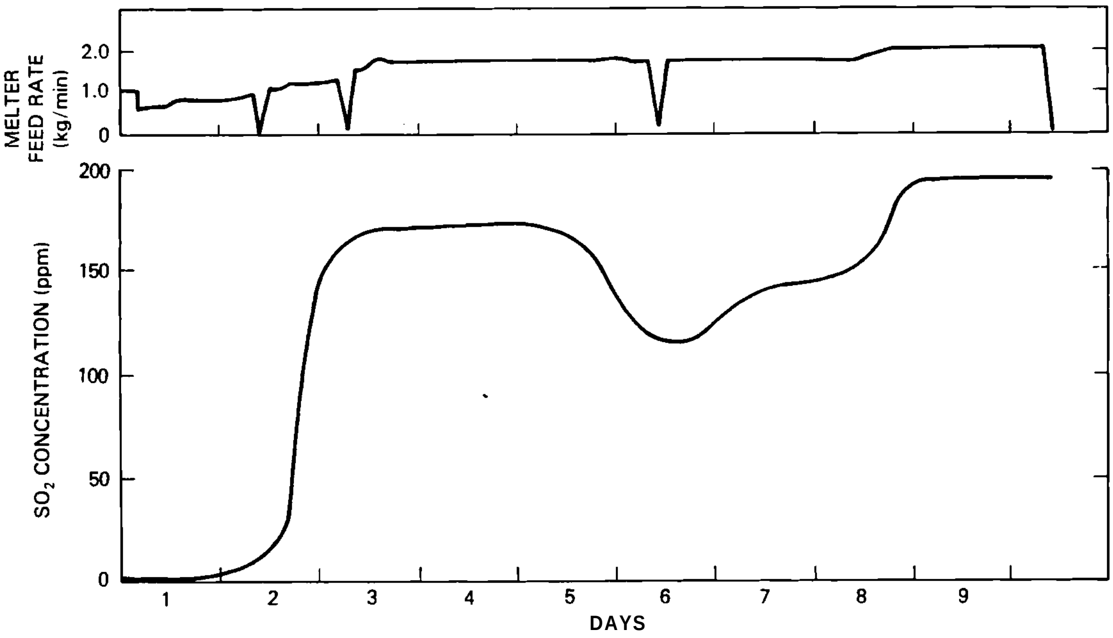

FIGURE 7. Melter SO_2 Emission Characteristics Accompanying a 240-h Test

NATURE OF MELTER FEED COMPONENT LOSSES

In order to characterize the pathways and magnitudes of melter feed component losses, a differential sampling system composed of an aerosol filter, condenser, and a series arrangement of three gas-scrubbing units was employed. The manner in which any given element is distributed across the five discrete sampling fractions of this device is indicative of the physical state(s) assumed by the effluent. Typical data generated with this differential sampling system during a formate-feed melter test are summarized in Table 6. The values listed in this table are melter decontamination factors (DFs), which are ratios of the rate at which feed components enter the melter to the rate at which they are evolved. Particulate DFs are partial DFs relating to only a single loss mechanism: aerosol emission. The data presented in this abridged table clearly show that melter gas-phase losses to the off-gas system are only significant for Cl, S, and B, which readily form volatile acid gases previously referred to.

This is not to say that melter-induced volatilization has no influence upon melter losses of other feed component elements. On the contrary, the low

TABLE 6. PSCM-6 Particulate and Total Feed Component DFs

Element	Average DF	
	Particulate	Total
Al	27,000	22,000
B	6,800	100
Cd	9.9	9.9
Cl	21	2.9
Cs	14	14
Fe	1,900	1,800
La	2,100	2,100
Mn	1,800	1,800
Na	300	300
S	11	5.5
Sr	1,800	1,800
Te	3.0	3.0
Zr	22,000	22,000

DFs associated with the semivolatile elements Cd, Cs, and Te, as well as Se and Sb, clearly underscore the importance of this volatilization process. What is being said is that apart from the mechanisms responsible for producing airborne effluents, particulate transport through the off-gas system is the predominant loss mechanism associated with liquid-fed melter operation.

CHARACTERISTICS OF MELTEK AEROSOLS

Since most melter off-gas system losses are associated with aerosol emission, establishing the characteristics of these aerosols was of particular interest. The size distribution of melter-generated aerosols was established using a cyclonic particle-size analysis system, which was described earlier. Table 7 details the manner in which melter particulate matter was distributed across the cyclonic sample fractions for different melter experiments. All melter tests, with the exception of PSCM-4, exhibited aerosol-size distributions which were bimodal. This suggests that the overall aerosol distribution may be comprised of two independent components, each having its own characteristic size distribution. Gross compositional dissimilarities between the

TABLE 7. Size Distribution of Melter Aerosols

Experiment	Average wt% Versus Cut Point			
	16 µm	6	1 µm	<1 µm
LFCM-7	76.7	2.8	8.5	11.9
PSCM-4	--	0.9	3.6	95.6
PSCM-5	13.5	3.9	20.2	62.2
PSCM-6	46.1	0.5	12.7	40.7
PSCM-7	7.5	3.2	9.4	79.9
PSCM-8	44.0	7.3	19.6	29.1

discrete cyclonic size fractions illustrated in Table 8 strongly reinforce this argument. Moreover, since the submicron size fraction detailed in this table (LFCM-7) contains only 12% of the total sample mass, but possesses essentially all the semivolatile matter of the sample, the mechanism responsible for the small-diameter component of the overall distribution is probably a volatilization/condensation process that occurs within the melter plenum. The compositions of the large cyclonic size fractions are very similar to those of the slurry feed as shown in Table 9. Consequently, the large component of the bimodal distribution must be associated with a gross entrainment mechanism.

Since the major melter loss mechanism associated with the radiologically important semivolatiles is associated with submicron aerosol emission, the elemental makeup of this size fraction is of particular interest. Table 10 presents representative submicron particulate compositional data collected during the PSCM-4 experiment. If a material balance for this submicron matter is established by assuming an oxide form' for all elements except for a stoichiometric quantity of Na, which is associated with the Cl in the sample, 99% of the matter present can be accounted for. It should be noted that while the submicron sample fraction is quite rich in semivolatiles, it is essentially salt (83 wt% NaCl).

MELTER EMISSION PERFORMANCE

Melter performance with regard to effluent emission is commonly expressed in terms of a unitless decontamination factor, or DF. By definition, a melter

TABLE 8. Elemental Distribution Across the Cyclonic Sampling System

Element	Distribution, %			
	16 µm	6 µm	1 µm	<1 µm
Al	96.2	0.9	2.5	0.4
B	87.8	1.8	7.8	2.6
Ba	83.7	5.8	10.5	0
Ca	77.7	2.7	15.2	4.4
Cd	10.7	0.8	7.3	81.2
Ce	92.1	0	7.9	0
Cr	46.4	21.7	23.3	8.6
Cs	7.5	0	5.4	87.1
Cu	82.6	4.9	4.2	8.3
Fe	77.3	2.6	17.0	3.1
La	91.9	1.5	6.1	0.5
Li	83.2	1.5	5.3	10.0
Mg	91.5	1.6	5.8	1.1
Mn	89.4	6.4	3.6	0.6
Mo	77.5	5.6	9.8	7.1
Na	68.8	1.7	5.6	23.9
Nd	93.4	0	6.6	0
Sb	100.0	0	0	0
Se	56.9	1.9	11.4	29.8
Si	92.0	1.8	5.6	0.6
Sr	77.6	2.8	19.6	0
Te	5.5	0.4	3.2	90.9
Ti	91.2	1.8	6.0	1.0
Zr	91.6	1.6	5.6	1.2

feed component DF is the ratio of the rate at which that particular feed component enters the melter to the rate at which it exists. Consequently, melter DFs are related to the liquid-fed melter process efficiencies for converting feed components into a borosilicate glass. Table 11 presents experimental feed component DFs for all pertinent DWPF melter tests conducted at PNL. The entries in this table are grouped according to feed type, and each group is

TABLE 9. Composition of 16 μm Cyclonic Sample Fraction

Elemental Oxides	Weight Percent	
	16 μm	Feed
Al_2O_3	3.4	5.1
B_2O_3	9.0	10.5
CaO	1.6	1.7
Fe_2O_3	14.4	12.7
La_2O_3	0.3	0.4
LiO_2	3.5	4.1
MgO	1.1	1.4
MnO	3.2	2.9
Na_2O	13.0	13.6
SiO_2	38.0	45.6
TiO_2	0.7	0.7
ZrO_2	0.3	0.4

ordered with respect to the experimental melter employed. This ordering is significant in the interpretation of the data.

The initial melter tests conducted with alkaline feed were, with one exception, all boosted experiments (see Table 1). Consequently, a major goal of all of these tests was to establish maximum melter feeding rates under a variety of plenum heating conditions. To complicate matters, a slurry feed system being developed during this same period was often responsible for inconsistent feed delivery to the melter. As a result, stable steady-state operating conditions during these early melter scoping tests were rarely, if ever, achieved. The spread in melter emission performance data during this initial testing phase is in large part a reflection of the unequilibrated conditions that existed when this data was collected. The average DFs listed for the alkaline feed components should, however, provide a fairly representative description of the ceramic melter effluent emission behavior that occurred during this initial development period.

With the exception of the LFCM-7 test (melter capacity scoping study), all acid feed melter experiments sought to establish operational stability under a

TABLE 10. Submicron Particulate Composition

Element	Elemental wt%	Assumed Form	Compound, wt%	Feed Composition, %
Al	0.04	Al_2O_3	0.08	4.95
B	0.07	B_2O_3	0.24	9.86
Ca	0.14	CaO	0.20	1.66
Cd	0.55	CdO	0.63	0.006
Cl	55.0	--	--	0.4
Cs	2.1	Cs_2O	2.2	0.044
Cu	0.06	CuO	0.09	--
Fe	0.29	Fe_2O_3	0.41	13.69
K	0.36	K_2O	0.43	--
Li	1.1	Li_2O	2.4	3.98
Mg	0.02	MgO	0.03	1.29
Mn	0.08	MnO_2	0.13	3.25
Na	33.7	$NaCl$ Na_2O	83.0 6.7	-- 13.88
Ni	0.03	NiO	0.04	0.76
Pb	0.04	PbO	0.05	--
Si	0.66	SiO_2	1.4	44.47
Te	0.56	TeO_2	0.71	0.006
Zn	0.02	ZnO	0.02	--
TOTAL			98.8	

variety of run conditions. Table 12 presents partial melter DFs associated with off-gas aerosol emission for the PSCM-5 and PSCM-6 experiments. The data were collected over several days of stable, steady-state melter operation using three independent sampling devices. The internal agreement between results obtained in each test is indicative of the stability associated with each of these experiments. Consequently, effluent results of individual acid feed experiments should be more representative of average melter behavior than were those associated with the alkaline feed.

TABLE 11. Melter Effluent Emission Characteristics

	Alkaline Feed Melter DFs					Acid Feed Melter DFs[(a)]							
Element	PSCM-1	LFCM-4	PSCM-2	LFCM-6	Average	LFCM-7	PSCM-3	PSCM-4	PSCM-5	PSCM-6[(a)]	PSCM-7	PSCM-8[(b)]	Avg.
Al	11000	530	990	330	3200	190	6000	23000	14000	22000	26000	2200	13000
B	210	130	160	90	150	75	200	230	140	100	210	390	190
Ca	1840	260	610	180	720	62	1100	1900	1100	1200	2600	340	1200
Cd	190	70	47	80	100	8.0	--	9.2	5.7	9.9	6.5	5.6	7.5
Cl	3.1	2.2	3	2.7	2.8	--	4	5	1.5	2.9	6.4	4.7	4.1
Cs	51	57	3	10	30	12	3.8	16	9.4	14	13	130	28
Fe	3800	260	680	230	1200	69	1600	2000	1100	1800	2800	570	1400
La	--	--	--	--	--	--	--	--	10000	2100	3600	590	4100
Li	1900	310	340	160	680	89	2600	3200	730	1300	1100	1600	1500
Mg	9000	350	920	260	2600	120	8200	--	3500	7800	11000	1600	5400
Mn	5700	420	630	330	1800	76	3300	2100	7100	1800	3700	600	2700
Na	830	340	130	90	350	60	900	180	160	300	290	710	370
Nd	--	--	--	--	--	--	--	--	--	2500	4100	540	2400
Ni	1500	260	--	930	900	--	9400	1400	580	1100	3100	4000	3300
Ru	32	26	48	13	30	16	--	--	--	--	--	--	--
S	1	1	19	11	8	--	8	16	4.5	5.5	2.9	10	7.8
Sb	--	1800	100	--	950	67	--	--	440	--	710	130	430
Se	--	--	--	--	--	1	--	--	130	--	40	2.5	58
Si	15000	420	1600	280	4300	120	3000	9200	5300	13000	8700	1900	5900
Sr	7400	204	640	290	2100	55	640	250	--	1800	4200	550	1200
Te	170	62	58	210	130	5.6	32	3.1	3.1	3.0	24	7.6	11
Ti	--	--	1400	170	790	120	4100	8700	7200	5900	15000	1900	6100
Zr	--	--	--	--	--	--	--	5000	13000	22000	9400	1900	10000
TOTAL ±σ	1100	290	430	180±10	500	120 ±50	980	490±30	480±90	800±80	1200 ±100	1000 ±150	720

(a) Frit-165 used for PSCM-6 through PSCM-8. Frit-131 used for all other tests.

(b) High Al, low Fe feed employed.

TABLE 12. Steady-State Aerosol Emission Characteristics

PSCM-5 Boosted Test

Sample Type(a)	Feed Rate, L/h	Particulate Loading,(b) mg/L	DF
C	51	0.55	470
S	72	0.49	460
S	79	0.44	510
C	81	0.61	440
HEPA	81	--	370
S	86	0.48	492
C	93	0.78	440
HEPA	93	--	670
ALL			480

PSCM-6 Boosted/Unboosted Test

Sample Type(a)	Feed Rate, L/h	Particulate Loading,(b) mg/L	DF
S	68	0.29	820
HEPA	68	--	810
C	67	0.37	840
S	74	0.25	910
C	90	0.41	700
S	91	0.28	840
HEPA	90	--	720
S	58(c)	0.32	870
C	58(c)	0.54	660
ALL			800

(a) C = cyclone; S = differential samples; HEPA = absolute filtration.
(b) STP.
(c) Unboosted operation.

A comparison of melter DFs achieved with alkaline and acidic waste slurries reveals that, with only a single exception, higher effective emission rates (lower DFs) were observed for the radiologically important semivolatiles when acidified melter waste was employed. The reducing power of the formic acid feed component apparently promotes volatilization in the plenum and thereby produces greater effective off-gas losses of these elements.

Ruthenium is an exception to the above statement. Ever since melter experiments with a formate feed formulation began, no significant airborne ruthenium has been detected in melter exhaust streams, except for the very atypical LFCM-7 test. Feed and glass sample analyses, on the other hand, indicate significant ruthenium melter losses (DF = 2), and yet no specific sink has been conclusively identified to account for these losses. In all probability, ruthenium is being reduced by the formic acid to its elemental state, whereupon it is lost to the melter floor as slag. A surface plateout mechanism is a possible, but less likely, explanation for these losses; however, no evidence of off-gas-line plating has ever been found. A thorough examination of the melter and its plenum revealed slag generation to be responsible for the observed ruthenium losses.

The effect of feed boosting upon melter emissions has been studied under controlled conditions. If the previous melter stability comments are neglected, Table 11 strongly suggests that melter DFs are dramatically reduced when boosting is employed. However, tests designed to illustrate this effect have failed to show any significant relationships between feeding rates and melter emissions. Table 12 presents gross aerosol DF values associated with the boosted PSCM-5 and PSCM-6 tests. Clearly, these data show no correlation between feeding rates and DFs. Moreover, the boosted PSCM-6 experiment did not utilize electric radiant lid heaters for the entire melter test, yet no significant differences in melter emissions were observed throughout the experiment. Consequently, this data suggests that electric radiant plenum heaters can be employed to boost liquid feeding rates of ceramic melters without significantly deteriorating melter performance.

The implementation of feed-boosting techniques, however, is not without operational difficulties. The high exhaust stream temperatures (>600°C) resulting from the auxiliary plenum heaters can cause the formation of fused off-gas line deposits and accelerated material corrosion rates. A cooling spray (see Figure 2) has successfully controlled exiting melter exhaust gas temperatures to 400°C or less. However, the spray nozzle itself acts to collect entrained feed. These feed deposits ultimately grow to form a local obstruction to melter off-gas flow. Although these deposits are soft and easily removed, the current cooling spray configuration clearly compromises melter off-gas system design.

MELTER IDLING TEST

Because of the high (~1000°C) plenum temperatures associated with idling joule-heated ceramic melters, volatilization losses of radiologically important glass components during these periods could overwhelmingly influence the overall melter source term. The composition of typical melter idling emissions, which appears in Table 13, verifies the importance of this loss mechanism for the semivolatiles. In order to determine the overall importance of this melter loss mechanism, emission rates of semivolatile elements were investigated as a function of plenum temperature and, consequently, of the glass surface viscosity. Temperature control was maintained through use of plenum water sprays, which cooled but did not disturb the surface of the melter glass pool.

TABLE 13. Melter Idling Deposits

Oxides	Weight Percent Gray Deposits	White Deposits	Glass
Al_2O_3	1.2	0.11	3.7
B_2O_3	14.2	1.6	10.0
CaO	0.22	0.46	1.2
CdO	0.02	0.02	0.009
Cr_2O_3	0.57	0.58	0.02
Cs_2O	3.7	8.3	0.05
Fe_2O_3	0.10	0.17	14.8
K_2O	0.79	0.85	*
Li_2O	1.92	2.6	4.4
MgO	0.05	0.05	1.4
MnO_2	0.05	0.05	3.9
Na_2O	31.0	31.0	15.7
NiO	0.25	0.02	1.2
RuO_2	0.82	2.1	0.01
Sb_2O_3	0.01	0.01	0.02
SiO_2	0.02	0.47	45.1
SrO	0.005	0.005	0.02
TeO_2	0.70	0.70	0.002
TiO	0.01	0.01	0.8
ZnO	0.02	0.02	0.008

---

* Used in sample preparation.

This study was initiated immediately after a 120-h liquid-fed melter test (PSCM-5). With a 42 L/h water spraying rate and the melter under automatic resistance control, the melter glass surface was cooled to the point that it formed a continuous, nonconvective layer above the bulk melter glass pool (with plenum at 280°C). At a 27 L/h spray rate, the surface viscosity decreased significantly. Convective mixing opened vents in the glass surface that migrated at random across the melter glass pool. However, plenum temperatures were not high enough to melt feed deposits formed upon the melter walls and lid during the preceding PSCM-5 experiment. Finally, the cooling spray was terminated and the melter was allowed to idle at a fixed current rate, which slowly brought the melter plenum up to 850°C. Samples were collected from the plenum during all phases of this study.

The results obtained from these plenum samples are yraphically summarized in Figure 8, which characterizes the emission rates of the semivolatile elements under various idling conditions (temperature) employed during this test. These data indicate that emission rates of all semivolatile elements decreased as a function of time after the completion of PSCM-5 at a 42 L/h water-spraying rate. Reducing the cooling spray rate to 27 L/h increased both plenum temperature and semivolatile emission rates; however, an equilibrated plenum temperature was not achieved during the brief 24-h period of reduced spraying.

Termination of the water-cooling spray increased the plenum temperature steadily to the point where plenum surface deposits formed during PSCM-5 began to melt and "burn" away. The dramatic peaking of emission rates of the semivolatile elements occurred during this period. The fact that all semivolatiles do not form maxima at the same point in time is most probably due to temperature, which was steadily increasing throughout the interval over which these maxima occurred.

The plenum temperature during the last two sampling periods was ~850°C, and all plenum surfaces appeared clean. The emission rates during these periods are, with the exception of Se and Te, significantly greater than the minimum emission rates exhibited by these elements during full 42 L/h spray cooling. However, these elevated idling emission rates are still significantly below those rates observed during moderate liquid feeding conditions.

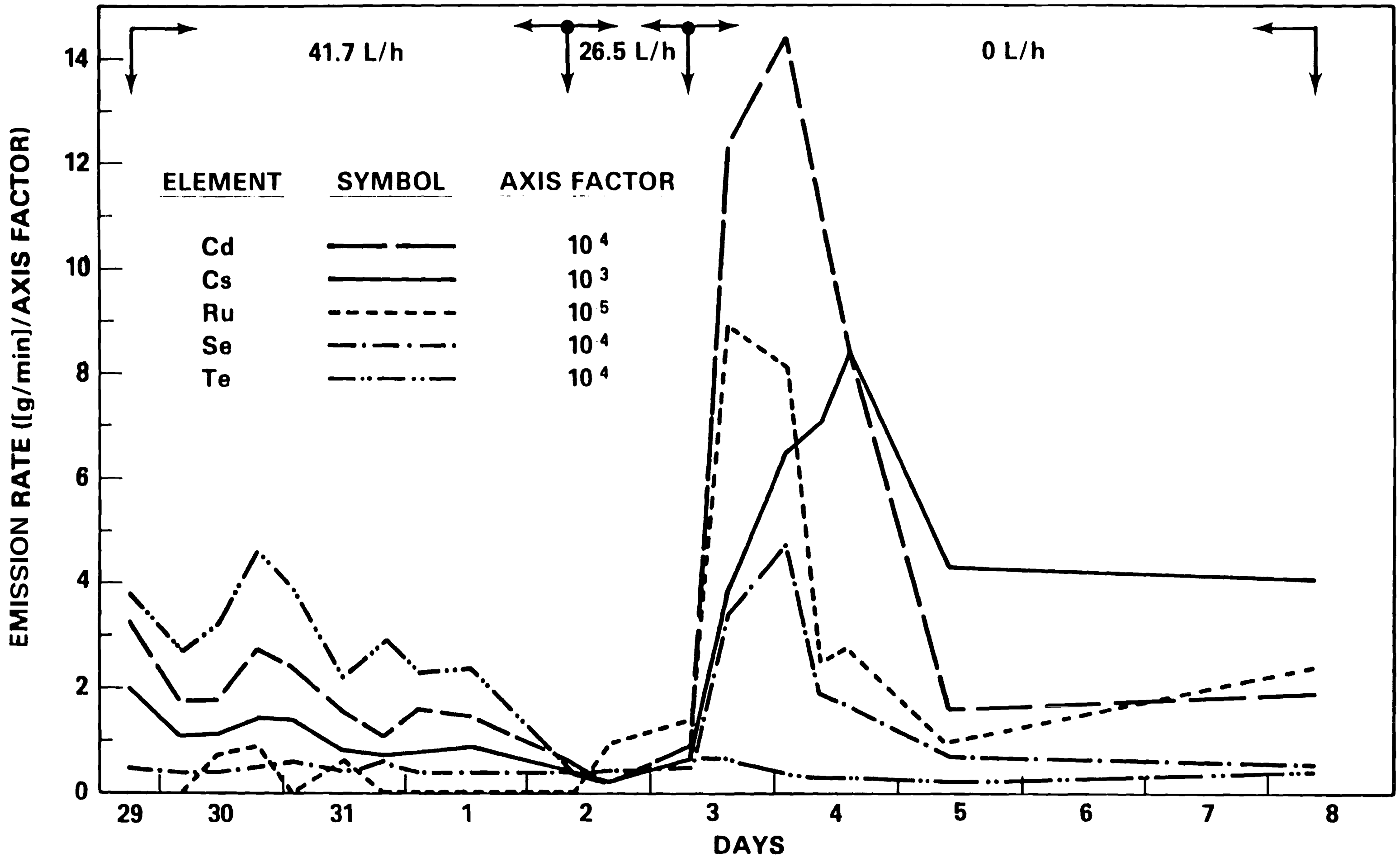

FIGURE 8. Melter Idling Emission Rates of Semivolatile Elements

Specifically, the Cs emission rate expected from the PSCM for a liquid feeding rate of 50 L/h (1.1 kg/min) would be about 10 mg/min. This is more than twice the value observed during the hot melter idling conditions. Consequently, it appears that the plenum cooling approach, although capable of reducing emission rates of most semivolatiles (by a factor of 10 for Cs), is of little practical value in reducing the overall radiological burden of the melter off-gas system.

It should be noted that the effect of directly feeding water onto the surface of an idling melter has also been investigated as an alternative method for reducing idling emissions. This approach was, however, a less satisfactory means of cooling the plenum and melter glass surface than was the plenum spray approach. The water feeding technique produced a high degree of entrainment and aerosol carryover into the off-gas system. Moreover, at the water feeding rates used (45 L/h), convective mixing was actually exacerbated, although total melter surface flooding was never attempted. On the other hand, the water plenum spray initiated no observed entrainment, and minimized or eliminated convective surface mixing.

MELTER SLAG FORMATION

After formic acid was added to the SRL reference feed composition, unaccountable losses of semivolatile spikes were observed. The most probable explanation for these feed component losses was melter production of insoluble metallic slag. Examination of the melter floor, after draining, confirmed that metallic slag formation had indeed occurred and was responsible for significant losses of Ru, Se, and Te. The major metallic component of the harvested nodules was, however, Ni, which because of its wt% in the feed is capable of producing significant slag accumulations on the melter floor. This in turn could seriously affect the service life of a production melter if slag generation or its accumulation is not controlled.

MOLTEN SALT ACCUMULATION

Due to the potential steam explosion hazards associated with the presence of molten salts within liquid-fed melters, the composition and accumulation rates of immiscible melter salt layers have been investigated. Time-dependent compositional behavior was assessed following PSCM-7. Salt samples extracted promptly after the PSCM-7 test were composed of alkali metal compounds of sulfate (75 wt%) and chloride (25 wt%). Samples extracted two days after termination of PSCM-7 were essentially all alkali sulfates. The presence of halogen salts in a molten sulfate phase during melter operation is somewhat disquieting since halogen salts have been shown to sensitize the water-molten Na_2SO_4 interactions. As a result, safety considerations may necessitate molten salt phase control.

A molten sulfate salt phase accumulates in a melter when the sulfate composition of the feed exceeds the capacity of the glass to incorporate it. The rate at which it accumulates will not only depend upon glass and feed characteristics, but will also depend upon melter off-gas loss rates of sulfur. Table 14 summarizes the behavior of sulfur for all formate feed tests for which adequate data exists. Although the sulfur distributional results are quite variable, a few general conclusions can be drawn: If the sulfur content of the feed is kept below -0.025 wt%, accumulations of Na_2SO_4 probably will not occur. On the other hand, if the glass capacity is exceeded by the sulfur in the feed, the excess will be distributed equally between a molten salt phase and the off-gas system.

TABLE 14. Relative Melter Production and Loss Rates of Sulfur

	Wt% Sulfur		Fractional Production/ Loss Rates of Sulfur		
Melter Test	Feed	Glass	Glass	Off Gas	Molten Salt
PSCM-3	0.05	0.09	>1	>0.13	--
PSCM-4	0.081	0.044	0.54	>0.06	<0.40
PSCM-5	0.056	0.067	>1	0.22	--
PSCM-6	0.049	0.025	0.51	0.18	0.31
PSCM-7	0.070	0.035	0.50	0.34	0.16
PSCM-8	0.082	<0.02	<0.24	0.10	>0.66

CLOSE-COUPLED SCRUBBER PERFORMANCE

A close-coupled venturi ejector scrubber with cyclonic disengagement was added to the PSCM melter off-gas system prior to the PSCM-7 test. Since melter exhaust fouling of the off-gas system is most probable between the melter and the quencher, close coupling of a quench scrubber is an off-gas system necessity. Consequently, the performance characteristics of the close-coupled venturi ejector were carefully evaluated during PSCM-7 and PSCM-8, and the results obtained are summarized in Table 15. The variances in scrubber performance between these two tests can be ascribed to differences in off-gas particle size distributions and steam loadings produced by gross feed compositional differences. PSCM-8 generated larger aerosols on the average and possessed much higher off-gas water loadings (80% versus 60%) than did PSCM-7 (see Appendix for more details). The combined effect of these two factors can easily account for the observed differences in scrubber performance.

The overall system performance of the melter and scrubber combination was found to be quite invariant throughout the duration of each of the two tests. System upsets such as overfeeding during PSCM-8 or the use of a melter air sparge in PSCM-7 did not affect the overall system DF, although the melter and scrubber efficiencies were diametrically affected. This behavior is consistent with disturbances that would serve to increase gross entrainment losses.

MELTER OFF-GAS FLOW RATES

The off-gas flow rates of the two liquid-fed melters have been examined over the past year as part of the SRL-DWPF melter development program. During this period of study, two separate feed formulations have been used, and a variety of melter operational running conditions have been employed. The results of these studies have shown that both feed composition and melter feeding rates have a preponderant influence upon the stability of melter off-gas flow rate.

TABLE 15. **Close-Coupled Scrubber Particulate DFs**

Element	Scrubber DFs	
	PSCM-7	PSCM-8
Al	81	5900
B	5.2	6000
Ba	--	--
Ca	90	79
Cd	19	14
Cl	--	37
Cr	32	100
Cs	18	11
Cu	20	260
F	11	--
Fe	260	3600
La	52	800
Li	23	63
Mg	--	220
Mn	470	1500
Na	20	33
Nd	140	--
Ni	120	150
Pb	12	13
S	7.7	75
Sb	23	36
Se	7.9	3
Si	180	10000
Sr	9.1	360
Te	14	13
Ti	13	--
Zn	23	900
Zr	36	--
TOTAL	9	54

The effect of feed composition upon melter flow rate behavior is related to the physical ability of the feed components to form a structurally sound insulating layer (cold cap) between the incoming liquid feed and the hot glass surface. As portions of the insulating cold cap become calcined, structural collapse occurs, bringing dammed-up liquid feed into contact with the extremely hot glass surface. This results in the flashing off of the water component (and volatile reaction products) of the feed, producing a flow pulse or an off-gas surge. The magnitude and extent of these surges are naturally dependent upon the amount of liquid feed present on the cold cap that is delivered to the hot glass surface. Consequently, an erratic flow rate from the melter exhaust is often indicative of an unstable, overfed operational condition. Exhaust flow rate patterns associated with stable and unstable melter operation are illustrated in Figure 9.

The two melter feed formulations used in these studies exhibited significantly different melter off-gas properties. The alkaline waste formulation produced a noisy, erratic melter flow rate with surges as high as seven times that of the average flow. The acid feed, on the other hand, possessed a very compliant, nonbridging cold cap, which reduced the frequency and magnitude of off-gas surging events. Average melter flow characteristics associated with each of these feed formulations are summarized in Table 16. These data clearly show the stabilizing influence of the formic acid feed component upon melter flow rate behavior.

Due to the conservative, stable manner in which most PSCM runs were conducted, PSCM flow rate data associated with acidified feed are probably more representative of average melter behavior than are the values associated with the LFCM. The LFCM data, on the other hand, can be used in assessing the effects of heavy melter feeding conditions upon melter off-gas flow rate.

CORROSION

Extensive metal corrosion has been observed in liquid-fed melter plenums and in associated melter off-gas lines and processing equipment. The nature of the corrosion observed suggests acidic chemical attack by volatile halogens and

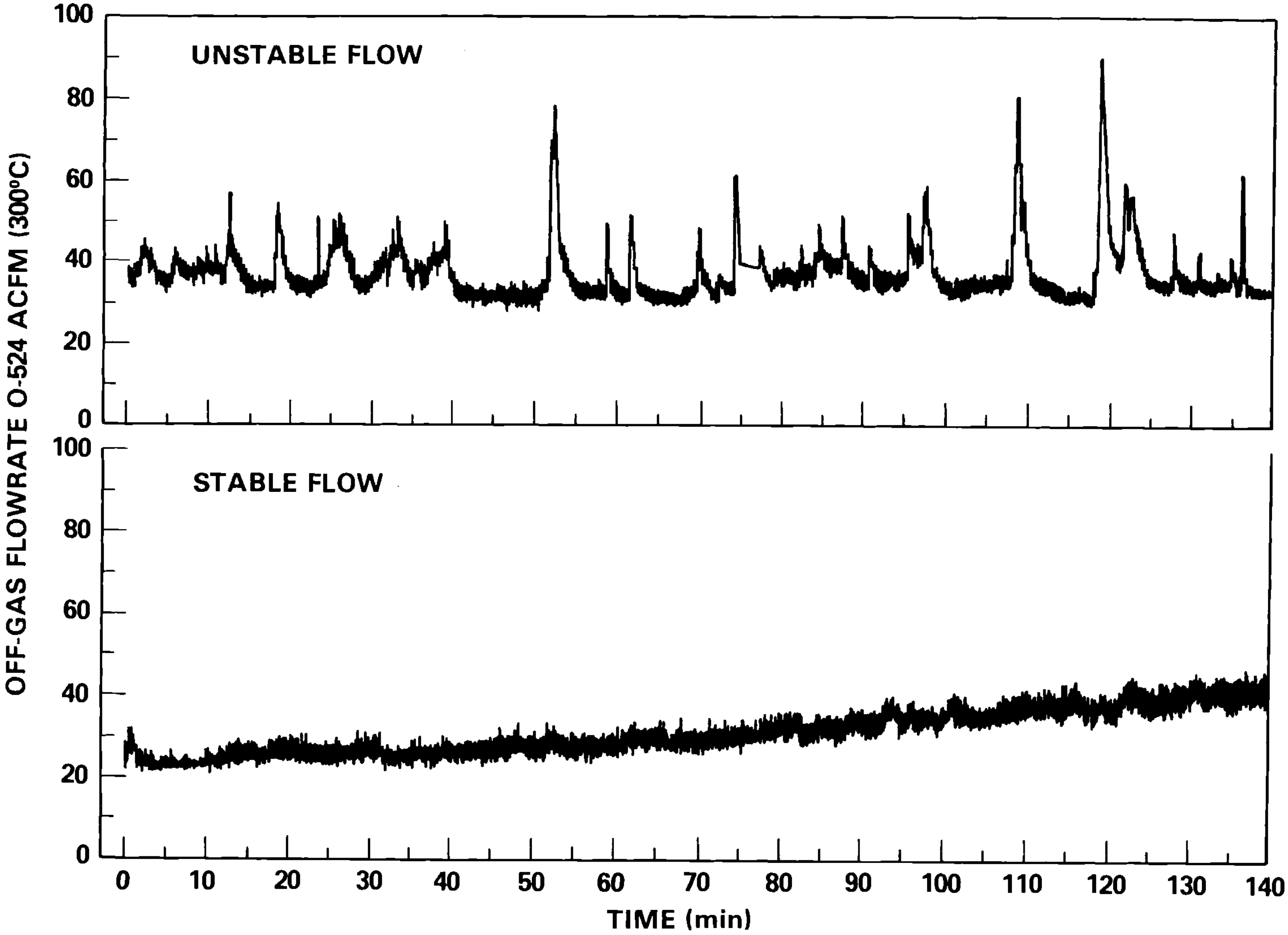

FIGURE 9. Typical Off-Gas Flow Rate Behavioral Patterns Associated with Liquid-Fed Melters

TABLE 16. Liquid-Fed Melter Flow Rates

Experiment	Feed	Average, Flow, scfm	Maximum Surge, scfm	Average Surge Duration, min
LFCM-4	Alkaline	90	620	3
LFCM-6	Alkaline	90	470	3
PSCM-3	Acid	70	220	3
LFCM-7	Acid	240	710	3
PSCM-4	Acid	70	300	4
PSCM-5	Acid	80	230	3
PSCM-6	Acid	80	190	3

sulfur compounds. In order to identify suitably corrosive-resistant materials for the melter off-gas treatment system, corrosion coupons representing different groups of alloys were exposed to the plenum environment of liquid-fed melters during processing (300 to 500°C) and idling (850°C) conditions. The extent of corrosion as a function of operating conditions was established gravimetrically through coupon weight loss. The results of these studies, which are summarized in Table 17, indicate that the corrosion rates occurring during actual liquid feeding are much greater than those occurring during hot idling, although temperature cycling between feeding and idling accelerates overall corrosion rates. In addition, titanium, tantalum and all alloys having high iron concentrations were unsuitable for liquid-fed melter service. The most promising alloys are those possessing a content low in iron and high in nickel or cobalt, and a chromium content greater than 20%. Inconel-625 and the Haynes alloys were the most corrosive-resistant materials employed during this study.

CONCLUSIONS

The off-gas studies discussed in this report have sought to establish the effluent characteristics of liquid-fed joule-heated ceramic melters. The results of these studies have shown particulate emission to be responsible for most melter effluent losses. Moreover, a large fraction of the total particulate mass evolved from an operating melter is conveyed to the off-gas system by

TABLE 17. Corrosion Sample Results

Material	Exposure, h		Weight Change g/cm2	Cor. Rate cm/yr	Observations			Approximate Composition, wt%					
	Idling	Operating			Spalling	Deposits(a)	Color(b)	Cr	Co	Fe	Ni	Mo	W
Inconel®-690	1134	214	-0.025	0.020	Light	Light	Blk-Silver	30	--	9.5	60	--	--
	198	214	-0.014	0.074	Light	None	Black						
	1256	214	-0.036	0.023	Light	Light	Multi						
	320	330	-0.011	0.015	Light	Light	Black						
Inconel®-625	1134	214	+0.015		None	Heavy	Brown	21.5	--	2.5	61	9	--
	198	214	+0.007		None	Heavy	Brn-Silver						
	1256	330	+0.013		None	Heavy	Brn-Black						
	320	330	+0.012		None	Heavy	Brn-Silver						
Inconel®-617	122	116	-0.004	0.008	Med-Pits	Medium	Gr-Silver	22	12.5	1.5	52	9	--
	122	116	-0.013	0.024	Med-Pits	Medium	Gr-Silver						
Inconel®-600	122	116	-0.008	0.015	Medium	Light	Multi	15.5	--	8	76	--	--
	122	116	-0.002	0.004	Medium	Light	Multi						
Haynes®-188	1134	214	+0.059			Very Light	Bl-Black	22	40	3	10	--	15
	198	214	+0.004		Light	Light	Bl-Black						
Haynes®-25	1134	214	+0.005		Light	Light	Bl-Black	21	54	3	10	--	15
	198	214	+0.003	0.008	Light	Light	Bl-Black						
	60	110	+0.001		None	None	Black						
RA®-330	1134	214	-0.025	0.020	Medium	None	Multi	18	--	47	35	--	--
	198	214	-0.036	0.185	Medium	None	Gr Spots						
RA®-446	1134	214	-0.18	0.145	Heavy	None	Multi	25	--	75	--	--	--
	198	214	-0.17	0.472	Heavy	None	Multi						
Titanium	122	116	-0.063	0.210	Heavy	None	Silver-Brn	--	--	--	--	--	--
Tantalum	122	116	-3.3	>3	Disappeared								

(a) Feed material sintered on coupon surface.
(b) Bl - Blue; Blk - Black; Brn - Brown; Gr - Green.
® Inconel is a registered trademark of Huntington Alloys, Huntington, West Virginia.
® Haynes is a registered trademark of the Cabot Corporation, Kokomo, Indiana.
® RA is a registered trademark of Rolled Alloys, Detroit, Michigan.

submicron aerosols which are almost exclusively responsible for semivolatile transport. Melter operational conditions have had little effect upon these results as long as quasi-steady-state conditions are maintained. Even hot melter idling conditions do not significantly affect the overall melter source term.

Melter-generated gases have been found to be potentially flammable as well as corrosive. Hydrogen generation presents the greatest flammability hazard of the combustibles generated by liquid-fed melters. Off-gas dilution was required during a melter test to maintain the H_2 concentration below 70% of its lower flammability limit in the quenched melter exhaust. The combustible gas CO has never achieved a quenched off-gas concentration greater than 1/10 of its flammability limit. Auxiliary plenum heating significantly reduces melter emission rates of both these combustible gases.

Significant concentrations of acidic volatile compounds of sulfur and the halogens exist in unquenched melter off-gas streams independent of melter operation. These gases have been responsible for extensive corrosion observed in melter plenums and in associated off-gas lines and processing equipment. Alloys possessing low iron, high nickel or cobalt, and high chromium content are the most suitable for liquid-fed melter service.

REFERENCES

Bjorklund, W. J. 1982. Defense Waste Vitrification Studies During FY-1981. PNL-4366, Pacific Northwest Laboratory, Richland, Washington.

Bonner, W. F. 1979. The High-Level Waste Immobilization Program: An Overview. PNL-3094, Pacific Northwest Laboratory, Richland, Washington.

Buelt, J. L., and C. C. Chapman. 1978. Liquid-Fed Ceramic Melter: A General Description Report. PNL-2735, Pacific Northwest Laboratory, Richland, Washington.

Conroy, A. R., W. H. Manning, and W. C. Bauer. 1966. "The Role of Sulfate in the Melting and Fining of Glass Batch." Glass Ind 47(2):84-89.

Ethridge, L. J. 1983. Defense Waste Vitrification Studies During FY 1982. PNL-4834, Pacific Northwest Laboratory, Richland, Washington.

APPENDIX

OFF-GAS DATA COMPILATION FOR LIQUID FEEDING OF CERAMIC MELTERS

APPENDIX

OFF-GAS DATA COMPILATION FOR LIQUID FEEDING OF CERAMIC MELTERS

INTRODUCTION

Off-gas and effluent characterization studies have been estabished as part of the SRL-DWPF melter development program being conducted at PNL. The objective of these studies is to establish the off-gas properties of liquid-fed joule-heated melters as a function of melter operational parameters. The scope of these studies is quite broad and covers all aspects of off-gas concern including

- effluent characterization
- flow rate behavior
- corrosion effects
- emission abatement.

The purpose of this appendix is to present all off-gas data compiled since liquid-fed melter tests began in support of DWPF. During this period, 13 major melter experiments have been conducted. These are listed below according to abbreviation and date:

Experiment[a]	Date
LFCM-2	September 1980
LFCM-3	November 1980
PSCM-1	December 1980
LFCM-4	January 1981
PSCM-2	March 1981
LFCM-6	June 1981
PSCM-3	July 1981
LFCM-7	August 1981
PSCM-4	December 1981
PSCM-5	January 1981
PSCM-6	March 1982
PSCM-7	May 1982
PSCM-8	June 1982

(a) LFCM and PSCM refer to the Liquid Fed Ceramic Melter and Pilot-Scale Ceramic Melter, respectively.

The details concerning these experiments are fully described and documented in melter test summary documents (Bjorklund 1982; Ethridge 1983). As an aid in reading this report, all pertinent melter operational parameters associated with each experiment to be discussed are listed in Table A.1.

Both melters being studied in this report share a common 0.1-m (4-in.) stainless steel off-gas system consisting of an ejector venturi, a downdraft condenser, and a packed scrubbing tower. The arrangement of these components is illustrated in Figure A.1. In addition to these common off-gas elements, both melters are equipped with a close-coupled HEPA filter receptacle and a total (condensible and noncondensible) off-gas flowmeter. However, since the PSCM off-gas HEPA filtration capability was added during lid modifications of this melter, total off-gas filtration data were not available for the PSCM-3 experiment.

An additional venturi ejector was added to the PSCM off-gas system during May 1982. The wet scrubber was close coupled to the PSCM melter by a 2-m length of 15-cm (6-in.) pipe. The performance of this scrubber was evaluated during the last two tests (PSCM-7 and -8) covered in this appendix.

EFFLUENT CHARACTERIZATION

LFCM-2 - SEPTEMBER 1980

Briefly, LFCM-2 was a 120-h test to demonstrate a steady-state glass production of 40 kg/h-m^2 using lid boosting (see Table A.1 for more details). During this run, a 5.9-kg (13-lb) plug formed in a horizontal section of off-gas-line ~3 m (10 ft) from the melter lid. The off-gas temperature at this location ranged between 400 and 600°C throughout the duration of plug formation. Figure A.2 schematically illustrates the components of the LFCM off-gas line that were later disassembled for inspection. Figures A.3 through A.5 are photographs of the piping sections called out in Figure A.2. The composition of the plug materials is compared with that of the feed in Table A.2, where an oxide composition has been assumed except for the anions. With the exception of the anions, the three most highly enriched elements in the plug relative to

TABLE A.1. Liquid-Fed Melter Operational Parameters

Operational	Equipment												
Parameters	LFCM-2	LFCM-3	LFCM-4	PSCM-1	PSCM-2	LFCM-4	PSCM-3	LFCM-7	PSCM-4	PSCM-5	PSCM-6	PSCM-7	PSCM-8
Feed Rate, kg/h-m^2	80	50	90	45	110	100	62	130	120	135	165	95	140
Glass Production, Rate, kg/h-m^2	37	21	41	22	50	45	28	57	39	46	65	41	49
Boosting type	Elect. Lid Heat	None	Elect. Lid Heat	None	Propane Combustion	Elect. Lid and Plasma Torch	None	Elect. Lid Heat	None	Elect. Lid Heat	Elect. Lid Heat	None	Elect. Lid Heat
Boosting Power, kW	~25	--	30	--	35	40	--	15	--	36	55	--	45
Off-Gas Temp., °C	300-600	325	375	375	375	350	210	250	275	375	400	280	360
Off-Gas Cooling, gph	None	None	2	None	6	5	None	Variable	None	6	6	None	8
Experiment Duration, hours	120	24	120	120	120	120	135	120	107	99	138	115	232

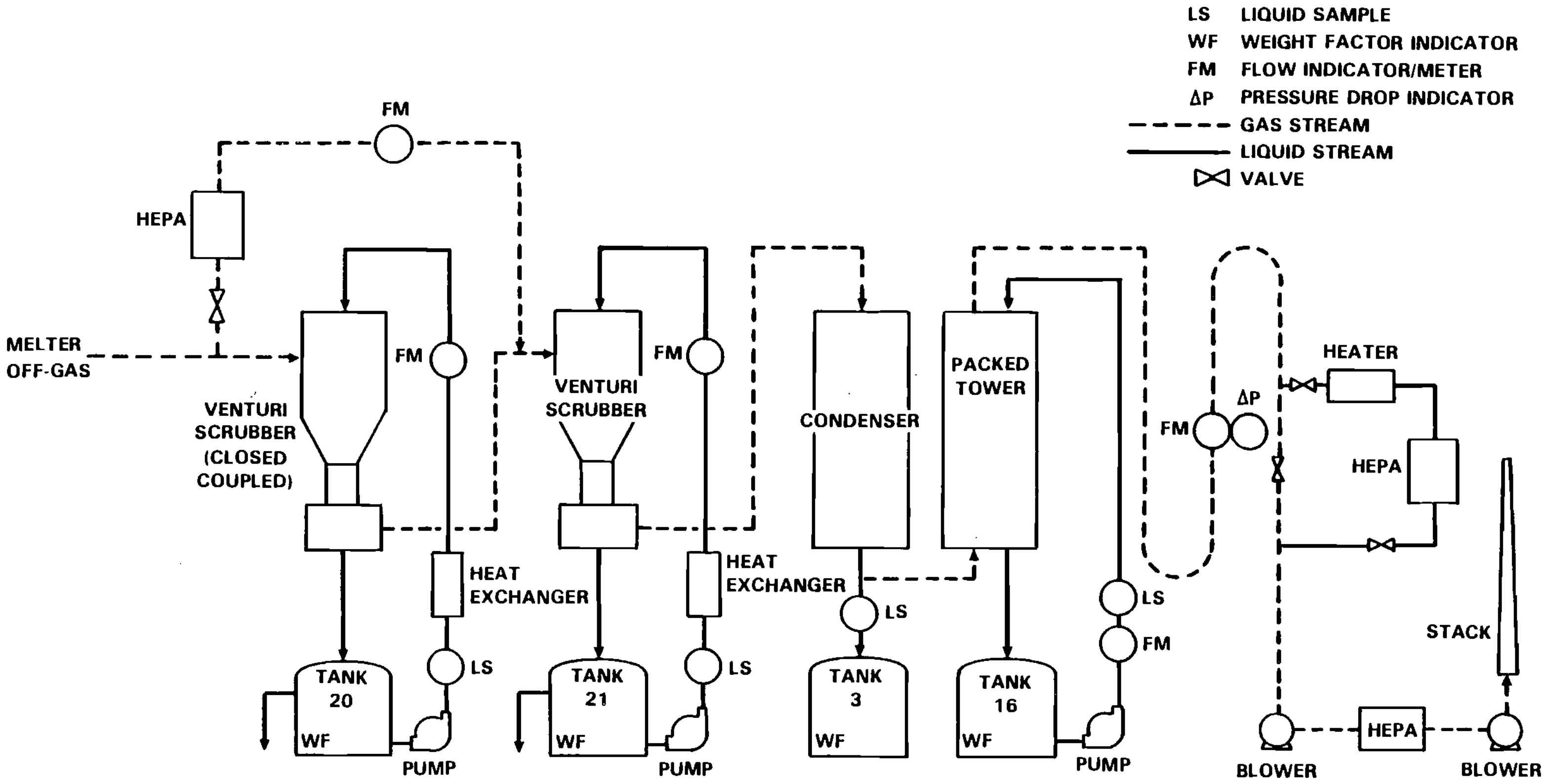

FIGURE A.1. Off-Gas Treatment System

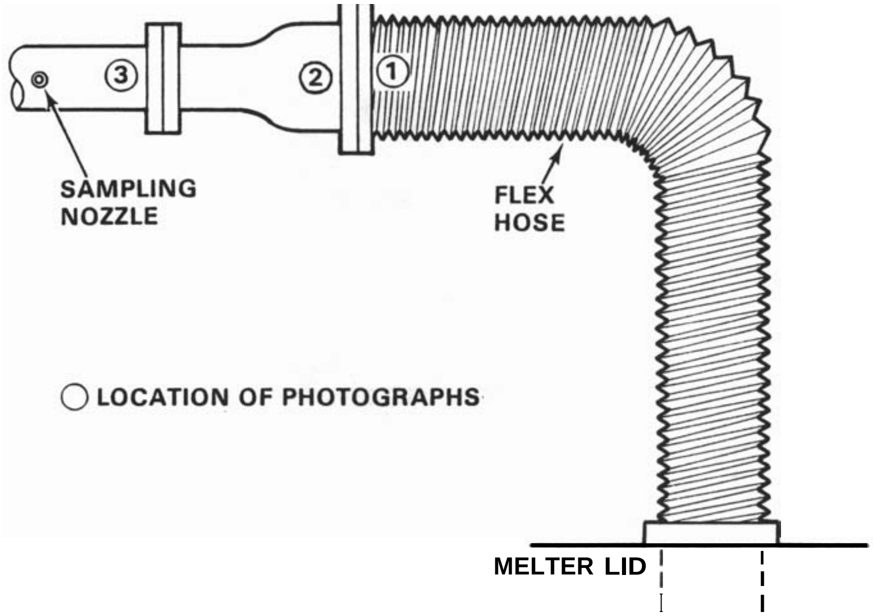

FIGURE A.2. LFCM-2 Off-Gas Line Schematic

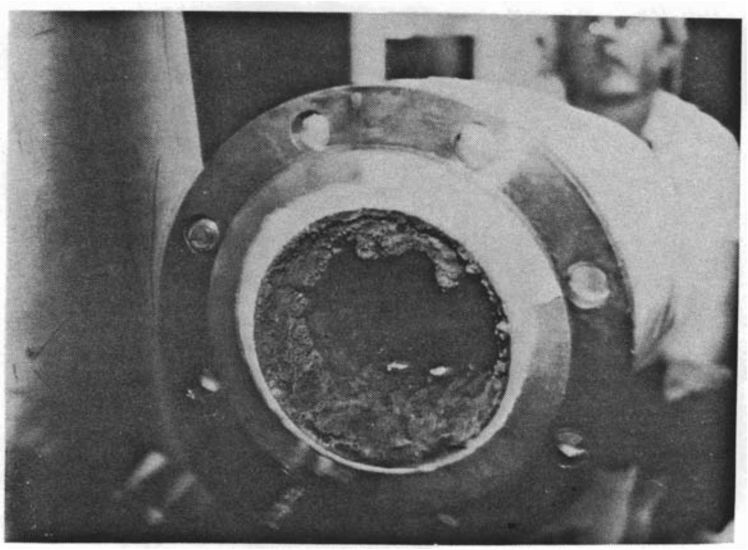

FIGURE A.3. LFCM-2 #1

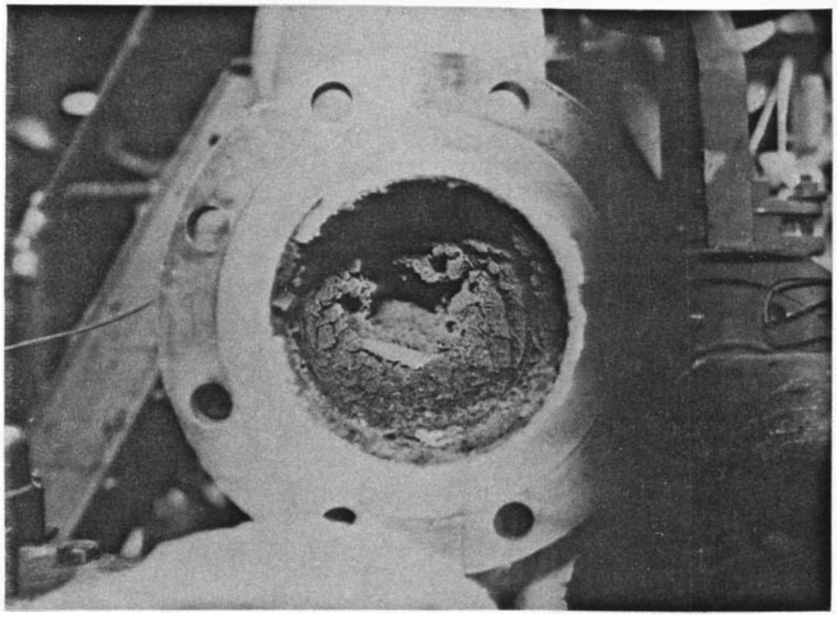

FIGURE A.4. LFCM-2 #2

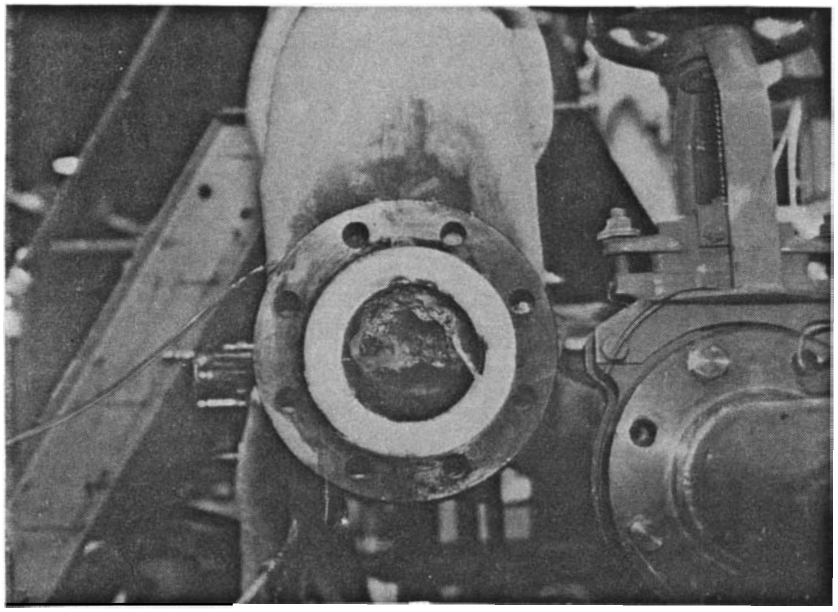

FIGURE A.5. LFCM-2 #3

TABLE A.2. LFCM-2 Plug Composition

Elemental Oxides	Average wt% in Plug	Wt% Feed 9/18/82 2030 h	Wt% Ratio Plug/Feed
Al_2O_3	1.67	2.96	0.56
B_2O_3	4.62	3.78	1.22
CaO	4.40	4.62	0.95
Cl^-	10.00	--	--
Cr_2O_3	0.42	--	--
Cs_2O	0.26	0.04	6.5
F^-	0.24	--	--
Fe_2O_3	20.3	10.9	1.86
Li_2O	2.02	2.42	0.83
MgO	0.22	0.11	2.00
MnO_2	1.21	3.67	0.32
Na_2O	16.9	13.0	1.30
NiO	2.49	1.32	1.89
RuO_2	0.30	0.01	30.0
SiO_2	31.0	35.0	0.89
$SO_4^=$	1.9	0.003	0.630
SrO	0.04	0.02	2.0
TeO_2	0.07	0.004	17.5
TiO_2	0.07	0.03	2.33
ZnO	0.08	0.04	2.0

the feed are Ru, Te and Cs. Significant quantities of stainless steel corrosion products, including Ni and Cr, were also present as part of the plug material.

Total decontamination factors (DFs) associated with melter feed components were calculated from analytical results obtained from the condensible off-gas sampling train and the composition and weight of all process-line deposits. These results appear in Table A.3. The DFs obtained for sulfates, nitrates, and fluorides are upper limits since total analysis for these anions was not possible.

TABLE A.3. LFCM-2 Decontamination Factors

Element	Minimum	Maximum	Average DFs
Al	3750	7700	4900
B	180	530	260
Ca	540	950	740
Cd(a)	120	560	340
Cl	9	32	17
Cs	30	70	40
F(b)	--	--	>175
Fe	330	950	420
Li	690	1120	920
Mg	340	640	480
Mn	550	2400	1580
N(b)	--	--	>350
Na	290	400	340
Ni	330	520	430
Ru	1.3	27	7
S	--	--	<19
Sb(a)	310	580	480
Se	80	430	210
Si	630	1200	940
Sr	250	520	380
Te	49	80	60
Ti	280	2300	1100
Zn	290	360	350
	Total Avg. Oxide DF		564

(a) Due to limitations of analyzing equipment, the DFs reported are minimum values based on the ICP detection limit.

(b) Unknown feed composition. Value given in mg of effluent/kg of glass produced.

The classical scattering aerosol spectrometer was used to characterize the off-gas loading and size distribution of entrained particulate matter during the LFCM-2 experiment. The results obtained from this instrument during a 15-min sampling interval are illustrated in Figure A.6. Assuming particulate sphericity and an average bulk density of 4 g/cm^3, the average off-gas loading during this measurement period was 7 x 10^{-4} g/scf.

No noncondensible off-gas data was generated during the run.

LFCM-3 - NOVEMBER 1980

This 24-h melter experiment was conducted to test the LFCM operational characteristics without lid heating. Effluent sampling was limited to the use of the off-gas scrub train previously described, and to the use of gas cylinders for obtaining grab samples of noncondensible gases. The analytical results obtained from these samples are summarized in Table A.4. This table

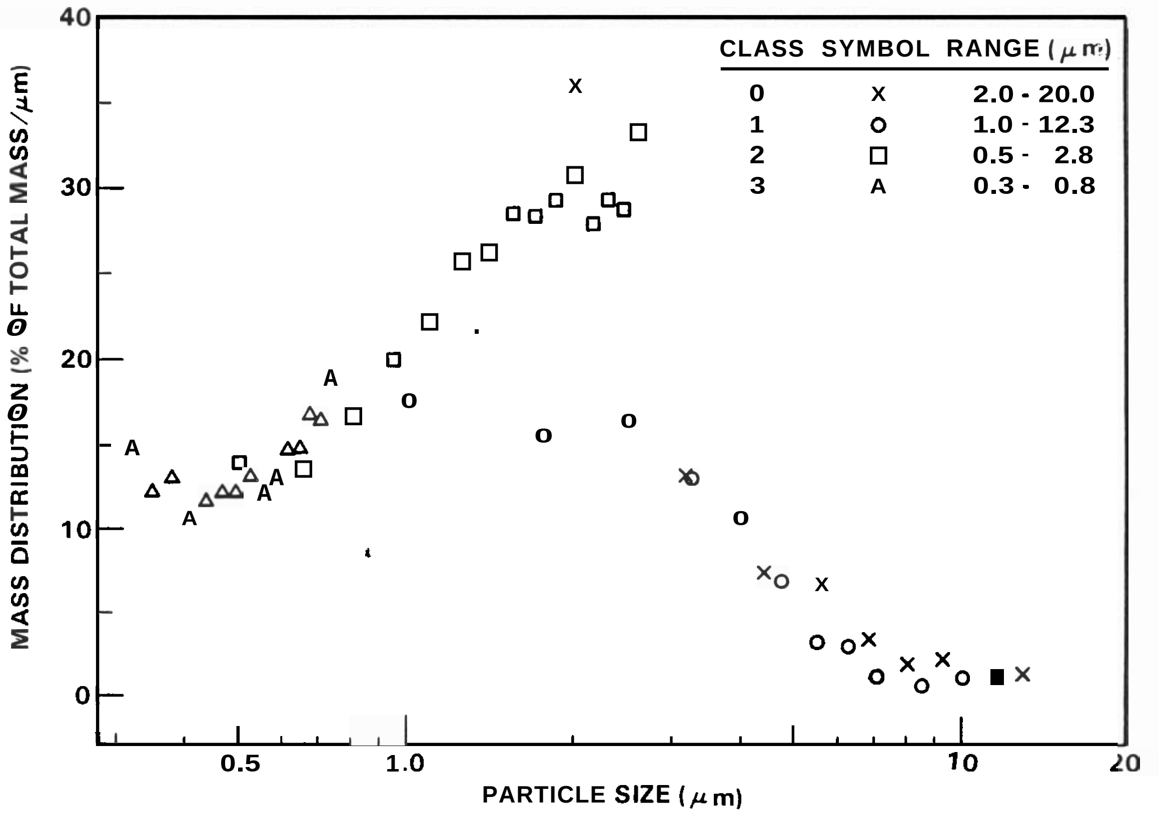

FIGURE A.6. LFCM-2 Mass-Size Particle Distribution

TABLE A.4. LFCM-3 Decontamination Factors

Element	Average DF	DF Ratio LFCM-3/LFCM-7
Al	2400	1.6
B	121	0.46
Ca	1850	2.50
Cd	84	<0.2
Cl	9	0.53
Cs	7	0.18
Fe	690	1.64
Li	660	0.72
Mg	1800	3.75
Mn	3100	1.94
Na	280	0.82
Ni	430	1.00
Ru	60	8.57
S	5	0.26
Si	2600	2.77
Sr	1500	3.95
Te	270	4.43
TOTAL OXIDE	480	0.86

presents the DFs associated with LFCM-3 feed components and compares these values to those obtained from the LFCM-2 test. DFs were higher during LFCM-3 than during LFCM-2 for most feed components, although the total oxide DFs of these two experiments are more or less comparable.

PSCM-1 - DECEMBER 1980

The 120-h PSCM-1 experiment represented the first test of the pilot-scale ceramic melter since it was converted to liquid feeding. No boosting techniques were employed during this December test. All pertinent operational parameters associated with this run are summarized in Table A.1.

In preparation for this experiment, all appropriate off-gas-line components were preweighed so that the extent of off-gas deposition within the process lines could be assessed after completion of the run. However, very little deposition was found, as is illustrated in Figures A.7 through A.21. Figure A.7 is an off-gas-line schematic identifying the off-gas components which were disassembled for inspection at the end of the PSCM-1 test. Figures A.8 through A.21 are photographs of these components. The total deposition mass which was scraped from these components amounted to 68 g. The analyses of these deposits were conducted by SRL. Table A.5 summarizes these analytical results and compares them with the previous LFCM-2 deposits whenever possible.

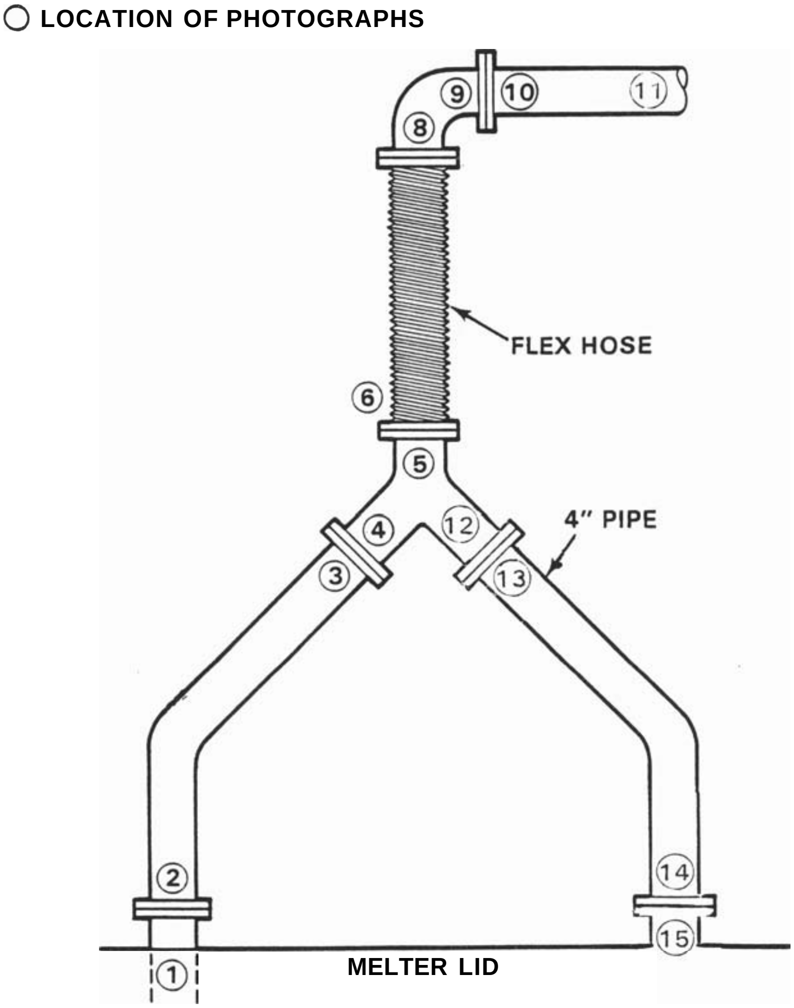

FIGURE A.7. PSCM-1 Off-Gas-Line Schematic

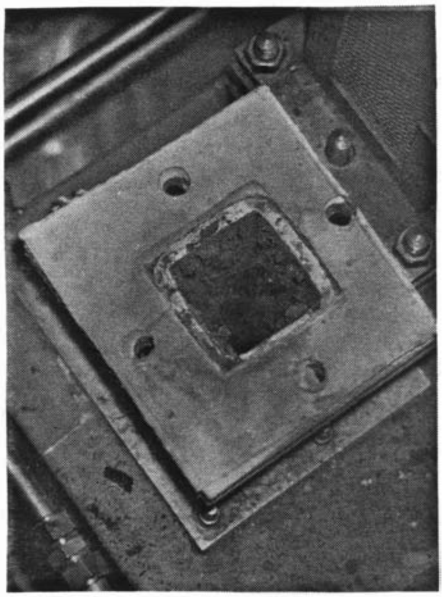

FIGURE A.8. PSCM-1 #1

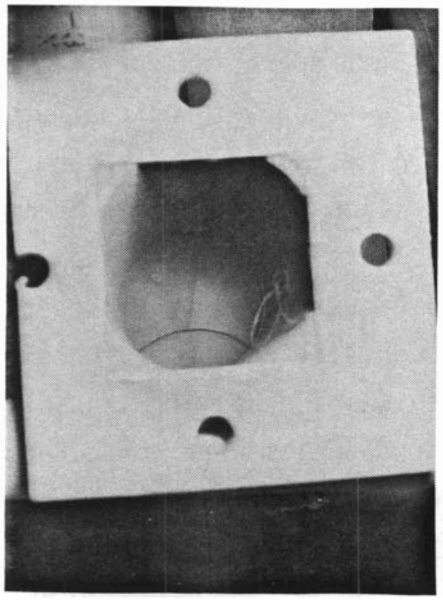

FIGURE A.9. PSCM-1 #2

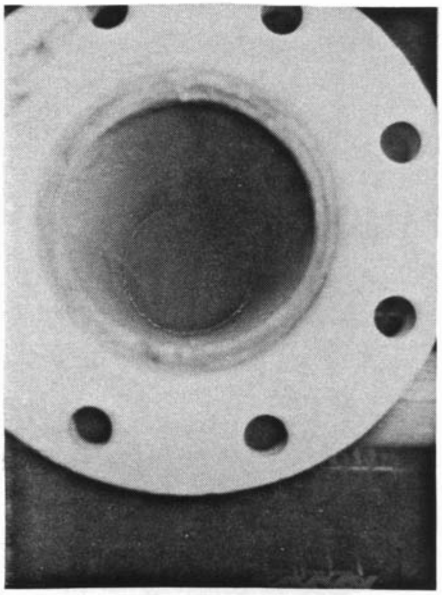

FIGURE A.10. PSCM-1 #3

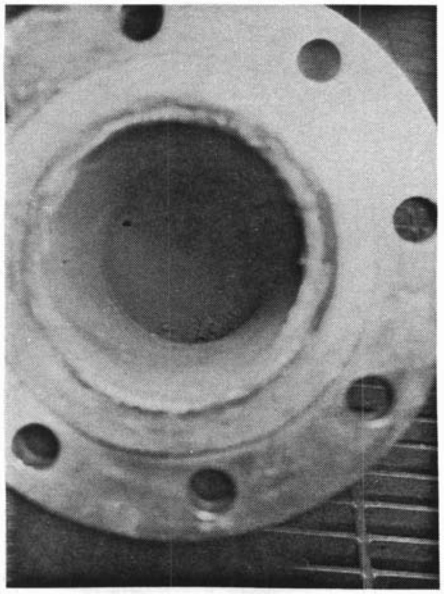

FIGURE A.11. PSCM-1 #4

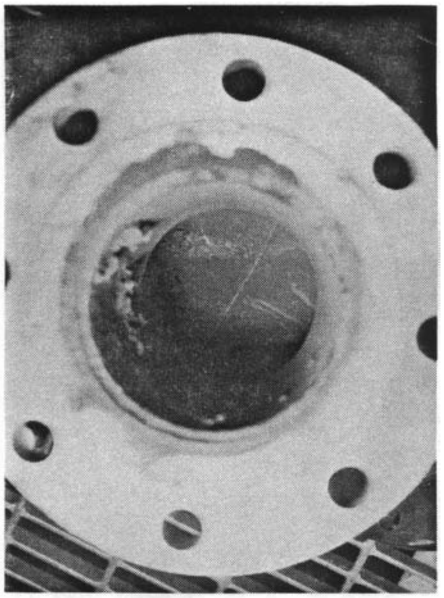

FIGURE A.12. PSCM-1 #5

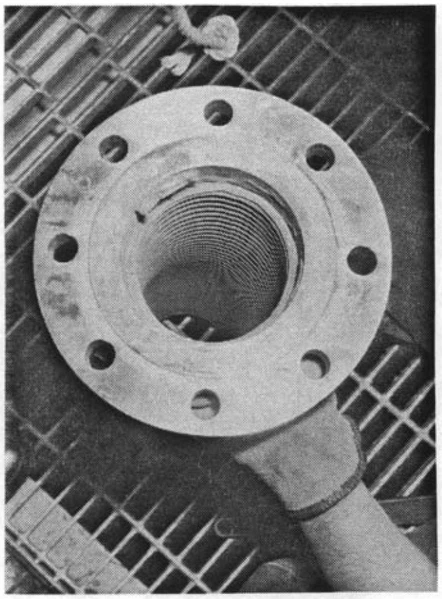

FIGURE A.13. PSCM-1 #6

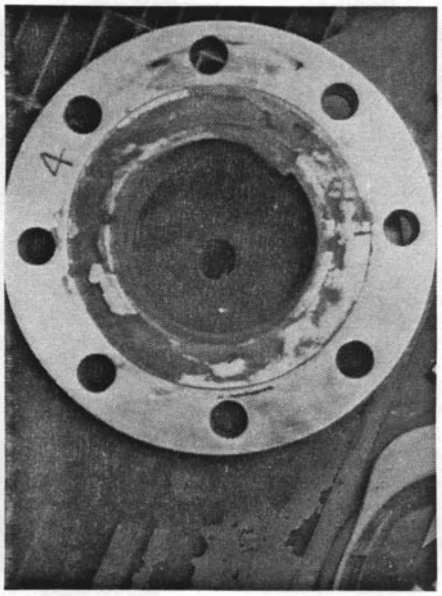

FIGURE A.14. PSCM-1 #8

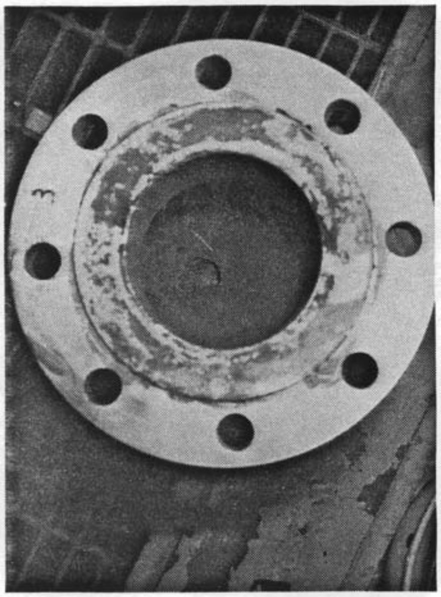

FIGURE A.15. PSCM-1 #9

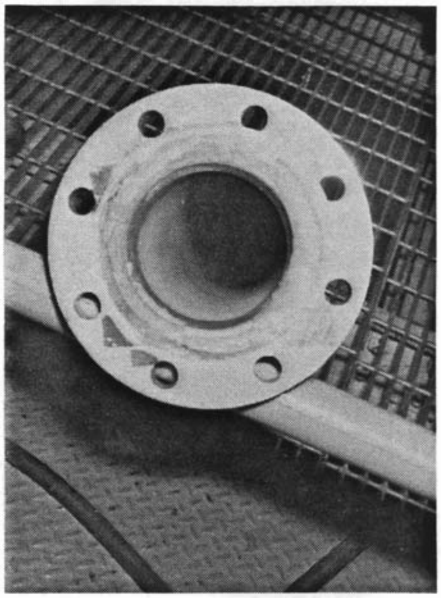

FIGURE A.16. PSCM-1 #10

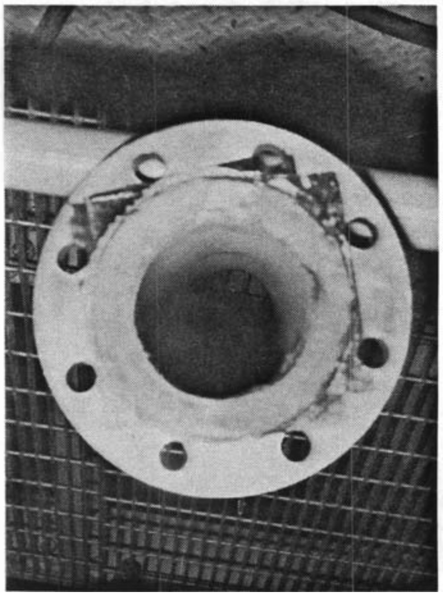

FIGURE A.17. PSCM-1 #11

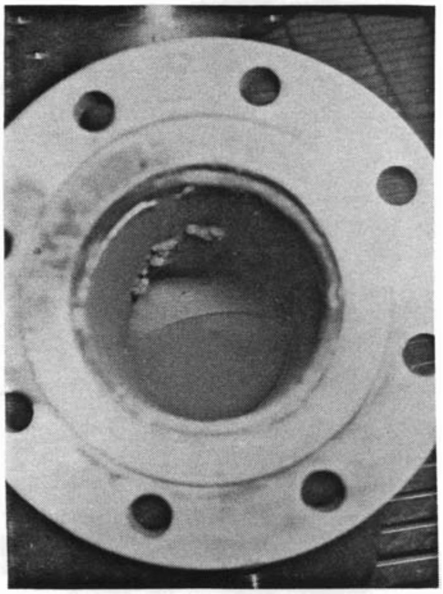

FIGURE A.18. PSCM-1 #12

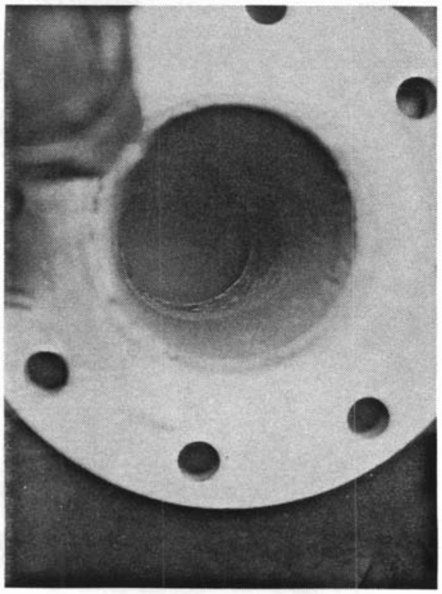

FIGURE A.19. PSCM-1 #13

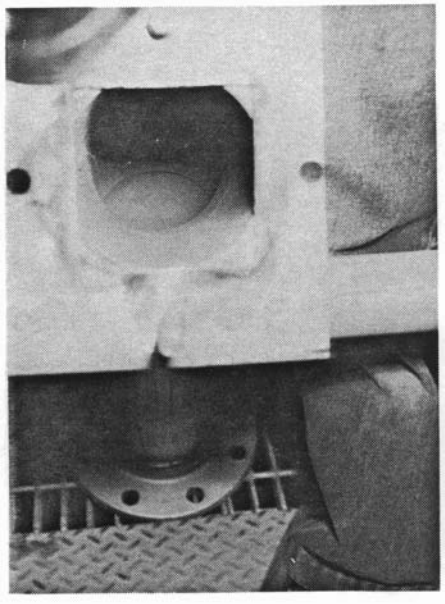

FIGURE A.20. PSCM-1 #14

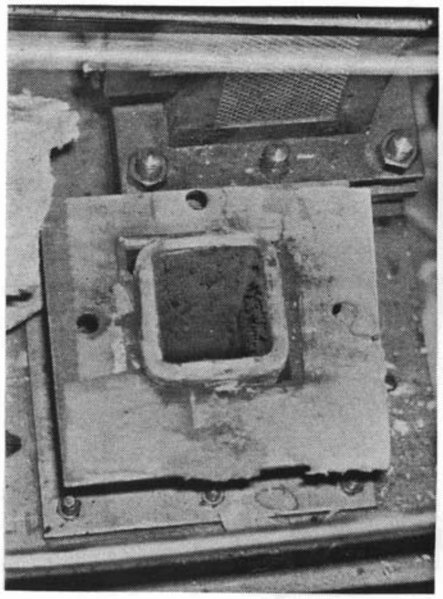

FIGURE A.21. PSCM-1 #15

Idling deposits were also collected from these same process line components two months after completion of PSCM-1. These deposits were highly enriched with the semivolatile elements Cs, Ru, and Te, and the anion $SO_4^=$. These results are included in Table A5 for comparison.

The feed component DFs achieved with PSCM-1 are summarized in Table A.6. Again, these values are compared to those obtained from the two previous melter runs LFCM-2 and LFCM-3. Clearly, much less volatilization and entrainment occurred during PSCM-1 than in the two previous experiments discussed in this report.

Grab samples taken from PSCM-1 plenum were analyzed using a gas mass spectrometer. These results are summarized in Table A.7. Aeration of the feed slurry with CO_2 and the oxidation of the coal component of the feed are responsible for the unusually high concentrations of CO_2 in the melter plenum. Oxygen, on the average, appears to be slightly depleted with regard to room air, which is consistent with moderate inleakage rates and feed component oxidation. Although Sample B appears to be enriched in oxygen (relative to nitrogen), no observable frothing or reboil occurred during that or any other sampling period.

TABLE A.5. PSCM-1 Process Line Deposits

Elemental Oxides	Weight Percent			
	PSCM-1	Idling	LFCM-2	Feed
Al_2O_3	--	1.2	1.7	3.6
B_2O_3	4.6	14.2	4.6	9.9
CaO	--	0.22	4.4	1.2
CdO	--	0.02	--	0.01
Cl^-	--	0.5	10.0	--
Cr_2O_3	--	0.57	0.42	0.02
Cs_2O	0.80	3.7	0.26	0.06
F^-	--	0.02	0.24	--
Fe_2O_3	10.0	0.10	20.0	16.0
LiO_2	--	1.92	2.0	4.1
MgO	--	<0.05	0.22	1.4
MnO_2	--	0.05	1.2	3.8
Na_2O	20.0	31.0	17.0	15.5
NiO	--	0.25	2.5	1.5
RuO_2	--	0.82	0.30	0.02
Sb_2O_3	--	<0.01	--	0.008
SiO_2	--	<0.02	31.0	44.0
$SO_4^=$	--	62.0	1.9	--
SrO	--	<0.005	0.04	0.02
TeO_2	--	0.70	0.07	0.01
TiO	--	<0.01	0.07	0.70
ZnO	--	0.02	0.08	0.008

LFCM-4 - JANUARY 1981

LFCM-4 was a 120-h experiment using lid heaters to boost feeding rates and an off-gas cooling nozzle to maintain the melter exhaust temperature at 375°C. One objective of this run was to evaluate the effect of off-gas temperature upon process-line deposition rates. The deposits that formed within the components making up the melter exhaust line are shown in Figures A.23 through A.27. The location of these components relative to the melter are identified in Figure A.22. Although the deposition rate during this run was

TABLE A.6. PSCM-1 Decontamination Factors

Element	PSCM-1 Average DF	DF Ratios PSCM-1/LFCM-2	DF Ratios PSCM-1/LFCM-3
Al	11000	7.33	4.58
B	210	0.81	1.74
Ca	1800	2.49	1.00
Cd	190	0.56	2.26
Cl	3.1	0.13	0.34
Cs	50	1.28	7.28
Fe	3800	9.05	5.51
Li	1900	2.06	2.88
Mg	9000	18.80	5.00
Mn	5700	3.56	1.84
Na	830	2.44	2.96
Ni	1500	3.49	3.49
Ru	32	4.57	0.53
S	1.0	0.05	0.20
Si	15000	15.96	5.77
Sr	7400	19.47	4.93
Te	170	2.79	0.63
TOTAL	1140	2.04	2.38

TABLE A.7. PSCM-1 Noncondensible Off-Gas Results

Sample	Molar Composition, % (dry) CO_2	Ar	O_2	N_2	CO	H_2
A	2.86	1.06	7.11	88.9	<0.01	0.08
B	6.35	0.88	19.8	73.0	<0.01	<0.01
C	1.81	0.96	17.0	80.1	<0.01	0.03
D	4.54	0.95	14.9	79.6	<0.01	<0.01
E	1.50	1.03	11.8	85.6	<0.01	<0.01

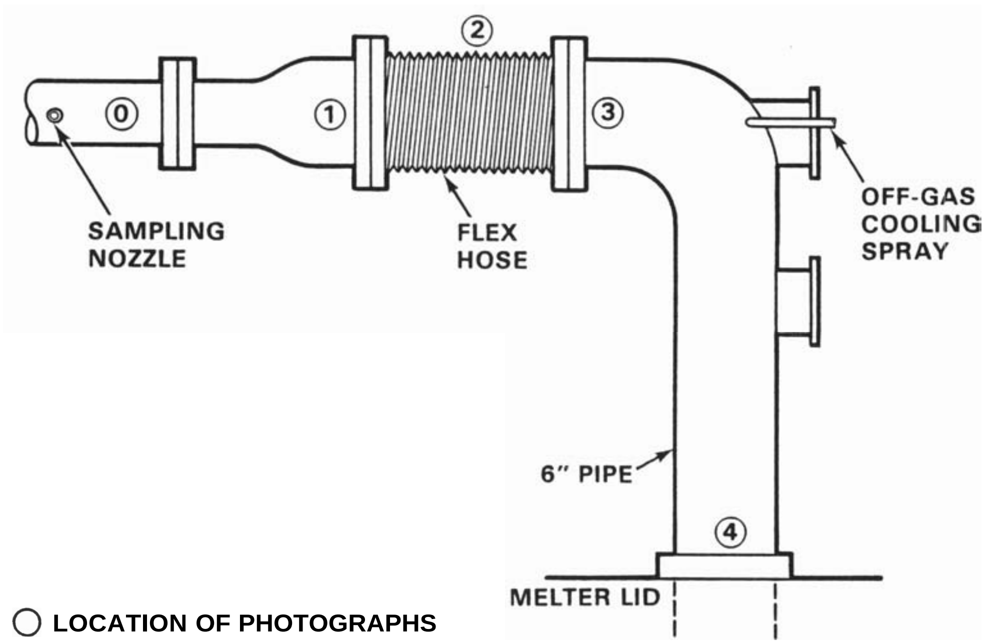

FIGURE A.22. LFCM-4 Off-Gas-Line Schematic

FIGURE A.23. LFCM-4 #4

FIGURE A.24. LFCM-4 #3

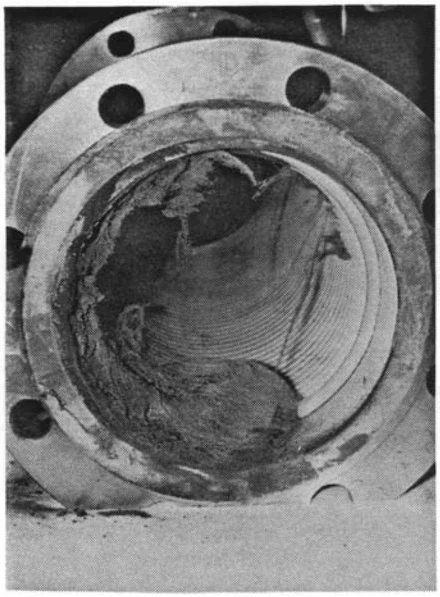

FIGURE A.25. LFCM-4 #2

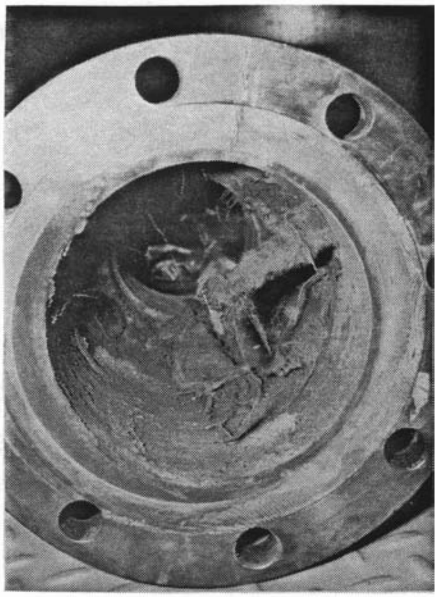

FIGURE A.26. LFCM-4 #1

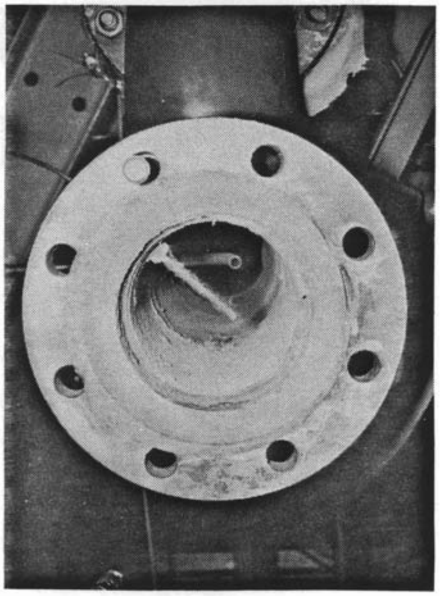

FIGURE A.27. LFCM-4 #0

greater than in the previous PSCM-2 experiment, the total quantity of material deposited was only 560 g (–1 lb), which is a vast improvement over the 5.9-kg (13-lb) deposit formed during LFCM-2. The composition of the material collected from these pipe components is summarized in Table A.8, and is compared with previously obtained process-line deposition data. It is clear from this table that all melter-generated pipe deposits investigated to date possess comparable compositions.

Total feed component DFs obtained for the LFCM-4 test are summarized in Table A.9. These values are also compared with DF results obtained from all previous experiments described in this report. Although overall volatilization

TABLE A.8. LFCM-4 Pipe Deposition Composition

Elemental Oxides	Weight Percent			
	LFCM-4	PSCM-1	LFCM-2	Feed
Al_2O_3	2.0	--	1.7	3.5
B_2O_3	5.6	4.6	4.6	9.9
CaO	6.5	--	4.4	1.2
CdO	0.08	--	--	0.01
Cr_2O_3	0.31	--	--	0.02
Cs_2O	0.31	0.80	0.26	0.06
Fe_2O_3	14.0	10.0	20.0	16.0
LiO	3.4	--	2.0	4.1
MgO	2.5	--	0.22	1.4
MnO_2	3.4	--	1.2	3.8
Na_2O	15.0	20.0	17.0	16.0
NiO	--	--	2.5	1.5
RuO_2	0.16	--	0.3	0.02
Sb_2O_3	--	--	--	0.003
SiO	31.0	--	31.0	44.0
SrO	0.05	--	0.04	0.02
TeO_2	0.11	--	0.07	0.01
TiO	0.11	--	0.07	0.70
ZrO_2	0.29			--

TABLE A.9. LFCM-4 Decontamination Factors

Element	LFCM-4 Average DF	DF Ratio LFCM-4/LFCM-2		
		LFCM-4/LFCM-2	LFCM-4/LFCM-3	LFCM-4/PSCM-1
Al	530	0.35	0.22	0.05
B	130	0.5	1.07	0.62
Ca	260	0.35	0.14	0.14
Cd	70	<0.20	0.83	0.37
Cl	2.2	0.13	0.24	0.71
Cs	60	1.42	8.14	1.12
Fe	260	0.62	0.38	0.07
Li	310	0.34	0.47	0.16
Mg	350	0.73	0.19	0.04
Mn	420	0.26	0.14	0.07
Na	340	1.00	1.21	0.41
Ni	260	0.60	0.60	0.17
Ru	26	3.7	0.43	0.81
S	1.0	0.05	0.20	1.0
Sb	1800	<3.8	--	--
Si	420	0.45	0.16	0.03
Sr	200	0.54	0.14	0.03
Te	62	1.01	0.23	0.36
TOTAL	290	0.52	0.60	0.25

and entrainment is higher for LFCM-4 than for all the previous runs, the emissions of several semivolatiles are lower in LFCM-4 than they were in the two previous LFCM tests.

Particulate entrainment occurring during LFCM-4 was characterized by HEPA filtration. The particulate DFs listed in Table A.10 were calculated using both HEPA and off-gas-line deposition data. The elemental (oxide) composition of HEPA-trapped particulates is also listed in this table along with the feed makeup composition. Clearly, the composition of the HEPA-trapped material cannot be explained by a simple feed entrainment model.

TABLE A.10. LFCM-4 Particulate Data

Elemental Oxides	DF	Weight Percent HEPA	Weight Percent Feed
Al_2O_3	1580	1.44	3.5
B_2O_3	1250	5.32	10.0
CaO	620	1.34	1.2
CdO	220	0.04	0.01
Cr_2O_3	--	0.23	0.02
Cs_2O	100	0.70	0.06
Fe_2O_3	660	15.1	16.0
LiO	840	3.21	4.1
MgO	900	0.87	1.4
MnO_2	1100	2.64	3.8
Na_2O	600	19.0	15.5
NiO	--	--	1.5
Ru_2O_3	25	0.64	0.02
Sb_2O_3	--	--	0.008
SeO_2	--	--	0.008
SiO_2	1100	26.4	44.0
SrO	595	0.20	0.02
TeO_2	130	0.18	0.01
TiO_2	--	0.49	0.70
ZnO	--	0.06	0.008
ZrO_2	--	0.22	--
TOTAL	600		

A summary of the gas chromatographic analysis of the LFCM-4 plenum gas composition appears in Table A.11. Due to the high melter inleakage rates, the oxygen-nitroyen ratios of the plenum gas samples were indistinguishable from room air during the melter run. As in PSCM-1, aeration of the feed slurry with CO_2, and the oxidation of coal present in the feed, are responsible for the high concentrations of CO_2 in the melter plenum.

Gas-scrubbing techniques were utilized for investigating the nature of idling emissions associated with LFCM-4. Sampling was begun 7 days after the

TABLE A.11. LFCM-4 Noncondensible Off-Gas Composition

	Percent			
Date	CO_2	O_2 (a)	N_2	CO, ppm
01/20/81	1.1	21.0	78.0	<10
01/20/81	0.3	21.3	77.5	<10
01/21/81	0.5	21.6	77.0	<10
01/22/81	0.9	21.0	77.2	<10
01/22/81	0.7	21.4	77.0	320
01/22/81	0.3	21.4	78.3	250
01/23/81	0.4	21.4	77.3	>100
01/23/81	0.6	20.8	77.7	570
01/23/81	0.4	21.5	77.2	310

(a) Includes ~1% Ar.

completion of LFCM-4, and again after 14 days. These data appear in Table A.12 along with the final composition of the LFCM-4 glass. The data in this table indicate that the semivolatile elements and compounds present in the molten glass matrix are escaping at rates which are proportional to their concentrations and volatilities.

PSCM-2 - MARCH 1981

One of the main objectives of PSCM-2 was to investigate the effect of combustion (propane) boosting upon melter feeding rates. The effect of using an off-gas cooling-spray nozzle upon melter emissions was also assessed. Further details concerning PSCM-2 operational parameters and constraints are summarized in Table A.1.

The nature of the off-gas-line deposits which were assessed after the run are summarized in Figures A.28 through A.42. Figure A.28 identifies the components of the process exhaust line where material deposits occurred. Figures A.29 through A.42 are photographs of these off-gas-line components. The largest deposition formed in the throat of the melter lid exhaust port. This deposit is thought to have resulted from the operation and positioning of the

TABLE A.12. LFCM-4 Idling Emissions

Element	Weight Percent 1 Week	 2 Weeks	 Glass
Al	0.06	--	3.2
B	10.2	2.2	5.6
Ca	0.33	0.01	1.5
Cd	0.17	--	0.036
Cl	1.07	71.0	0.19
Cr	1.7	0.23	--
Cs	6.7	1.6	0.06
Fe	8.3	0.20	20.0
K	1.5	--	--
Li	2.8	0.78	3.2
Mg	--	--	1.5
Mn	0.12	0.002	5.2
Na	61.7	18.7	20.0
Ni	0.82	0.04	2.2
Ru	0.11	0.02	0.006
S	0.21	1.4	--
Sb	--	--	0.03
Si	2.9	1.0	37.0
Sr	--	--	0.04
Te	1.0	0.13	0.07
Ti	0.03	--	--
Zr	0.02	--	--

---

* Calculated from all detectable elements.

off-gas cooling nozzle just downstream from the plug formation site. Total depositions in the off-gas-line, including as much of the lid plug as could be collected, amounted to –2 kg, which represents 0.1% of the total oxides fed to the melter during this experiment.

The composition of the deposits collected from PSCM-2 off-gas-line components is summarized in Table A.13. Table A.14 compares the weighted, average

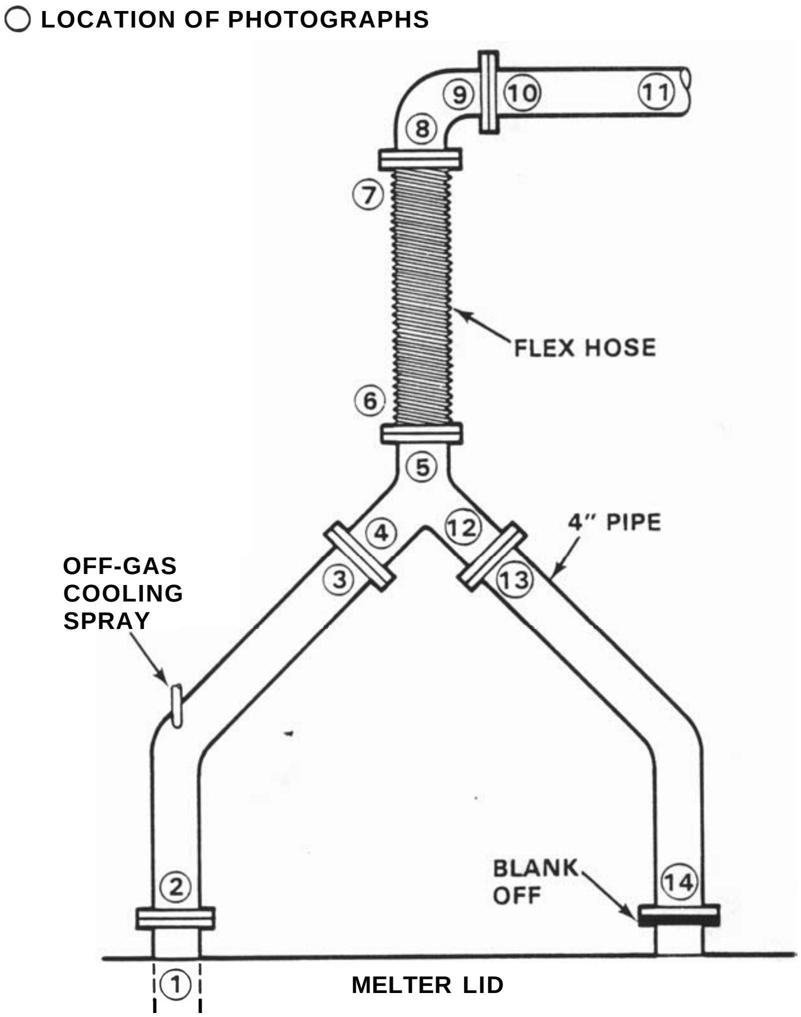

FIGURE A.28. PSCM-2 Off-Gas-Line Schematic

composition of these PSCM-2 deposits with the off-gas-line deposits formed in previous melter experiments. Composition of all off-gas-line deposits are similar, but not strictly representative of the feed.

Experimental feed component DFs determined during PSCM-2 are listed in Table A.15, where they are compared to all previous melter runs discussed in this report. It is clear from this table that combustion boosting, in conjunction with increased feeding rates, has dramatically increased effluent

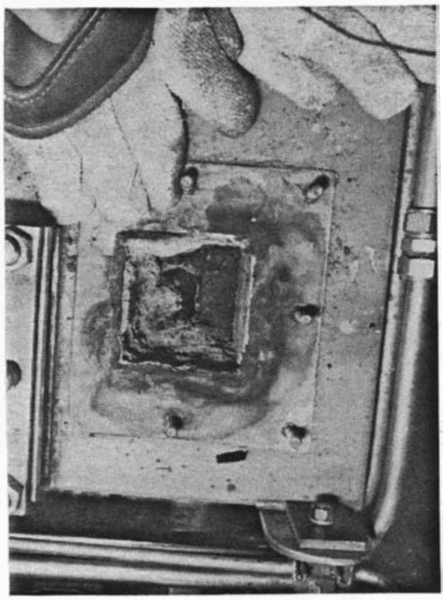

FIGURE A.29. PSCM-2 #1

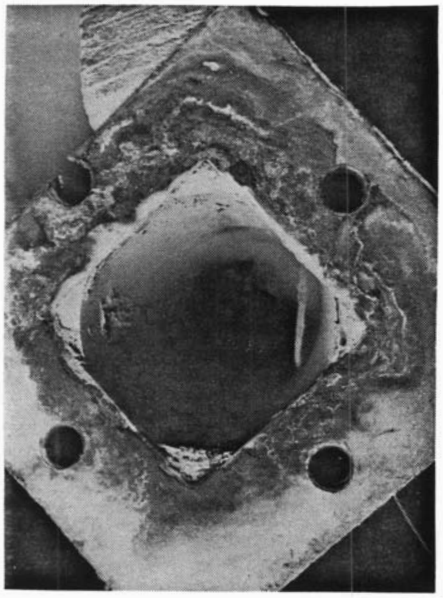

FIGURE A.30. PSCM-2 #2

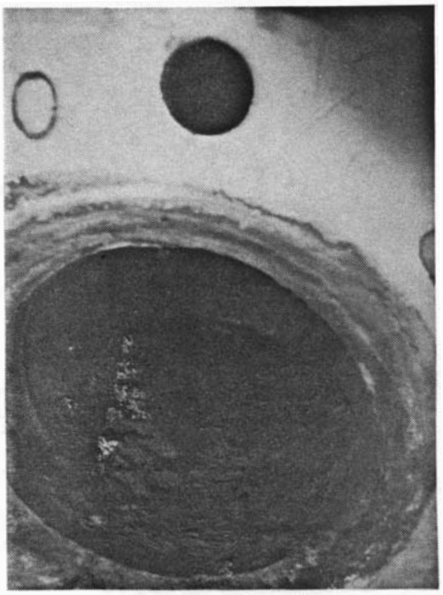

FIGURE A.31. PSCM-2 #3

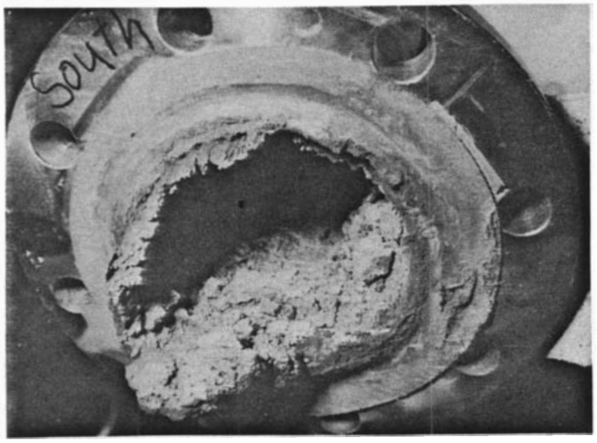

FIGURE A.32. PSCM-2 #4

FIGURE A.33. PSCM-2 #5

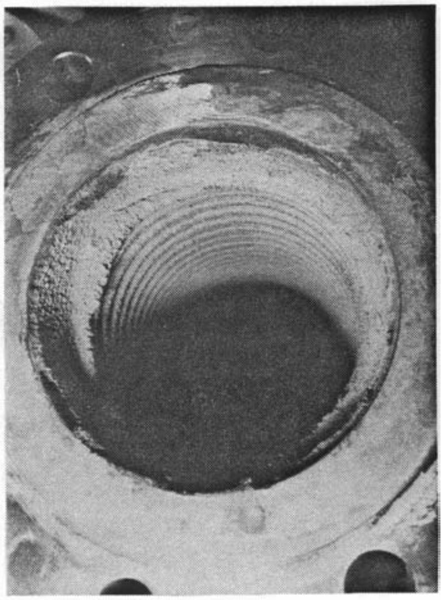

FIGURE A.34. PSCM-2 #6

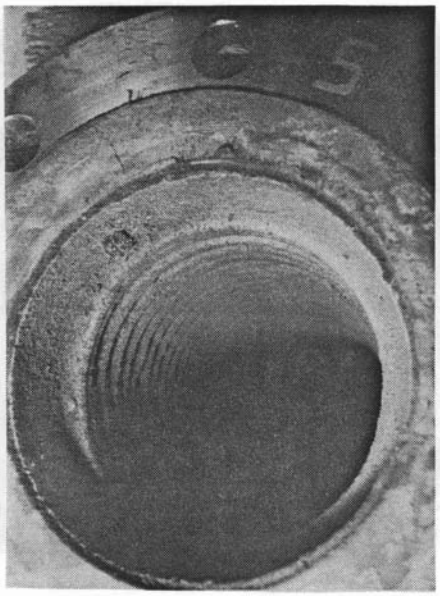

FIGURE A.35. PSCM-2 #7

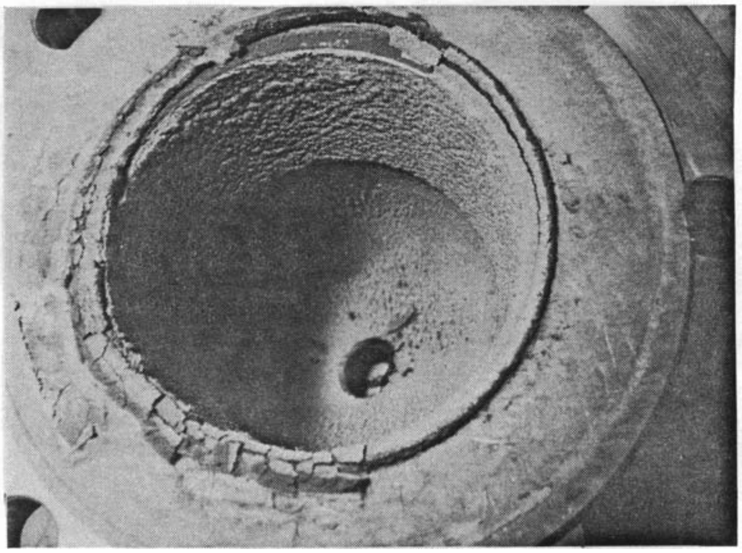

FIGURE A.36. PSCM-2 #8

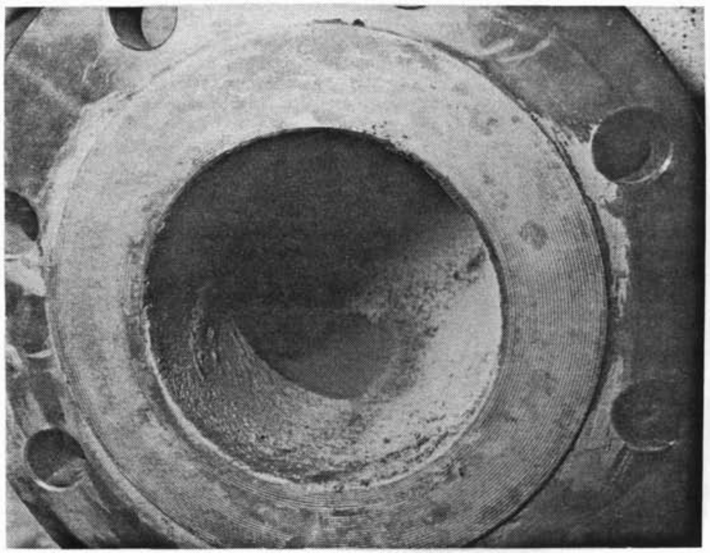

FIGURE A.37. PSCM-2 #9

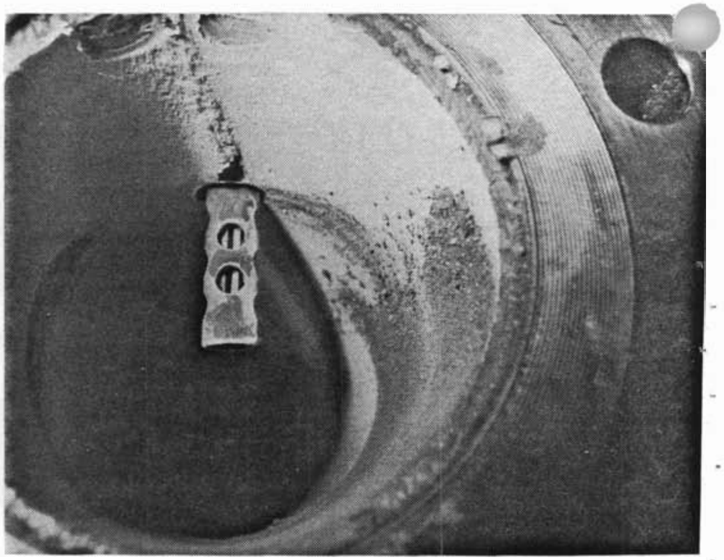

FIGURE A.38. PSCM-2 #10

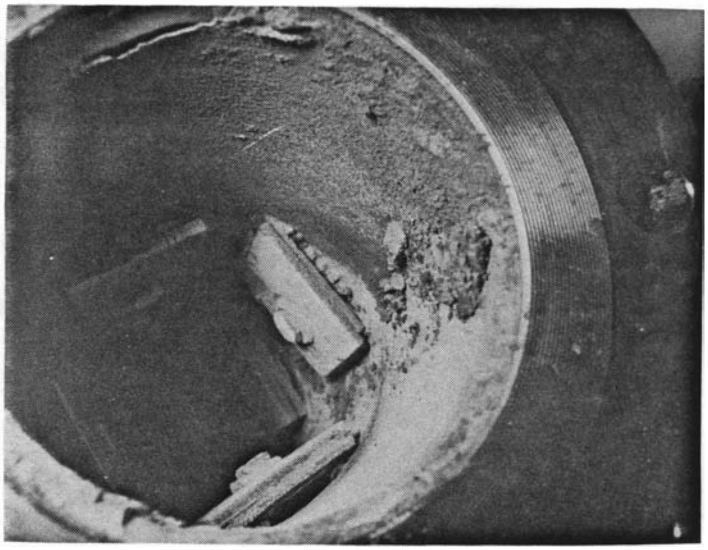

FIGURE A.39. **PSCM-2** #11

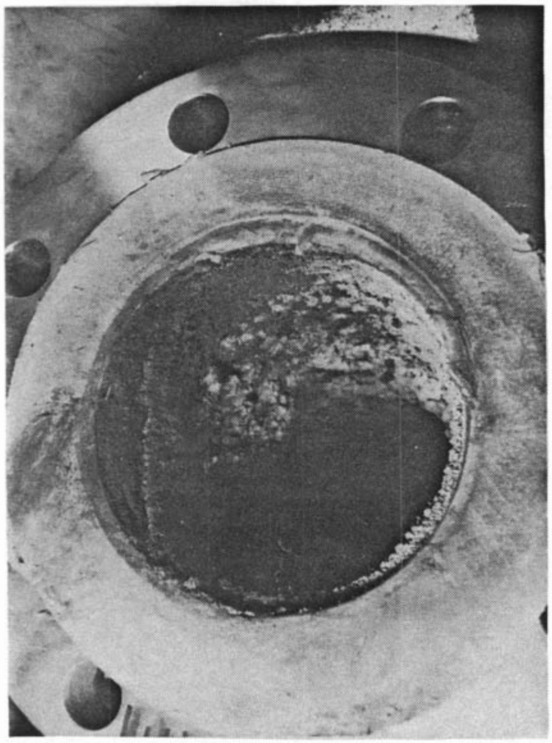

FIGURE A.40. PSCM-2 #12

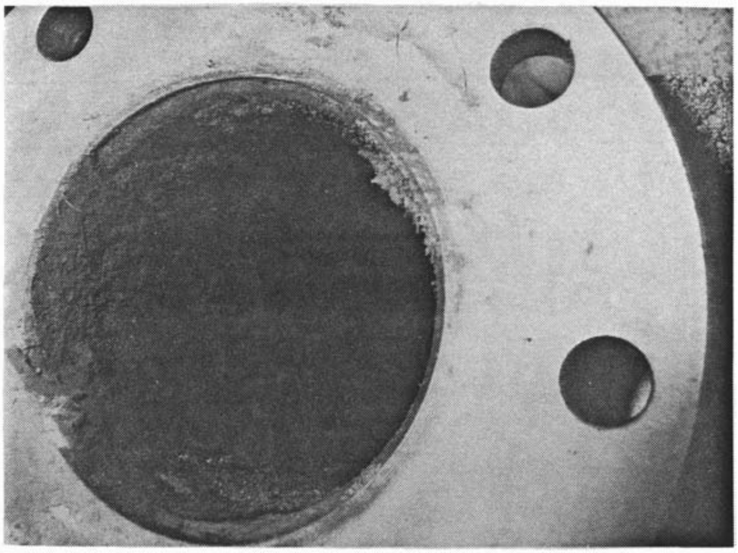

FIGURE A.41. PSCM-2 #13

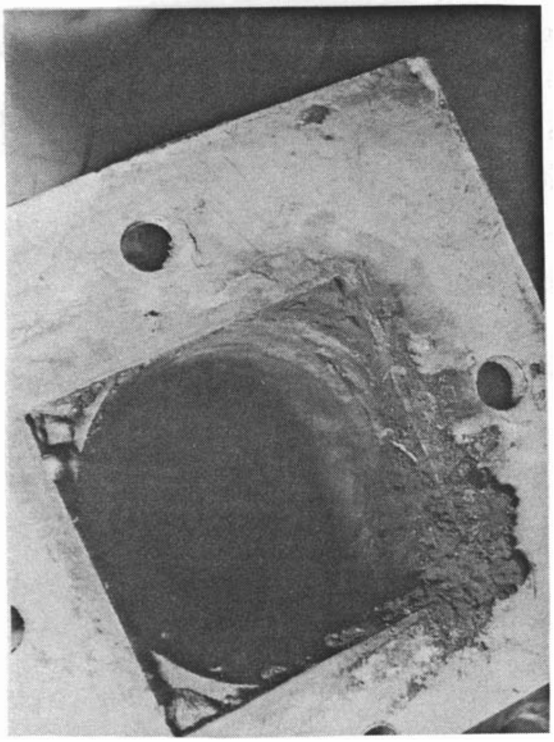

FIGURE A.42. PSCM-2 #14

TABLE A.13. PSCM-2 Pipe Deposits

Elemental Oxides	Weight Percent "Y"	Flex Hose	Inside Lid	Corrosion Test	90° Elbow
Al_{23}	1.8	1.5	1.5	1.6	1.2
B_2O_3	4.0	3.7	1.6	5.0	3.1
CaO	4.8	3.6	3.5	3.7	3.6
CdO	0.04	0.10	0.02	0.08	0.10
Cl^-	6.63	10.7	19.8	9.56	22.9
Cs_2O	0.35	1.34	0.44	1.0	1.22
Cr_2O_3	0.98	0.90	0.36	0.50	0.91
F^-	0.096	0.05	0.13	0.097	0.15
Fe_2O_3	16.0	15.0	10.5	13.0	14.0
LiO	3.0	2.6	2.8	3.0	2.6
MgO	1.1	0.70	0.85	0.80	0.66
MnO_2	3.9	3.4	3.3	3.6	4.2
Na_2O	13.0	16.6	23.0	17.0	21.0
NiO	2.5	2.4	1.8	1.9	2.6
RuO_2	0.10	0.35	0.11	0.22	0.26
Sb_2O_3	<0.04	--	<0.04	--	--
Se	0.097	0.11	0.006	0.13	0.28
SiO_2	25.0	21.0	21.0	27.0	13.0
$SO_4^=$	3.03	9.45	6.02	3.89	5.79
SrO	0.038	0.03	0.03	0.03	0.03
TeO_2	0.06	0.10	0.07	0.08	0.08
TiO_2	0.46	0.38	0.38	0.50	0.25
ZnO	0.025	0.025	0.02	0.02	0.05
ZrO_2	0.23	0.16	0.20	0.22	0.13

TABLE A.14. Compositional Comparison of Off-Gas-Line Deposits

Elemental Oxides	Weight Percent			
	PSCM-2	LFCM-4	PSCM-1	LFCM-2
Al_2O_3	1.6	2.0	--	1.7
B_2O_3	3.4	5.6	4.6	4.6
CaO	4.1	6.5	--	4.4
CdO	0.05	0.08	--	--
Cr_2O_3	0.78	0.31	--	--
Cs_2O	0.11	0.31	0.80	0.26
Fe_2O_3	14.2	14.0	10.0	20.0
LiO	2.9	3.4	--	2.0
MgO	0.92	2.5	--	0.22
MnO_2	3.6	3.4	--	1.2
Na_2O	16.8	15.0	20.0	17.0
NiO	2.3	--	--	2.5
RuO_2	0.17	0.16	--	0.3
Sb_2O_3	<0.04	--	--	--
SiO	22.7	31.0	--	31.0
SrO	0.03	0.05	--	0.04
TeO_2	0.07	0.11	--	0.07
TiO	0.42	0.11	--	0.07
ZrO_2	0.20	0.29	--	--

emission rates. Of the previous melter runs, only LFCM-4, which itself utilized electric lid boosting to maximize feeding rates, exhibited a lower overall DF.

Since one of the primary objectives of the PSCM-2 test was to investigate the effects of propane combustion boosting upon melter feeding rates, the gas composition of the melter plenum was of particular engineering interest. Gas chromatographic analysis of the plenum gases was conducted throughout the PSCM-2 experiment. The results of these analyses are illustrated in Fiyure A.43. The relationship between the concentrations of N_2, O_2, and CO_2 are consistent with the stoichiometry of total combustion of C_3H_8. That is, the

TABLE A.15. PSCM-2 Decontamination Factors

Element	PSCM-2 Average DF	DF Ratio			
		PSCM-2/LFCM-2	PSCM-2/LFCM-3	PSCM-2/PSCM-1	PSCM-2/LFCM-4
Al	990	0.20	0.41	0.090	1.9
B	160	0.62	1.30	0.76	1.2
Ca	610	0.82	0.33	0.33	2.3
Cd	47	0.14	0.56	0.25	0.67
Cl	3	0.17	0.33	0.96	1.4
Cs	3	0.075	0.43	0.059	0.053
Fe	680	1.60	0.99	0.18	2.6
Li	340	0.37	0.52	0.18	1.1
Mg	930	1.90	0.52	0.10	2.6
Mn	630	0.40	0.20	0.11	1.5
Na	130	0.39	0.46	0.16	0.38
Ru	48	6.90	0.80	1.5	1.8
S	19	>1.0	3.8	19.0	19.0
Sb	100	0.21	--	--	0.056
Si	1600	1.70	0.61	0.11	3.8
Sr	640	1.70	0.43	0.086	3.1
Te	58	0.95	0.21	0.34	0.93
Ti	1400	1.27	--	--	--
TOTAL	430	0.76	0.89	0.38	1.5

relative change in the percent composition of O_2, CO_2, and N_2, as a function of oxidation rate, will vary as -1:2/3:1/3, respectively, if complete combustion is assumed.

LFCM-6 - JUNE 1981

LFCM-6 was a 120-h experiment designed to characterize maximum feeding rates achievable utilizing both electric lid heaters and plasma torch boosting techniques. To minimize off-gas line deposition, a spray nozzle was used to introduce mechanically atomized water countercurrent to the exhaust flow at the

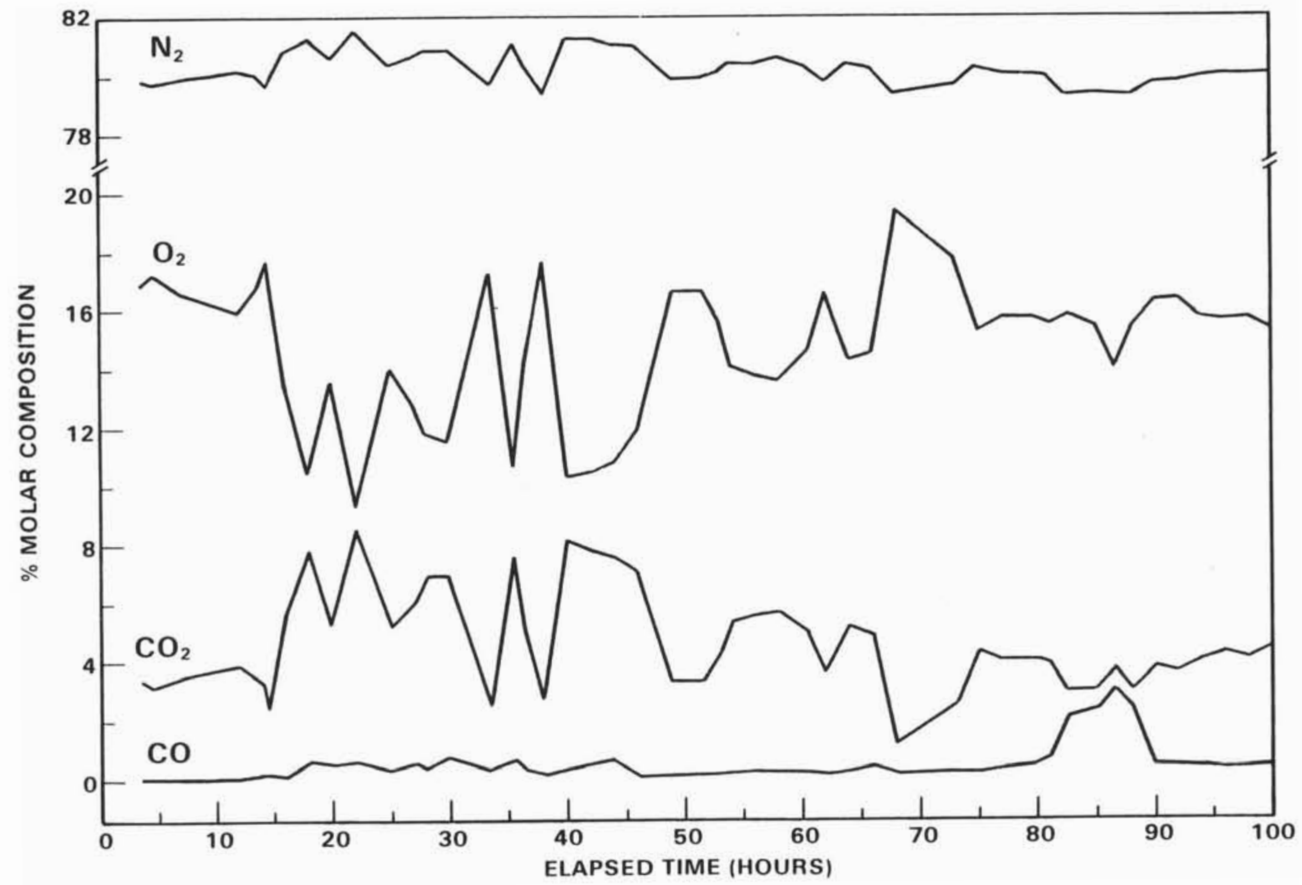

FIGURE A.43. PSCM-2 Plenum Off-Gas Composition entrance of the melter off-gas exhaust line. The locations of the off-gas line components are illustrated in Figure A.44. The deposits that did form in the melter off-gas line components are illustrated in Figures A.45 through A.50. It should be noted that the close-coupled vertical components had been cleaned 24 h prior to the end of the run in order to evaluate frit blasting as an off-gas cleaning technique. Nevertheless, the deposits that were removed by this technique were light and hairlike. The compositions of the deposits that formed in the various off-gas line components detailed in Figure A.44 are listed in Table A.16. A comparison of the weighted average composition of LFCM-6 line deposits with off-gas line deposits formed in previous melter experiments is detailed in Table A.17. Again, the similarities of these deposits are more striking than their minor differences. The semivolatiles Cs, Ru, Sb and Te, which are minor feed components but major radiological hazards, are enriched in these deposits.

Total feed component DFs for the LFCM-6 test are summarized in Table A.18. Efforts to establish a greater trace element homogeneity in the

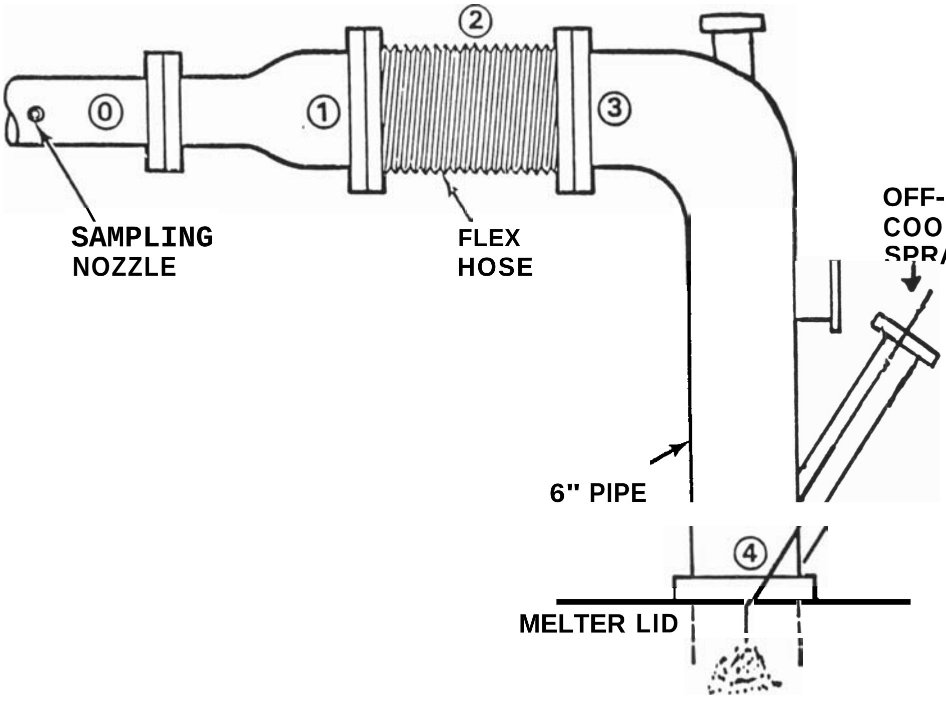

FIGURE A.44. LFCM-6 Off-Gas Line Configuration

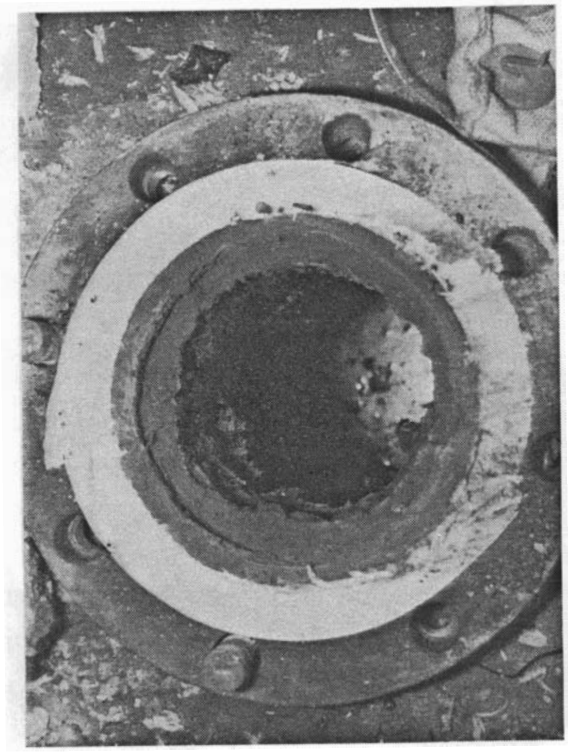

FIGURE A.45. LFCM-6 Melter Lid

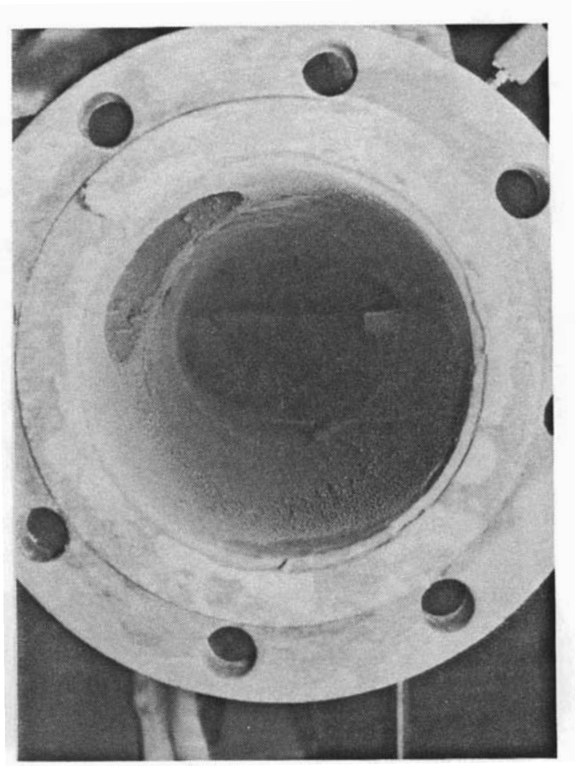

FIGURE A.46. LFCM-6 #4

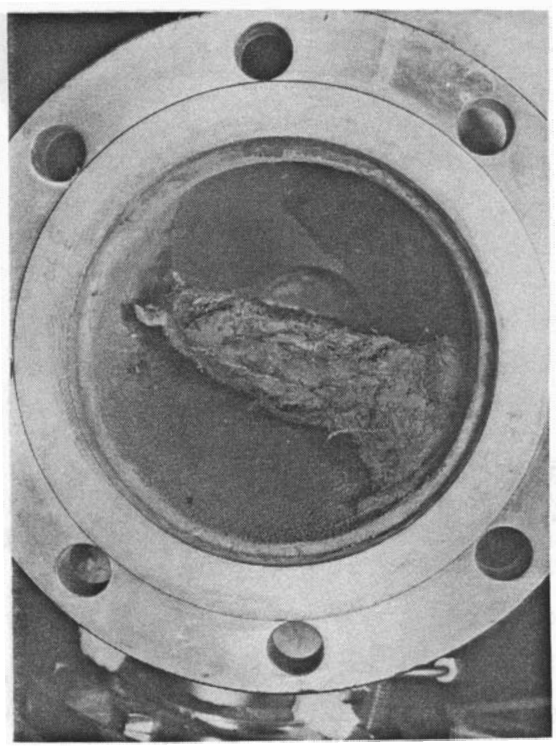

FIGURE A.47. LFCM-6 #3

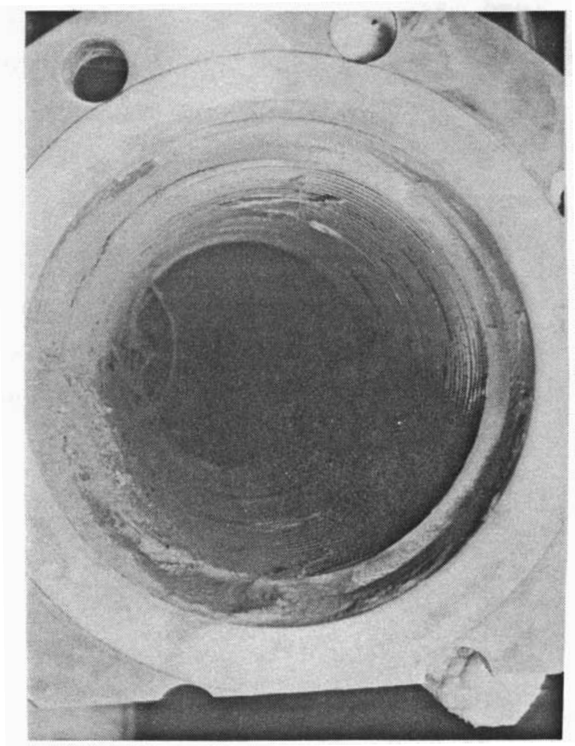

FIGURE A.48. LFCM-6 #2

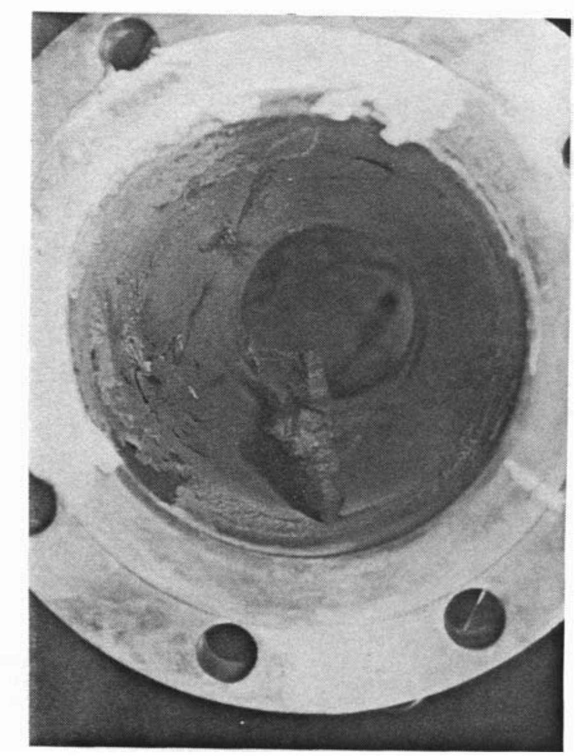

FIGURE A.49. LFCM-6 #1

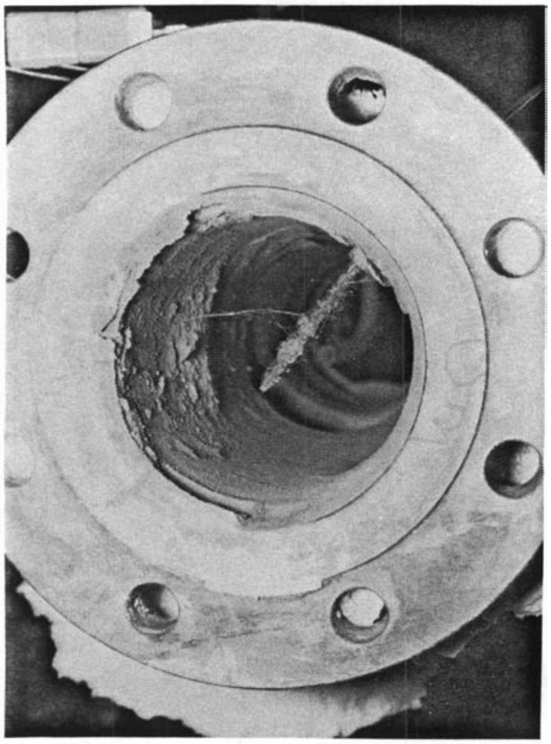

FIGURE A.50. LFCM-6 #0

feed makeup tanks appear to have produced much more consistent results between sampling runs than have been achieved in previous experiments. Also presented in this table is the total particulate DF as determined by absolute HEPA filtration. The agreement between these two sets of independent data is quite satisfying. Table A.19 compares the average LFCM-6 feed component DFs with those obtained from previous melter runs. Clearly, the LFCM-6 test exhibited the highest effective effluent emission rates of all liquid-fed melter runs conducted to date. Erratic, non-steady-state running conditions associated with this test are, no doubt, responsible for this result.

The use of plasma torches within an operating melter presents a potentially explosive hazard due to hydrogen generation resulting from plasma-initiated decomposition of H_2O. Tests of the plasma torches before LFCM-6 using building steam revealed that significant quantities of hydrogen (-4.5% dry basis) could be generated by this torch when low inleakage rates existed. Consequently, monitoring the noncondensible composition of the melter exhaust was of particular interest during this experiment. The results of these

TABLE A.16. LFCM-6 Off-Gas-Line Deposits

Elemental Oxides	Weight Percent					
	Sample Number					
	#1	#2	#3	#4	Average	Feed
Al_2O_3	1.6	1.9	1.8	2.1	1.9	3.5
B_2O_3	7.0	8.0	7.1	6.8	7.2	9.9
CaO	0.73	0.91	0.83	0.73	0.80	1.2
CdO	0.23	0.23	0.21	0.21	0.22	0.01
Cr_2O_3	0.16	0.13	0.08	0.09	0.10	0.02
Cs_2O	0.21	0.16	0.20	0.20	0.19	0.06
Fe_2O_3	13.7	12.3	12.0	11.0	12.0	16.0
La_2O_3	0.20	0.23	0.22	0.22	0.22	--
LiO	3.0	3.2	3.0	3.2	3.1	4.1
MgO	0.81	0.95	0.93	0.93	0.90	1.4
MnO_2	1.6	2.4	2.4	2.4	2.2	3.8
Na_2O	15.0	13.0	13.0	13.0	13.0	15.5
NiO	--	--	--	--	--	1.5
RuO_2	0.49	0.36	0.57	0.44	0.47	0.02
Sb_2O_3	--	0.03	0.03	0.04	0.03	0.008
SiO_2	30.0	34.0	32.0	32.0	32.0	44.0
SrO	0.02	0.03	0.02	0.02	0.02	0.02
TeO_2	0.06	0.05	0.05	0.06	0.06	0.01
TiO	0.78	0.88	0.62	0.61	0.72	0.70
ZrO_2	0.22	0.29	0.29	0.28	0.27	--

analyses are presented in Table A.20. Because of the large melter inleakage rates, hydrogen was not detectable (H_2 <0.1%) during the LFCM-6 test. Indeed, the inleakayes were high enough that the plasma torch support gas (Ar) had only a minimal effect upon the noncondensible off-gas composition. Argon and oxygen concentrations are combined in this table since they are not resolvable under the running conditions of the GC used in these analyses.

TABLE A.17. Melter Pipe Deposition Composition

Elemental Oxides	Weight Percent LFCM-6	PSCM-2	LFCM-4	PSCM-1	LFCM-2
Al_2O_3	1.9	1.6	2.0	--	1.7
B_2O_3	7.2	3.4	5.6	4.6	4.6
CaO	0.80	4.1	6.5	--	4.4
CdO	0.22	0.05	0.08	--	--
Cs_2O	0.19	0.11	0.31	0.80	0.26
Cr_2O_3	0.10	0.78	0.31	--	--
Fe_2O_3	12.0	14.2	14.0	10.0	20.0
LiO	3.1	2.9	3.4	--	2.0
MgO	0.90	0.92	2.5	--	0.22
MnO_2	2.2	3.6	3.4	--	1.2
Na_2O	13.0	16.8	15.0	20.0	17.0
NiO	--	2.3	--	--	2.5
RuO_2	0.47	0.17	0.16	--	0.3
Sb_2O_3	0.03	<0.04	--	--	--
SiO	32.0	22.7	31.0	--	31.0
SrO	0.02	0.03	0.05	--	0.04
TeO_2	0.06	0.07	0.11	--	0.07
TiO	0.72	0.42	0.11	--	0.07
ZrO_2	0.27	0.20	0.29	--	--

PSCM-3 - JULY 1981

The PSCM-3 experiment was the first large-scale test of a liquid-fed ceramic melter with a formate-based feed composition. Since the primary objective of this experiment was to assess the response of liquid-fed melters and supporting equipment with this new feed formulation, no feed-boosting techniques were employed during this test. Consequently, this experiment was very much like that of the PSCM-1 test, except for the feed composition. A comparison of all pertinent operating parameters associated with these PSCM experiments appears in Table 1. The location of the PSCM-3 off-gas exhaust line components are detailed in Figure A.51.

TABLE A.18. LFCM-6 Decontamination Factors

Elemental Oxides	Experimental DFs Sample Number #1	 #2	 #3	Average DF
Al	272	342	390	330
B	89	95	90	90
Ca	230	180	140	180
Cd	85	84	82	80
Cl	3	2	2	2
Cs	4	11	13	10
Fe	210	230	230	230
La	250	280	300	280
Li	150	160	170	160
Mg	237	273	276	260
Mn	210	330	400	330
Na	89	83	95	90
Ni	710	990	1100	930
Ru	10	22	9	13
S	10	8	16	11
Sb	>60	>100	>70	--
Si	284	260	290	280
Sr	290	300	270	290
Te	190	230	214	210
Ti	96	120	300	170
Zr	260	245	270	260
TOTAL	160	170	180	170
TOTAL PARTICULATE DF DETERMINED FROM HEPA				190

The extent of feed component deposition occurring within these off-gas exhaust lines is graphically displayed in Figures A.52 through A.62. Qualitatively, the depositions illustrated in these figures suggest that PSCM-3 produced higher overall emission rates than PSCM-1. Again, the only significant difference between these two PSCM experiments was the nature of the feed.

TABLE A.19. LFCM-6 Comparative DFs

Elemental Oxides	LFCM-6 Average DF	DF Ratio				
		LFCM-6 / LFCM-2	LFCM-6 / LFCM-3	LFCM-6 / PSCM-1	LFCM-6 / LFCM-4	LFCM-6 / PSCM-2
Al	330	0.067	0.14	0.030	0.62	0.33
B	90	0.35	0.74	0.43	0.69	0.56
Ca	180	0.24	0.097	0.099	0.69	0.30
Cd	80	>0.23	0.95	0.42	1.1	1.7
Cl	2	0.11	0.22	0.64	0.93	0.67
Cs	10	0.25	1.4	0.20	0.17	3.3
Fe	230	0.55	0.33	0.060	0.88	0.34
Li	160	0.17	0.24	0.084	0.52	0.47
Mg	260	0.53	0.14	0.028	0.74	0.28
Mn	330	0.21	0.11	0.58	0.79	0.52
Na	90	0.27	0.32	0.11	0.26	0.69
Ni	930	2.2	2.2	0.62	3.6	--
Ru	13	1.8	0.22	0.41	0.50	0.27
S	11	--	2.2	11.0	11.0	0.58
Si	280	0.30	0.11	0.019	0.67	0.18
Sr	290	0.77	0.19	0.039	1.4	0.45
Te	210	3.4	0.78	1.2	3.4	3.6
Ti	170	0.15	--	--	--	0.12
TOTAL OXIDE	170	0.30	0.35	0.15	0.59	0.40

Deposits were collected from various components of the off-gas line components illustrated in the previously discussed figures in order to establish their elemental composition. This compositional data appears in Table A.21. The average composition of these deposits is, not surprisingly, very much like those exhibited by deposits formed in previous melter tests using a neutralized feed as is shown in Table A.22.

Total melter feed component DFs associated with PSCM-3 have been established for most elemental constituents. These data appear in Table A.23. Overall, these results are strikingly similar to the data generated by the original pilot-scale melter experiment, PSCM-1. A comparison of PSCM-3 DFs

TABLE A.20. LFCM-6 Noncondensible Off-Gas Composition

Date	Time	CO_2	$[O_2+Ar]$	N_2	CO	Comments
5/31	22:06	0.19	20.4	78.4	--	
5/31	23:15	0.36	20.3	78.4	--	
6/01	17:01	0.81	19.8	78.5	0.026	
6/01	18:19	0.67	19.7	78.7	0.038	
6/01	19:41	0.64	19.8	78.6	0.015	
6/01	21:28	0.62	19.9	78.6	0.015	
6/01	22:39	0.72	20.0	78.3	0.035	
6/02	00:10	0.51	20.1	78.4	0.050	
6/02	18:09	0.74	19.6	78.7	--	No Feed
6/02	21:56	0.86	20.5	77.7	0.014	
6/02	22:35	0.13	20.7	78.2	--	No Feed
6/03	15:52	0.52	19.9	78.6	0.067	
6/03	17:31	0.49	19.5	79.0	0.025	
6/03	18:30	0.43	19.5	79.1	0.021	
6/03	19:19	0.48	20.0	78.5	0.050	
6/03	20:16	0.66	19.8	78.6	>0.01	
6/03	20:55	0.48	19.9	78.6	>0.01	
6/03	21:43	0.55	19.9	78.6	0.015	
6/03	22:28	0.51	20.0	78.5	0.032	
6/03	23:15	0.42	19.9	78.8	0.035	
6/04	18:19	0.27	21.0	77.7	0.018	Plasma Torch On
6/04	19:44	0.39	22.1	76.6	0.020	Plasma Torch On
6/04	20:47	0.58	21.9	76.6	0.017	Plasma Torch On
6/04	22:19	0.43	22.7	76.0	0.024	Plasma Torch On
6/04	23:18	0.48	22.8	75.8	0.017	Plasma Torch On

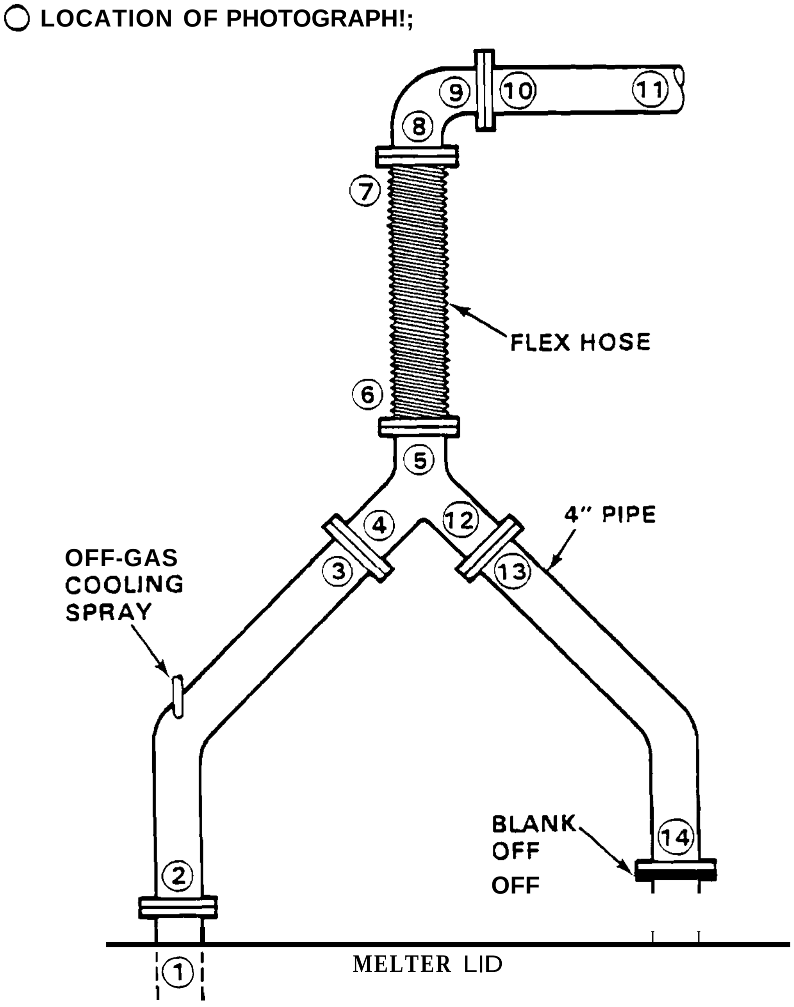

FIGURE A.51. PSCM-3 Off-Gas-Line Configuration

with DFs from all previous melter experiments covered in this report is presented in Table A.24. The effluent emission rates for PSCM-3 are lower than those exhibited by all other melter tests except PSCM-1. The low Cs DF associated with present data may not be an accurate measure of melter performance with regard to this element. The Cs composition of PSCM-3 feed was exceedingly low. On the other hand, the bulk glass within the melter possessed significant quantities of Cs from previous melter runs. Consequently, steady-state running conditions were never established for Cs during PSCM-3. The DF values for Ru and Sb are not available from this experiment.

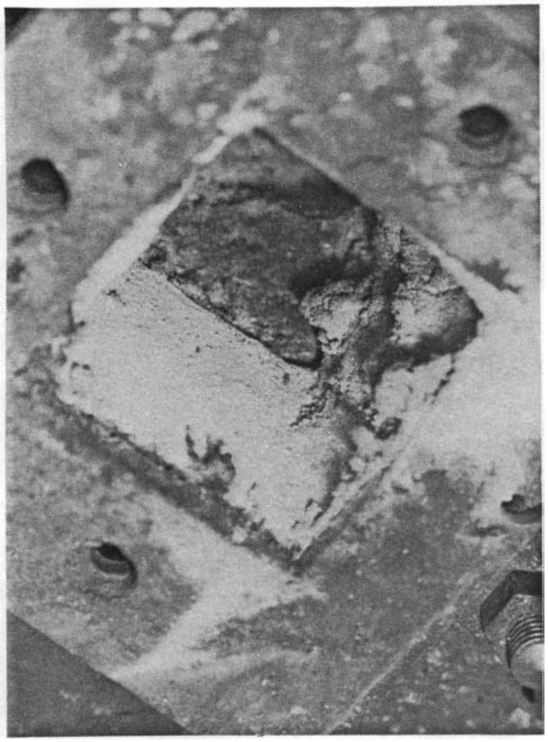

FIGURE A.52. PSCM-3 #1

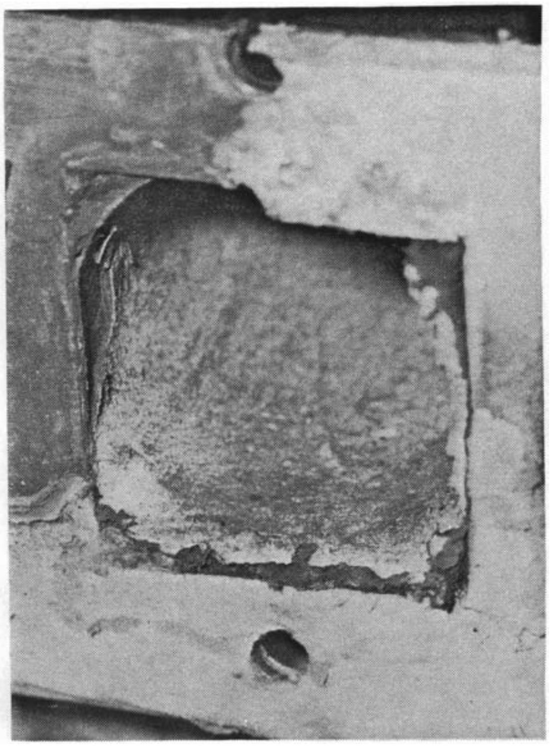

FIGURE A.53. PSCM-3 #2

FIGURE A.54. PSCM-3 #3

FIGURE A.55. PSCM-3 #4

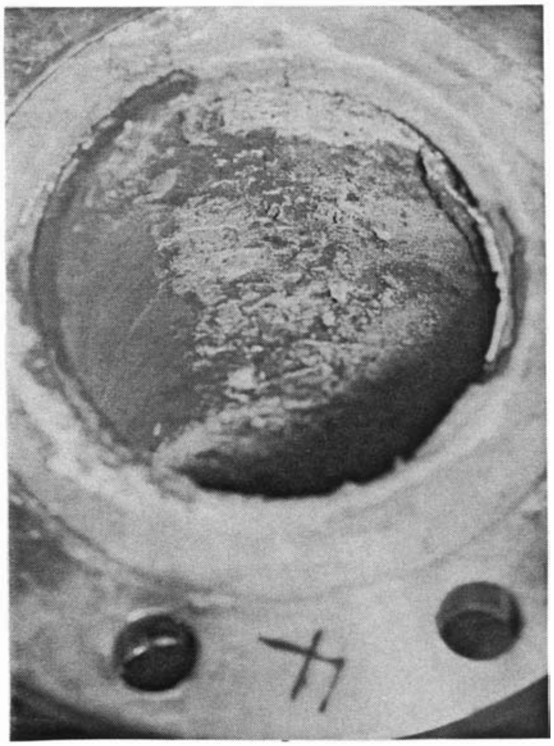

FIGURE A.56. PSCM-3 #5

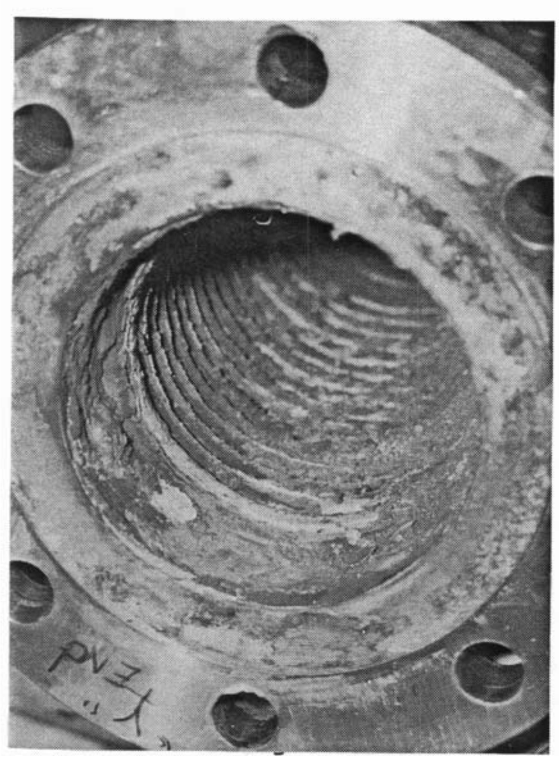

FIGURE A.57. PSCM-3 #6

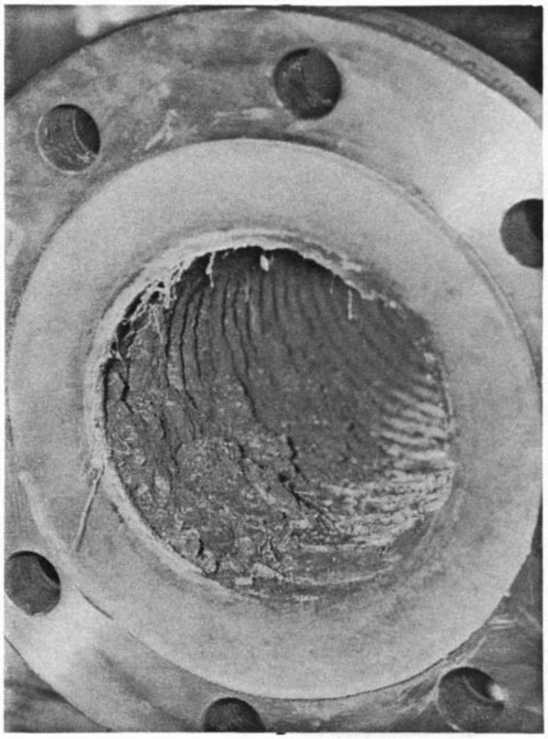

FIGURE A.58. PSCM-3 #7

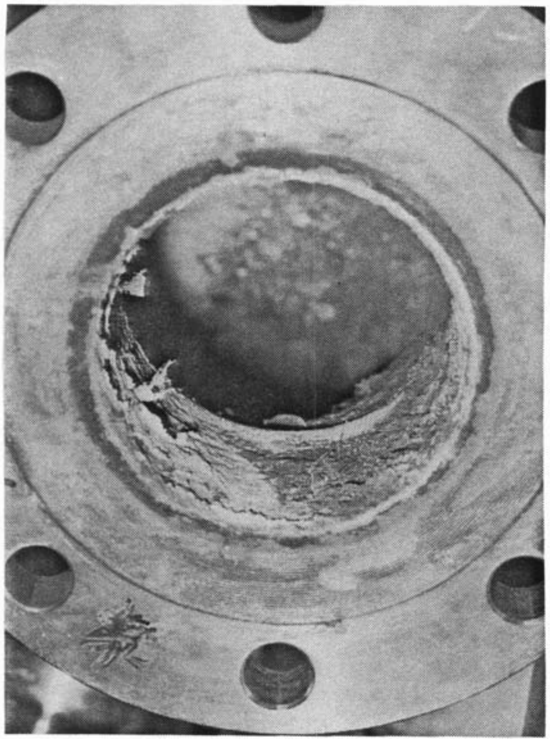

FIGURE A.59. PSCM-3 #8

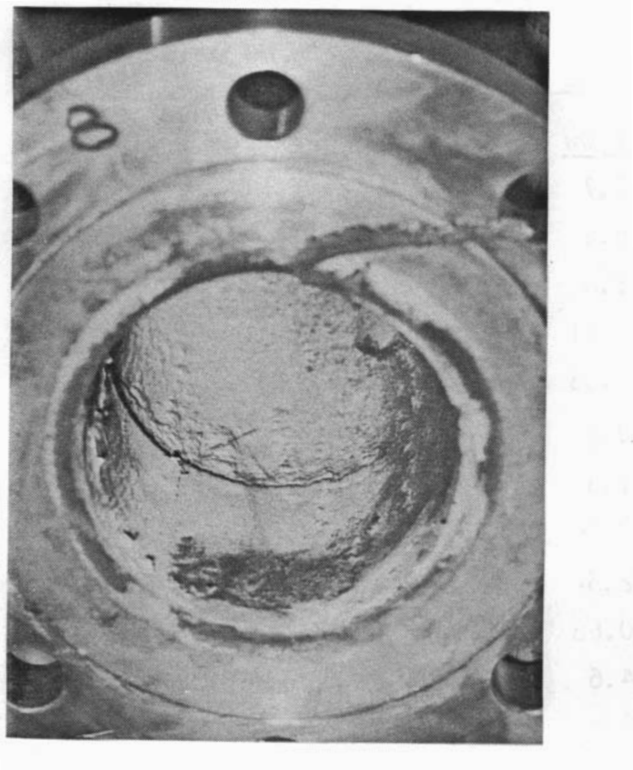

FIGURE A.60. PSCM-3 #9

FIGURE A.61. PSCM-3 #10

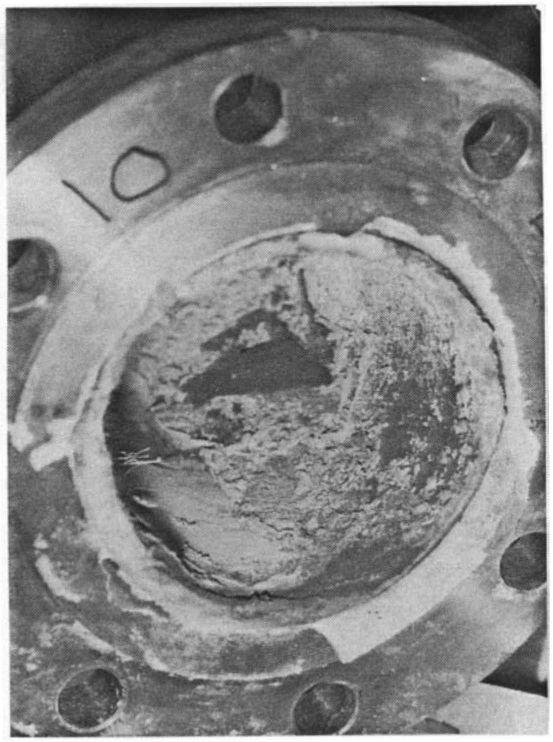

FIGURE A.62. PSCM-3 #11

TABLE A.21. PSCM-3 Pipe Deposition Composition

	Weight Percent					
Element, Oxide	Lid Port #1	Lid Port #15	Elbow	"Y"	Flex Hose	Horizontal Pipe
Al_2O_3	1.4	1.8	1.7	1.3	1.7	1.7
B_2O_3	5.0	5.5	5.5	5.4	6.0	5.0
CaO	1.6	1.9	1.6	1.6	1.8	1.6
CdO	0.09	0.08	0.11	0.15	0.10	0.09
Cs_2O	0.93	0.53	0.55	0.68	0.72	0.55
Cr_2O_3	0.14	0.15	0.21	--	0.12	0.17
Fe_2O_3	10.2	12.1	11.3	10.6	11.7	10.7
La_2O_3	0.19	0.21	0.20	0.19	--	--
LiO	2.5	2.3	2.5	2.5	2.5	2.4
MgO	0.61	0.71	0.68	0.60	0.69	0.64
MnO_2	4.3	5.3	4.6	4.3	4.9	4.8
Na_2O	18.5	14.2	14.5	18.0	15.0	14.4
NiO	0.89	1.2	1.0	0.92	1.1	1.2
RuO_2	0.11	0.04	0.11	0.03	0.29	0.08
Sb_2O_3	0.02	0.02	0.02	0.04	0.02	0.02
SiO_2	25.0	28.18	27.1	25.6	27.9	25.7
SrO	0.02	0.03	0.02	0.03	0.03	0.02
TeO_2	0.13	0.11	0.14	0.18	0.16	0.12
TiO	0.48	0.57	0.55	0.50	0.55	0.51
ZnO	0.06	0.08	0.07	0.05	0.07	--
ZrO_2	0.22	0.26	0.24	0.22	0.27	0.24
SeO_2	0.14	0.24	0.30	0.31	0.32	0.30

The composition of the noncondensible melter exhaust gases was of particular importance during this experiment due to the high organic loading of the feed. The possibility of generating H_2 and CO (water gas) in sufficient quantities to present an explosive hazard after the venturi ejector was of genuine concern. Consequently, a GC was utilized to identify all pertinent gas components present in the melter exhaust. Quantitative compositional data was generated by the GC for all gaseous components except H_2. This data appears in

TABLE A.22. Melter Pipe Deposit Composition

Element, Oxide	Weight Percent					
	PSCM-3	LFCM-6	PSCM-2	LFCM-4	PSCM-1	LFCM-2
Al_2O_3	1.6	1.9	1.6	2.0	--	1.7
B_2O_3	5.4	7.2	3.4	5.6	4.6	4.6
CaO	1.7	0.80	4.1	6.5	--	4.4
CdO	0.10	0.22	0.05	0.08	--	--
Cs_2O	0.66	0.19	0.11	0.31	0.80	0.26
Cr_2O_3	0.13	0.10	0.78	0.31	--	--
Fe_2O_3	11.1	12.0	14.2	14.0	10.0	20.0
LiO	2.5	3.1	2.9	3.4	--	2.0
MgO	0.66	0.90	0.92	2.5	--	0.22
MnO_2	4.7	2.2	3.6	3.4	--	1.2
Na_2O	15.8	13.0	16.8	15.0	20.0	17.0
NiO	1.1	--	2.3	--	--	2.5
RuO_2	0.11	0.47	0.17	0.16	--	0.3
Sb_2O_3	0.02	0.03	<0.04	--	--	--
SiO	26.6	32.0	22.7	31.0	--	31.0
SrO	0.03	0.02	0.03	0.05	--	0.04
TeO_2	0.14	0.06	0.07	0.11	--	0.07
TiO	0.53	0.72	0.42	0.11	--	0.07
ZrO_2	0.24	0.27	0.20	0.29	--	--

Figure A.63. A bipolar response of the GC detector for H_2 precluded area determination of the H_2 peak. However, GC responses for hazardous H_2 concentrations had been established previously. These served as comparative standards for the chromatograms generated during PSCM-3 and allowed operating safety, with regard to H_2, to be assessed throughout this experiment. In order to obtain the molar composition of H_2, grab samples were taken and analyzed by mass spectrometry. These results are included in Table A.25, which also contains a condensation of the data appearing in Figure A.63. From the data and flammability limits listed in this table, it is clear that dilution air was never required to eliminate potentially flammable conditions within the melter exhaust. However, these results also suggest that careful monitoring of

TABLE A.23. PSCM-3 Feed Component DFs

Elemental Oxides	DF Values		
	7/20/81	7/21/81	Average
Al	4800	7500	6000
B	210	180	200
Ca	1200	1000	1100
Cl	--	4	4
Cs	5.7	1.9	3.8
Fe	760	2500	1600
La	3400	6000	4700
Li	3000	2200	2600
Mg	11000	5300	8200
Mn	1500	5100	3300
Na	1200	600	900
Ni	3700	15000	9400
S	--	8	8
Sb	>117	>670	--
Si	2500	3600	3000
Sr	560	720	640
Te	45	20	32
Ti	2700	5600	4100
Zr	2500	1600	2000
TOTAL OXIDES	970	990	980

flammability conditions will have to be continued in all future experiments which utilize a formate-based feed.

The GC hydrogen response appears to be nonlinear in nature and insufficient data exists to construct a calibration curve. Because the amount of information is limited with regard to H_2 generation within liquid-fed melters, a trend curve has been constructed from chromatographic peak parameters which are monotonically related to concentration. It should be kept in mind that this data is not linearly related to concentration. This trend curve appears in Figure A.64.

Finally, an IR analyzer was utilized to examine the melter exhaust for the corrosive gas SO_2. At the high sensitivity settings required of this instrument, water vapor interferences proved to be an analytically limiting

TABLE A.24. PSCM-3 Comparative DFs

Elemental Oxides	PSCM-3 Avg. DF	DF Ratio PSCM-3 / LFCM-2	PSCM-3 / LFCM-3	PSCM-3 / PSCM-1	PSCM-3 / LFCM-4	PSCM-3 / PSCM-2	PSCM-3 / LFCM-6
Al	6000	1.2	2.5	0.55	11.0	6.1	18.0
B	200	0.77	1.6	0.95	1.5	1.2	2.2
Ca	1100	1.4	0.59	0.60	4.2	1.8	6.1
Cl	4	0.22	0.44	1.3	1.9	1.3	2.0
Cs	3.8	0.10	0.54	0.07	0.07	1.3	0.3
Fe	1600	3.8	2.3	0.42	6.2	2.4	7.0
Li	2600	2.8	3.9	1.4	8.4	7.6	16.0
Mg	8200	17.0	4.6	0.91	23.0	8.9	32.0
Mn	3300	2.1	1.1	0.58	7.9	5.02	10.0
Na	900	2.7	3.2	1.1	2.6	6.9	10.0
Ni	9400	22.0	22.0	6.3	36.0	--	10.0
S	8	--	1.6	8.0	8.0	0.44	0.73
Si	3000	3.2	1.1	0.20	7.1	1.9	11.0
Sr	640	1.7	0.43	0.09	3.1	1.0	2.2
Te	32	0.52	0.12	0.19	0.52	0.55	0.15
Ti	4100	3.7	--	--	--	2.79	24.0
TOTAL OXIDE	980	1.7	2.0	0.86	3.4	2.3	5.8

variable. Consequently, no conclusive data was generated with regard to melter-generated SO_2 emissions during PSCM-3. Further SO_2 monitoring studies will be discussed in the LFCM-7 effluents section.

LFCM-7 - AUGUST 1981

LFCM-7 represented the second liquid-fed melter experiment utilizing a formate-based slurry feed. Unlike the first test run (PSCM-3), LFCM-7 employed electric lid-heat boosting to maximize feeding rates. However, the run was structured to allow sampling to be conducted at various feeding rates with and without lid heat. One of the major objectives of this melter run was to evaluate real time off-gas-line cleaning techniques. Consequently, the post-run examination of the off-gas line was not carried out. However, it was observed that off-gas depositions were quite light and easily removed. None of the formations observed could have grown into local off-gas line restrictions.

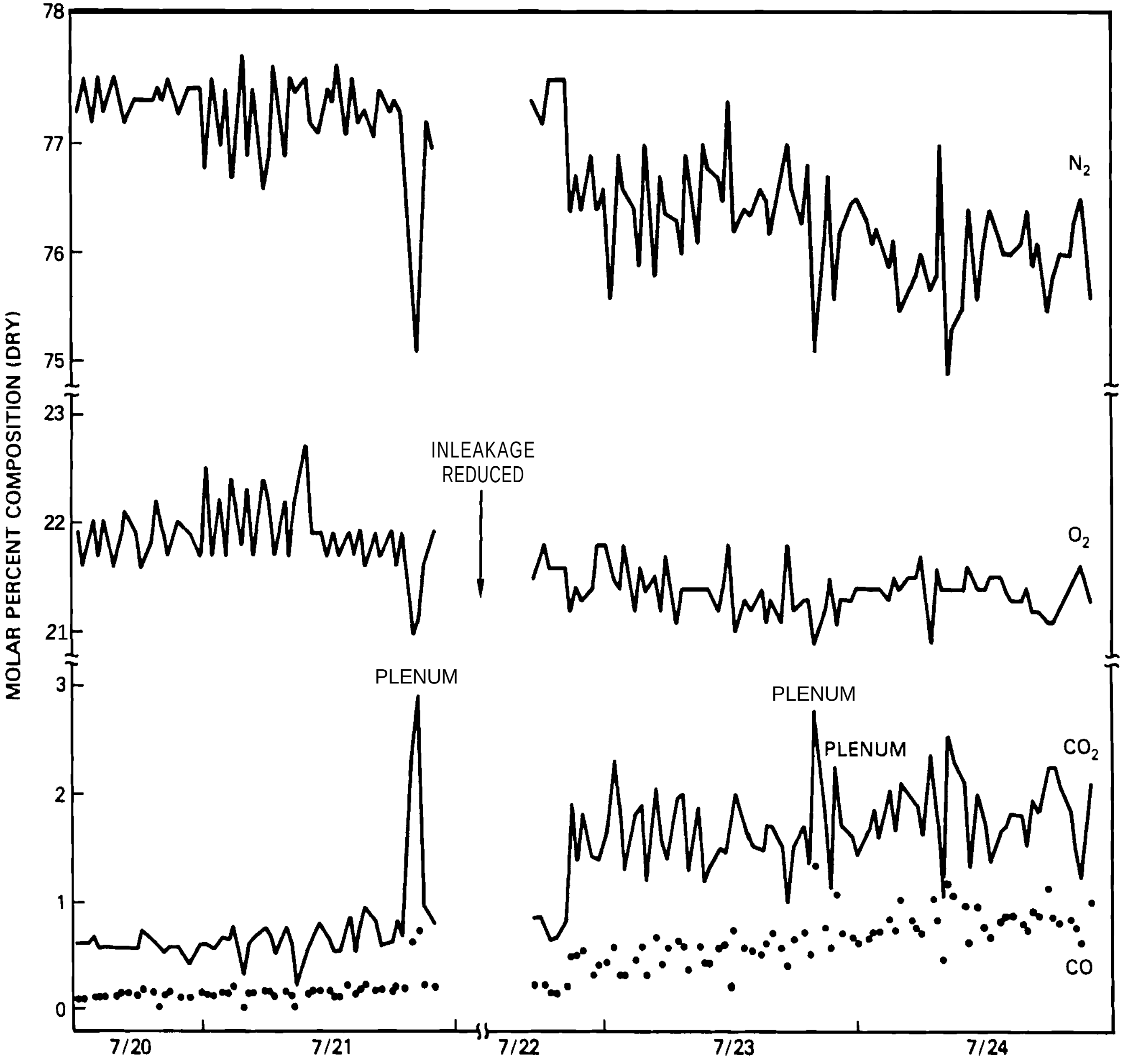

FIGURE A.63. PSCM-3 Noncondensible Off-Gas Composition

Effluent sampling of LFCM-7 emphasized the characterization of melter-yenerated aerosols. Sampling was conducted in order to establish the size distributions and concentrations of entrained particulate matter as a function of melter feeding rates. Size distribution information was obtained from a cyclone sampler consisting of a series arrangement of three cyclones and a

TABLE A.25. PSCM-3 Off-Gas Composition

		Molar Composition, %					
		Dry Basis					
Date	Data Type	CO_2	O_2(a)	N_2	CO(b)	H_2(b)	H_2O
7/20	Avg.	0.60	21.8	77.4	0.14	--	--
7/21	Avg.	0.79	21.9	74.8	0.19	--	--
7/22	Avg.	1.65	21.5	77.0	0.32	--	48
7/23	Avg.	1.42	21.3	76.1	0.58	0.64	74
7/24	Avg.	1.83	21.6	76.0	0.83	--	--
7/20 - 7/24	Hi	2.94	22.7	77.13	1.31	1.[illegible]	N/A
7/20 - 7/24	Lo	0.20	20.9	75.1	0.04	0.17	N/A

(a) Includes –1% argon.
(b) Lower flammability limit in air: H_2 - 4%; CO - 12.5%.

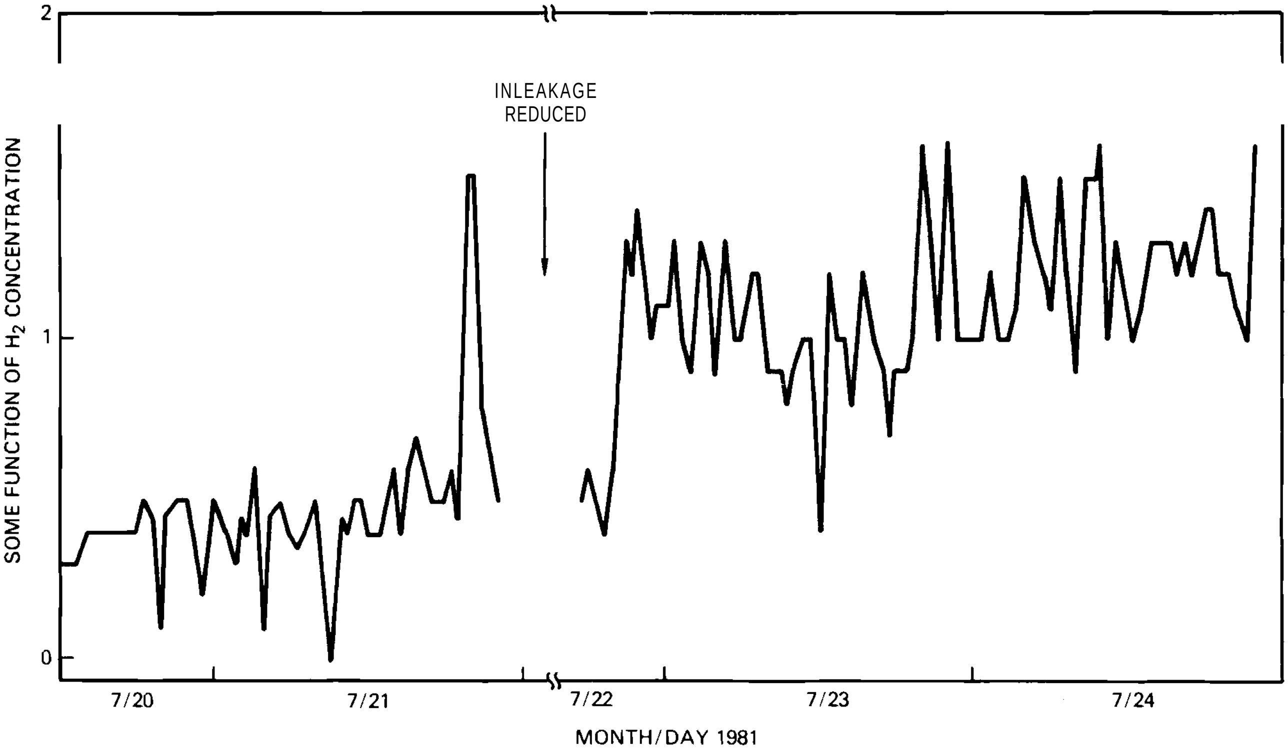

FIGURE A.64. H_2 Variation During PSCM-3 final absolute filter. The cut points of the cyclones employed were 16 µm, 6 µm and 1 µm. The absolute final filter is designed to collect submicron fines which are able to pass through all three preceding cyclones.

The data generated with this differential filtering system are summarized in Table A.26. The distribution of particulates generated by LFCM-7 is clearly bimodal in nature. Compositional analysis of these size fractions, including the condensate, appear in Table A.27. Clearly, the compositions of the various size fractions differ markedly with the semivolatile constituents strongly concentrated in the submicron fraction. This fact suggests that the two distributions making up the overall bimodal distribution probably result from independent processes.

Also presented in Table A.26 are total particulate off-gas loadings and total melter entrainment DFs. Neither of these quantities nor the size distribution data seem to be correlated with feeding or glass-production rates that occurred during the various sampling periods. However, sampling times were relatively short and feeding rates were fairly erratic.

Total aerosol loading of the off-gas stream was also assessed at various times during the run by diverting all off-gas flow through a preweighed HEPA filter. The net (dry) weight gains of these filters were then compared with the quantity of glass produced during the filtration periods to obtain total melter DFs. Concentration information was obtained through use of total off-gas flow rates, which were recorded continuously throughout the run. This data

TABLE A.26. Differential Particulate Data

Date	Sampling Period	Wt% Versus Cut Point 16 µm	6 µm	1 µm	<1 µm	Loading,$^{(a)}$ mg/L	DF	Average Rates Glass, kg/min	Feed, L/min
8/24	0727 - 0925	79.5	20	10.2	8.3	11	100	--	0.85
8/24	1635 - 1805	65.3	66	14.6	13.5	6.7	170	0.46	0.95
8/25	0553 - 0640	86.2	24	61	52	17	80	0.46	13
8/25	1415 - 1515	74.2	27	9.4	13.7	6.8	250	0.82	16
8/27	0811-0831	78.4	03	24	18.9	18	120	0.73	2.4
8/24-27	Average	76.7	28	8.5	11.9	3.5	140	--	--

(a) Actual steam-loaded volume reduced to STP.

TABLE A.27. Elemental Distribution Across Cyclonic Sampling System

	Elemental Distribution, %									
	Sample Fraction 8/25/81					Sample Fraction 8/27/81				
Element	16 µm	6 µm	1 µm	<1 µm	Cond.	16 µm	6 µm	1 µm	<1 µm	Cond.
Al	95.93	0.90	2.48	0.41	0.21	97.68	--	0.65	1.49	0.18
B	35.28	0.72	3.15	1.06	59.8	55.75	--	0.80	0.87	42.58
Ba	83.72	5.75	10.53	--	--	97.0	--	3.0	--	--
Ca	77.42	2.70	15.11	4.45	0.32	88.87	--	3.84	5.30	1.99
Cd	10.66	0.86	7.32	81.17	--	11.29	--	3.94	84.76	--
Ce	92.08	--	7.92	--	--					
Cr	46.40	21.70	23.31	8.59	--	98.58	--	1.42	--	--
Cs	7.49	--	5.41	87.10	--	13.79	--	2.20	84.01	--
Cu	82.64	4.85	4.23	8.27	--	60.83	--	4.99	34.19	--
Fe	72.12	2.56	16.97	3.14	0.20	92.19	--	3.98	3.48	0.36
La	91.95	1.48	6.09	0.48	--	98.84	--	1.16	--	--
Li	83.16	1.54	5.32	9.98	--	87.46	--	0.99	11.55	--
Mg	91.52	1.60	5.79	1.08	--	95.31	--	1.29	3.40	--
Mn	89.38	6.41	3.61	0.61	--	93.99	--	3.27	2.61	0.13
Mo	77.46	5.62	9.80	7.12	--	68.65	--	31.35	--	--
Na	68.80	1.70	5.62	23.86	0.03	66.52	--	1.25	32.15	0.08
Nd	93.45	--	6.55	--	--	100.0	--	--	--	--
Ni	--	--	--	--	100.0	--	--	--	--	100.0
Pb	--	--	--	--	--	--	--	5.62	94.38	--
Sb	100.0	--	--	--	--	--	--	--	--	--
Se	56.89	1.92	11.36	29.83	--	87.25	--	2.85	9.90	--
Si	91.86	1.79	5.61	0.60	0.14	96.71	--	1.15	1.24	0.89
Sr	77.57	2.80	19.62	--	--	95.56	--	4.44	--	--
Te	5.48	0.39	3.22	90.91	--	--	--	4.97	95.03	--
Ti	91.19	1.80	6.04	0.96	--	97.88	--	0.98	1.14	--
Zr	90.58	1.58	5.52	1.24	1.09	81.07	--	0.98	2.28	15.68

is presented in Table A.28 along with glass production rates. Again, no clear correlation appears to exist relating aerosol emission rates with feeding or glass production rates. Moreover, the average DF value (130) established with these filters is lower than the values achieved by the two previous LFCM experiments, which were 600 for LFCM-4 and 170 for LFCM-6. However, it compares quite well with the cyclonically derived value of 140.

TABLE A.28. HEPA Filtration Data

Date	Sampling Period	Sample Weight, g	Glass Rate, kg/min	Glass Weight, kg	Loading,[(a)] mg/L	DF
8/24	0805 - 1013	390	0.25	32	0.45	82
8/25	0648 - 0815	370	0.59	51	0.63	137
8/25	2233 - 2336	360	0.97	61	0.84	170
8/27	0900 - 0938	420	0.98	37	1.6	89
8/28	0442 - 0534	360	1.1	57	1.0	158
8/24-28	Average	---	--	--	0.9	130

(a) Based on an average total flow rate reduced to STP.

Additional off-gas particulate loading data were also generated by the prefilter associated with the off-gas differential sampling apparatus. This data is summarized in Table A.29. These particulate samples were collected over relatively long periods of time and thus should be less sensitive to the erratic nature of the LFCM-7 feeding rates. As with the previous data, off-gas loading and DFs are compared to feeding and glass production rates averaged over the sampling intervals. This data does exhibit a weak correlation between feeding or glass production rates and total particulate off-gas loading conditions. However, the quantity of entrained material per unit weight of feed processed (DF) appears to be independent of the feeding rates. In other words, this suggests that DFs are independent of the extent of development of the melter cold cap.

Particulate and total melter feed component DFs associated with the LFCM-7 test have been established for most elemental constituents (see Table A.30). A comparison of average LFCM-7 DFs with results obtained from previous melter experiments is presented in Table A.31. Clearly, melter effluent emission rates associated with the LFCM-7 experiment were, with few exceptions, the highest ever recorded since effluent studies began in August 1980. However, the average LFCM-7 melter DF value for Cs is higher than has been achieved in the previous three melter tests.

TABLE A.29. Particulate Data From Off-Gas Sampling Train

			Particulate		Average Rates	
Date	Sampling Period	Net Sample Weight, g	Loading,[(a)] mg/L	DF	Glass, kg/m	Feed, L/m
8/24	0913 - 1615	2.7	1.9	50	0.34	0.98
8/25	0840 - 1530	3.2	2.2	65	0.59	1.2
8/26	0833 - 1804	3.8	3.8	45	0.79	1.8
8/27	0857 - 1806	2.8	3.8	65	0.70	2.0
8/28	0830 - 1246	1.6	2.0	130	1.6	2.7
8/24-27	Average	--	2.7	71	--	--

(a) STP.

TABLE H.30. Particulate and Total Feed Component DFs

	Melter DFs											
	8/24		8/25		8/26		8/27		8/28		Ave.	
Element	Part	Total	Part	Total	Part	Total	Part	Total	part	Total	Part	Total
Al	136	132	92	91	71	71	139	139	540	530	200	190
B	56	44	72	53	59	46	103	80	260	150	110	75
Ca	41	40	52	52	36	36	63	63	120	120	62	62
Cd	11	10	8.1	8.1	5.3	5.3	6.6	6.6	10	10	8.2	8.0
Cs	16	16	24	24	9	9	4.5	4.5	5.9	5.9	12	12
Fe	48	48	65	65	49	48	64	63	130	120	71	69
La	--	--	92	92	69	69	109	109	290	290	140	140
Li	52	57	66	66	55	55	77	77	200	190	90	89
Mg	79	78	89	89	66	66	106	106	270	270	120	120
Mn	46	46	64	64	44	44	64	64	162	160	76	76
Na	50	50	65	64	43	43	50	50	93	91	60	60
Ru	--	--	--	--	16	16	--	--	--	--	16	16
Sb	54	54	86	86	62	62	--	--	--	--	67	67
Se	--	--	1	1	--	--	--	--	--	--	1	1
Si	70	70	82	82	65	65	102	101	270	260	120	120
Sr	35	35	44	44	32	32	45	45	140	140	55	55
Te	6.4	6.3	3.3	3.3	4	4	6.1	6.1	8.5	8.5	5.7	5.6
Ti	73	73	91	91	66	66	106	106	280	280	120	120
Zr	78	78	94	94	63	63	95	95	270	270	120	120

TABLE A.31. LFCM-7 Comparative DFs

Element	LFCM-7 Avg DF	DF Ratio						
		LFCM-7 / PSCM-3	LFCM-7 / LFCM-6	LFCM-7 / PSCM-2	LFCM-7 / LFCM-4	LFCM-7 / PSCM-1	LFCM-7 / LFCM-3	LFCM-7 / LFCM-2
Al	190	0.03	0.58	0.13	0.35	0.02	0.08	0.04
B	75	0.38	0.83	0.47	0.58	0.36	0.62	0.29
Ca	62	0.06	0.34	0.10	0.24	0.03	0.03	0.08
Cd	8	--	0.10	0.17	0.11	0.04	0.10	--
Cs	12	3.2	1.2	4.0	0.21	0.24	1.7	0.30
Fe	69	0.04	0.30	0.10	0.27	0.02	0.10	0.16
Li	89	0.03	0.56	0.10	0.25	0.01	0.05	0.18
Mg	120	0.01	0.46	0.13	0.34	0.01	0.07	0.25
Mn	76	0.02	0.23	0.12	0.18	0.01	0.02	0.05
Na	60	0.07	0.67	0.46	0.18	0.07	0.21	0.18
Ru	16	--	1.23	0.33	0.62	0.50	0.27	2.3
Sb	67	--	--	0.67	0.04	--	--	0.14
Se	1	--	--	--	--	--	--	0.004
Si	120	0.04	0.43	0.08	0.29	0.01	0.05	0.13
Sr	55	0.09	0.19	0.09	0.27	0.01	0.04	0.15
Te	5.6	0.18	0.03	0.10	0.09	0.03	0.02	0.09
Ti	120	0.03	0.71	0.09	--	--	--	0.11

Gross melter entrainment has been measured by several different approaches and at many different feed rates during LFCM-7. Table A.32 is a collection of all the gross DF values established during this experiment.

Due to the potential hazards associated with melter-generated H_2 and CO, noncondensible gas monitoring was conducted throughout the duration of LFCM-7. As in PSCM-3, the gas samples were extracted and analyzed by a GC at the exhaust of the venturi ejector (see Figure A.1). The compositional data generated with this sampling system is graphically illustrated in Figure A.65. The inleakage rates (90 scfm) for LFCM-7 were much greater than those occurring during the previous PSCM-3 test (~20 scfm). Consequently, CO and H_2 concentrations were never much of a safety concern throughout the run. In fact, H_2 was hardly detectable until one of the larger off-gas leaks was eliminated

TABLE A.32. Gross DF Values

Date	Sampling Period	Sampling Type[(a)]	Particulate Loading,[(b)] mg/L	Particulate DF	Average Rates Glass, kg/m	Average Rates Feed, L/m
8/24	0727 - 0925	C	1.08	120	--	0.85
8/24	0805 - 1013	HEPA	0.45	82	0.25	--
8/24	0913 - 1615	S	1.90	50	0.34	0.98
8/24	1635 - 1805	C	0.67	170	0.46	0.95
8/25	0553 - 0640	C	1.70	80	0.46	1.3
8/25	0648 - 0815	HEPA	0.63	137	0.59	--
8/25	0840 - 1530	S	2.2	65	0.59	1.2
8/25	1415 - 1515	C	0.67	245	0.82	1.6
8/25	2233 - 2336	HEPA	0.84	170	0.97	--
8/26	0833 - 1804	S	3.8	45	0.79	1.8
8/27	0811 - 0831	C	1.8	120	0.73	2.4
8/27	0900 - 0938	HEPA	1.6	89	0.98	--
8/27	0857 - 1806	S	3.8	65	0.70	2.0
8/28	0442 - 0534	HEPA	1.0	158	1.1	--
8/28	0830 - 1246	S	2.0	130	--	2.7
8/24-28	Average	ALL	1.61	115		

(a) C = cyclone S = differential sampler HEPA = absolute filtration.
(b) STP.

toward the end of the run. As in PSCM-3, H_2 concentrations were established using a gas mass spectrometer. This data, along with a condensation of the results appearing in Figure A.65, is presented in Table A.33. A curve showing H_2 concentration as a function of time, has been constructed from the GC data (see Section "PSCM-3, JULY 1981"). This curve, displayed in Figure A.66, is designed to give the reader a semiquantitative notion of the way in which H_2 concentrations varied throughout the LFCM-7 experiment. The reader is cautioned that the correlation presented in this figure is nonlinear.

The sampling difficulties encountered with the SO_2 monitor during PSCM-3 were eliminated, allowing SO_2 to be monitored during LFCM-7. However, no significant responses were recorded during the sampling periods employed. Thus, the upper concentration limit of SO_2 in the melter exhaust is 50 ppm.

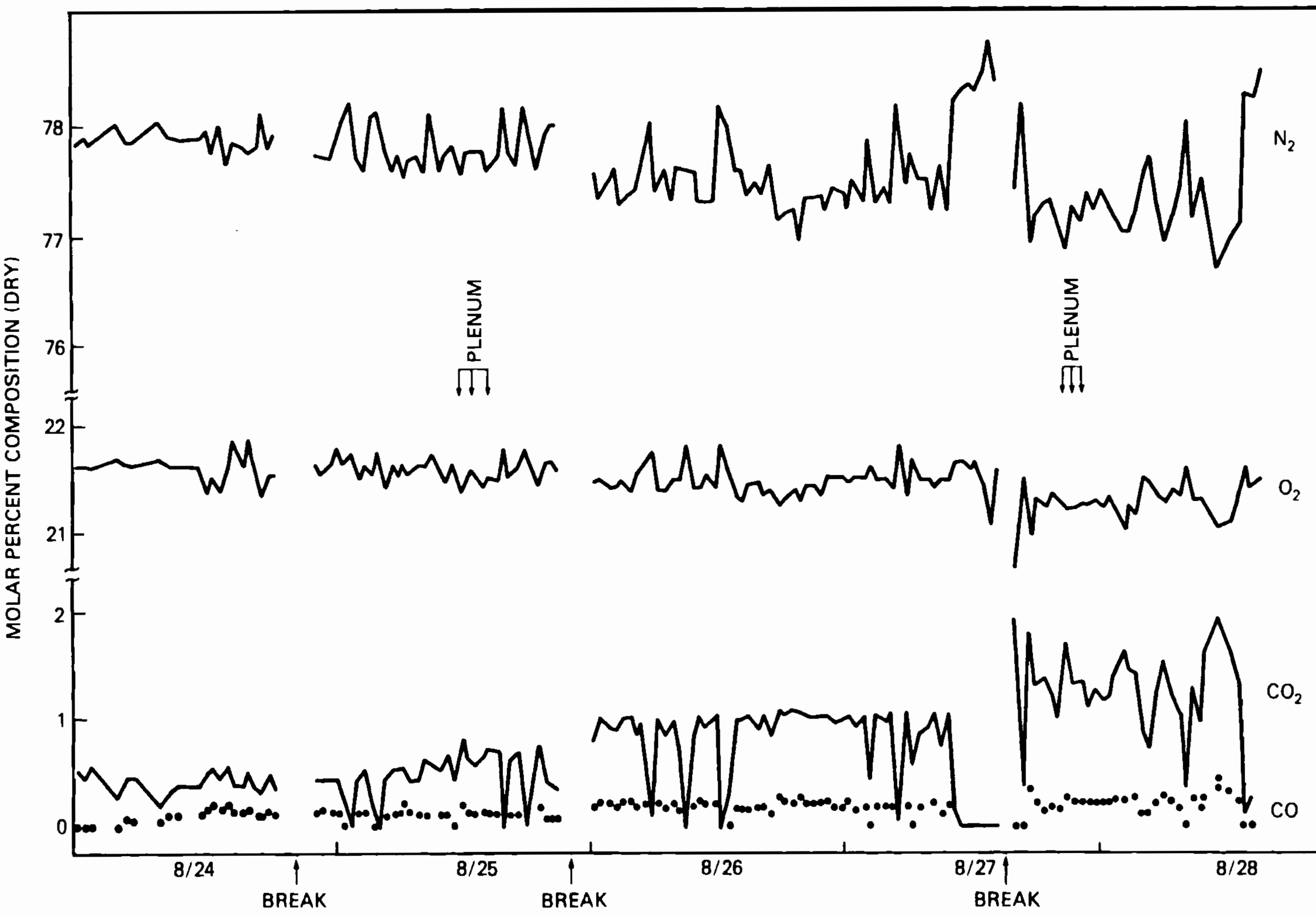

FIGURE A.65. LFCM-7 Noncondensible Off-Gas Composition

TABLE A.33. LFCM-7 Off-Gas Composition

		Molar Composition, %					
		Dry Basis					
Day	Data Type	CO_2	O_2(a)	N_2	CO	H_2	H_2O
8/23	Avy.	0.49	21.6	77.9	<20(b)	--	--
8/24	Avy.	0.43	21.6	77.8	0.12	--	22
8/25	Avg.	0.47	21.6	77.9	0.12	--	27
8/26	Avg.	0.91	21.4	77.5	0.18	--	35
8/27	Avg.	0.87	21.4	77.6	0.13	0.44	41
8/28	Avy.	1.19	21.3	77.4	0.21	0.63	46
8/23-28	Hi	2.2	21.8	78.8	0.44	0.63	46
8/23-28	Lo	0.03	20.9	76.3	<10(b)	0.40	22

(a) Includes ~1% Ar.
(b) In ppm.

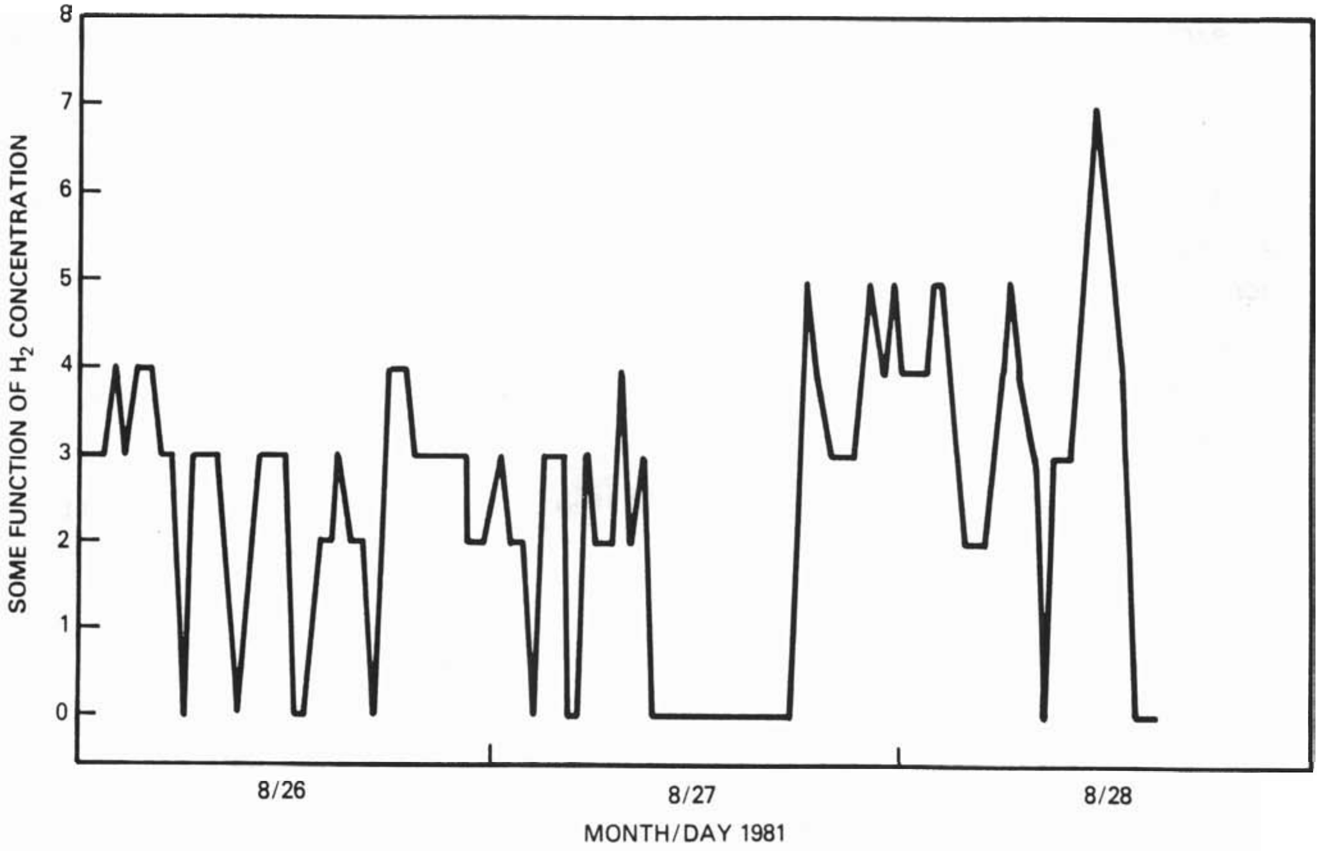

FIGURE A.66. H_2 Variation Duriny LFCM-7

PSCM-4 - DECEMBER 1981

PSCM-4 was a nonboosted, 109-h experiment designed to demonstrate a steady-state feeding capacity of 39 kg/h-m^2. Unlike the previous LFCM-7 experiment where inleakaye rates were very high and probably a contributing factor to the high entrainment observed during that test, PSCM-4 was conducted with a newly rebuilt melter, with very low air inleakage (20 scfm). As such, the performance of this melter is most suitably comparable to the previous, unboosted PSCM-1 and PSCM-3 tests, as is clearly shown in Table A.1. The off-gas-line deposits generated by the PSCM-4 melter are illustrated in Figures A.68 through A.70. The locations of these off-gas line components are illustrated in Figure A.67. A comparison of these photographs with those taken during PSCM-1 (see FY-1981 Summary) and PSCM-3 (see Section "PSCM-3, JULY 1981") reveals moderate entrainment rates associated with PSCM-4.

The magnitude of gross melter entrainment occurring during PSCM-4 was established by total HEPA filtration of the melter exhaust stream. These data appearing in Table A.34. Entrainment generated by the PSCM-4 test is greater than that observed during both the PSCM-1 and the PSCM-3 experiments.

The off gas was also sampled during PSCM-4 to establish individual melter feed component DFs. Table A.35 presents this data for all elemental feed components detected in the off-gas stream. The distribution of these effluents across sampling train components (particulate versus condensible) is also given in the table. Physically, the melter-generated effluents are predominantly particulate in nature, at least at the point at which they enter the off-gas system.

A possible exception to the above statement is the semivolatile element Ru. No airborne state or phase of this element was detected by any of the off-gas sampling experiments conducted during PSCM-4 in spite of a high feed loading for this element. The most plausible explanation for this observation is that Ru is being reduced by the formic acid in the feed and is subsequently lost to the melter floor as slag. A surface plate-out mechanism is a possible, but less likely explanation for these losses. However, no local deposits of Ru metal have been observed in off-gas line components.

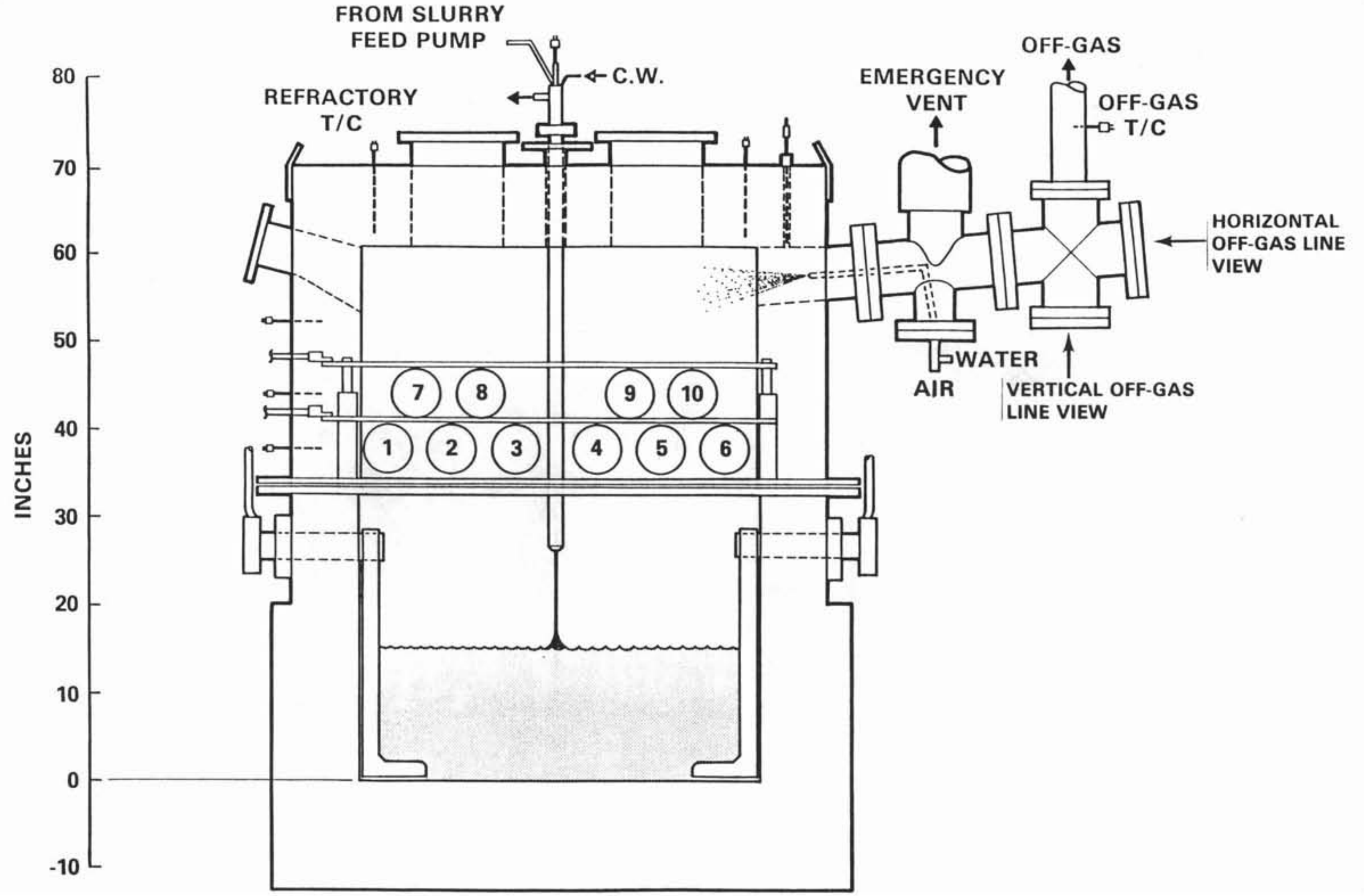

FIGURE A.67. PSCM Off-Gas-Line Configuration

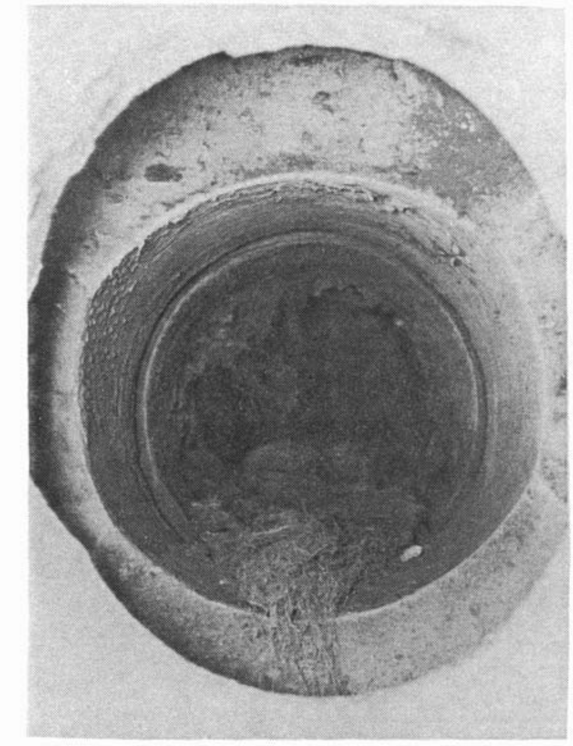

FIGURE A.68. PSCM-4 Off-Gas Line Horizontal Section

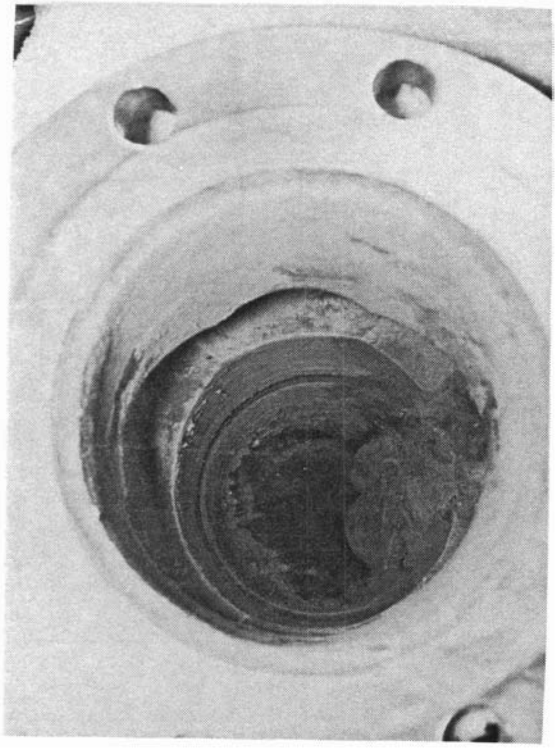

FIGURE A.69. PSCM-4 Off-Gas Line Horizontal Section

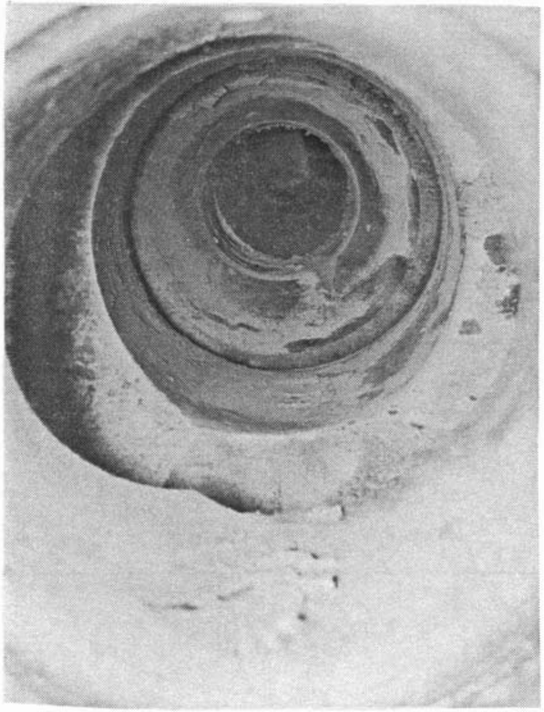

FIGURE A.70. PSCM-4 Off-Gas Line Vertical Section

TABLE A.34. PSCM-4 Aerosol DFs

Sampling Period		Sample Type	Feed Rate, L/h	DF
Date	Interval			
12/08	2242 - 0252	HEPA	62	516
12/10	0026 - 0600	HEPA	62	500
12/11	0200 - 1015	HEPA	67	509

TABLE A.35. Particulate and Total Elemental Melter DFs

	12/07/81		12/08/81		12/09/81		Average	
	DF		DF		DF		DF	
Element	Part	Total	Part	Total	Part	Total	Part	Total
Al	1.9×10^4	1.9×10^4	2.9×10^4	2.4×10^4	3.1×10^4	2.6×10^4	2.6×10^4	2.3×10^4
B	7.3×10^3	350	9.2×10^3	180	7.2×10^3	160	7.9×10^3	230
Ca	2.1×10^3	2.0×10^3	2.4×10^3	2.2×10^3	1.7×10^3	1.4×10^3	2.1×10^3	1.9×10^3
Cd	19	19	4.1	4.0	4.5	4.5	9.2	9.2
Cl	13	9.9	5.1	3.2	3.0	2.0	7	5
Cs	27	27	8.9	8.5	11	11	16	16
Fe	2.7×10^3	2.7×10^3	2.4×10^3	1.8×10^3	1.8×10^3	1.6×10^3	2.3×10^3	2.0×10^3
Li	1.6×10^3	1.6×10^3	700	677	7.6×10^3	7.2×10^3	3.3×10^3	3.2×10^3
Mn	2.6×10^3	2.6×10^3	2.7×10^3	2.2×10^3	2.2×10^3	1.6×10^3	2.5×10^3	2.1×10^3
Na	380	380	1.5	1.5	170	170	180	180
Ni	1.9×10^3	1.8×10^3	2.3×10^3	1.2×10^3	1.8×10^3	1.3×10^3	2.0×10^3	1.4×10^3
S	100	26	15	6.9	55	16	57	16
Si	8.2×10^3	8.1×10^3	1.4×10^4	1.2×10^4	1.1×10^4	7.6×10^3	1.1×10^4	9.2×10^3
Sr	--	--	310	310	190	190	250	250
Te	5	5	1.9	1.9	2.3	2.3	3.1	3.1
Ti	8.2×10^3	8.2×10^3	1.1×10^4	1.0×10^4	7.9×10^3	7.8×10^3	9.0×10^3	8.7×10^3
Zr	4.2×10^3	4.2×10^3	6.4×10^3	6.4×10^3	4.4×10^3	4.4×10^3	5.0×10^3	5.0×10^3

Individual melter feed component DFs observed in PSCM-4 are compared in Table A.36 with DFs collected from all previous melter experiments. This comparison reveals that PSCM-4 effluent emission rates are, on the average, lower than those observed during PSCM-3, but remain higher than those associated with PSCM-1, the "cleanest" melter experiment conducted to date.

TABLE A.36. PSCM-4 Comparative DFs

		DF Ratio							
	PSCM-4	PSCM-4	PSCM-4	PSCM-4	PSCM-4	PSCM-4	PSCM-4	PSCM-4	PSCM-4
Element	Avg. DF	LFCM-7	PSCM-3	LFCM-6	PSCM-2	LFCM-4	PSCM-1	LFCM-3	LFCM-2
Al	2.3 × 10^4	120	3.8	70	23	43	2.1	9.6	4.7
B	230	3.1	1.2	2.6	1.4	1.8	1.1	1.9	0.89
Ca	1.9 × 10^3	31	1.7	11	3.1	7.3	1.0	1.0	2.6
Cd	9.2	1.2	--	0.12	0.20	0.13	0.05	0.11	--
Cl	5	--	1.2	1.8	1.7	2.3	1.6	0.56	0.29
Cs	16	1.3	4.2	1.6	5.3	0.28	0.31	2.3	0.40
Fe	2.0 × 10^3	29	1.2	8.7	2.9	7.7	0.53	2.9	4.8
Li	3.2 × 10^3	36	1.2	20	9.4	10	1.7	4.8	3.5
Mn	2.1 × 10^3	28	0.64	6.4	3.3	5.0	0.37	0.68	1.3
Na	180	3.0	0.20	2.0	1.4	0.53	0.22	0.64	0.54
Ni	1.4 × 10^3	--	0.15	1.5	--	5.4	0.93	3.3	3.3
S	16	--	2.0	1.5	0.84	16	16	3.2	0.84
Si	9.2 × 10^3	77	3.1	33	5.8	22	0.61	3.5	9.8
Sr	250	4.6	0.39	0.86	0.39	1.2	0.03	0.17	0.66
Te	3.1	0.55	0.10	0.01	0.05	0.05	0.02	0.01	0.05
Ti	8.7 × 10^3	72	2.1	51	6.2	--	--	--	7.9
Zr	5 × 10^3	--	--	--	--	--	--	--	--

Total aerosol DFs were also extracted from the data presented in Table A.35. These values, combined with the HEPA data previously discussed, are summarized in Table A.37. Overall, the entrainment DF values were fairly consistent throughout the run, with an average value of 630. This is lower than the values from both the PSCM-1 and PSCM-3 experiments, but is still quite respectable.

The size distribution of particulate matter conveyed to the off-gas system by the unboosted PSCM-4 melter was also investigated during this test by a four-stage cyclonic particle-size separator having 16 μm, 6 μm, 1 μm and <1 μm cut points. The results of this study are summarized in Table A.38. Unlike the previous LFCM-7 experiment where >80% of the melter entrained mass was

TABLE A.37. PSCM-4 Gross Aerosol DFs

Sampling Period		Feed Rate,		
Date	Interval	Sample Type	L/h	DF
12/07	1715 - 2018	S - FILTER[(a)]	52	970
12/08	1848 - 2218	S - FILTER	60	460
12/8-9	2241 - 0252	HEPA	62	520
12/09	1650 - 2302	S - FILTER	63	470
12/10	0026 - 0600	HEPA	62	500
12/10	1720 - 2306	S - FILTER	66	980
12/11	0200 - 1015	HEPA	67	510
12/07-11	Average	ALL		630

(a) Sample stream filter.

TABLE A.38. PSCM-4 Particulate Size Data

Sampliny Period		Wt% Versus Cut Point			
Date	Interval	16 μm	6 μm	1 μm	<1 μm
12/07	1811 - 1901	0	3.4	4.7	91.9
12/08	2202 - 2212	0	0	0	100.0
12/09	1712 - 1720	0	0	9.6	90.4
12/10	1950 - 1959	0	0	0	100.0
	Average	0	0.9	3.6	95.6

collected by the 16 μm cyclone, PSCM-4 emitted predominantly submicron aerosols. The composition of PSCM-4 submicron particulate matter is presented in Table A.39. As was the case during LFCM-7, the submicron melter-generated aerosol was highly enriched with semivolatile elements relative to the feed. If a material balance is conducted for this submicron matter by assuming an oxide form for all elements except for a stoichiometric quantity of Na, which is associated with the Cl in the sample, 98.8% of the matter present can be accounted for. It should be noted that the submicron particulate sample is 83% NaCl.

The noncondensible composition of the melter exhaust was determined by a GC at 30-min intervals throughout the duration of PSCM-4. The percentages of

TABLE A.39. PSCM-4 Submicron Particulate Composition

Element	Elemental Wt%	Elemental Form	Compound Wt%	Feed Composition, %
Al	0.04	Al_2O_3	0.08	4.95
B	0.07	B_2O_3	0.24	9.86
Ca	0.14	CaO	0.20	1.66
Cd	0.55	CdO	0.63	0.006
Cl	55.0	--	--	0.4
Cs	2.1	Cs_2O	2.2	0.044
Cu	0.06	CuO	0.09	--
Fe	0.29	Fe_2O_3	0.41	13.69
K	0.36	K_2O	0.43	--
Li	1.1	Li_2O	2.4	3.98
Mg	0.02	MgO	0.03	1.29
Mn	0.08	MnO_2	0.13	3.25
Na	33.7	NaCl Na_2O	83.0 6.7	-- 13.88
Ni	0.03	NiO	0.04	0.76
Pb	0.04	PbO	0.05	--
Si	0.66	SiO_2	1.4	44.47
Te	0.56	TeO_2	0.71	0.006
Zn	0.02	ZnO	0.02	--
Total			98.8	

N_2, O_2+Ar, CO, CO_2 and H_2 are plotted in Figure A.71. The H_2 data presented in Figure A.71 is included to illustrate H_2 concentration trends only. The GC response function for this molecule has not been determined. A summary of off-gas composition is presented in Table A.40.

Off-gas concentrations of SO_2 were also continuously measured during part of PSCM-4 (see Figure A.71 and Table A.40). Table A.41 compares the SO_2 off-gas monitoring data with average SO_2 values derived from off-gas scrubbing data. The low values obtained from the SO_2 monitor resulted from the unavoidable interaction of this gas with condensed-phase H_2O and/or the presence of SO_3.

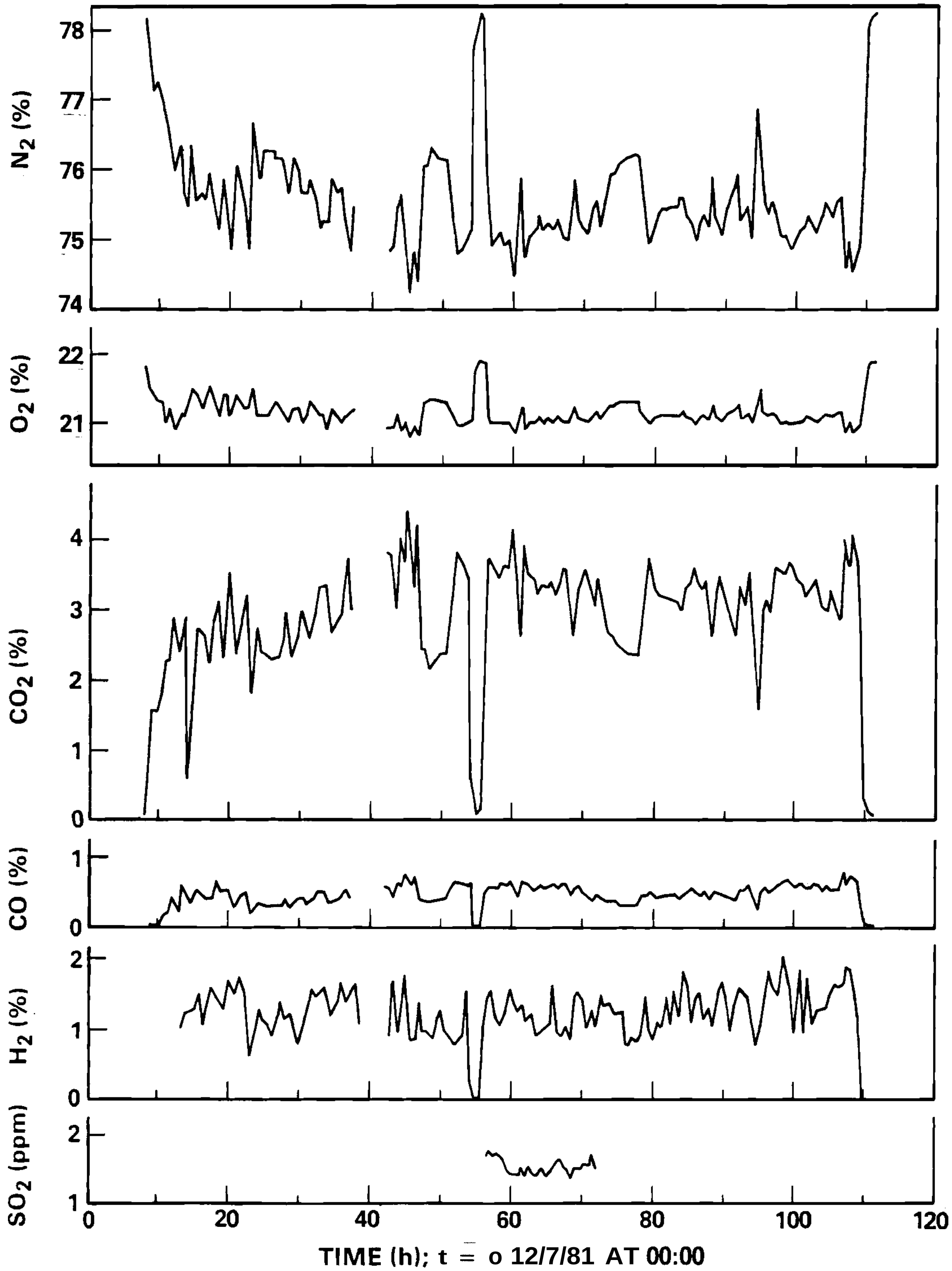

FIGURE A.7 1. PSCM-4 Off-Gas Cornposition

TABLE A.40. PSCM-4 Noncondensible Off-Gas Composition

		Molar Composition, %						
		Dry Basis						
Date	Data Type	CO_2	O_2[(a)]	N_2	CO	H_2	SO_2 ppm	H_2O
12/07	Avg.	2.5	20.9	76.3	0.37	--	--	77.0
12/08	Avg.	3.0	20.7	75.8	0.43	--	--	80.5
12/09	Avg.	3.0	20.7	75.8	0.48	1.3	1.5	78.6
12/10	Avg.	3.0	20.8	75.8	0.42	--	>2.0	81.1
12/11	Avg.	3.0	20.7	75.8	0.49	1.0	>2.0	--
12/7-11	Hi	4.4	21.0	77.1	0.75	1.3	>2.0	81.1
12/7-11	Lo	0.5	20.4	74.5	0.20	1.0	1.34	77.0

(a) Includes -1% Ar.

TABLE A.41. PSCM-4 SO_2 Off-Gas Concentration

Sampling Period		SO_2 Concentration, ppm (Vl/Vl)	
Date	Interval	Gas Scrub	Gas Monitor
12/07	1715 - 2018	1.8	--
12/08	1848 - 2218	7.6	--
12/09	1650 - 2320	12.0	1.5 (Avg.)
12/10	1720 - 2306	23.0	>2.0
12/11	0800 - 1300	--	>2.0

During the PSCM-4 run, samples were taken of the scrubbing solution from the venturi scrubber and the packed tower. The analyses of the solutions were used to calculate a melter DF and a venturi DF. These results are based on the assumption that the venturi scrubber and the packed tower collected greater than 99% of the material leaving the melter, and that the venturi scrubbing solution had reached steady state. PSCM-4 was a smooth, steady run, so the steady-state assumption should be good.

The results of the analysis are shown in Table A.42. Calcium was left out of the analysis because of large amounts added to the venturi scrub solution to neutralize the condensate and retard corrosion. The total oxide DF compared very well with values reported for the HEPA filters (500 average).

TABLE A.42. Melter Decontamination Factors

Element	Melter DFs	Venturi DFs
Al	7300	44
B	160	44
Cd	6	50
Cs	12	54
Fe	1300	3.7
La	2600	79
Li	940	46
Mg	550	62
Mn	2000	98
Na	170	51
Nd	1770	H
Ru	N/A	N/A
Sb	840	H
Si	2500	66
Sr	400	58
Te	2	H
Ti	3800	H
Zr	3500	H
TOTAL OXIDES	590	50

H = High.

PSCM-5 - FEBRUARY 1982

PSCM-5 was a 99-h experiment designed to characterize maximum feeding rates achievable utilizing electric lid heat boosting. As such, it represents the second boosted experiment utilizing the new formate feed composition. As revealed in Section "LFCM-7, AUGUST 1981," the first boosted test (LFCM-7) with the formate-feed formulation exhibited melter DFs, which were generally the lowest ever recorded. Consequently, the effluent behavior associated with this experiment was of keen interest.

The off-yas lines of the pilot-scale melter were visually examined upon completion of the PSCM-5 test. Melter depositions were greatest around off-gas line penetrations, which tended to collect glass strands and other debris. Overall, the conditions of the melter off-yas lines were quite similar to what was found at the conclusion of the previous melter test (PSCM-4). The largest accumulation of melter debris developed around the off-gas line spray nozzle, which is located at the plenum exhaust port. These deposits did not significantly restrict off-gas flow, but would present a problem under prolonged continuous melter operation.

The extent of gross melter aerosol emission was established during PSCM-5 through HEPA filtration of the entire melter exhaust stream. The results obtained from these filtration studies are summarized in Table A.43.

Although the data available are limited, the average DF value (~500) extracted from this filtration study is basically the same as was obtained during the unboosted PSCM-4 test.

Particulate and total feed component DFs were also measured during PSCM-5 and are summarized in Table A.44. It is clear from this and the previous studies that, apart from the mechanisms responsible for producing airborne effluents, particulate transport through the off-gas system is the predominant loss mechanism associated with liquid-fed melter operation. This is apparently not true, however, for Ru. Again, as in PSCM-4, no airborne Ru was detected in PSCM-5 melter exhaust, even though feed and glass analyses indicate significant Ru melter losses. No specific sink for the element has yet been conclusively identified to account for these losses.

Table A.45 compares PSCM-5 melter feed component DFs with those measured during all previous melter tests. PSCM-5 exhibited greater overall effluent emission rates than did the unboosted PSCM-4 test. However, much higher feed component DFs were achieved during PSCM-5 than were recorded during the previous boosted LFCM-7 test, which also employed a formate-based feed.

TABLE A.43. PSCM-5 Gross Melter Entrainment

Sampling Period		Melter Entrainment	
Date	Interval	% Loss	DF
1/27	1820 - 2135	0.27	370
1/28	1920 - 2400	0.15	670

TABLE A.44. PSCM-5 Particulate and Total Feed Component DFs

	DF							
	1/26/82		1/27/82		1/28/82		Average	
Element	Part	Total	Part	Total	Part	Total	Part	Total
Al	1.5×10^4	1.4×10^4	1.4×10^4	1.3×10^4	1.4×10^4	1.4×10^4	1.4×10^4	1.4×10^4
B	3.9×10^3	130	4.3×10^3	160	3.9×10^3	120	4.0×10^3	140
Ca	880	860	1.1×10^3	1.1×10^3	1.2×10^3	1.2×10^3	1.1×10^3	1.1×10^3
Cd	6.0	5.9	5.7	5.7	5.4	5.4	5.7	5.7
Cl	3.8	1.8	3.2	1.5	3.2	1.1	3.4	1.5
Cs	8.8	8.8	10	10	9.5	9.5	9.4	9.4
Fe	1.5×10^3	1.3×10^3	1.3×10^3	1.0×10^3	1.4×10^3	1.0×10^3	1.4×10^3	1.1×10^3
La	7.0×10^3	7.0×10^3	8.1×10^3	8.1×10^3	1.6×10^4	1.6×10^4	1×10^4	1.0×10^4
Li	640	640	830	830	730	730	730	730
Mg	2.9×10^3	2.9×10^3	3.7×10^3	3.7×10^3	3.8×10^3	3.8×10^3	3.5×10^3	3.5×10^3
Mn	8.5×10^3	7.5×10^3	9.2×10^3	6.3×10^3	1.0×10^4	7.6×10^3	6.2×10^3	7.1×10^3
Na	150	150	170	170	150	150	160	160
Nd	6.8	6.8	--	--	--	--	--	--
Ni	1.1×10^3	640	1.1×10^3	500	1.1×10^3	590	1.1×10^3	580
S	11	2.8	28	5.6	26	5.2	22	4.5
Sb	580	350	720	720	330	340	540	440
Se	--	--	110	110	140	140	130	130
Si	5.5×10^3	4.8×10^3	5.7×10^3	5.4×10^3	6.3×10^3	5.6×10^3	5.8×10^3	5.3×10^3
Te	2.2	2.2	2.8	2.8	4.40	4.40	3.1	3.1
Ti	7.6×10^3	7.6×10^3	--	--	6.8×10^3	6.8×10^3	7.2×10^3	7.2×10^3
Zr	1.2×10^4	1.2×10^4	--	--	1.4×10^4	1.4×10^4	1.3×10^4	1.3×10^4

Particle size analysis of melter-entrained aerosols was conducted during PSCM-5 using a cyclonic separator system. Table A.46 summarizes the distribution of the melter-generated aerosols through the four stages of this differential particle-size analyzer. Unlike PSCM-4, which produced predominantly submicron aerosols, the boosted PSCM-5 melter exhibited a bimodal particle distribution much like that observed in the boosted LFCM-7 test. However, the full distribution associated with PSCM-5 was weighted much more heavily toward the submicron region than was LFCM-7s.

TABLE A.45. PSCM-5 Comparative DFs

Element	PSCM-5 Avg. DF	DF Ratio PSCM-5 / PSCM-4	PSCM-5 / LFCM-7	PSCM-5 / PSCM-3	PSCM-5 / LFCM-6	PSCM-5 / PSCM-2	PSCM-5 / LFCM-4	PSCM-5 / PSCM-1	PSCM-5 / LFCM-3	PSCM-5 / LFCM-2
Al	14 x 10^4	0.61	74.0	2.3	42.0	14.0	26.0	1.3	5.8	2.8
B	140	0.61	1.9	0.70	1.6	0.88	1.1	0.67	1.2	0.54
Ca	1.1 x 10^3	0.58	18.0	1.0	6.1	1.8	4.2	0.60	0.59	1.5
Cd	5.7	0.62	0.71	--	0.07	0.12	0.08	0.03	0.07	--
Cl	1.5	0.30	--	0.38	0.56	0.50	0.68	0.48	0.17	0.09
Cs	9.4	0.59	0.78	2.5	0.94	3.1	0.16	0.18	1.3	0.24
Fe	1.1 x 10^3	0.55	16.0	0.69	4.8	1.6	4.2	0.29	1.6	2.6
La	1 x 10^4	--	--	--	--	--	--	--	--	--
Li	730	0.23	8.2	0.28	4.6	2.2	2.4	0.38	1.1	0.79
Mg	3.5 x 10^3	--	29.0	0.43	13.0	3.8	10.0	0.39	1.9	7.2
Mn	7.1 x 10^3	3.4	93.0	2.2	22.0	11.0	17.0	1.2	2.3	4.5
Na	160	0.89	2.7	0.18	1.8	1.2	0.47	0.19	0.57	0.48
Ni	580	0.41	--	0.06	0.62	--	2.2	0.39	1.4	1.4
S	4.5	0.28	--	0.56	0.41	0.24	4.50	4.50	0.90	0.24
Sb	440	--	6.6	--	--	4.4	0.24	--	--	0.91
Se	130	--	--	--	--	--	--	--	--	--
Si	5.3 x 10^3	0.58	44.0	1.8	19.0	3.3	13.0	0.35	2.0	5.6
Te	3.1	1.0	0.55	0.10	0.01	0.05	0.05	0.02	0.01	0.05
Ti	7.2 x 10^3	0.83	60.0	1.8	42.0	5.1	--	--	--	6.6
Zr	1.3 x 10^4	2.6	--	--	--	--	--	--	--	--

TABLE A.46. PSCM-5 Differential Particulate Data

Sampling Period Date	Interval	Wt% Versus Cut Point 16 μm	6 μm	1 μm	<1 μm	Particulate Loading,[a] mg/L	DF	Feed Rate, L/h
1/26	1738 - 1749	18.6	2.9	19.8	58.7	0.43	590	51
1/27	1758 - 1805	14.4	6.7	22.83	56.0	0.61	440	81
1/28	1730 - 1738	7.5	2.5	18.0	72.0	0.78	435	89
	Average	13.5	3.9	20.2	62.2			

(a) STP.

The compositions of the various cyclonic particulate size fractions were analyzed to establish the nature of semivolatile melter emissions. The resultant data appearing in Table A.47 suggest that most of the effluent mass associated with the radiologically important semivolatiles is conveyed to the melter off-gas system as submicron particulate matter.

Gross melter aerosol emissions can be characterized from most of the sampling data which has already been presented. Table A.48 summarizes all gross particulate melter DF values derived from these data. Comparison of this data with corresponding results from the nonboosted PSCM-4 experiment reveal only a slight increase in effective melter entrainment associated with the present test. Based upon past LFCM experiments, it is surprising that the lid heat boosting associated with PSCM-5 did not have a more pronounced effect upon melter entrainment.

Noncondensible melter off-gas data was collected during this experiment using a GC (analyzing for O_2, N_2, CO and CO_2) as well as continuous gas monitors (analyzing for H_2, O_2, CO and CO_2). The GC data is displayed in Figure A.72. Figure A.73 is a plot of the continuous data taken at 15-min intervals, which provides a higher resolution study of H_2, O_2, CO and CO_2 than is afforded by the GC. Baseline drifts were observed in both O_2 and H_2 data. The oxygen data was corrected by approximating the nonlinear drift by a series of linear segments (a piecewise linear relationship). The H_2 drift, which amounted to 0.25% H_2 at the end of the run, was probably due to gradual changes in the dewpoint of the sample stream and was not corrected. The discontinuities present in these data plots are produced by instrument calibrations. Table A.49 summarizes all the noncondensible off-gas compositional data taken during PSCM-5.

Off-gas deposits were taken from the off-gas lines and viewports after PSCM-5. The results are shown in Table A.50. The results are similar to each other and to past runs, which have shown off-gas-line deposits enriched in Cl, Cs, Na, S, Te, Cd, and Ru.

TABLE A.47. Elemental Distribution Across Cyclonic Aerosol Size Fractions

	Elemental Distribution, %							
	Size Fraction 1/26/82				Size Fraction 1/28/82			
Element	16 µm	6 µm	1 µm	<1 µm	16 µm	6 µm	1 µm	<1 µm
Al	60.5	6.1	29.3	4.1	49.7	12.8	30.6	7.0
B	30.3	9.6	53.2	6.9	23.1	14.9	55.4	6.6
Ba	40.4	9.6	43.1	7.0	30.3	17.6	48.0	4.1
Ca	27.1	7.3	58.3	7.3	24.6	14.4	56.1	4.9
Cd	4.6	2.5	18.0	74.8	2.1	3.8	17.2	76.9
Ce	53.9	--	46.1	--	--	--	100.0	--
Cl	2.5	1.6	15.3	80.6	5.2	11.4	60.2	23.3
Co	--	--	58.8	41.2	--	9.7	33.2	57.1
Cr	4.2	2.6	22.0	71.2	19.0	17.9	30.3	32.8
Cs	2.0	1.9	18.6	77.6	1.5	3.8	22.0	72.2
Cu	7.4	4.1	27.6	61.0	5.9	6.4	21.7	66.0
F	64.5	25.8	9.7	0	15.1	11.1	61.7	12.0
Fe	36.1	10.1	46.8	7.0	23.6	17.5	54.2	4.7
K	--	1.3	26.5	72.2	--	4.3	25.9	69.8
La	41.5	9.2	44.3	5.0	31.8	14.7	50.2	3.3
Li	8.9	2.7	29.7	58.7	6.5	7.0	31.0	55.5
Mg	20.2	6.6	66.3	6.9	20.8	14.1	59.9	5.2
Mn	66.2	7.1	21.2	5.6	50.7	14.7	30.1	4.5
Mo	--	--	--	--	--	--	--	100.0
Na	3.3	1.4	15.5	79.8	2.6	3.5	18.5	75.4
Nd	43.4	10.3	46.3	--	25.4	11.8	40.2	22.7
Ni	23.6	9.3	37.9	29.1	24.0	14.9	48.2	12.9
P	--	--	100.0	--	24.6	17.1	58.3	--
Pb	--	--	22.8	77.2	--	11.0	18.8	70.2
Ru	--	--	--	--	--	--	26.2	13.8
Sb	--	--	9.6	90.4	--	--	14.8	85.2
Se	0	5.4	92.0	2.6	33.9	3.2	53.7	9.2
Si	29.0	7.6	50.0	13.4	15.5	12.7	49.1	22.7
S	6.1	18.9	19.1	55.9	21.4	13.2	56.4	8.9
Sr	9.1	2.9	67.7	20.4	36.6	9.1	53.5	0.8
Te	2.4	3.0	52.0	42.7	1.4	4.1	27.1	67.4
Ti	39.5	42.2	5.9	39.5	29.3	20.4	46.3	4.0
Zn	16.2	10.4	34.5	39.0	19.7	18.2	31.1	31.0
Zr	24.7	8.6	58.7	8.2	18.6	17.3	59.0	5.1

TABLE A.48. PSCM-5 Gross Entrainment DFs

Sampling Period		Sample Type(a)	Feed Rate, L/h	Particulate Loading,(b) mg/L	DF
Date	Interval				
1/26/82	1739 - 1749	C	51	0.55	470
1/26/82	2201 - 2345	S	72	0.49	460
1/27/82	0818 - 1130	S	79	0.44	510
1/27/82	1758 - 1805	C	81	0.61	440
1/27/82	1820 - 2135	HEPA	81	--	370
1/28/82	0732 - 1143	S	86	0.48	492
1/28/82	1730 - 1738	C	93	0.78	440
1/28/82	1920 - 2400	HEPA	93	--	670
1/26-28	Average	ALL	80	0.56	480

(a) S = differential sampler; C = cyclone; HEPA = absolute filter.
(b) STP.

PSCM-6 - MARCH 1982

PSCM-6 was a 138-h melter experiment designed to test a new **frit** composition which could prove to form a more durable glass product. This experiment was nominally run under the same conditions as the previous PSCM-5 test (see Table A.1) except that the plenum heater power was increased. However, the last 18 hours of the experiment were conducted without lid heat boosting, allowing comparisons to also be made with the previous PSCM-4 test.

The extent of melter-generated off-gas depositions were assessed at the conclusion of this test. As in the previous PSCM test, off-gas line deposits were generally quite light. The only significant accumulations occurred around devices projecting into the off-gas lines. Qualitatively, less "hairlike" effluent (fine glass strands) was found in the off-gas lines during the present test than during previous tests involving the 131 **frit**.

Overall melter aerosol DFs were determined at two separate feeding rates by HEPA filtration of the melter exhaust stream. These data, which do not include contributions from off-gas line deposits upstream of the filter, appear in Table A.51. These results suggest that gross melter entrainment has been

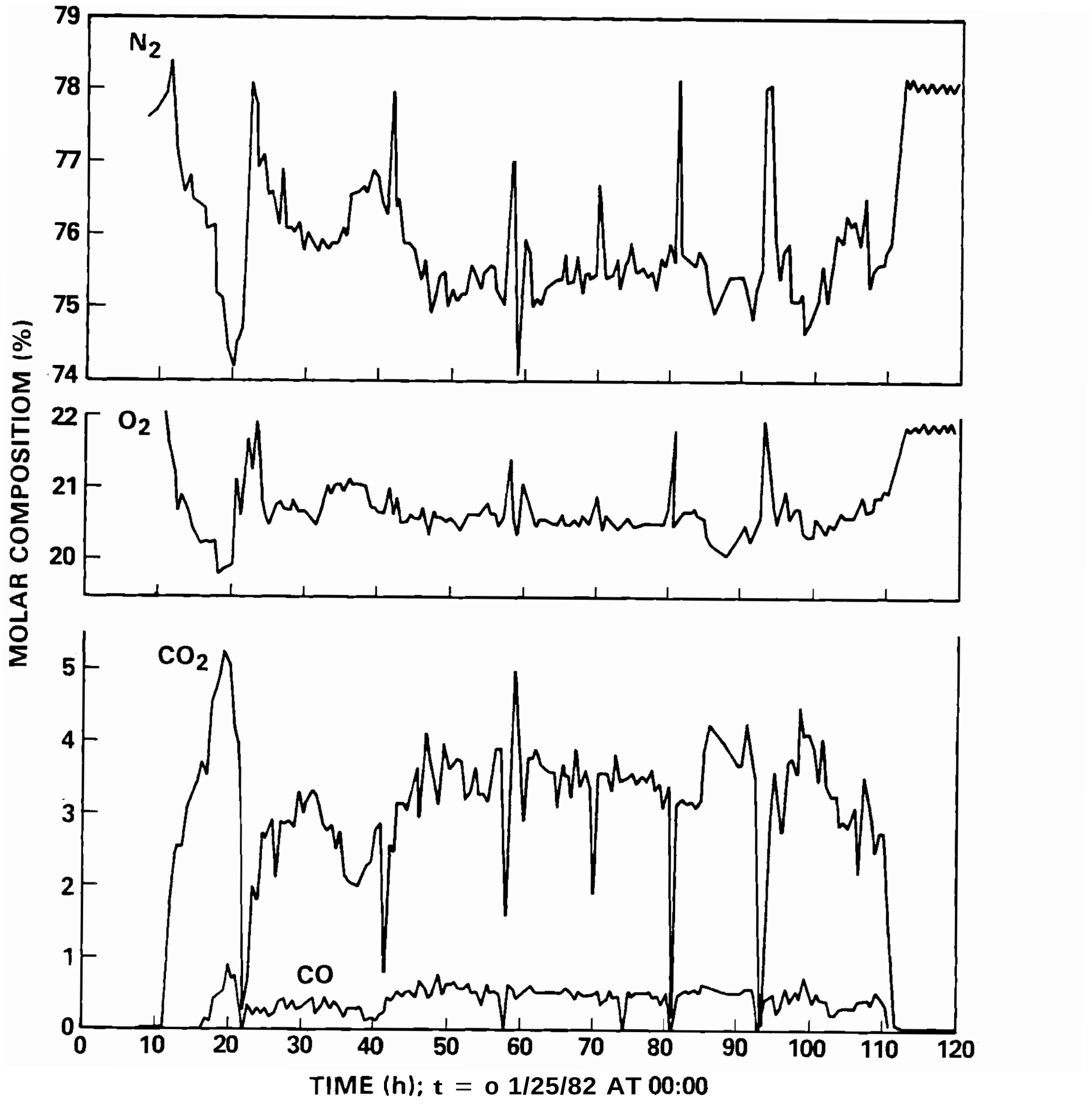

FIGURE A.72. PSCM-5 Off-Gas Composition

reduced more than for both the PSCM-4 and PSCM-5 experiments, which exhibited average DFs of ~500 and 600, respectively.

The effect of melter operation upon individual feed component DFs was also examined during the PSCM-6 experiment. Table A.52 presents partial particulate DFs and total overall melter DFs. The absence of Ru from this table strengthens the argument that the formic acid feed component must be responsible for Ru

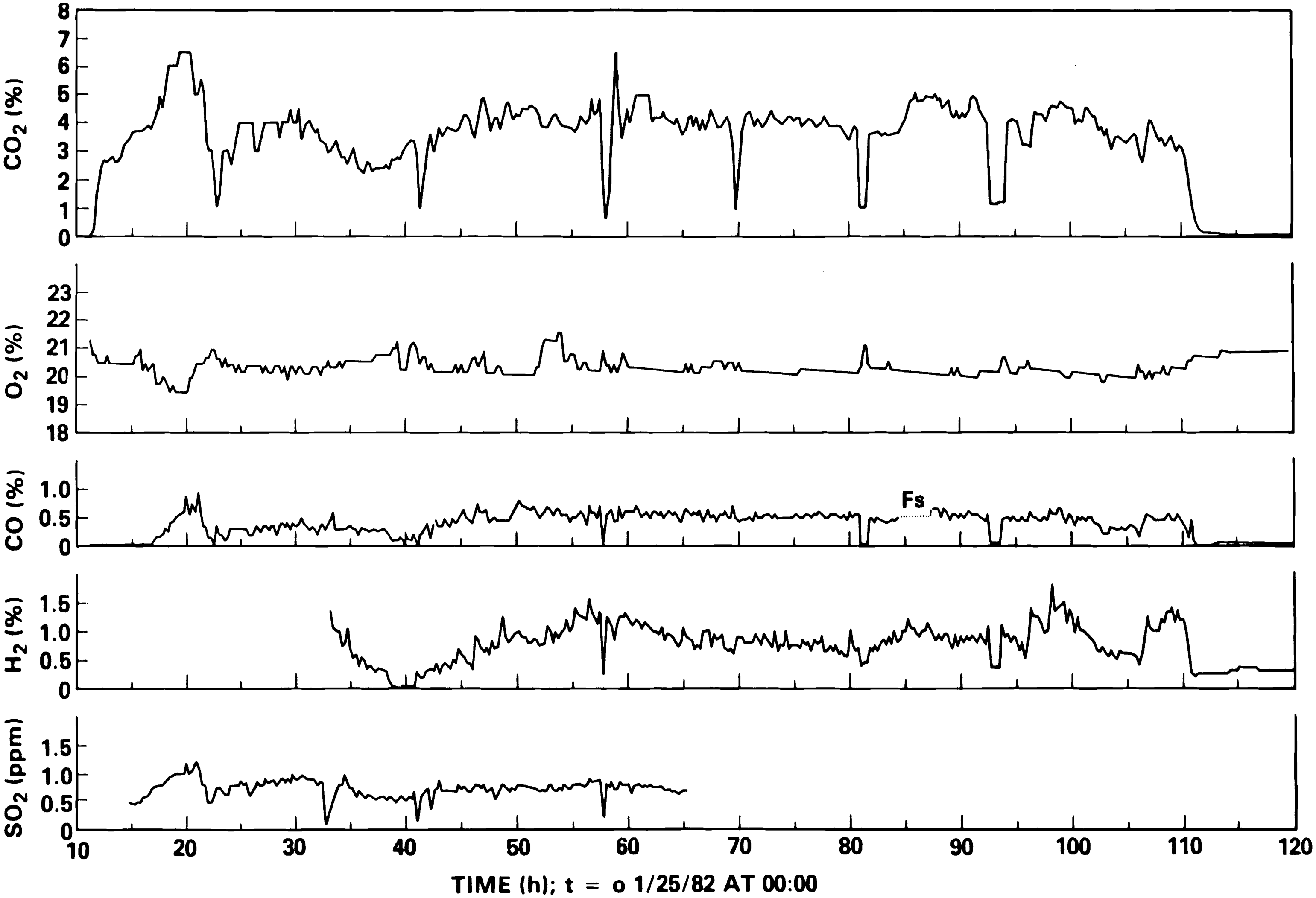

FIGURE A.73. PSCM-5 Off-Gas Composition

TABLE A.49. PSCM-5 Noncondensible Off-Gas Composition

Date	Data Type	Molar Composition, %						
		Dry Basis						
		CO_2	O_2 (a)	N_2	CO	H	SO_2 ppm	H_2O
1/25	Avg.	2.4	21.0	76.4	0.18	--	0.79	--
1/26	Avg.	2.7	20.6	76.2	0.32	0.48	0.75	81.8
1/27	Avg.	3.4	20.6	75.4	0.52	1.0	0.76	80.3
1/28	Avg.	3.2	20.6	75.7	0.45	0.81	--	83.1
1/29	Avg.	2.2	21.1	76.5	0.27	0.96	--	--
1/25-29	Hi	6.5	21.2	76.9	0.9	1.8	1.25	83.1
1/25-29	Lo	2.0	19.8	74.1	0.1	--	0.5	80.3

(a) Includes –1% Ar.

TABLE A.50. PSCM-5 Off-Gas-Line Deposits

Element	Weight Percent			
	South Viewport	North Viewport	Off-Gas Line Exiting Melter	PSCM-5 Feed
Al	0.72	--	1.8	2.7
B	0.92	0.19	2.1	3.3
Ca	0.64	0.02	1.83	1.2
Cd	0.10	0.12	0.15	0.007
Cl	16.0	37.0	5.3	0.40
Cr	0.82	0.85	0.17	<0.01
Cs	2.1	2.1	0.31	0.05
F	0.26	7.3	0.66	<0.01
Fe	5.4	0.30	8.9	8.9
La	0.10	--	0.22	0.30
Li	0.950	0.40	1.53	1.9
Mg	0.21	--	0.61	0.80
Mn	0.56	0.08	1.08	1.8
Na	17.4	14.0	11.0	10.0
Ru	1.22	1.6	0.05	0.014
S	3.2	3.7	1.8	0.05
Si	6.5	0.12	15.3	21.0
Sr	--	--	0.02	0.018
Te	0.17	0.12	0.21	0.009
Ti	0.16	0.02	0.37	0.42
Zr	0.30	0.03	0.22	0.30

TABLE A.51. PSCM-6 Gross Melter Entrainment

Sampling Period		Feed Rate, kg/min	DF
Date	Interval		
3/24	0036 - 1117	1.5	810
3/25-26	2024 - 0040	2.0	720

melter losses (dropout). No airborne Ru has been observed during the last three melter experiments and, yet, idling emissions of particulate Ru are quite easily detected (see section on Melter Idling).

A comparison of the average PSCM-6 feed component DFs with all previous melter tests is tabulated in Table A.53. With the exception of LFCM-7, no dramatic changes in melter effluent characteristics have been observed since the introduction of the new formate feed formulation (PSCM-3).

Particle size sampling of PSCM-6-generated aerosols was also conducted using a cyclonic differential particle-size separator system. Data collected with this device during three distinct operational modes of the PSCM-6 melter are summarized in Table A.54. The size distribution of aerosols collected during PSCM-6 appears to be quite similar to that exhibited by PSCM-5. Moreover, this data suggests that lid heating has, at best, only a minor effect upon the size distribution of melter-generated aerosols.

Compositional analysis of the various particle-size fractions collected by the cyclone was conducted to establish the functional dependence of elemental loss on particle size. The resultant distribution appears in Table A.55. As has been found in all previous cases, the major carrier responsible for semivolatile melter losses is submicron particulate matter.

A summary of all measurements of melter aerosol DFs appears in Table A.56. The agreement between these results is quite satisfying. Moreover, the consistency of these results suggest that melter entrainment has not been strongly influenced by either feeding rates or lid heat boosting techniques. In addition, the average melter entrainment DF associated with PSCM-6 is greater than has been achieved by either the nonboosted PSCM-4 or the boosted PSCM-6

TABLE A.52. PSCM-6 Particulate and Total Feed Components DFs

	DF									
	3/23/82		3/24/82		3/25/82		3/26/82		Average	
Element	Part	Total	Part	Total	Part	Total	Part	Total	Part	Total
Al	1.3×10^{4}	9.3×10^{3}	2.2×10^{4}	2.0×10^{4}	1.8×10^{4}	1.6×10^{4}	5.6×10^{4}	4.4×10^{4}	2.7×10^{4}	2.2×10^{4}
B	2.8×10^{3}	105	3.0×10^{3}	100	3.2×10^{3}	100	1.8×10^{4}	110	6.8×10^{3}	100
Ca	750	730	770	760	890	890	2.4×10^{3}	2.4×10^{3}	1.2×10^{3}	1.2×10^{3}
Cd	2.2	2.2	2.7	2.7	32	32	2.5	2.5	9.9	9.9
Cl	26	2.6	15	1.9	11	2.2	33	4.7	21	2.9
Cs	17	17	14	14	8.0	8.0	17	17	14	14
Fe	1.4×10^{3}	1.4×10^{3}	1.8×10^{3}	1.7×10^{3}	1.8×10^{3}	1.8×10^{3}	2.4×10^{3}	2.3×10^{3}	1.9×10^{3}	1.8×10^{3}
La	2.2×10^{3}	2.2×10^{3}	1.7×10^{3}	1.7×10^{3}	1.8×10^{3}	1.8×10^{3}	2.8×10^{3}	2.8×10^{3}	2.1×10^{3}	2.1×10^{3}
Li	1.2×10^{3}	1.2×10^{3}	1.4×10^{3}	1.4×10^{3}	--	--	1.2×10^{3}	1.2×10^{3}	1.3×10^{3}	1.3×10^{3}
Mg	3.5×10^{3}	3.5×10^{3}	2.3×10^{3}	2.3×10^{3}	2.3×10^{3}	2.3×10^{3}	2.3×10^{4}	2.3×10^{4}	7.8×10^{3}	7.8×10^{3}
Mn	1.4×10^{3}	1.4×10^{3}	1.5×10^{3}	1.5×10^{3}	1.7×10^{3}	1.7×10^{3}	2.6×10^{3}	2.6×10^{3}	1.8×10^{3}	1.8×10^{3}
Na	330	320	360	360	280	280	240	230	300	300
Nd	3.4×10^{3}	3.4×10^{3}	1.8×10^{3}	1.8×10^{3}	1.9×10^{3}	1.9×10^{3}	3×10^{3}	3×10^{3}	2.5×10^{3}	2.5×10^{3}
Ni	1.2×10^{3}	1.2×10^{3}	700	670	1.1×10^{3}	1.0×10^{3}	2.1×10^{3}	1.6×10^{3}	1.3×10^{3}	1.1×10^{3}
S	2.4	1.9	5.0	3.8	22	12	13	4.4	11	5.5
Si	6.3×10^{3}	5.0×10^{3}	3.9×10^{4}	1.5×10^{4}	3.5×10^{4}	1.3×10^{4}	4.5×10^{4}	2×10^{4}	3.1×10^{4}	1.3×10^{4}
Sr	1.7×10^{3}	1.7×10^{3}	1.5×10^{3}	1.5×10^{3}	1.5×10^{3}	1.6×10^{3}	2.4×10^{3}	2.4×10^{3}	1.8×10^{3}	1.8×10^{3}
Te	2.7	2.7	3.5	3.5	2.7	2.7	3.1	3.1	3.0	3.0
Ti	6.0×10^{3}	6.0×10^{3}	5.0×10^{3}	5.0×10^{3}	5.5×10^{3}	5.5×10^{3}	7.2×10^{3}	7.2×10^{3}	5.9×10^{3}	5.9×10^{3}
Zr	9.3×10^{3}	9.3×10^{3}	1.3×10^{4}	1.3×10^{4}	1.7×10^{4}	1.7×10^{4}	4.9×10^{4}	4.9×10^{4}	2.2×10^{4}	2.2×10^{4}

TABLE A.53. PSCM-6 Comparative DFs

Element	PSCM-6 Avg. DF	DF Ratio PSCM-6 / PSCM-5	PSCM-6 / PSCM-4	PSCM-6 / LFCM-7	PSCM-6 / PSCM-3	PSCM-6 / LFCM-6	PSCM-6 / PSCM-2	PSCM-6 / LFCM-4	PSCM-6 / PSCM-1	PSCM-6 / LFCM-3	PSCM-6 / LFCM-2
Al	2.2×10^4	1.6	0.96	120	3.7	67	22	41	2.0	9.2	4.5
B	100	0.71	0.43	1.3	0.50	1.1	0.63	0.77	0.48	0.83	0.39
Ca	1.2×10^3	1.1	0.63	19	1.1	6.7	2.0	4.6	0.65	0.65	1.62
Cd	9.9	1.7	1.1	1.2	--	0.12	0.21	0.14	0.05	0.12	--
Cl	2.9	1.9	0.58	--	0.73	1.1	0.97	1.3	0.94	0.32	0.17
Cs	14	1.5	0.88	1.2	3.7	1.4	4.7	0.25	0.27	2.0	0.35
Fe	1.8×10^3	0.55	1.6	26	1.1	7.8	2.6	6.9	0.47	2.6	4.3
La	2.1×10^3	2.6	--	--	--	--	--	--	--	--	--
Li	1.3×10^3	1.8	0.41	15	0.50	8.1	3.8	4.28	0.68	2.0	1.4
Mg	7.8×10^3	2.2	--	65	0.95	30	8.5	22	0.87	4.3	16
Mn	1.8×10^3	0.25	0.86	24	0.55	55	2.9	4.3	0.32	0.58	1.14
Na	300	1.9	1.7	5.0	0.3	3.3	2.3	0.88	0.36	1.1	0.89
Nd	2.5×10^3	--	--	--	--	--	--	--	--	--	--
Ni	1.1×10^3	1.9	0.79	--	0.12	1.2	--	4.2	0.73	2.6	2.6
S	5.5	1.2	0.34	--	0.69	0.50	0.29	5.5	5.5	1.1	0.29
Si	1.3×10^4	2.4	1.4	110	4.3	46	8.1	31	0.87	5.0	14
Sr	1.8×10^4	--	7.2	33	2.8	6.2	2.8	8.8	0.24	1.20	4.8
Te	3.0	0.97	0.97	0.54	0.09	0.01	0.05	0.05	0.02	0.01	0.05
Ti	5.9×10^3	0.82	0.68	49	1.4	35	4.2	--	--	--	5.36
Zr	2.2×10^4	1.7	4.4	--	--	--	--	--	--	--	--

TABLE A.54. PSCM-6 Differential Particle Size Data

Sampling Period Date	Interval	Wt% Versus Cut Point 16 µm	6 µm	1 µm	<1 µm	Particulate Loading, mg/L	DF	Feed Rate, kg/min	Lid Heat (?)
3/24	1125 - 1137	67.1	0.9	14.9	17.1	0.37	840	1.5	Yes
3/25	1220 - 1229	38.6	--	14.6	46.8	0.41	700	2.0	Yes
3/26	1430 - 1453	32.5	0.7	8.6	58.2	0.54	660	1.3	No

experiments. Although the differences in these DFs are not startling, the result may be a reflection of the new glass formulation which has distinguished the PSCM-6 test.

The noncondensible composition of the melter-generated exhaust was continuously recorded during PSCM-6 using real-time gas monitors. A composite plot of all the gas data generated appears in Figure A.74. The most interesting feature of this figure is the absence of significant combustible gas concentrations throughout most of the run. Only after the lid heaters had been turned off did H_2 and CO concentrations increase to significant levels.

TABLE A.55. Feed Component Distribution Across Cyclonic Aerosol Size Fractions

	Elemental Distribution, %											
	3/24/82				3/25/82				3/26/82			
	Size Fraction				Size Fraction				Size Fraction			
Element	16 µm	6 µm	1 µm	<1 µm	16 µm	6 µm	1 µm	<1 µm	16 µm	6 µm	1 µm	<1 µm
Al	92.8	--	2.8	4.4	75.5	--	13.4	11.1	89.8	--	10.2	--
B	69.7	--	19.7	10.6	39.3	--	35.0	25.7	68.0	--	27.3	4.7
Ba	79.6	--	9.8	10.6	25.6	--	34.0	40.4	77.8	--	26.2	--
Ca	61.4	--	23.5	15.0	41.1	--	38.9	20.0	58.4	--	36.6	5.0
Cd	14.3	--	16.5	69.1	6.3	--	9.9	83.8	12.2	--	10.9	76.9
Ce	100.0	--	--	--	--	--	--	--	100.0	--	--	--
Cl	78.4	--	15.1	6.5	19.8	--	44.4	35.8	1.7	--	6.2	92.2
Co	98.5	--	1.5	--	29.1	--	11.0	59.9	30.1	--	16.0	53.9
Cr	95.5	--	1.9	2.5	91.3	--	4.6	4.1	84.4	--	9.3	6.3
Cs	24.0	--	21.0	55.0	2.55	--	13.2	84.3	23.7	--	9.2	67.1
Cu	65.0	--	13.2	21.8	23.4	--	27.1	49.5	27.5	--	20.7	51.7
Dy	81.8	--	18.2	--	46.8	--	53.2	--	55.6	--	44.4	--
F	93.5	--	4.2	2.3	18.9	--	64.9	16.2	1.7	--	10.0	88.3
Fe	86.4	--	10.1	3.5	73.9	--	23.6	2.4	60.2	--	35.9	3.9
K	24.5	--	16.3	59.2	2.3	--	13.0	84.7	11.3	--	7.5	81.1
La	81.8	--	18.2	--	46.9	--	44.5	8.5	56.5	--	40.1	3.4
Li	37.5	--	8.9	43.6	17.1	--	19.9	63.0	18.4	--	9.1	72.5
Mg	64.3	--	12.4	23.3	35.8	--	28.4	35.9	85.5	--	14.5	--
Mn	66.3	--	31.3	2.5	61.3	--	34.8	4.0	57.9	--	37.7	4.4
Mo	33.4	--	18.5	48.1	33.9	--	15.6	50.5	49.1	--	15.7	35.2
Na	43.0	--	13.5	43.6	8.5	--	14.2	77.3	16.4	--	6.3	77.4
Nd	60.0	--	40.0	--	39.7	--	60.3	--	51.8	--	48.2	--
Ni	94.3	--	5.2	0.5	63.0	--	30.8	6.2	59.6	--	32.0	8.4
P	--	--	--	100.0	--	--	--	100.0	100.0	--	--	--
Pb	15.5	--	15.2	64.3	5.3	--	15.1	79.6	35.4	--	1.2	63.4
Si	64.8	--	12.3	22.8	38.2	--	24.9	36.8	51.9	--	31.4	16.7
S	67.5	--	25.7	6.8	11.8	--	67.0	21.2	77.3	--	2.9	19.8
Sr	60.8	--	27.0	12.2	40.7	--	27.3	32.0	56.5	--	30.0	13.5
Te	14.7	--	17.7	67.6	51.3	--	48.7	--	11.7	--	23.7	64.6
Ti	51.7	--	48.3	--	5.20	--	12.2	82.6	94.6	--	5.4	--
Zn	52.0	--	11.5	36.5	25.8	--	22.9	51.2	40.0	--	22.4	37.7
Zr	79.0	--	21.0	--	55.3	--	39.8	4.9	81.8	--	14.8	3.3

Apparently an 850°C plenum temperature is more than sufficient to burn all combustibles before they were able to pass into the off-gas line. The discontinuities present in these data plots are produced by instrument calibrations. A summary of this gas compositional data is tabulated in Table A.57.

TABLE A.56. PSCM-6 Aerosol DFs

Sampling Period		Sample Type[a]	Feed Rate, L/h	Particulate	
Mo/d	Interval			Loading, mg/L	DF
3/23	1735 - 1920	S	68	0.29	820
3/24	0036 - 1117	HEPA	--	--	810
3/24	1125 - 1137	C	67	0.37	840
3/24	1615 - 1841	S	74	0.25	910
3/25	1220 - 1229	C	90	0.41	700
3/25	1620 - 1835	S	91	0.28	840
3/25	2024 - 0040	HEPA	--	--	720
3/26	0915 - 1141	S	58	0.32	870
3/26	1430 - 1453	C	58	0.54	660
3/23-26	Average	ALL			800

(a) S = sample train; C = cyclone; HEPA = absolute filtration.

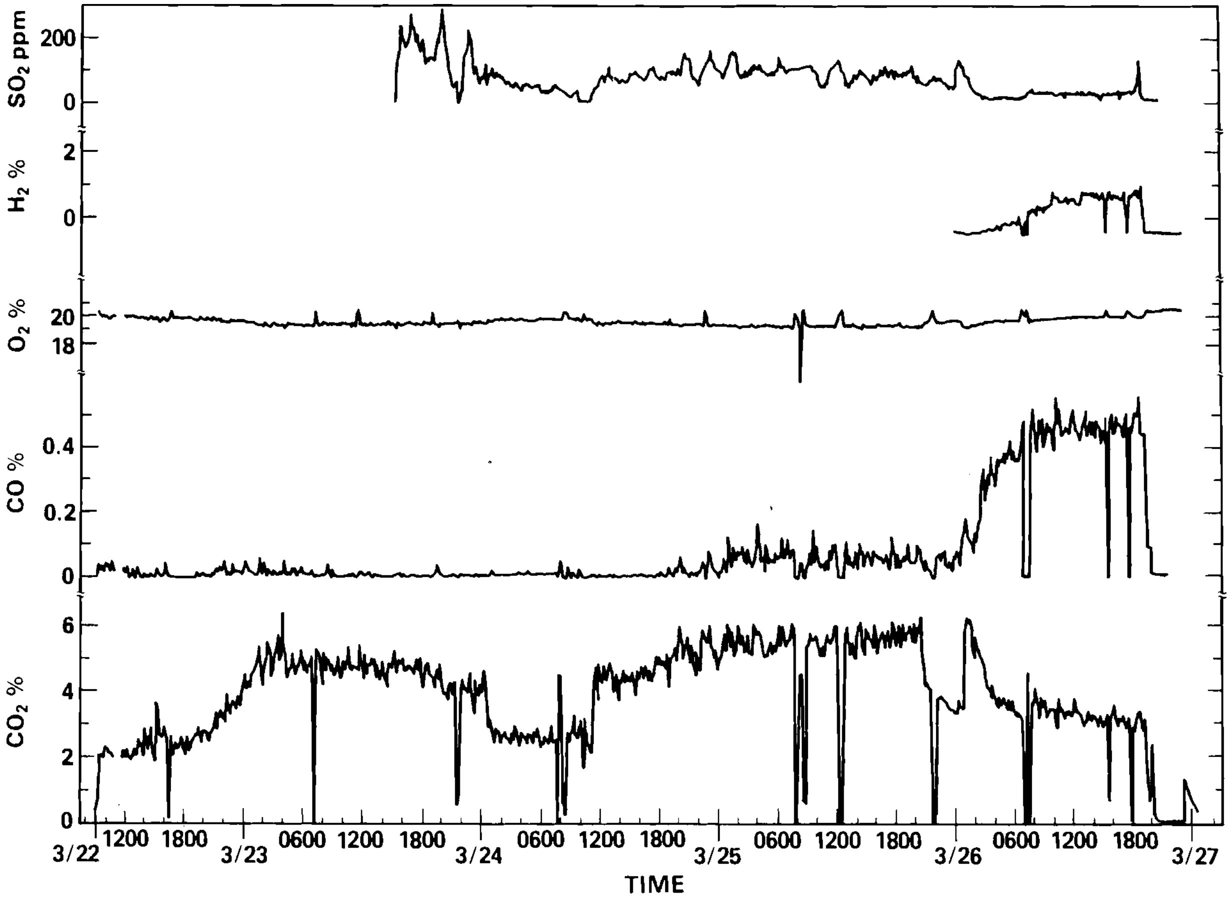

FIGURE A.74. PSCM-6 Off-Gas Composition

TABLE A.57. PSCM-6 Off-Gas Composition

		Molar Composition, %						
	Data	Dry Basis						
Date	Type	CO_2	O_2(a)	N_2	CO		SO_2(a)	H_2O
3/22	Avg.	2.6	19.8		0.002	--	--	--
3/23	Avg.	5.2	19.0	--	0.011	--	154	66
3/24	Avg.	3.9	18.8	--	0.014	--	69	67
3/25	Avg.	5.3	18.7	--	0.060	--	85	69
3/26	Avg.	3.7	19.3	--	0.382	1.1	27	55

(a) ppm.

The nature of combustible gas generation within an operating melter was also investigated during PSCM-6. Figure A.75 portrays the time-dependent compositional behavior of the melter exhaust stream upon feed interruption or termination. With the exception of SO_2, none of the melter-generated gases increased in concentration when feeding was terminated. This fact implies that volatile decomposition and reaction products generated from the melter feed are formed soon after introduction of the feed into the melter environment. Consequently, chemically reactive organic feed components within the melter cold cap apparently do not accumulate significantly under steady-state feeding conditions.

On the other hand, the increase in terminal SO_2 exhaust concentration (illustrated in Figure A.75) suggests that sulfur, as Na_2SO_4, may be accumulating within the melter as a molten salt. Post-run inspection of the idling melter glass surface later proved this. This observation stimulated speculation that accumulations of Na_2SO_4 could be responsible for changes in the melting capacity of liquid-fed melters during the initial –24 h of liquid feeding (the startup phase). Melter emissions of SO_2 during the PSCM-8 test further support this notion, as will be shown in the next section.

Off-gas deposits were taken from the off-gas lines and viewports after PSCM-6. The results are shown in Table A.58. These results are similar to each other and to past runs, which have shown off-gas-line deposits enriched in Cl, Cs, Na, S, Te, Cd, and Ru. The overflow sampling port shows the most

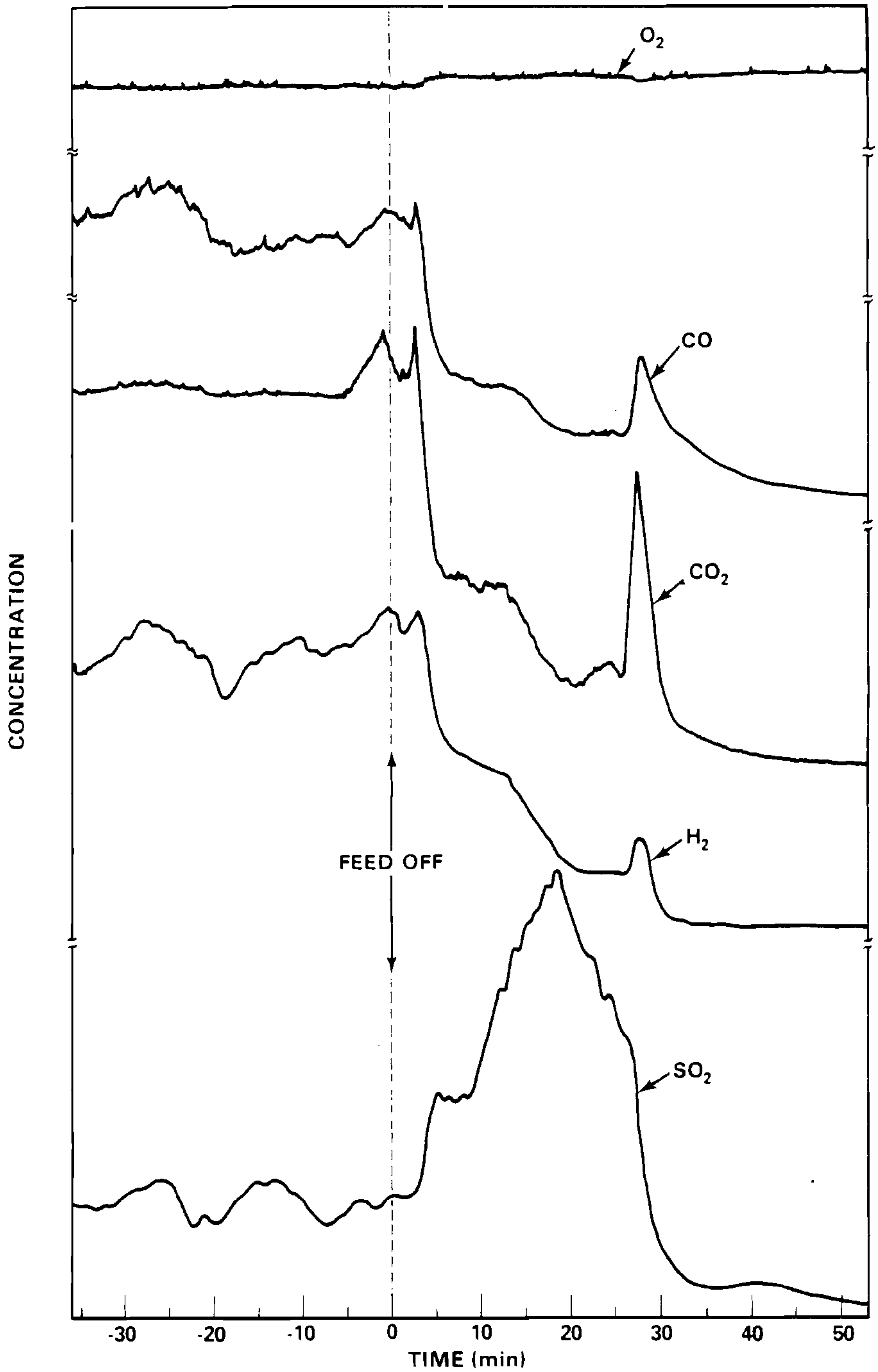

FIGURE A.75. Melter Off-Gas Compositional Behavior Associated with Feed Termination. (The **t** = 30 min compositional spike is due to the injection of a small quantity of liquid feed.)

TABLE A.58. Off-Gas-Line Deposits (wt%) - PSCM-5 & -6

Element	South Viewport	North Viewport	Off-Gas Line Exiting Melter	Overflow Sample Port	Off-Gas Cooling Nozzle	PSCM-6 Feed
Al	0.37	0.33	0.21	1.0	1.39	2.7
B	0.34	0.35	1.41	0.48	0.82	2.2
Ca	0.26	0.34	0.43	0.16	3.84	1.1
Cd	0.20	0.15	0.17	0.02	0.38	0.004
Cl	18.0	17.0	18.0	36.0	4.3	0.42
Cr	3.2	0.04	2.96	0.09	0.21	<0.01
Cs	1.4	1.1	0.52	3.3	0.26	0.05
F	0.25	0.28	1.2	0.39	0.8	<0.01
Fe	2.3	7.6	21.7	0.41	10.9	7.1
La	0.02	0.02	0.01	--	0.15	0.05
Li	0.84	0.51	0.71	0.97	1.33	2.33
Mg	--	--	--	--	0.41	0.46
Mn	0.33	0.41	1.63	--	2.68	2.1
Na	20.4	15.0	8.4	2.3	5.54	7.6
Ru	0.60	1.8	--	0.53	0.04	0.014
S	8.0	4.3	2.8	2.7	3.2	0.05
Si	2.4	2.3	2.4	0.41	16.0	25.0
Sr	0.005	--	--	--	0.05	0.018
Te	0.26	0.35	0.08	0.09	0.76	0.007
Ti	0.05	0.08	0.01	--	0.05	0.07
Zr	0.21	0.08	0.09	0.08	0.34	0.57

enrichment in the semivolatiles because all the deposits come from volatilization, while the other deposits contain volatilized and entrained material.

PSCM-7 - MAY 1982

PSCM-7 was a 115-h nonboosted melter experiment designed to assess the effect of increased slurry solids loading (decreased water loadiny) upon maximum achievable melter feeding rates. In addition, an air sparge was utilized at the conclusion of this experiment to test the effects of forced melter glass convection upon feed melting rates. The new glass former, Frit-165, which was utilized for the first time during PSCM-6, was also employed during PSCM-7.

There was little melter off-gas-line deposition apparent at the conclusion of PSCM-7. The minor accumulations that did occur all formed around off-gas line penetrations as in the past. The overall deposition rate associated with PSCM-7, however, appeared to be less than that of the previous boosted PSCM-6 experiment.

Gross melter DF was measured during steady state feeding by HEPA filtration of the entire melter exhaust stream. The resultant DF, which appears in Table A.59, is significantly higher than the –800 value recorded during PSCM-6, and further confirms the qualitative statement made above with regard to PSCM-7 off-gas line deposition rates.

Differential sampling of the PSCM-7 melter off-gas stream was also conducted in order to establish individual melter feed component DFs. Table A.60 presents these data in terms of partial particulate and total overall melter DFs. As has been the case for all formate feed tests, no airborne Ru was detectable in the PSCM-7 off-gas stream.

A comparison of average melter feed component DFs for PSCM-7 with all previous liquid-fed melter tests is given in Table A.61. Overall, the emissions during PSCM-7 are some of the lowest ever recorded. However, Cs DFs are quite comparable to all previous PSCM formate feed tests.

Particulate size analysis of the melter-generated aerosols was also conducted during PSCM-7. The results of these studies are summarized in Table A.62. The size distributions of PSCM-7 aerosols are much like those from previous PSCM tests (bimodal in nature) except that the overall, distribution is much more heavily weighted by the small diameter component during PSCM-7.

Compositional analysis of the various particle-size fractions collected by the cyclone was conducted to establish the dependence of elemental loss on

TABLE A.59. Gross Melter DF

Date	Period	HEPA Weight, kg Initial	 Final	Feed Rate, kg/min	DF
5/20-21/82	1925 - 0446	9.20	9.34	1.1	1.4×10^3

TABLE A.60. PSCM-7 Particulate and Total Feed Components DFs

Element	5/18 DFs Part	5/18 DFs Total	5/20 DFs Part	5/20 DFs Total	5/21 DFs[(a)] Part	5/21 DFs[(a)] Total	Average DFs Part	Average DFs Total
Al	3.3×10^4	2.6×10^4	4.7×10^4	4.3×10^4	8.2×10^3	8.2×10^3	29,000	2,600
B	1.2×10^4	204	1.0×10^4	214	1.9×10^3	202	8,000	210
Ca	3.5×10^3	3.2×10^3	3.8×10^3	3.6×10^3	921	910	2,700	2,600
Cd	8.0	8.0	4.0	4.0	7.4	7.4	6.5	6.5
Cl	15.7	11	12	4.8	9.5	3.3	12	6.4
Cs	16.2	16.2	13	13	10.2	10.2	13	13
Fe	3.9×10^3	3.9×10^3	5.2×10^3	3.0×10^3	1.4×10^3	1.4×10^3	3,500	2800
La	3.2×10^3	3.2×10^3	6.5×10^3	6.5×10^3	1.2×10^3	1.2×10^3	3,600	3,600
Li	1.4×10^3	1.4×10^3	1.3×10^3	1.3×10^3	678	678	1,100	1,100
Mg	1.5×10^4	1.5×10^4	1.4×10^4	1.4×10^4	3.2×10^3	3.2×10^3	11,000	11,000
Mn	5.5×10^3	5.4×10^3	4.8×10^3	4.4×10^3	1.2×10^3	1.2×10^3	3,800	3,700
Na	345	345	323	322	191	191	290	290
Nd	6.4×10^3	6.4×10^3	5.7×10^3	5.7×10^3	311	311	4,100	4,100
Ni	6.2×10^3	5.4×10^3	6.0×10^3	1.6×10^3	2.7×10^3	2.4×10^3	5,000	3,100
S	40	3.0	359	1	64.9	4.6	150	2.9
Sb	730	730	793	793	620	620	710	710
Se	2.8	2.8	90	90	28.8	28.8	40	40
Si	1.5×10^4	1.1×10^4	1.9×10^4	9.8×10^3	5.4×10^3	5.3×10^3	13,000	8,700
Sr	5.3×10^3	5.3×10^3	6.2×10^3	6.2×10^3	960	960	4,200	4,200
Te	8.4	8.4	23	23	43.3	43.3	24	24
Ti	7.6×10^3	7.6×10^3	3.3×10^4	3.3×10^4	5.1×10^3	5.1×10^3	15,000	15,000
Zr	2.0×10^4	2.0×10^4	2.8×10^4	3.3×10^3	4.9×10^3	4.9×10^3	18,000	9,400

(a) Air sparge In operation.

particle size. The resultant distributional data appear in Table A.63. As in all previous cases, the major carrier responsible for semivolatile melter losses is submicron particulate matter.

The performance of the newly installed venturi ejector was also evaluated during the present test. In this study, off-gas aerosol DFs were established for individual effluent species. This data appears in Table A.64. The values listed are consistent with anticipated performance.

A summary of melter-scrubber performance as determined by off-gas particulate loading appears in Table A.65. The data are quite consistent. The low melter and high scrubber DFs recorded on 5/21 resulted from melter sparging. Apparently, sparginy increased gross feed component carryover into the

TABLE A.61. PSCM-7 Comparative DFs

Element	PSCM-7 Average DF	DF Ratio										
		PSCM-7 / PSCM-6	PSCM-7 / PSCM-5	PSCM-7 / PSCM-4	PSCM-7 / LFCM-7	PSCM-7 / PSCM-3	PSCM-7 / LFCM-6	PSCM-7 / PSCM-2	PSCM-7 / LFCM-4	PSCM-7 / PSCM-1	PSCM-7 / LFCM-3	PSCM-7 / LFCM-2
Al	26,000	1.2	1.8	1.1	135.0	4.3	78.0	26.0	49.0	2.3	11.0	5.2
B	210	2.1	1.5	0.9	2.8	1.0	2.3	1.3	1.6	1.0	1.7	0.80
Ca	2,600	2.1	2.3	1.4	42.0	2.3	14.0	4.2	1.0	1.4	1.4	3.5
Cd	6.5	0.65	1.1	0.70	0.81	--	0.08	0.14	0.09	0.03	0.08	0.02
Cl	6.4	2.2	4.2	1.3	--	1.6	2.4	2.1	2.9	2.0	0.71	0.37
Cs	13	0.94	1.4	0.82	1.1	3.5	1.3	4.4	0.23	0.26	1.9	0.33
Fe	2,800	1.6	2.6	1.4	42.0	1.8	12.0	4.1	11.0	0.79	4.2	6.7
La	3,600	1.7	0.36	--	--	--	--	--	--	--	--	--
Li	1,100	0.87	1.5	0.35	12.0	0.43	7.0	3.3	3.6	0.59	1.7	1.2
Mg	11,000	1.4	3.1	0.01	89.0	1.3	41.0	11.0	30.0	1.2	6.0	22
Mn	3,700	2.0	0.52	1.8	48.0	1.1	11.0	5.8	8.7	0.64	1.2	2.3
Na	290	0.95	1.8	1.6	4.8	0.32	3.2	2.2	0.84	0.34	1.0	0.85
Nd	4,100	1.65	--	--	--	--	--	--	--	--	--	--
Ni	3,100	2.8	5.4	2.2	--	0.33	3.4	--	12.0	2.1	7.3	7.3
S	2.9	0.52	0.64	0.18	--	0.36	0.26	0.15	2.9	2.9	0.57	0.15
Sb	710	--	1.6	--	10.0	--	--	7.1	0.40	--	--	1.5
Se	40	--	0.31	--	40.0	--	--	--	--	--	--	0.19
Si	8,700	0.67	1.6	0.95	72.0	2.9	31.0	5.4	20.0	0.58	3.4	9.3
Sr	4,200	2.3	--	16.0	75.0	6.5	14.0	6.5	20.0	0.56	2.8	11
Te	24	8.3	8.0	8.0	4.5	0.78	0.12	0.43	0.40	0.15	0.09	0.41
Ti	15,000	2.6	2.1	1.8	130.0	3.7	89.0	10.0	0.02	0.02	0.05	13
Zr	9,400	0.43	0.72	1.9	0.01	0.01	0.01	0.01	0.01	0.01	0.01	0.01

TABLE A.62. Cyclonic Melter Aerosol Size Analysis

Date	Period	Feed Rate, kg/min	Weight Percent 16 μm	 6 μm	 1 μm	 <1 μm
5/19/82	1645 - 1806	1.1	7.6	4.0	9.4	79.0
5/21/82	0542 - 0729	1.2	7.3	2.5	9.4	80.8

off-gas system, which reduced overall melter emission performance (DF). However, the fact that the scrubber DF increased during this same period suggests that melter sparging must generate large-diameter aerosols which are easily removed by the close-coupled ejector venturi. Moreover, the overall system DF (melter + scrubber) during sparging is not significantly different than during nonsparging periods, which further reinforces the above argument.

The PSCM-7 melter test was distinguished by very low inleakage rates (10 to 15 scfm). Moreover, since this test did not employ lid heaters, plenum oxidation rates of combustible gases were quite slow. As a result, very high concentrations of H_2 and CO were generated by the melter throughout the test as is clearly shown in Figure A.76. Although CO presented no particular off-gas problem, melter exhaust stream dilution was required to maintain H_2 below 70% of its lower flammability limit. The peak concentration of H_2 recorded during this test was 3.5%.

After PSCM-7, molten salt samples were skimmed from the glass surface of the melter. Samples were taken four times on different days to determine the fate of the salt layer. The weight and molar percents for each element are shown in Table A.66. The salt layer diminished with time, and the last sample taken on 6/08 was very difficult to obtain. The last two samples may have had some glass mixed in with the salt, so only the leachable constituents are reported. The salt layer appears to volatilize and, in a few weeks, is almost indistinguishable from the molten glass. The chloride salts disappear first. The majority of the salt layer appears to be Na_2SO_4. An attempt to match up cations and anions is shown in Table A.67, where Na was combined with sulfates, where possible.

TABLE A.63. Elemental Distribution Across Cyclonic Size Fractions

	Elemental Distribution, %									
	Size Fraction 5/19/82					Size Fraction 5/31/82				
Element	16 µm	6 µm	1 µm	<1 µm	Cond.	16 µm	6 µm	1 µm	<1 µm	Cond.
Al	67.0	10.2	20.8	2.1	--	41.8	8.5	17.5	32.2	--
B	0.8	0.2	0.7	0.1	98.2	0.9	0.3	1.02	0.07	97.7
Ba	49.5	--	50.5	--	--	21.32	19.8	58.8	--	--
Ca	34.2	11.4	44.2	10.2	--	31.28	13.53	43.6	8.9	2.6
Cd	1.7	1.4	4.7	92.3	--	1.9	2.6	5.9	89.6	--
Cl	1.0	0.8	3.1	26.0	69.1	2.1	2.4	4.9	46.7	43.9
Co	7.3	--	12.4	80.3	--	5.8	5.1	9.4	79.7	--
Cr	22.9	5.2	9.7	6.7	55.4	29.3	19.0	10.6	22.5	18.5
Cs	1.3	1.3	4.6	92.8	--	1.2	1.5	3.7	93.6	--
Cu	5.2	3.8	10.2	78.0	2.8	7.6	3.8	9.9	78.7	--
Dy	41.4	9.7	48.8	--	--	35.9	12.7	51.4	--	--
F	1.2	0.7	2.5	14.9	80.6	0.8	0.9	1.9	13.2	83.1
Fe	30.2	10.5	46.8	9.0	3.6	28.1	12.8	48.3	6.6	4.2
La	31.2	11.1	47.5	10.3	--	29.8	13.6	52.2	4.4	--
Li	6.7	2.2	8.3	82.8	--	6.7	3.8	8.8	80.7	--
Mg	58.6	8.1	33.3	--	--	59.3	--	40.7	--	--
Mn	34.3	10.9	45.5	7.2	2.0	32.2	14.0	47.0	6.2	0.6
Mo	56.6	--	43.4	--	--	24.5	--	12.0	63.4	--
Na	2.8	1.6	5.8	89.8	--	3.2	2.9	5.6	88.3	--
Nd	32.6	9.5	47.6	10.3	--	29.4	11.2	46.4	13.0	--
Ni	21.7	8.3	25.6	18.0	26.4	27.9	13.1	26.4	21.8	10.8
P	8.3	--	--	91.7	--	--	--	--	--	--
Pb	1.5	1.4	5.9	91.1	--	3.3	3.0	9.0	84.7	--
S	--	--	0.2	0.7	99.1	--	0.1	0.3	1.0	98.6
Sb	19.1	3.0	13.1	64.8	--	9.8	5.2	9.0	76.0	--
Se	9.0	4.9	6.9	79.3	--	8.6	9.1	15.8	66.5	--
Si	53.3	9.7	27.9	5.4	3.7	47.7	13.8	27.1	5.1	6.2
Sr	38.9	11.5	49.6	--	--	27.5	13.6	25.9	33.1	--
Te	10.0	6.6	31.0	52.4	--	1.8	2.5	7.2	88.5	--
Ti	13.4	35.0	34.3	17.3	--	29.4	6.5	13.2	50.8	--
Zn	1.5	1.0	2.9	84.7	9.8	9.6	3.8	23.5	22.3	40.9
Zr	54.7	14.6	19.9	10.8	--	48.3	15.2	29.7	6.8	--

TABLE A.64. PSCM-7 Close-Coupled Scrubber Particulate DFs

Element	DFs			
	5/18	5/20	5/21	Avg.
Al	--	2.0	160	81
B	1.9	1.7	12	5.2
Ba	--	1.0	--	--
Ca	50	32	190	90
Cd	17	19	21	19
Co	--	36	--	36
Cr	33	--	32	32
Cs	17	17	21	18
Cu	23	16	22	20
F	11	10	12	11
Fe	350	43	400	260
La	--	14	90	52
Li	20	22	29	23
Mn	430	410	560	470
Na	17	20	24	20
Nd	--	--	140	140
Ni	82	46	220	120
Pb	2.7	16	20	12
S	12	3.3	7.7	7.7
Sb	19	27	24	23
Se	17	3.0	3.6	7.9
Si	200	25	330	180
Sr	--	9.1	--	9.1
Te	19	15	9.3	14
Ti	--	6.1	21	13
Zn	4.1	23	43	23
Zr	49	9.1	51	36

PSCM-8 - JUNE 1982

PSCM-8 was a boosted 232-h test which utilized a new slurry feed composition possessing a higher alumina and lower iron content than the standard feed formulation. This new feed was expected to produce a higher viscosity ylass than observed with Frit-165. Since both feed and glass alterations might be expected to affect the effluent characteristics of the slurry-fed melter, off-gas studies were of special interest during the test.

TABLE A.65. PSCM-7 Gross Aerosol DFs

Sampling Period		Sample Type	Feed Rate, kg/min	DF	
Date	Interval			Melter	Scrubber
5/18	1755 - 2033	Scrub	0.75	1100	8
5/19	1645 - 1806	Cyclo	1.10	1300	--
5/20	1442 - 1715	Scrub	1.15	1100	9
5/20	1925 - 0446	HEPA	1.1	1400	--
5/21	0542 - 0723	Cyclo	1.15	1300	10
5/21(a)	1620 - 1731	Scrub	1.40	540	18

(a) Sparge testing.

Because of its length, this experiment was a good test of the total melter off-gas system. The only difficulty encountered was associated with the buildup of entrained matter about the off-gas cooling spray nozzle (see Figure A.2). These spray nozzle accumulations restricted melter off-gas flow, which necessitated cleaning halfway through the PSCM-8 experiment. The soft, nonfused deposits were easily removed. Figure A.77 is a photograph of the spray nozzle deposits that had accumulated by the end of the PSCM-8 test. These deposits had formed after the mid-run cleaning operation. The only other off-gas-line depositions were found around line penetrations, and these were quite limited in size. Figure A.78 illustrates the unobstructed condition of the horizontal off-gas line between the melter and the close coupled scrubber at the end of the PSCM-8.

Although accumulations of melter entrained matter restricted melter off-gas flow, the extent of effective entrainment was moderately low. Data from HEPA filtration of the entire melter exhaust stream was used to establish overall melter aerosol performance. This data appears in Table A.68.

Although this DF value for PSCM-8 is lower than that achieved in PSCM-7, it is quite respectable when compared to results obtained from all other PSCM tests utilizing formate feed.

Melter performance with respect to individual feed components was also established during PSCM-8. This data appears in Table A.69. The most startling aspect of data present in this table is the high DF values recorded for

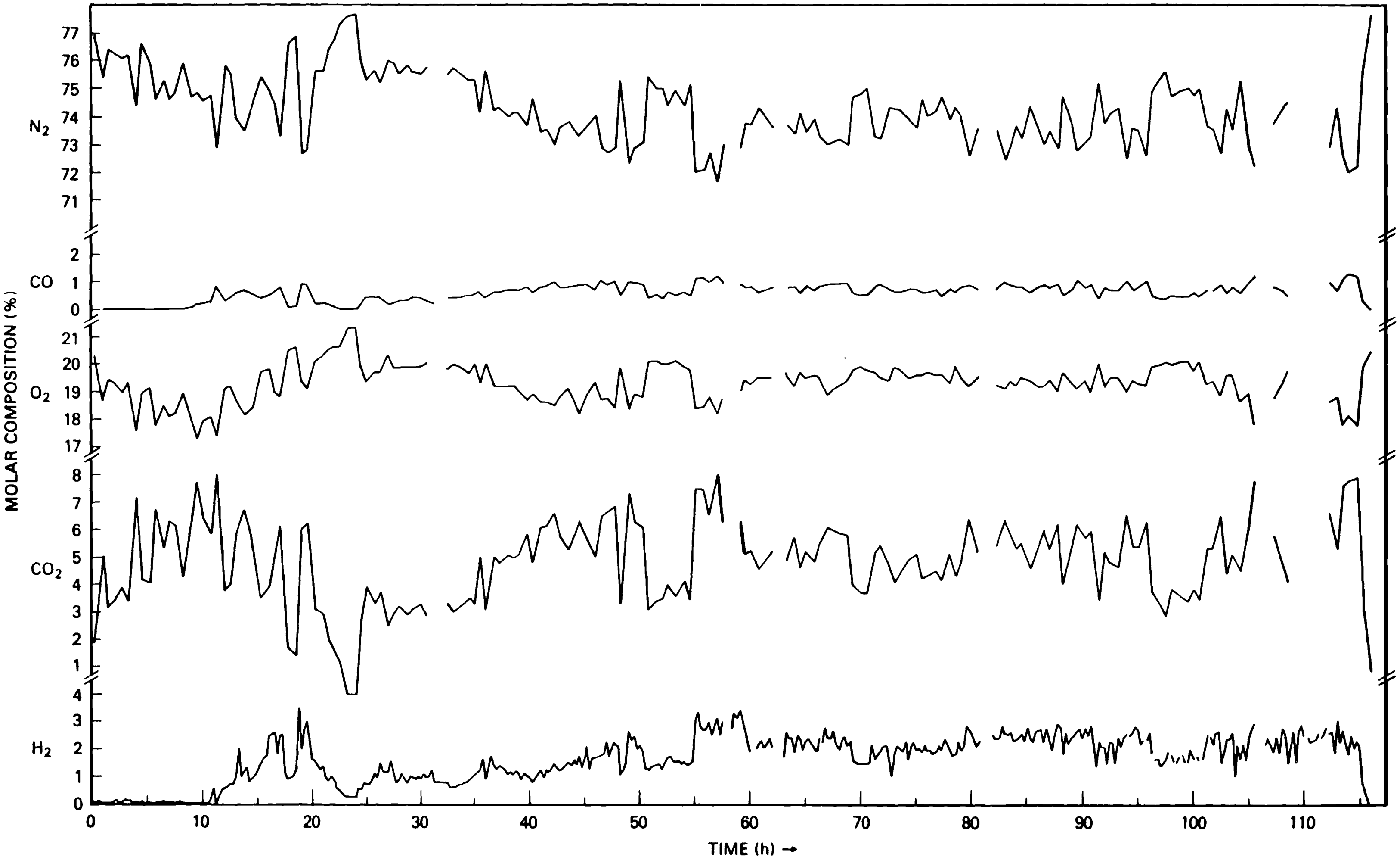

FIGURE A.76. PSCM-7 Off-Gas Composition

TABLE A.66. Melter Surface Samples After PSCM-7

Element	5/22/81		5/24/82		6/01/82		6/08/82	
	Wt%	M[(a)]	Wt%	M[(a)]	Wt%	M[(a)]	Wt%	M[(a)]
B	0.08	0.007	0.08	0.007	0.28	0.02	0.005	--
Ca	0.46	0.011	0.50	0.013	0.11	0.003	0.04	0.001
Cl	20.1	0.57	0.21	0.01	2.9	0.08	1.6	0.05
Cs	0.13	0.001	0.05	--	--	--	--	--
F	0.73	0.04	0.20	0.01	0.28	0.02	0.19	0.01
Li	3.4	0.49	3.7	0.53	4.0	0.58	0.35	0.05
Na	28.2	1.22	25.5	1.11	26.8	1.16	25.7	1.12
S	49.6	0.52	71.2	0.74	62.8	0.65	70.0	0.73
Si	0.04	0.001	0.04	0.001	2.8	0.10	--	--
Sr	0.008	--	0.02	--	0.02	--	0.005	--
TOTAL	2.86	2.42	2.61	1.96				

(a) M = moles/100 grams.

TABLE A.67. Assumed Salt Compounds for PSCM-7, wt%

Elemental Oxides	Weight Percent			
	5/22	5/24	6/01	6/08
Na_2SO_4	73.8	79.0	82.4	79.5
NaCl	10.0	--	--	--
Li_2SO_4	--	20.0	7.7	--
LiCl	15.0	0.4	3.4	2.1
LiF	0.5	0.2	0.5	0.2
	0.5	1.0	2.3	--
SO_4[(a)]	--	--	--	17.0

(a) Ions with unknown counterpart.

Cs. PSCM-8 exhibited a Cs DF a factor of 10 higher than the average obtained from all previous formate feed tests. In fact, the greatest formate feed Cs DF recorded prior to the PSCM-8 test was 16, which was achieved during the non-boosted PSCM-4 experiment. Glass compositional data further reinforces this Cs off-gas data by reporting much higher Cs capacities than have been experienced

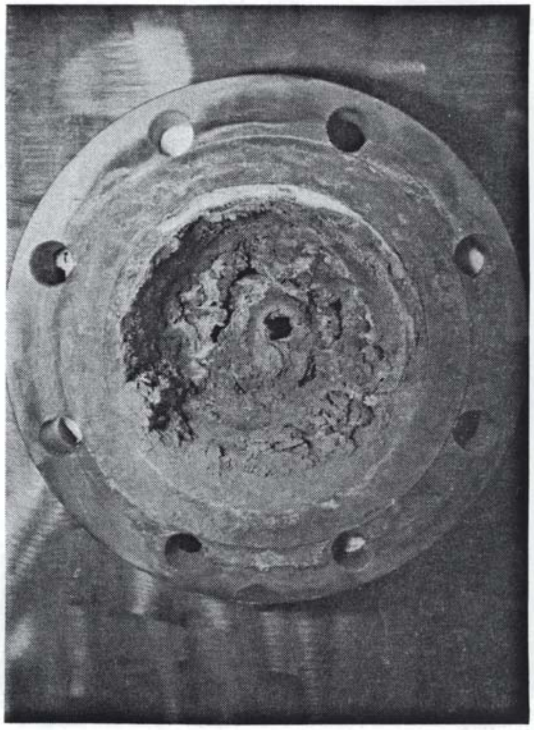

FIGURE A.77. Material Buildup in Melter Plenum Exhaust Port - Axial Hose was Where Spray Nozzle was Located

FIGURE A.78. Horizontal Off-Gas Line

TABLE A.68. Gross Melter Aerosol DF

Date	Interval	Feed Rate, kg/min	DF
6/19-20	0447 - 1426	1.7	820

in the past. These results are quite exciting and have important implication if these results are reproducible. This new feed/glass formulation should be tested further.

The average melter feed component DFs listed in Table A.69 are compared with DFs collected from all previous melter tests in Table A.70. These results show that, with the exception of Cs, PSCM-8 exhibits rather average emission performance characteristics.

TABLE A.69. PSCM-8 Particulate and Total Melter Feed Component DFs

Element	6/17 DFs		6/18 DFs		6/22 DFs		6/23 DFs		Average DF	
	Part	Total	Part	Total	Part	Total	Part	Total	Part	Total
Al	2600	2600	3100	3100	1795	1795	1100	1100	2200	2200
B	2900	150	2800	120	1800	1200	950	97	2100	390
Ca	340	340	370	340	440	440	260	260	350	340
Cd	4.8	4.8	3.8	3.8	5.0	5.0	8.8	8.8	5.6	5.6
Cl	35	4.5	39	4.2	20	3.6	44	6.6	34	4.7
Cs	120	120	86	86	72	72	250	250	130	130
Fe	630	630	640	640	640	640	380	380	570	570
La	360	360	520	520	500	500	980	980	590	590
Li	1700	1700	1500	1500	2100	2100	930	930	1600	1600
Mg	1940	1940	2100	2100	1500	1500	660	660	1600	1600
Mn	590	590	750	750	660	660	400	400	600	600
Na	830	830	770	770	760	760	490	490	710	710
Nd	400	400	500	500	450	450	790	790	540	540
Ni	3600	3600	3700	3700	3000	3000	5900	5900	4000	4000
S	20	12	16	9.7	30	14	13	7.3	19	10
Sb	52	52	110	110	120	120	230	230	130	130
Se	18	4.0	23	2.4	22	2.2	27	1.5	22	2.5
Si	2600	2600	2600	2600	1600	1600	760	760	1900	1900
Sr	560	560	570	570	670	670	390	390	550	550
Te	6.6	6.6	8.3	8.3	6.2	6.2	9.5	9.5	7.6	7.6
Ti	3300	3300	2200	2200	1300	1300	690	690	1900	1900
Zr	2500	2500	2600	2600	1600	1600	700	700	1900	1900

Size distributions of PSCM-8 aerosols established using a cyclonic sampliny system are summarized in Table A.71. As expected, the overall particle size distribution is bimodal. However, the small-diameter component of this distribution is not so heavily weighted as it was in PSCM-7. The usual differences in composition between the large- and small-diameter fractions are also present in PSCM-8 samples, as illustrated in Table A.72. Semivolatile aerosols are again found to be almost exclusively submicron. Selenium volatility is also suggested, but caution in interpretation is advised since this has not been observed previously, and since a new analytical technique for Se analysis was employed.

The off-gas performance of the close-coupled venturi ejector was also evaluated for melter-generated aerosols. Table A.73 presents scrubber DF values evaluated for individual aerosol feed components. The DFs obtained

TABLE A.70. PSCM-8 Comparative DFs

Element	PSCM-8 Avy. DF	DF Ratio											
		PSCM-8/PSCM-7	PSCM-8/PSCM-6	PSCM-8/PSCM-5	PSCM-8/PSCM-4	PSCM-8/LFCM-7	PSCM-8/PSCM-3	PSCM-8/LFCM-6	PSCM-8/PSCM-2	PSCM-8/LFCM-4	PSCM-8/PSCM-1	PSCM-8/LFCM-3	PSCM-8/LFCM-2
Al	2200	0.08	0.10	0.15	0.09	11	0.36	6.5	2.2	4.0	0.20	0.90	0.44
B	390	1.9	3.9	2.8	1.7	5.2	2.0	4.4	2.4	3.0	1.9	3.2	1.5
Ca	340	0.13	0.29	0.31	0.18	5.6	0.31	1.9	0.57	1.3	0.19	0.19	0.47
Cd	5.6	0.87	0.57	0.98	0.61	0.70	--	0.07	0.12	0.08	0.03	0.07	0.02
Cl	4.7	0.74	1.6	3.2	0.95	--	1.2	1.8	1.6	2.2	1.5	0.53	0.28
Cs	130	10.0	9.4	14	8.2	11	34	13	44	2.3	2.6	18	3.3
Fe	570	0.21	0.32	0.52	0.29	8.3	0.36	2.5	0.84	2.2	0.15	0.83	1.4
La	590	0.16	0.28	0.06	--	--	--	--	--	--	--	--	--
Li	1600	1.4	1.2	2.1	0.49	17	0.60	9.7	4.6	5.0	0.82	2.4	1.7
Mg	1600	0.14	0.20	0.44	--	12	0.19	6.0	1.7	4.4	0.17	0.86	3.2
Mn	600	0.16	0.33	0.08	0.29	7.9	0.18	1.8	0.95	1.4	0.11	0.19	0.38
Na	710	2.5	2.4	4.4	4.0	11	0.79	7.9	5.5	2.1	0.86	2.5	2.1
Nd	540	0.13	0.21	--	--	--	--	--	--	--	--	--	--
Ni	4000	1.3	3.7	7.0	2.9	--	0.43	4.4	--	15	2.7	9.4	9.4
S	10	3.8	2.0	2.4	0.67	--	1.3	0.98	0.57	10	10	2.2	0.57
Sb	130	0.18	--	0.29	--	1.9	--	--	1.3	0.07	--	--	0.27
Se	2.5	0.06	--	0.02	--	2.5	--	--	--	--	--	--	0.01
Si	1900	0.22	0.15	0.36	0.21	15	0.63	6.8	1.2	4.5	0.13	0.73	2.0
Sr	550	0.13	0.30	--	2.2	1.0	0.86	1.9	0.86	2.7	0.07	0.37	1.4
Te	7.6	0.31	2.6	2.5	2.5	1.4	0.24	0.04	0.13	0.12	0.05	0.03	0.13
Ti	1900	0.12	0.32	0.26	0.21	15	0.45	11	1.3	--	--	--	1.7
Zr	1900	0.20	0.08	0.14	0.37	--	--	--	--	--	--	--	--

TABLE A.71. PSCM-8 Particulate Analysis of Melter-Generated Aerosols

Sampling Period		Weight Percent Versus Cut Point			
Date	Interval	16 µm	6 pm	1 µm	<1 µm
6/18	0833 - 1004	38.2	5.0	24.1	32.7
6/21	0815 - 1200	41.2	7.3	21.1	30.4
6/22	2010 - 2301	52.8	9.5	13.5	24.2

during the present test are, on the average, much higher than those recorded during the previous PSCM-7 test. This is due to differences in both particle size and water loading. PSCM-8 generated larger aerosols and produced much higher off-gas water loadings [80% versus 60%] than did PSCM-7.

The size and composition of aerosols exiting the close-coupled off-gas scrubber were investigated using a scanning electron microscope (SEM). Figure A.79 shows the collected particulates under various degrees of magnification. Two filter samples were taken, corresponding to a low (21 L) and high (120 L) volume exposure. Unfortunately, both filters were too highly loaded to conduct a statistically significant particle size analysis. However, by comparing filter pore size (0.2 µm) with impacted particulate matter at 10,000X magnification, it is clear that the particle size distribution of aerosols being carried downstream of the close-coupled scrubber is weighted quite strongly by submicron particulate matter. The composition and size of representative particles which are called out in Figure A.79 are detailed in Figure A.80. Clearly, the concept of average composition has no real meaning when dealing with individual particles.

Table A.74 summarizes the gross aerosol off-gas performance of both the PSCM melter and the close-coupled scrubber during PSCM-8. The deterioration of melter performance on 6/23 was caused by unstable melter operation which occurred when the flow of feed was interrupted. The melter was not able to recover from this interruption and overfeeding resulted. As can be seen from Table A.74, the overall melter performance deteriorated, but the scrubber efficiency increased which acted to maintain the overall system performance. As in the sparging situation in PSCM-7, overfeeding apparently generates relatively large diameter aerosols which are easily removed by the close-coupled ejector venturi.

TABLE A.72. PSCM-8 Elemental Distribution Across Cyclonic Fractions

	Elemental Distribution, %														
	6/18 Sample Fraction					6/21 Sample Fraction					6/22 Sample Fraction				
Element	16 µm	6 µm	1 µm	<1 µm	Cond.	16 µm	6 µm	1 µm	<1 µm	Cond.	16 µm	6 µm	1 µm	<1 µm	Cond.
Al	80.3	10.3	9.0	0.3	--	75.8	3.3	11.4	1.0	8.5	66.5	7.3	4.5	21.7	--
B	2.4	0.2	0.4	0.1	96.9	2.6	0.1	0.4	0.1	96.9	4.6	0.6	0.6	0.8	93.4
Ba	88.5	11.5	--	--	--	66.1	--	33.9	--	--	71.5	28.5	--	--	--
Ca	29.5	8.0	43.7	18.8	--	29.5	8.6	46.6	15.3	--	39.0	13.5	30.1	17.0	0.4
Cd	18.0	3.5	14.6	≤3.9	--	19.3	13.0	12.8	54.9	--	36.9	9.4	14.5	39.2	--
Ce	26.4	1.2	72.4	--	--	23.5	2.1	48.3	26.1	--	--	11.9	42.4	45.7	--
Cl	0.9	0.3	1.4	8.0	89.4	1.5	0.5	0.7	3.7	93.7	2.6	1.2	1.1	5.8	89.3
Co	--	--	67.8	32.2	--	--	--	--	--	--	--	--	--	--	--
Cr	61.5	1.0	24.3	13.2	--	74.8	--	16.0	9.2	--	54.3	9.7	11.1	24.9	--
Cs	2.9	2.9	12.5	81.7	--	4.4	7.5	13.6	74.5	--	10.1	1.2	1.7	87.0	--
Cu	37.0	8.0	39.1	15.9	--	20.0	3.5	17.2	59.3	--	22.4	10.8	49.7	17.1	--
Dy	51.3	--	48.7	--	--	66.1	--	33.9	--	--	35.9	12.9	18.3	32.9	--
Fe	57.6	12.7	27.4	2.0	0.3	63.2	1.4	35.4	--	--	41.2	13.6	13.6	31.6	--
Gd	--	--	--	--	--	24.1	--	37.2	38.7	--	25.4	12.1	23.8	38.7	--
K	--	--	--	--	--	--	3.5	67.4	29.1	--	--	--	--	--	--
La	51.5	9.4	39.1	--	--	54.3	5.4	40.3	--	--	33.9	12.2	15.1	38.8	--
Li	36.9	4.9	17.8	40.4	--	46.0	9.4	17.3	27.3	--	62.9	9.9	13.2	14.0	--
Mg	56.4	2.2	30.9	10.5	--	61.4	2.1	34.1	2.4	--	64.2	10.3	12.8	12.7	--
Mn	56.9	12.7	30.0	0.4	--	58.5	2.0	38.9	0.6	--	38.9	12.7	14.4	34.0	--
Mo	12.7	0.8	48.3	38.2	--	7.0	12.4	28.8	51.8	--	--	--	--	--	--
Na	17.5	3.6	20.6	58.3	0.1	21.1	15.2	18.3	45.3	0.1	31.0	5.7	13.7	49.5	0.1
Nd	47.0	3.4	49.6	--	--	48.9	4.3	37.7	9.1	--	29.5	12.4	17.6	40.5	--
Ni	--	53.2	--	46.8	--	--	14.4	72.5	13.1	--	46.0	18.0	24.5	11.5	--
Pb	27.1	1.8	--	71.1	--	8.3	13.0	2.5	76.2	--	38.3	15.7	8.4	37.6	--
S	11.7	6.9	27.1	19.0	35.3	2.4	1.6	27.7	44.6	23.7	3.1	2.0	20.5	49.8	24.6
Sb	27.4	3.3	38.8	30.5	--	18.3	38.7	27.7	15.3	--	33.3	16.0	48.2	2.5	--
Se	3.8	0.9	4.3	--	91.0	0.6	0.1	0.4	73.3	25.6	1.4	0.4	1.1	9.5	87.7
Si	82.6	7.1	5.6	3.1	1.6	87.0	1.3	8.4	1.9	1.4	67.1	9.1	5.0	18.3	0.5
Sr	46.6	14.1	39.3	--	--	36.0	6.4	30.9	26.7	--	44.1	13.2	22.5	20.2	--
Te	7.0	1.0	14.2	77.8	--	7.8	9.8	13.6	68.8	--	16.2	8.0	27.4	48.4	--
Ti	69.0	3.8	18.7	8.5	--	83.0	--	17.0	--	--	58.5	14.7	--	26.8	--
Zn	46.4	2.4	35.2	16.0	--	41.0	1.8	42.1	15.1	--	21.7	9.7	16.6	34.8	17.2
Zr	81.1	6.9	6.3	5.7	--	89.4	--	7.8	2.8	--	65.1	9.6	4.9	20.4	--

TABLE A.73. Particulate Melter Scrubber DFs

Element	Melter Scrubber DFs 6/17	6/18	6/22	6/23	Average
Al	4000	2800	7700	9200	5900
B	3600	3800	9800	6900	6000
Ca	77	75	97	70	79
Cd	11	10	17	20	14
Cl	24	19	66	39	37
Cr	100	84	180	39	100
Cs	11	10	11	12	11
Cu	320	130	260	320	260
Fe	2000	2500	4900	4900	3600
La	590	600	1200	--	800
Li	41	35	49	130	63
Mg	100	110	370	280	220
Mn	1300	1200	2000	1600	1500
Mo	34	5.4	43	22	26
Na	21	20	30	64	33
Ni	91	97	140	259	150
Pb	12	7.5	16	17	13
S	61	58	62	120	75
Sb	--	26	47	--	36
Se	2.6	1.6	2.6	3.5	2.6
Si	5100	4700	15000	16000	10000
Sr	300	360	550	240	360
Te	14	12	13	14	13
Zn	160	140	2400	--	900

The compositional behavior of noncondensible melter exhaust components during the PSCM-8 experiment are graphically displayed in Figure A.81. Being a boosted test, exhaust concentrations of combustibles were quite low. Carbon monoxide was rarely over 0.5% and exhibited a maximum overall experiment maximum of only ~0.75%. H_2 was hardly ever detectable.

However, large excursions in the concentrations of all noncondensible gases occurred during melter flow surges. The behavior of some of the more important melter off-gas stream components accompanying an excursion three times the average flow is detailed in Figure A.82. The off-gas behavior

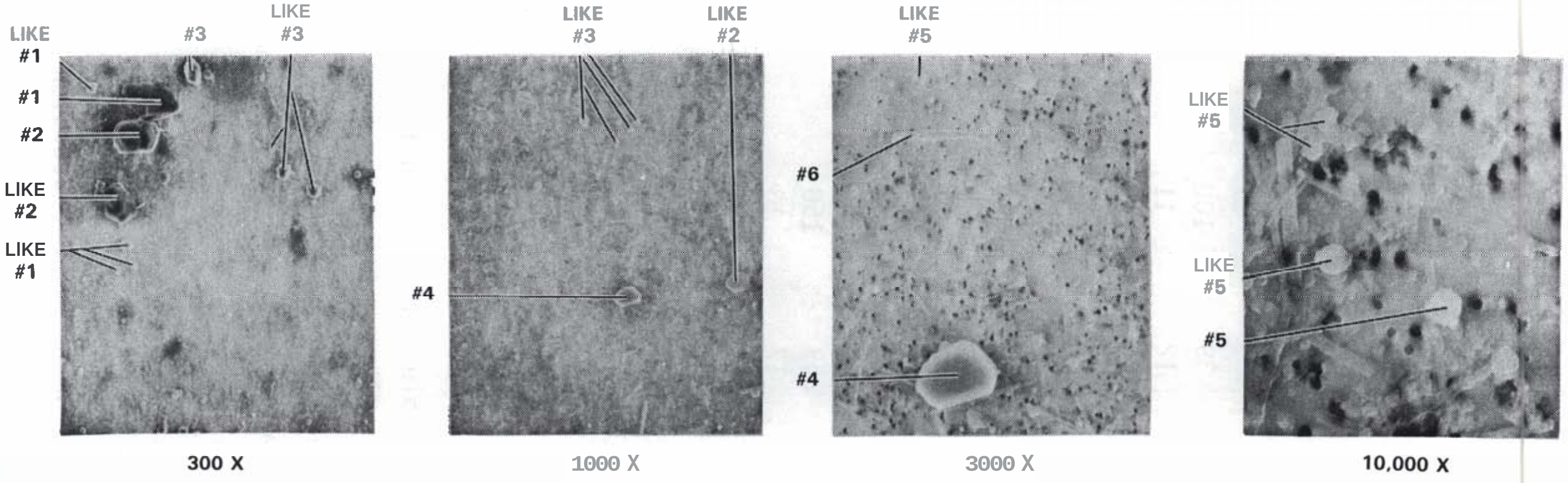
PSCM-8 LOW LOADING

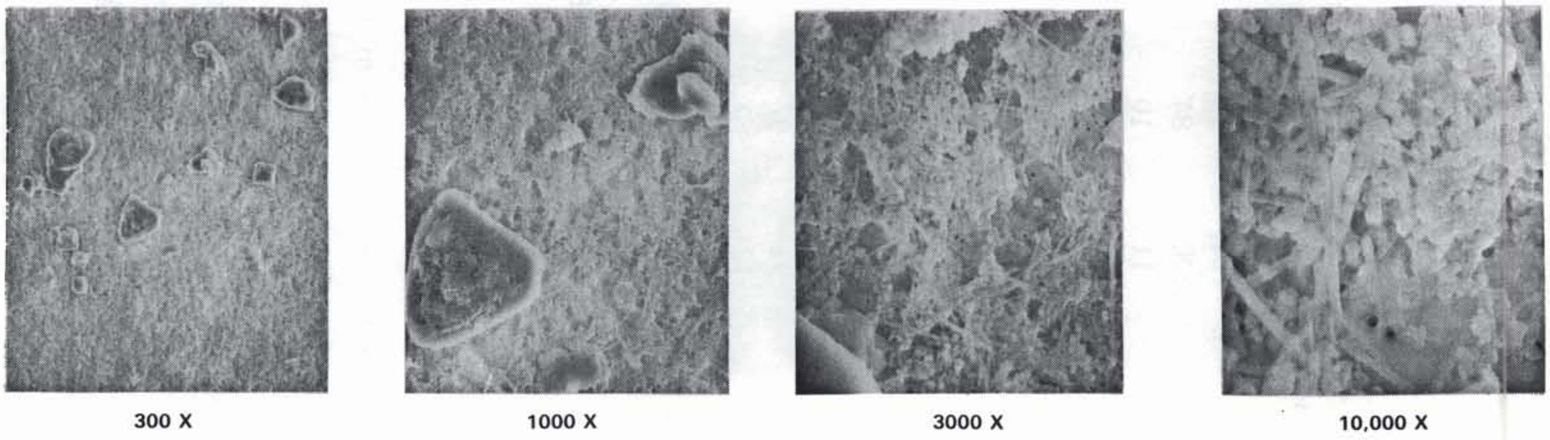
PSCM-8 HIGH LOADING

FIGURE A.79. SEM Photographs of Particulate Samples Taken Downstream of the Close-Coupled Scrubber

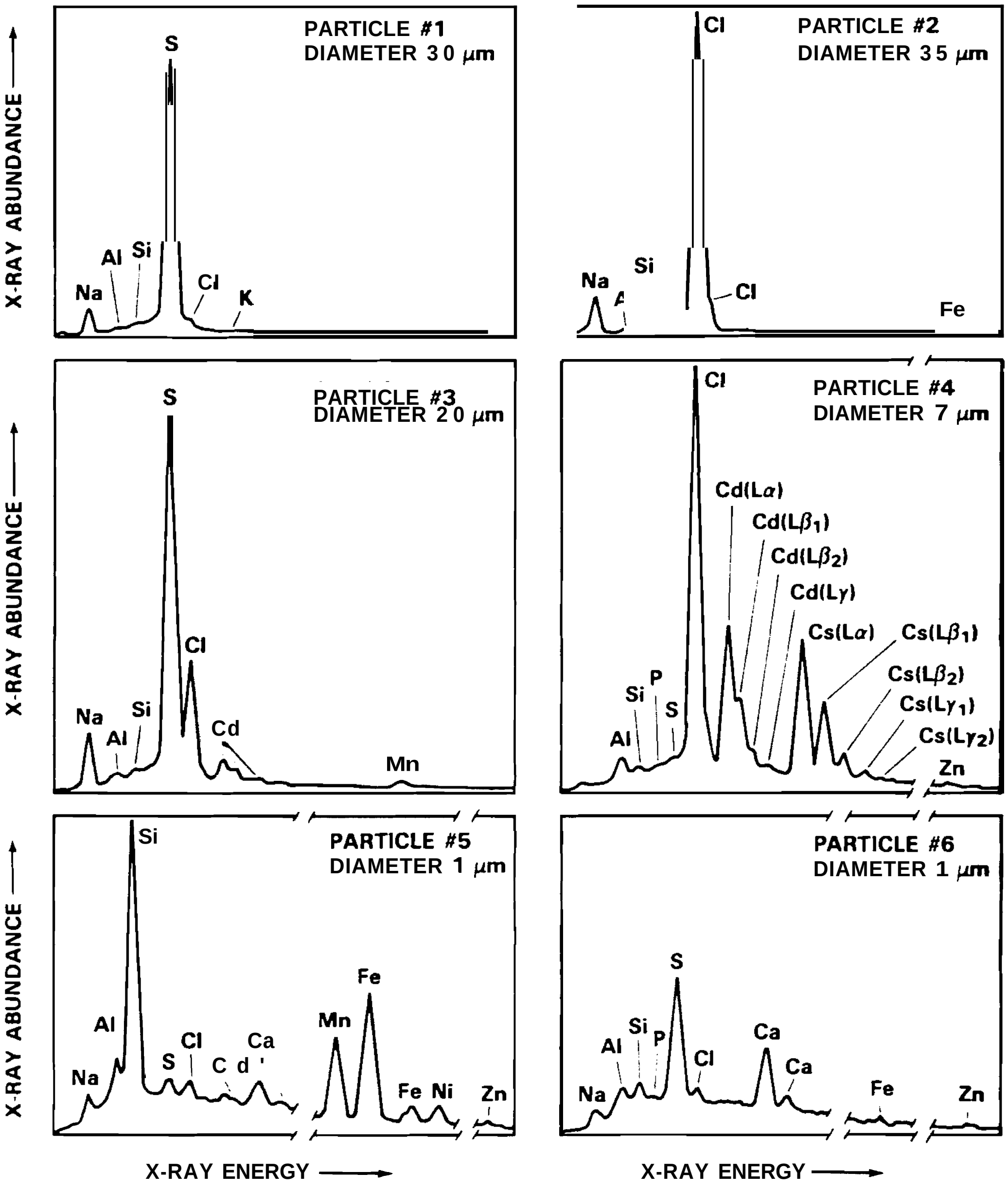

FIGURE A.80. X-Ray Fluorescence Spectra of Individual Particles Called Out in Figure A.79

exhibited in this figure is typical of all off-gas surging events observed during PSCM-8. However, caution should be used in interpreting the hydrogen spike in Figure A.82 because it may be due in part to a pressure fluctuation in the sampling line stimulated by the melter event.

TABLE A.74. PSCM-8 Gross Aerosol DFs

Sampling Period		Sample	Feed Rate,	DF	
Date	Interval	Type	kg/min	Melter	Scrubber
6/17	1017 - 1157	Scrub	1.7	1100	67
6/18	0833 - 1004	Cyclo	1.6	1200	--
6/18	1143 - 1346	Scrub	1.7	1100	44
6/19-20	0447 - 1426	HEPA	1.7	820	--
6/21	0815 - 1200	Cyclo	1.7	1200	--
6/22	1001 - 1327	Scrub	2.0	950	51
6/22	2010 - 2301	Cyclo	2.0	870	--
6/23	0847 - 1436	Scrub	1.7	580	110

During the PSCM-6 run (see Section "PSCM-6 - MARCH 1982"), SO_2 exhaust concentrations increased when feeding was terminated at the conclusion of the run, which suggested that Na_2SO_4 was accumulating within the melter. This was indeed found to be the case, as was later demonstrated in a post-run inspection of the idling melter glass surface. This stimulated speculation that accumulations of Na_2SO_4 could be responsible for changes in the melting capacity of liquid-fed melters that occur during the initial 24 h of liquid feeding (the startup phase). PSCM-8 melter emissions of SO_2 further support this notion, as is shown in Figure A.83. During the initial feeding phase, when the melter's ability to handle feed was limited, feed-rate-normalized SO_2 emission rates were uncharacteristically low, indicating that Na_2SO_4 was probably accumulating. As processing continued at a fixed feeding rate, SO_2 emission rates yradually increased along with the melting capacity of the liquid-fed melter. Apparently a molten Na_2SO_4 phase aids in the feed melting process.

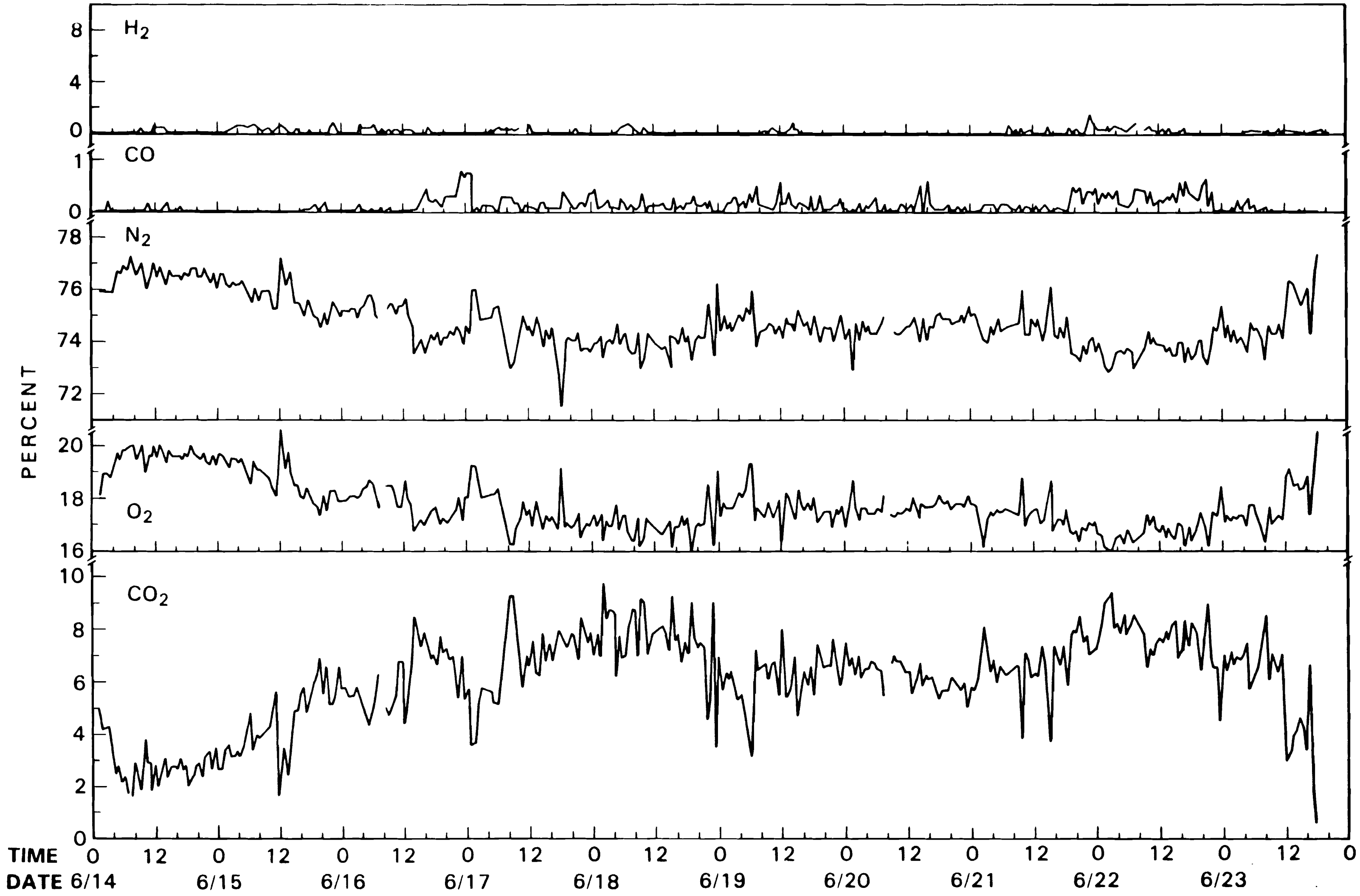

FIGURE A.81. PSCM-8 Off-Gas Composition

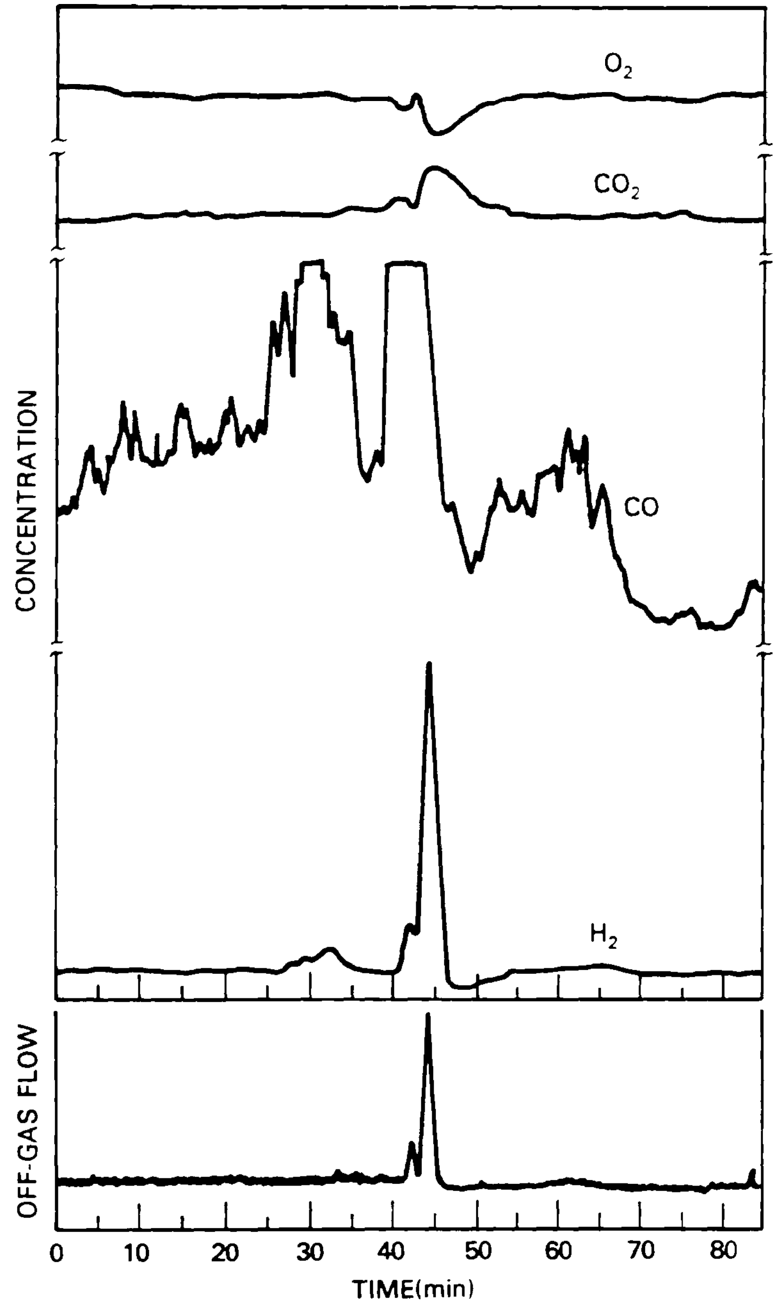

FIGURE A.82. Compositional Behavior of Noncondensible Melter Exhaust Gases Accompanying a Flow Surge. Maximum Extent of the Surge Event: Flow 3X; H_2 <3.5; CO >>0.5%; CO_2 15%; O_2 17%

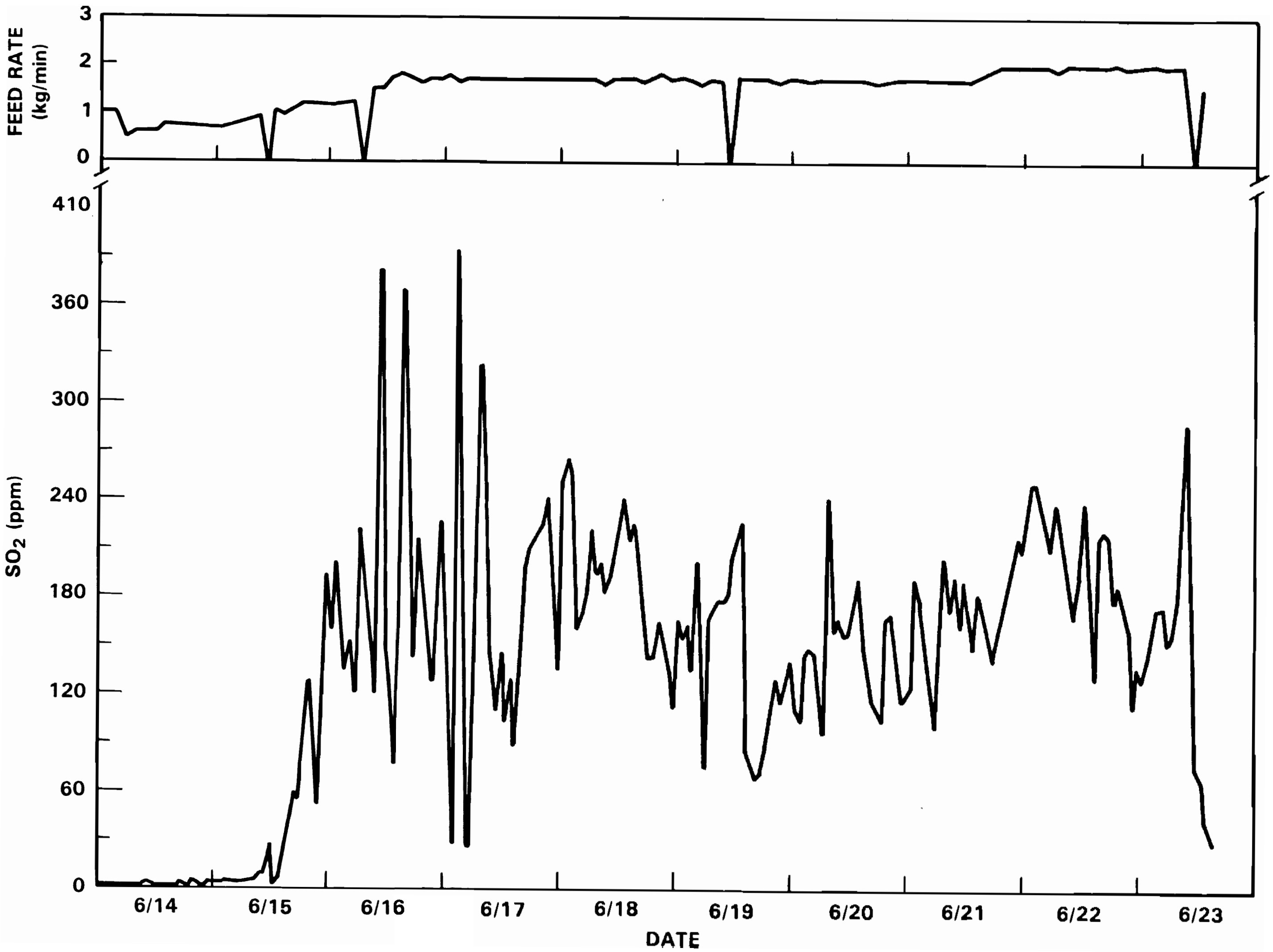

FIGURE A.83. Melter SO_2 Emission haracteristics Accompanying ~240-h Test

OFF-GAS FLOW RATES

Flow rate behavior has been studied for all melter experiments (except PSCM-2) conducted since January 1, 1981. These include 1) two experiments (LFCM-4 and LFCM-6) utilizing a neutralized waste composition, 2) four tests (PSCM-3, LFCM-7, PSCM-4 and PSCM-5) involving the new formate feed composition, 3) two tests (PSCM-6 & PSCM-7) employing a formate-feed composition and new frit, and 4) one test processing a high Al, low Fe formate feed. The results obtained from each test will now be discussed separately.

LFCM-4 - JANUARY 1981

The off-gas flow rates of liquid-fed melters were first examined during the LFCM-4 experiment. What was observed was a noisy, erratic flow rate consisting of frequent suryes mixed with periods of relative calm. Portions of the strip-chart record generated by the flow transducer during this experiment are illustrated in Figure A.84. The conditions illustrated in this figure represent extremes within which the melter operations were maintained. A statistical analysis of the magnitude and duration of surging was conducted during an active 8-h period of continuous melter operation. These results are summarized in Table A.75. The uncertainties listed with the averages represent one standard deviation of the data examined and, consequently, are measures of the spread or dispersion of this data (i.e., 68% of all data examined statistically lie within one standard deviation of the average).

During the LFCM-4 experiment, a significant number of off-gas surges exceeded the full-scale range of the flow transducer employed. These events were reexamined in order to extract information regarding their frequency, duration and extrapolated flows (triangular approximation). This data appears in Table A.76, where all emergency venting occurrences are so designated. It should be noted that conductance-limiting restrictions involving loaded HEPA filters and/or valve throttliny of the system exhaust were responsible for the brief melter pressurizations that led to the emergency venting situations. The flows recorded during these melter pressurizations are probably not totally ascribable to the events which triggered the venting occurrence but, rather,

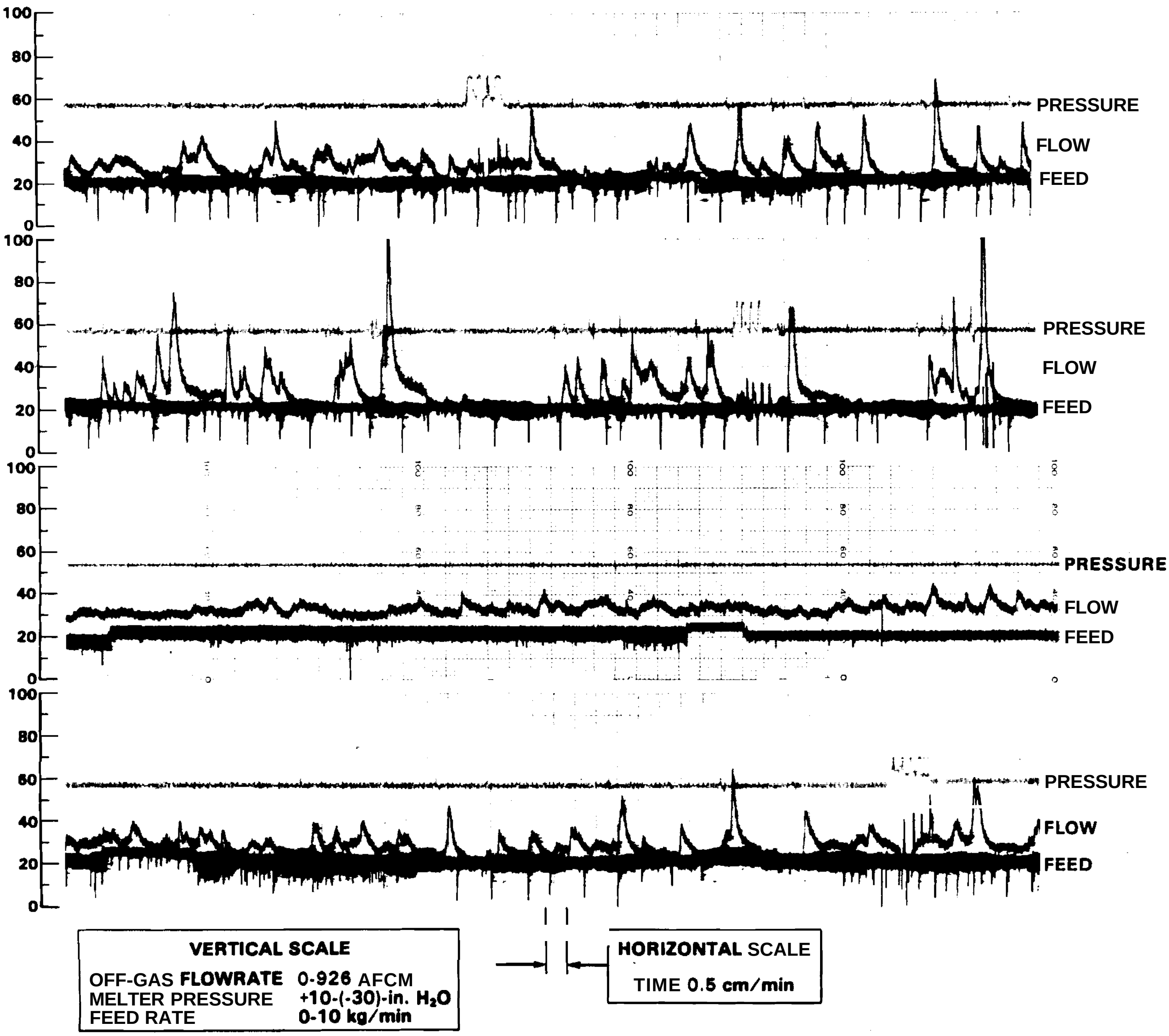

FIGURE A.84. LFCM-4 Off-Gas Flow Rate Behavior

are due (in part) to atmosphere flowback into the melter through the venting butterfly valve. This situation results primarily from the slow response time of the venting valve, coupled with an automated melter exhaust system that attempts to maintain a negative plenum pressure even when the melter is opened to the atmosphere.

TABLE A.75. Flow Surging Characteristics During LFCM-4[a]

Steady-State Flow, scfm	Average[b] Surye Flow ± σ, scfm	Average Surge Duration ± σ, min
90	220 ± 80	2 ± 1

(a) Study conducted over an 8-h period on 1/22/81.
(b) Total average flow (steady-state plus spike) is listed.

TABLE A.76. Frequency, Duration and Extent of LFCM-4 Surges

Date	Time	Duration, min	Flow, scfm	Vent
1/21/81	1328	1.8	450	Yes
	1600	2.4	450	
	1655	3.0	450	Yes
	1845	0.5	450	
1/22/81	1300	1.0	470	
	1345	1.5	520	
	1440	1.5	570	Yes
	1505	1.0	500	
	1515	3.2	450	
	1700	3.2	450	
	1815	3.2	450	
	1820	2.7	580	
	1948	3.2	590	Yes
	2040	2.3	620	Yes

LFCM-6 - JUNE 1981

One of the main objectives of the flow rate studies during LFCM-6 was to characterize the maximum flow surges generated by normal melter operation. Because off-gas surges extend beyond the dynamic range of the flow transducer employed during LFCM-4, a flow transducer was employed during the June run that responded to surge impulses but was relatively insensitive to the average flow rate. The maximum flow surges were cataloged and treated statistically. These results are summarized in Table A.77. It should be noted that no emergency venting occurred during this run. On the other hand, care was exercised to minimize conductance-limiting situations within the melter off-gas system.

PSCM-3 - JULY 1981

The modest off-gas characteristics of the unboosted pilot-scale melter allowed both the average and surging flows to be characterized by a single off-gas flow transducer. The data generated during PSCM-3 are summarized in Table A.78.

Melter flow rate behavior appears to have been drastically altered by the nature of the new formate feed. No longer is flow rate characterized by an erratic surging behavior; rather, a quiet, stable flow rate appears to be the dominant feature associated with steady-state melter operations.

LFCM-7 - AUGUST 1981

Due to the quiescent nature of PSCM-3 flow, a flow transducer capable of measuring the average flow rate was utilized in LFCM-7. It was hoped that the dynamic range of this transducer would be adequate for any surges which might be generated by this formate-fed, lid-boosted melter. This, indeed, did turn out to be the case, where only a single significant event occurred in ~120 h of melter operation. This event did cause melter pressurization, which initiated emergency venting. The maximum flow recorded during this event was a factor of 3 greater than the average flow. It should be noted that a partially-loaded

TABLE A.77. LFCM-6 Surging Flow Rate Behavior

Mean Surge Flow, scfm	Data Dispersion (1-σ), scfm	Maximum Flow, scfm
185	63	465

TABLE A.78. PSCM-3 Flow Rate Behavior

Flow (scfm)		Surges a % Average Flow		
Avg.	Max.	200	300	400
70	220	11	2	0

HEPA filter (ΔP ~10 in.) was present in the off-gas line when this event occurred. In addition, the water present in a seal pot, which was blown into the hot off-gas line by the pressurization, accounted for some of the flow recorded during this event. A summary of all pertinent off-gas flow rate data generated during LFCM-7 appears in Table A.79.

PSCM-4 - DECEMBER 1981

During PSCM-4, the total off-gas flow was measured to characterize melter off-gas flow surges. The data collected are shown in Table A.80. It should be noted that 22 of the surges that were >50% above the average flow occurred during a period when the melter surface was completely covered by a cold cap and when the melter seemed to be accumulating feed. The feed rate appeared to be higher than the melter's processing capabilities during that period. Later, the same feed rate was being processed with little surging, but the cold cap was not complete, and feed was not accumulating in the melter. These data indicate that frequent surges >50% above average off-gas flow rate occur when the melter is being overfed.

TABLE A.79. LFCM-7 Flow Rate Behavior

Flow Rate, scfm			
Steady State			Surges
Minimum	Maximum	Average	Maximum
190	270	240	710

TABLE A.80. Off-Gas Surging Behavior

Flow Characteristics	Rate
Average flow	70 scfm
Maximum surge flow	145 scfm
Number of surges, >150% average	26
Average surge length	4 minutes
Range of surge lengths	0.5 - 8 minutes
Maximum surge volume	~1000 ft^3

PSCM-5 - JANUARY 1982

During the January PSCM-5 test, the off-gas flow was measured with a Ramapd target-type flowmeter. As the run progressed, the flowmeter collected deposits which affected the calibration of the instrument; however, the changes between readings are believed to be proportional. Surges in the off-gas flow were categorized by using the ratio of the surge to the average flow. The ratios were separated into stable and unstable operating periods, and these values are shown in Table A.81. The stable and unstable periods were identified by observation of the cold cap through the melter viewport. These data represent only the first two days of the PSCM-5 test due to flowmeter malfunctions. Off-gas flow chart recordings of stable and unstable periods are shown in Figure A.85. As can be seen, unstable periods are characterized by frequent high spikes in flow.

PSCM-6 - MARCH 1982

The off-gas flow rate was quite stable during most of PSCM-6. On March 21, the first day of the run, the melter was overfed because the glass temperatures were low. This overfeeding was responsible for all recorded off-gas surges. This data is shown in Table A.82. The overfeeding situation described above was determined by visual observation of the melter cold cap. The unstable melter operation occurred between 0200 and 1100 hours on March 21.

During steady-state operation, no off-gas surges occurred, and the Ramapo flowmeter recorded an average gas flow rate of 120 scfm. This flow rate

TABLE A.81. PSCM-5 Off-Gas Flow Rate Behavior

Flow Characteristics	Stable	Unstable
Maximum surge ratio	1.8	2.9
Average surge ratio	1.4	1.9
Average flow rate, acfm[(a)]	180	180
Average surge duration, min	3	3
Maximum surge duration, min	15	5

(a) Calculated average from feed rate with off gas at 400°C.

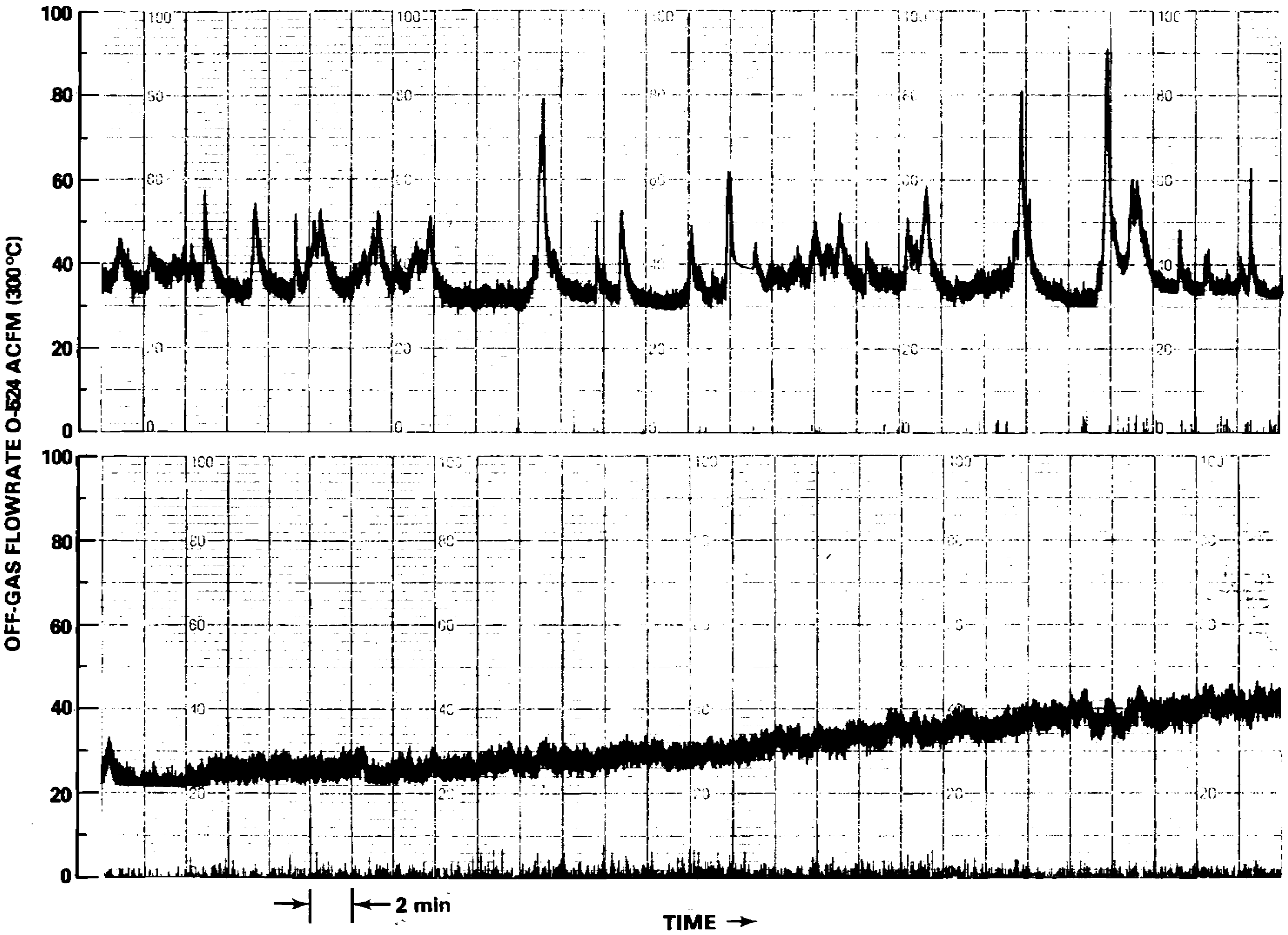

FIGURE A.85. PSCM-5 Off-Gas Flow Characteristics

TABLE A.82. PSCM-6 Off-Gas Flow Characteristics

Flow, scfm		Surges, Greater than Percent of Average Flow		
Average	Maximum	150%	200%	300%
80(a)	190	7	4	0

(a) Average during period of surges Feed rate 0 to 1.2 kg/min.

occurred with a slurry feed rate of 2 kg/min. The Ramapo flowmeter results were compared to a periodically checked pitot tube, which indicated an off-gas flow rate of 100 scfm. This indicates the Ramapo flowmeter gives reasonable values which might be slightly high because of the particulate in the off-gas lines.

The noncondensible gas flow was periodically measured with a pitot tube and calculated from the average CO and CO_2 concentrations in the gas. The flow was calculated for seven different time periods representing the periods before and after the use of a sampling HEPA filter. The carbon content in the feed was used with feeding rate and CO + CO_2 exhaust concentration data to determine the total noncondensible gas flow. The results are shown in Table A.83.

The values calculated from both methods compare very well and indicate that a small leak is present in the HEPA filter holder. This leak would not affect HEPA filter results. The air-atomized water spray nozzle used to cool the off gas contributed ~5 scfm to the noncondensible gas flow. The total inleakage into the melter was about 25 scfm.

PSCM-7 - MAY 1982

During PSCM-7, the total melter off-gas flow rate was monitored using the pressure drop across an orifice plate. The orifice was designed to detect and record large fluctuations in the off-gas flow rate. A graphical display of this flow data is shown in Figure A.86. This graph is a qualitative index of the off-gas flow rate instabilities and is compared to the melter operational stability index also shown in Figure A.86. Overall, there were >150 surges in PSCM-7; most of them occurred near the beginning of the test.

TABLE A.83. Noncondensible Gas Flow (scfm)

Date	Time	Average Pitot Tube Reading	Calculated From CO $+CO_2$ Concentrations	HEPA Filter Status
3/23	0033 - 2400	30	28	Out
3/24	0036 - 1117	45	48	In
3/24	1117 - 0100	NA	30	Out
3/25	0132 - 2400	33	31	Out
3/25	2024 - 2400	41	43	In
3/26	0040 - 0302	NA	33	Out
3/26	0302 - 1410	30	35	Out

The melter stability index is determined by feed rate and power input factors. The off-gas stability index is determined by counting the number of surges in a 1-h period, which exceeded two times the calculated average flow rate. If more than 10 surges were found, an index of 10 was given to that period. The section marked with "cyclone" may not be comparable to other areas because a particulate sampling cyclone placed in front of the orifice could have affected the orifice's operations. "Ramapo" indicates that the data were taken with a Ramapo flowmeter because the orifice flowmeter was bypassed at that time.

As a comparison, the off-gas flow rate stability[(a)] index during PSCM-6 was only above a value of two once, while the rest of the run had only a total of three surges. PSCM-6 was a much more stable test than was PSCM-7.

PSCM-8 - JUNE 1982

The total off-gas flow rate was monitored during PSCM-8 and is shown in Table A.84. An orifice flowmeter was used for most of the experiment, and a Ramapo flowmeter was used when a HEPA filter sample was being collected. The

---

(a) Currently, "stability" is a subjective decision made by the shift engineer, taking into consideration visual and recorded data and current melter behavior. The purpose of these analyses are to quantify a variable or measurement to use in place of subjective judgment.

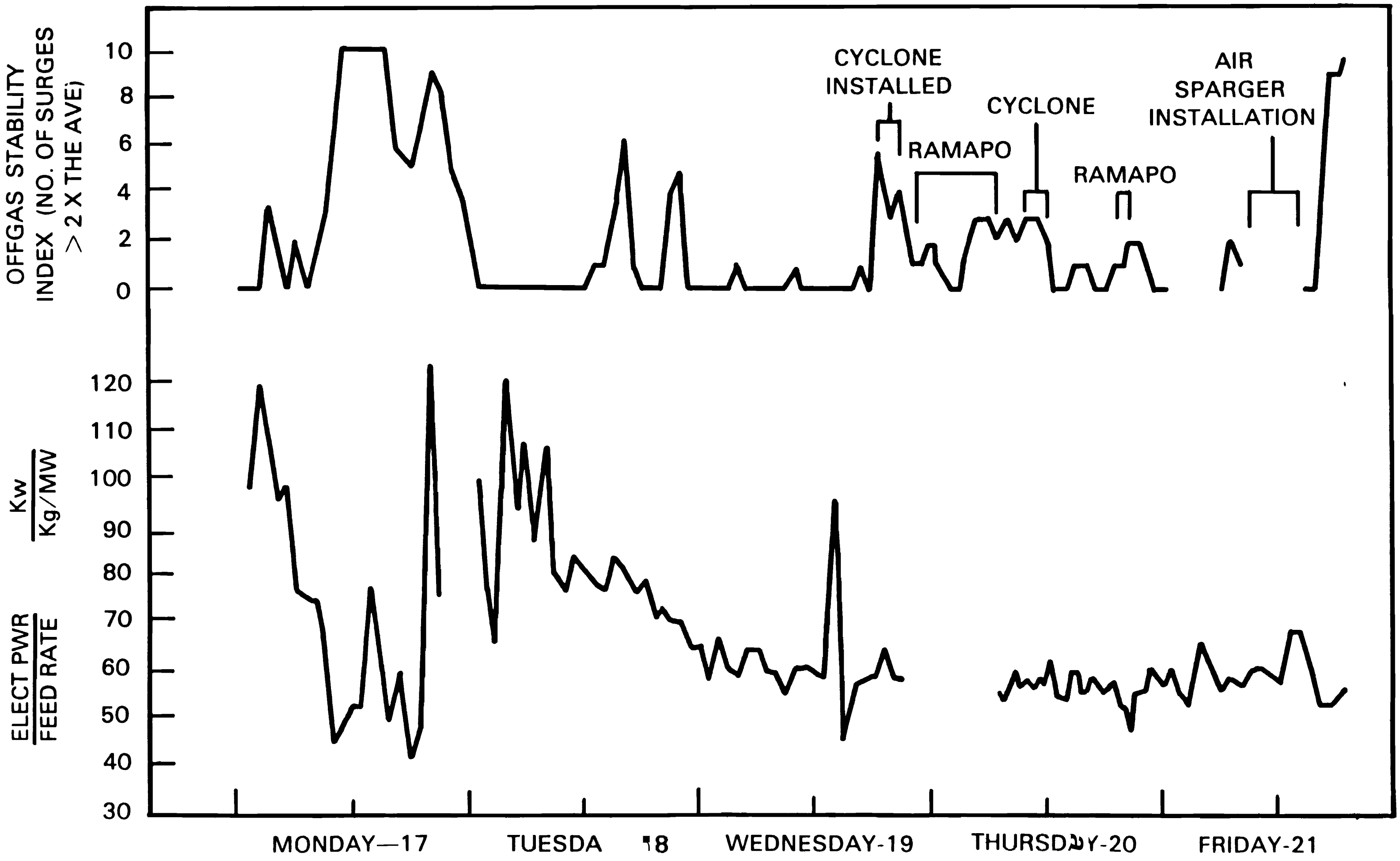

FIGURE A.86. Qualitative Index of Off-Gas Flow Rate Instabilities

TABLE A.84. PSCM-8 Flow Data

Flow, acfm		Number of Surges >% Average				Average Surge Duration
Average	Maximum	150	200	250	300	
138	391	17	4	4	1	3 min

Total number of surges = 26.

noncondensible flow was periodically checked with a pitot tube. The average flow rate of the noncondensible gases was 16 scfm before the HEPA filter sample, 30 scfm when the HEPA filter was valved in, and 22 when the HEPA filter was valved out again. PSCM-8 exhibited much more stable off-gas flow behavior than previous PSCM tests. The average flow rate recorded by the orifice flowmeter was comparable to the calculated value obtained from the noncondensible flow and melter feeding rates. The orifice flowmeter value was 140 acfm, and the calculated value was 190 acfm.

MELTER IDLING TESTS

Melter emission rates of semivolatile elements were investigated under various idling conditions at the conclusion of PSCM-5. Briefly, melter emission rates were determined by direct plenum sampling as a function of plenum temperature and surface glass viscosity. Temperature control was maintained through use of plenum water sprays, which cooled but did not disturb the surface of the melter glass pool. A brief qualitative description of melter characteristics during the test follows.

At a water spraying rate of 43.5 L/h and with the melter running under automatic resistance control, the glass surface was cooled to the point that it formed a continuous nonconvective layer above the bulk melter glass pool (plenum 280°C). At 26.5 L/h, the surface viscosity decreased significantly. Convective mixing opened vents, or fumaroles, in the glass surface that migrated at random across the melter glass pool. However, plenum temperatures were not high enough to melt feed deposits formed upon the melter walls and lid during PSCM-5. Finally, the cooling spray was terminated and the melter was allowed to idle at a fixed current rate, which slowly brought the melter plenum up to 850°C. Samples were collected from the plenum during all phases of this study.

The results obtained from these plenum samples are summarized in Figure A.87, which characterizes the emission rates of the semivolatile elements under various idling conditions (temperature) employed during this test. These data indicate that emission rates of all semivolatile elements decreased as a function of time after the completion of PSCM-5 under the influence of a 42 L/h water spraying rate. Reducing the cooling spray rate to 27 L/h measurably increased both plenum temperature and semivolatile emission rates; however, an equilibrated plenum temperature was not achieved during the brief period (24 h) of reduced spraying.

Termination of the water-cooling spray increased the plenum temperature steadily to the point where plenum surface deposits formed during PSCM-5 began to melt and "burn" away. This period was responsible for the dramatic peaking

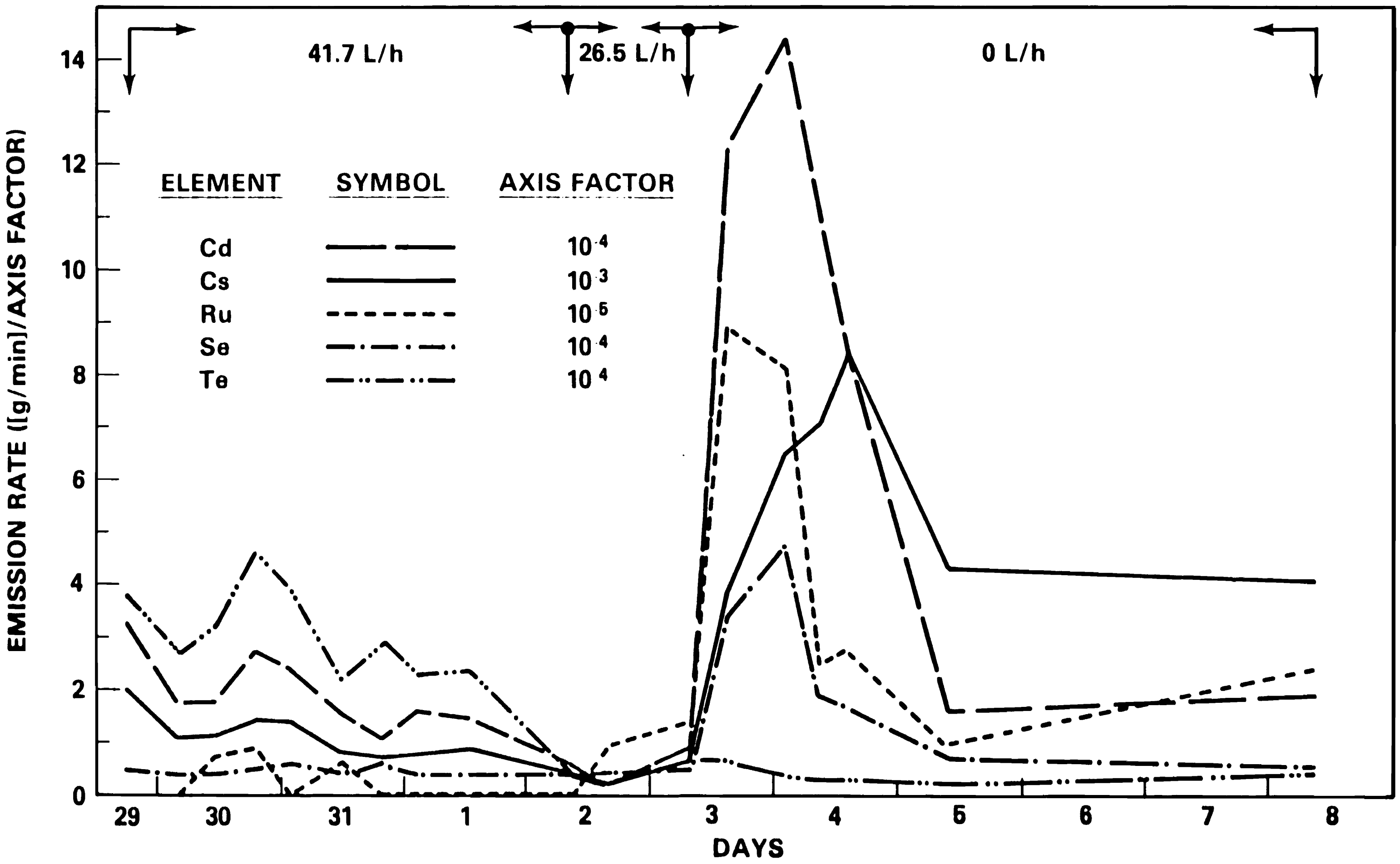

FIGURE A.87. Melter Idling Emission Rates of Semivolatile Elements of emission rates of the semivolatile elements. The fact that all semivolatiles do not form maxima at the same point in time is probably due to temperature, which was steadily increasing throughout the interval over'which these maxima occur.

The plenum temperature during the last two sampling periods was ~850°C, and all plenum surfaces appeared clean. The emission rates during these periods are, with the exception of Se and Te, significantly greater than the minimum emission rates of these elements during full 42 L/h spray cooling. However, these elevated idling emission rates are still significantly below those rates observed during moderate liquid feeding conditions. Specifically, the Cs emission rate expected from the PSCM for a liquid feeding rate of 50 L/h (1.1 kg/min) would be ~8 mg/min. This is twice the value observed during hot melter idling conditions. Consequently, it appears that the plenum cooling approach, although capable of reducing emission rates of most semivolatiles (by a factor of 10 for Cs), is of little practical value in reducing the overall melter off-gas radiological burden.

At the conclusion of PSCM-4 the effect of water feeding on the idling melter was investigated. The plenum spray appears to be far superior to direct water feeding as a means of cooling the plenum and melter glass surface. The water feeding technique produced a high degree of entrainment and aerosol carryover into the off-gas system. Moreover, at the water feeding rates used (45 L/h), convective mixing was actually exacerbated (total melter flooding was never attempted). On the other hand, the water plenum spray did not initiate entrainment, and minimized or eliminated convective surface mixing.

CORROSION

Metal corrosion has been observed in the plenum and off-gas equipment in two liquid-fed melters operated by PNL, the LFCM and the PSCM. The LFCM was constructed with an externally insulated Inconel® plenum liner and an Inconel off-gas port, while the PSCM melter has an internally insulated lid. The internal insulation is Alfrax-57. The off-gas port is made of Inconel-690 with a Cr_2O_3 plasma-sprayed coating. The only other metal in the PSCM is the Inconel plenum heater thimbles, the feed nozzle and the metal corrosion samples. Both melters use the same stainless steel off-gas system, which consists of a venturi scrubber, a packed tower and a blower. The corrosion of metal parts exposed to the melter off gas will be discussed in the following sections. The operating conditions of the melters during various tests are shown in Table A.85.

LFCM

Six experiments were conducted with the LFCM between September 1980 and September 1981 and, duriny that time, a variety of metal parts have corroded. The first component which failed was a stainless steel flex hose installed in the LFCM off-gas line. The hose corroded badly during the first experiment (LFCM-2) after 15 days of idling and 7 days of melter operation. The flex hose was brittle and full of holes near the welded joints. The metal was also flaking badly. Analysis of the corroded metal showed considerable amounts of chloride (Cl) and sulfur (S). The analysis also showed a high chromium (Cr) concentration in relation to the iron (Fe) and nickel (Ni) present in stainless steel. The corroded pieces were magnetic, indicating that the Ni was being attacked by S and Cl, which is typical of sulfidation attack. (Sulfidation causes high Cr-Fe alloys to become magnetic like the flex hose.)

It was also noted that the deposits downstream of the flex hose had high concentrations of Fe and Ni relative to their concentrations in the glass. Analysis of the plug material is shown in Table A.86. Because Fe and Ni are not considered volatile, the extra Fe and Ni probably came from the flex hose

TABLE A.85. Melter Operation Summary

	LFCM					PSCM						
Run No.	2	3	4	5	6	7	3	4	5	6	7	8
Operating plenum temperature, °C	400-800	350	600	--	600	500	250	350	550	700	300	800
Idling plenum temperature, °C	~900	~900	~900	~900	~900	~900	~900	~900	~900	~900	~900	~900
Off-gas operating temperature, °C	300-600	325	325	--	300	250	350	300	400	400	275	400
Days idling before run	15	38	73	30	97	79	116	30(a)	42	49	53	27
Days of operation	9	1	5	1	5	5	5	5	5	6	5	10
Plenum boosting power, kW	25	0	30	6	45	17	0	0	36	55	0	45

(a) New lid.

TABLE A.86. Composition of Material From Off-Gas Plug

Elemental Oxides	Average Wt% in Plug	Wt% Feed 9/18/72 at 2030 h	Ratio of Wt% Plug/ Wt% Feed
Al_2O_3	1.67	2.96	0.56
B_2O_3	4.62	3.78	1.22
CaO	4.40	4.62	0.95
Cs_2O	0.26	0.04	3.0
Fe_2O_3	20.3	10.9	1.86
Li_2O	2.02	2.42	0.83
MgO	0.22	0.11	2.00
MnO_2	1.21	3.67	0.32
Na_2O	16.9	13.0	1.30
NiO	2.49	1.32	1.89
RuO_2	0.30	0.01	30.0
SiO_2	31.0	35.0	0.89
SrO	0.04	0.02	2.0
TeO_2	0.07	0.004	17.5
TiO_2	0.07	0.03	2.33
ZnO	0.08	0.04	2.0

corrosion products. The flex hose corrosion was also caused by high-temperature cycling and flex hose stresses that were induced when tilting the melter. The plenum temperature during this period varied between 400 and 800°C.

Since LFCM-2, the off-gas temperature has been kept below 400°C by using a water-cooling spray during operation. During idling, the off-gas flow was decreased, so the off-gas temperature is relatively low a few feet from the melter, and the new flex hose has not corroded significantly.

About seven months after the flex hose corroded, signs of liner failure occurred. Some metal strips (Inconel-601) on the underside of the melter lid were observed to be hanging down from the melter lid.

After the lid failure was observed, a temperature excursion occurred, raising the glass temperatures above 1400°C. After the temperature excursion, the melter lid was inspected with a metallic mirror, and about 50% of the lid's metal underside was missing, as shown in Figure A.88.

The Inconel-601 walls were relatively undamaged. The difference in damage between the walls and lid could be caused by the different stresses in the lid, or the different temperatures encountered. The walls form the protective shield for the plenum heaters, which keeps the walls above 900°C during operation, while the lid temperature cycles between 400 and 1000°C.

After the next LFCM run, the badly-corroded off-gas port (Sch. 40 Inconel-601 pipe) broke away from the lid while the off-gas lines were being disassembled for inspection. Unlike Inconel, the port possessed magnetic properties. Analysis by x-ray diffraction showed layers of $NiCrO_4$, $NiFe_2O_4$ spinels, and metallic Ni. The analysis by SEM revealed large amounts of Cl and S in the void spaces, which indicates there was Cl and S attack.

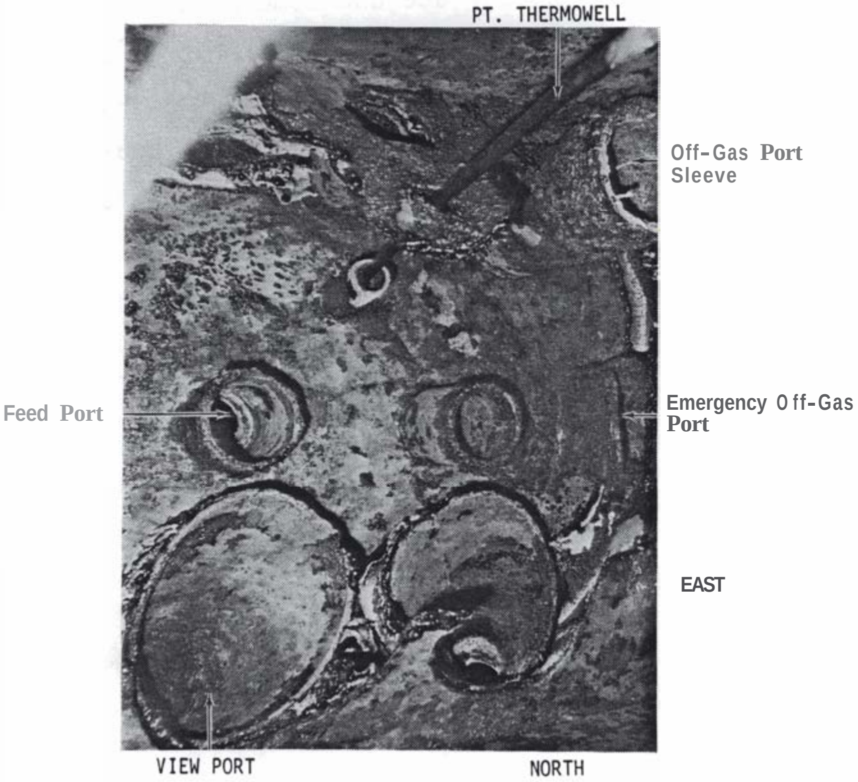

FIGURE A.88. Underside of LFCM Lid North

Analysis of off-gas line deposits formed during idling periods have shown NaCl concentrations ranging from 20 to 90% and S concentrations as high as 30%. These analyses indicate sulfidation attack, but do not rule out the possibility that the high temperature excursion contributed to the port's premature failure.

After the incidents mentioned above, the off-gas port was replaced and corrosion samples were mounted in the LFCM plenum. The corrosion resistance of the metal samples are shown in Table A.87. Visual observations indicate that Inconel-690 and -625 are the best alloys of the group.

The ability of the coatings to survive the plenum atmosphere is largely due to surface preparation, coating selection and a precisely controlled application technique. The oxide coating used and the application combination are shown in Tables A.88 and A.89.

All the oxide-coated samples spalled severely except for Cr_2O_3, where only a little coating was lost. The Ni-Cr base coat alone did not spall, but there was some attack at the coating surface and some physical changes at the coating substrate interface which have not been defined at this point. Spalling and coating changes can be seen in Figures A.89 through A.94. A possible explanation for the spalling is that the small coupons were heated too high during the deposition step, severely cornpressiny the ceramic layer upon cooling. The

TABLE A.87. Metallic Corrosion Sample Results

Material	Visual Observation
Tantalum	No longer on sample rack; disappeared
Titanium(a)	Large flakes, deep pits; badly corroded
Inconel-690	Discolored spots
Inconel-625	Discolored spots
Inconel-617	Discolored, green spots; obvious metal loss
Inconel-600	Many discolored spots
304 SS	Lots of flaking metal; oxidizing rapidly

(a) Only one sample. Other materials had two samples each.

TABLE A.88. Protective Coating Off-Gas Samples

	Bond Coating		Outer Coating		Surface Preparation	
Sample No.	METCOID	Thickness, μm	METCOID	Thickness, μm	Cleaned	Blasted
1	--	--	--	--	X	
2	--	--	--	--		X
3	43F-NS	380	--	--	X	
4	43F-NS	380	--	--		X
5	43C	250	--	--	X	
6	43C	250	--	--		X
7	443	250	--	--	X	
8	443	250	--	--		X
9	443	250	105SF	250		X
10	443	250	105	250		X
11	443	250	106	250		X
12	443	250	202NS	250		X
13	443	250	201	250		X
14	443	250	201B-NS-1	250		X

already weakened coating then spalled off when cycled back up to the plenum temperature. The pictures are grouped in pairs; the one marked CONTROL is an unexposed sample with the same type of coating as the plenum sample portrayed in the adjacent picture. The light shaded areas are the metal substrates and the areas with mixed shading are the coatings. Figures A.89 and A.90 are photos of the Ni-Cr base coat, which shows very little corrosion, but it does show the base coat substrate interaction. Figures A.91 and A.92 are photos of the Ni-Cr-6% Al base coat with a Cr_2O_3 secondary coat, showing some cracking of the oxide coat and the same base coat-substrate interaction shown in Figures A.89 and A.90. Figures A.93 and A.94 are photos taken of the ZrO-coated sample with a Ni-Cr base coat. A great deal of cracking and material loss of the ceramic layer are evident. These pictures are typical of the other coated samples. These results suggest that more work is needed to develop and refine coating techniques.

TABLE A.89. Spray Powder Characteristics

Spray Powder	Powder ID	Constituent	Percent	Range, µm	Comments
Nickel-Chromium Alloy	43F-NS	Ni Cr	80 20	-53 +10	Best single coating for oxidation resistance to 980°C.
Nickel-Chromium Alloy	43C	Ni Cr	80 20	-105 +10	Good bond coat + O_2 barrier to 980°C.
Nickel-Chromium/ Aluminum Composite	443	Al Ni-Cr	60 Balance	-120 +45	Best bond coat + O_2 barrier to 980 °C.
Ceramic	105SF	Al_2O_3 SiO_2 Other Oxides	98.5 0.5 1.5	-25 +05	Wear resistant.
White Alumina	105	Al_2O_3 SiO_2 Other Oxides	98.5 1.0 Balance	-53 +15	Resists erosion from 840 to 1650°C. Wear resistant.
Chromium Oxide	106	Cr_2O_3	98	-90 +15	Resists abrasion, cavitation & erosion to 540°C. Insoluble in acids, alkalis and alcohol.
Zirconium Oxide Composite	202NS	ZrO_2 Y_2O_3	80 20	-90 +10	Resists thermal shock and particle erosion to 1650°C.
Zirconium Oxide	201	ZrO_2 CaO Al_2O_3 Other Oxides	80 5 0.5 Balance	-90 +10	Resists thermal shock and particle erosion above 845°C.
Zirconium Oxide Composite	201B-NS-1	ZrO_2 $CaCO_3$	92 8		Resists thermal shock and particle erosion above 845°C.

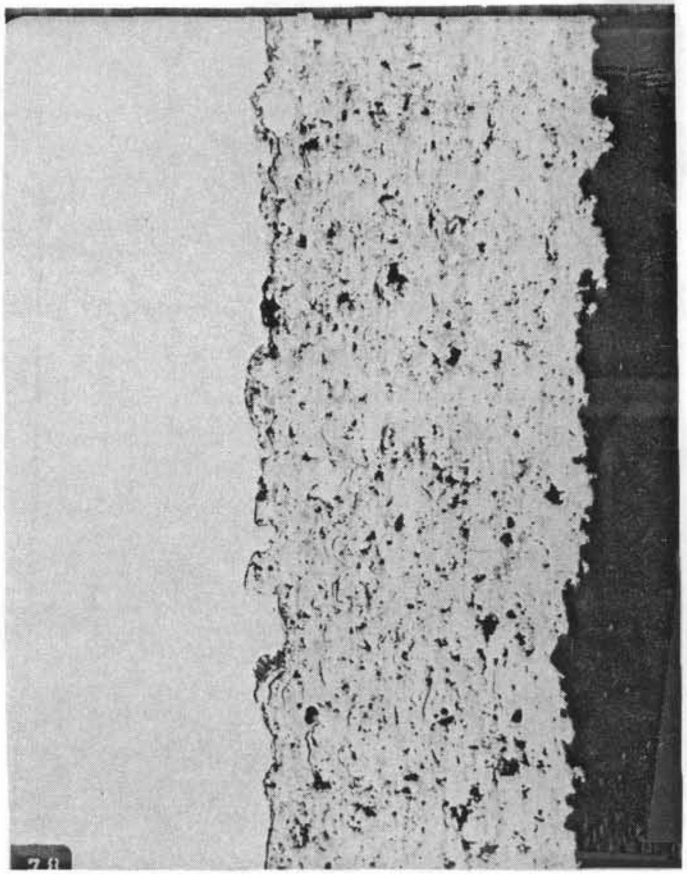

#4 Control 100X

FIGURE A.89. SEM Photograph of Ni-Cr Base Coat Under 100X Magnification - Control

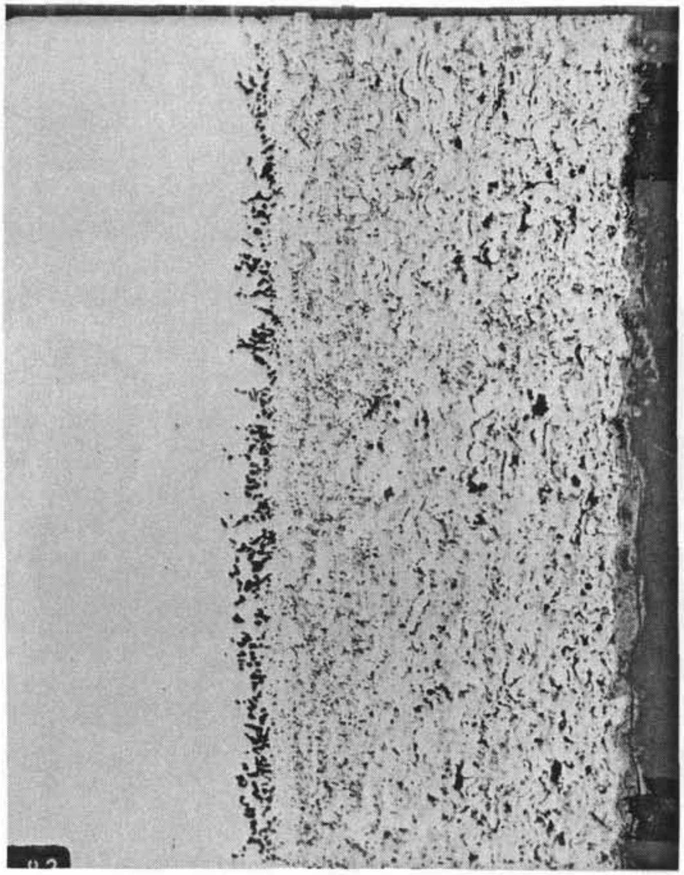

#4 100X

FIGURE A.90. SEM Photograph of Ni-Cr Base Coat Showing Very Little Corrosion Under 100X Magnification

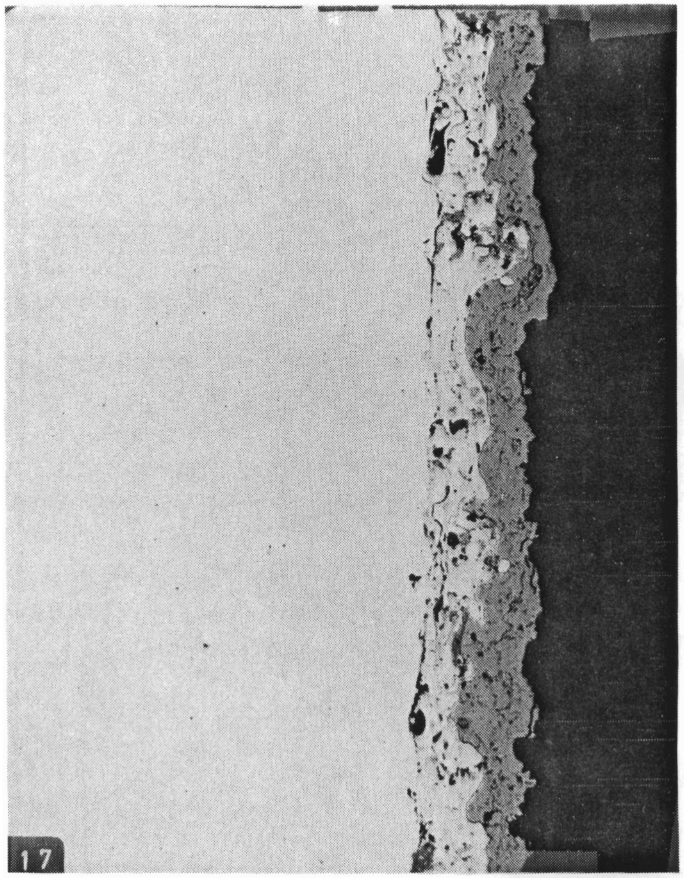

#11 Control 100X

FIGURE A.91. SEM Photograph of Ni-Cr-6% Base Coat with a Cr_2O_3 Secondary Coat Under 100X Magnification - Control

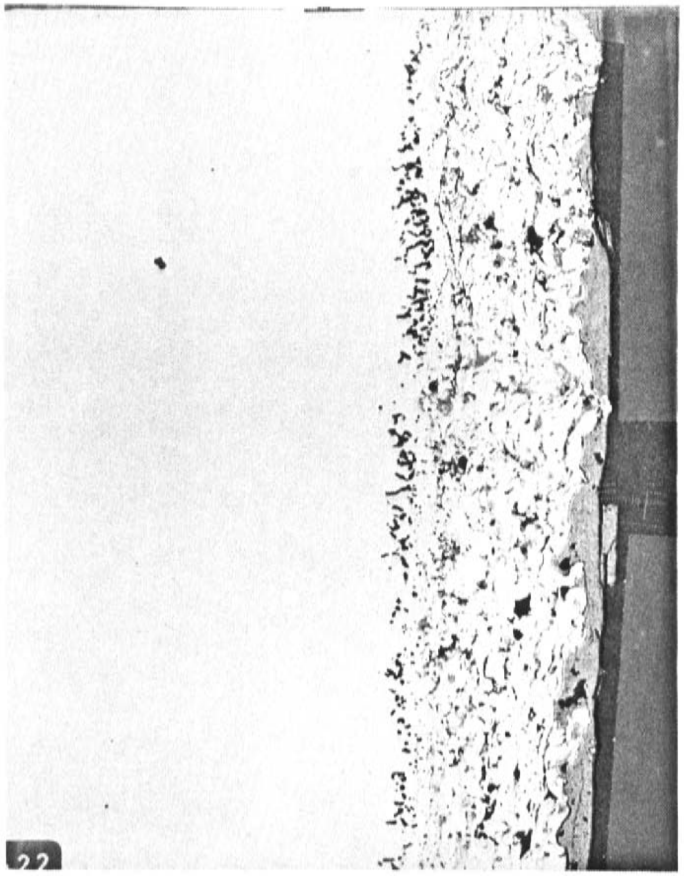

#11 100X

FIGURE A.92. SEM Photograph of Ni-Cr-6% Base Coat with a Cr_2O_3 Secondary Coat and Some Cracking Under 100X Magnification

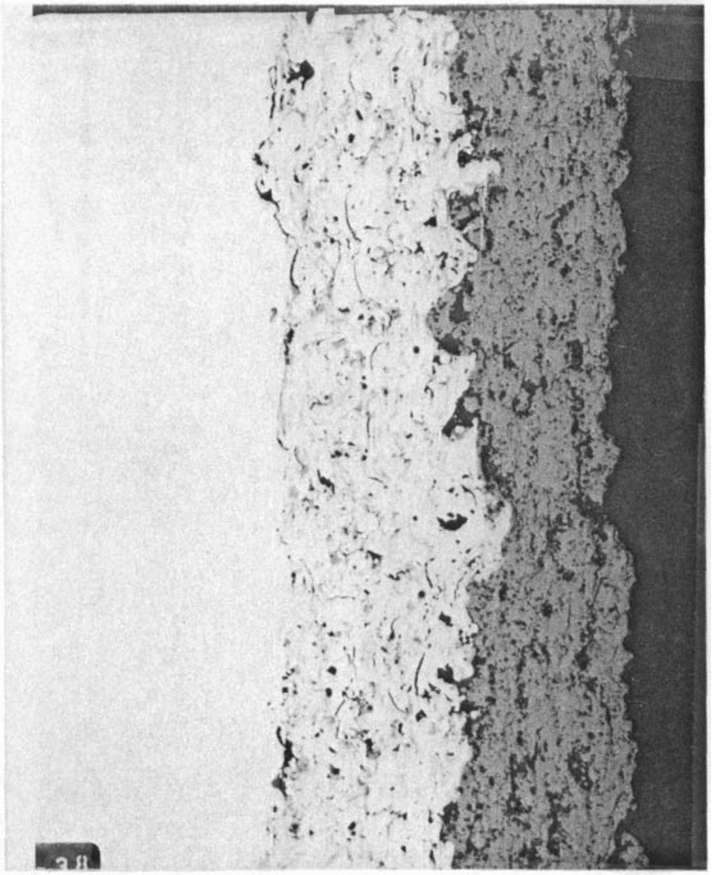

#12 Control 100X

FIGURE A.93. SEM Photograph of ZrO-Coated Sample with a Ni-Cr Base Coat Under 100X Magnification - Control

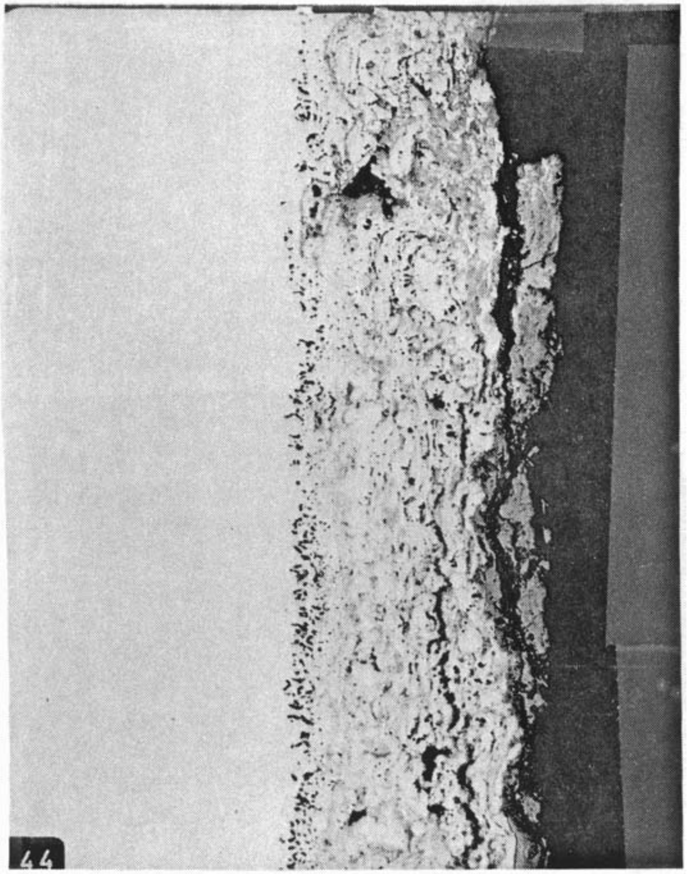

#12 100X

FIGURE A.94. SEM Photograph of ZrO-Coated Sample with a Ni-Cr Base Coat Under 100X Magnification

The most promising coupon samples from the LFCM tests were combined with additional metal samples for testing in the PSCM plenum after the LFCM tests were discontinued. The corrosion samples were chosen to represent different groups of alloys, and the exposure time was varied so the separate effects of idling and melter operation could be determined. The physical appearance and weight of the metal samples were recorded before and after exposure, and the results are shown in Table A.90. Some samples had tenacious particle deposits, so the corrosion rates shown may be low. The deposits also make sample comparison difficult, but the adherence of the deposit may indicate that the surface of the samples is in good condition; the samples with heavy spalling had no deposits.

Examination of the metal samples indicates that idling is not the major contributor to metal corrosion, since duplicate alloys exposed to lengthy idling periods have lower corrosion rates than samples primarily exposed to operating conditions. The cycling between idling and operation could be a cause of corrosion since all the coupons were subjected to cycling. The results also indicate that titanium, tantalum and alloys with high iron concentrations are very susceptible to corrosion.

The alloys' corrosion rate appears to be directly related to the iron concentration, as is clearly shown by comparing corrosion results obtained from RA-446, RA-330, Inconel-615 and the Haynes alloys (see Table A.90). The most promising alloys appear to have low iron, high nickel or cobalt, and 20 to 25% chromium. The cobalt-based alloys are yenerally considered more corrosion resistant to sulfidation corrosion and should be considered in place of nickel-based alloys.

SEM micrographs were obtained of the cross-sections of the best alloys, which include Inconel-690 and -625, Haynes 188 and 25, and Hastelloy X. (see Figures A.95 through A.103). Figure A.95 is an unexposed Inconel-625 sample for comparison. A summary of the samples' conditions and exposures is given in Table A.91. Overall, the micrographs show Cr migration to the surface of the alloys and voids underneath the Cr_2O_3 layer. The samples all appear depleted in Ni or Co, with segregation of the Ni and Cr. Most of the micrographs show CrS underneath the Cr_2O_3 layer typical of sulfidation or hot corrosion. A more detailed description of the coupon samples examined is given below.

TABLE A.90. Corrosion Data

Material	Corrosion Exposure, h		Rate, mm/yr	Observations			Approximate Composition, Wt%					
	Idling	Operating		Pitting	Spalling	Deposits	Co	Cr	Fe	Mo	Ni	W
Inconel®-690	1340	700	*0.23	N	M	N	--	30	9.5	--	60	--
	1270	584	0.26	N	M	N						
	340	584	0.43	N	L	N						
	460	700	0.17	N	M	N						
Inconel®-625	460	700	*0.03	N	--	H	--	21.5	2.5	9	61	--
	1270	584	0.03	N	--	L						
	340	584	t	N	--	L						
	1390	700	*0.01	Small Pits	--	M						
Haynes®-188	1270	584	*0.07	N	M	H	49	22	<3	--	22	15
	340	584	0.05	N	L	M						
	100	232	*3.6	One Wide Pit	Pitted	N						
Haynes®-25	1270	584	t	N	H	L	54	21	<3	--	10	15
	160	480	0.55	N	MH	L						
	340	584	*0.04	N	MH	L						
	100	232	9.6	One Wide Pit	Pitted	L						
HA''-330	1270	584	0.38	N	H	N	--	18	47	--	35	--
	340	584	0.62	N	M	N						
RA®-446	1170	352	1.9	N	H	N	--	25	75	--	--	--
	238	352	3.7	N	H	N						
Hastelloy X	100	232	*0.94	One 1" dia pit	Pitted	L	1.5	23	18.5	9	47	0.6
Hastelloy C-4	100	232	>48	Disappeared	--	N	--	16	3	15	65	--
Hastelloy S	40	138	40	Badly Pitted	L	N	--	16	3	15	65	--
Inconel-600	222	348	0.23	N	M	L	--	15.5	8	--	76	--
Inconel-617	122	116	0.16	Pitted	--	M	12	22	1.5	9	52	--
Tantalum	122	116	30	Disappeared	--	--	--	--	--	--	--	--
Titanium	122	116	2.1	Pitted Badly	H	N	--	--	--	--	--	--

* Samples were not washed before obtaining final weight.
® Inconel is a registered trademark of Huntington Alloys.
® Haynes is a registered trademark of the Cabot Corporation, Kokomo, Indiana.
® RA is a registered trademark of Rolled Alloys, Detroit, Michigan.
H Heavy
M Medium
L Light
N None

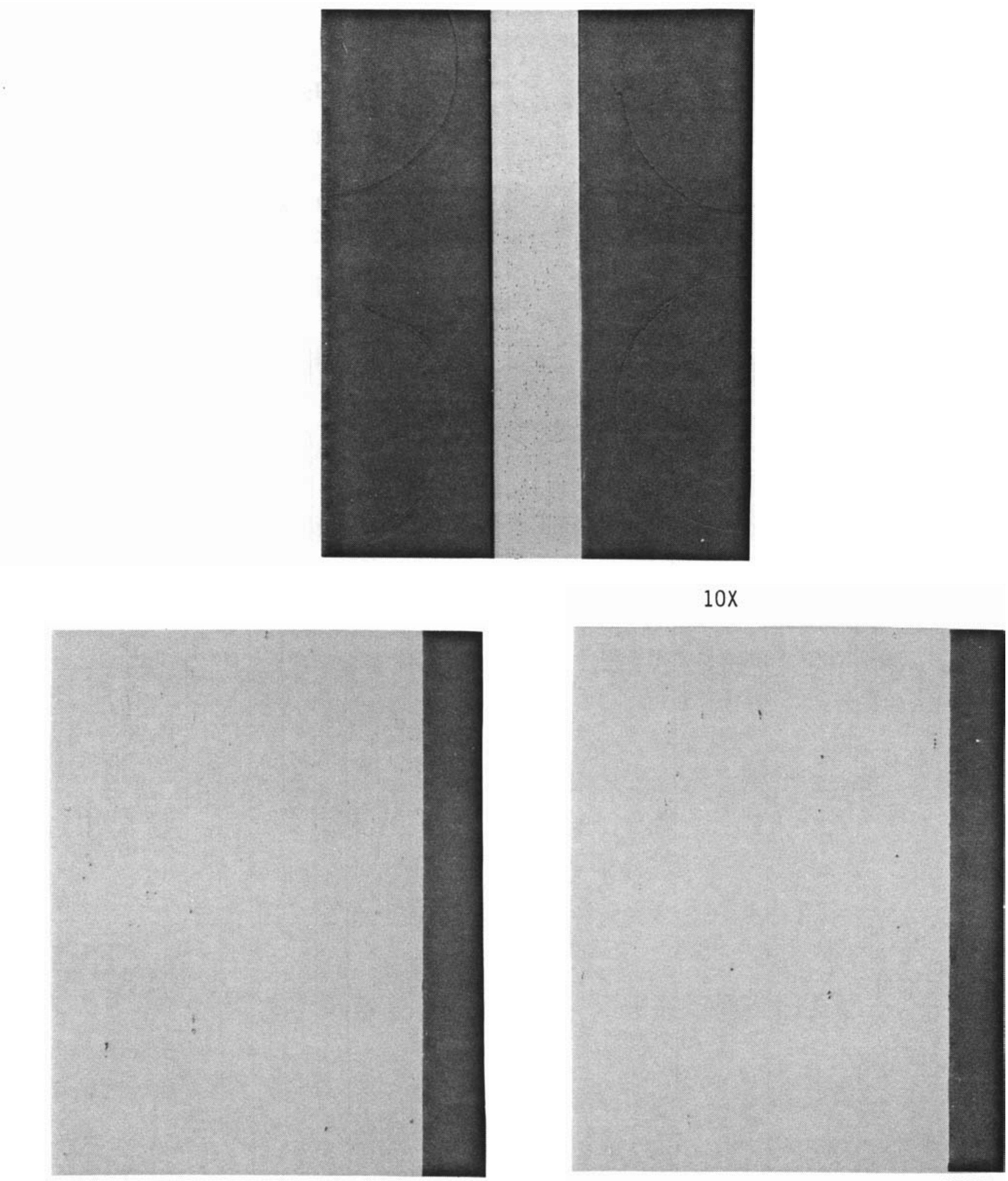

10X

100X

250X

FIGURE A.95. Inconel-625 Unexposed Sample Under 10X, 100X and 250X SEM Magnification

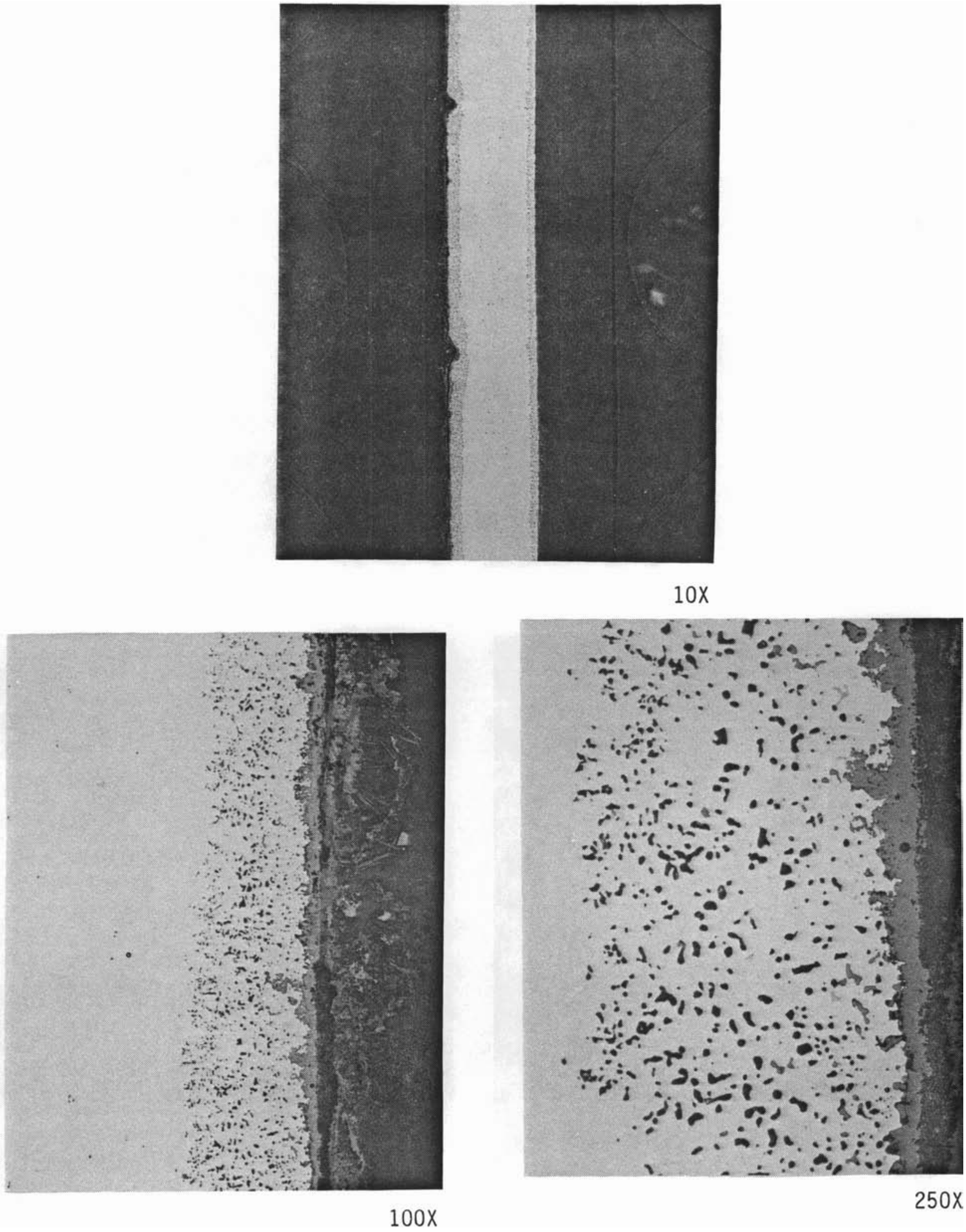

10X

100X

250X

FIGURE A.96. Inconel-625 Sample Under 10X, 100X and 250X SEM Magnification

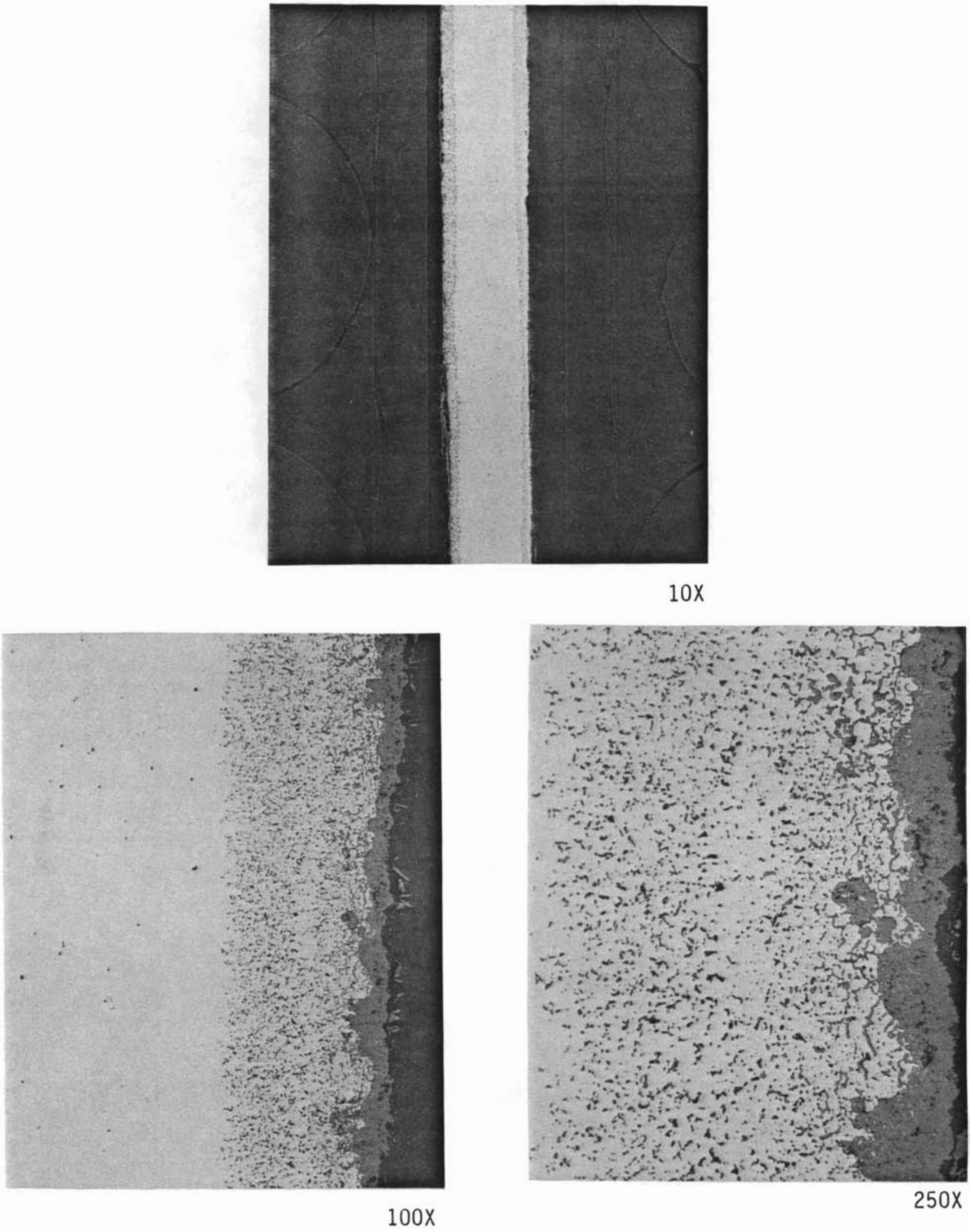

10X

100X

250X

FIGURE A.97. Inconel-625 Sample Under 10X, 100X and 250X SEM Magnification

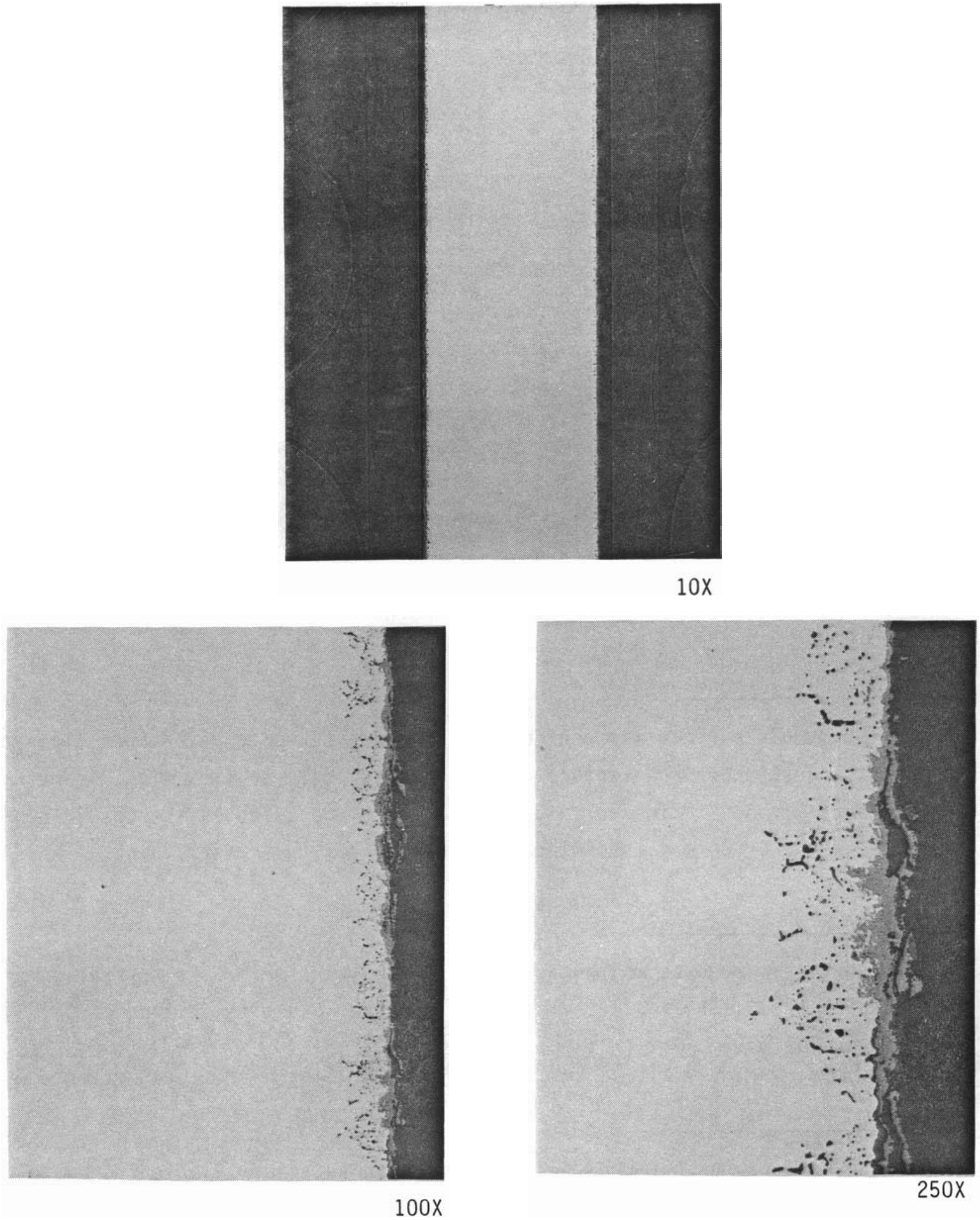

10X

100X

250X

FIGURE A.98. Hastelloy Sample X Under 10X, 100X and 250X SEM Magnification

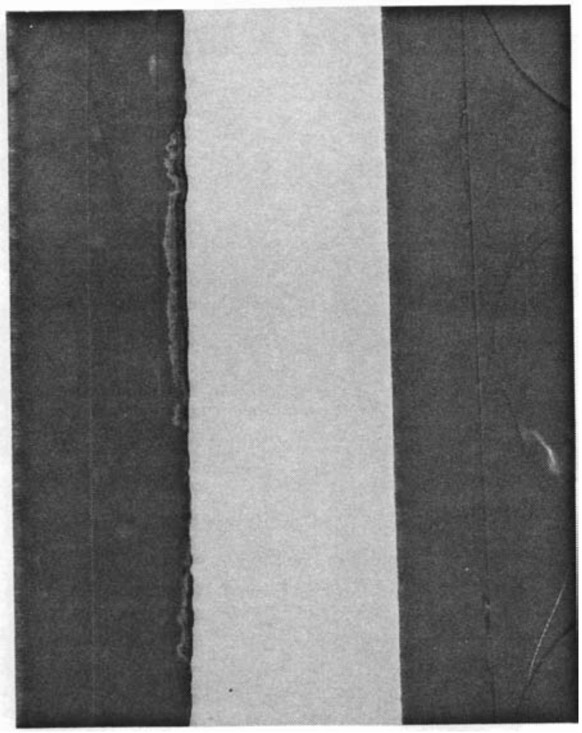

FIGURE A.99. Haynes 188 Sample #1 Under 10X SEM Magnification

Figure A.96 - Inconel-625 #2

The sample surface was enriched in Fe and appears to have other glass components. Just under the surface was a Cr-enriched layer with significant amounts of Ti and S. The solid grey area above the voids is the Cr_2O_3 layer and below the Cr_2O_3 was Inconel-625 depleted of Cr, with many voids.

Figure A.97 - Inconel-625 #1

The glass deposits on the surface of Cr_2O_3 had small NiCr crystals. Underneath the Ni-Cr is a metal matrix of Inconel-625 with islands of Cr, S, and some Ni.

Figure A.98 - Hastelloy X

The surface was enriched in Fe and with an adjacent layer enriched in Cr. The substrate was the Hastelloy X composition slightly depleted in Cr.

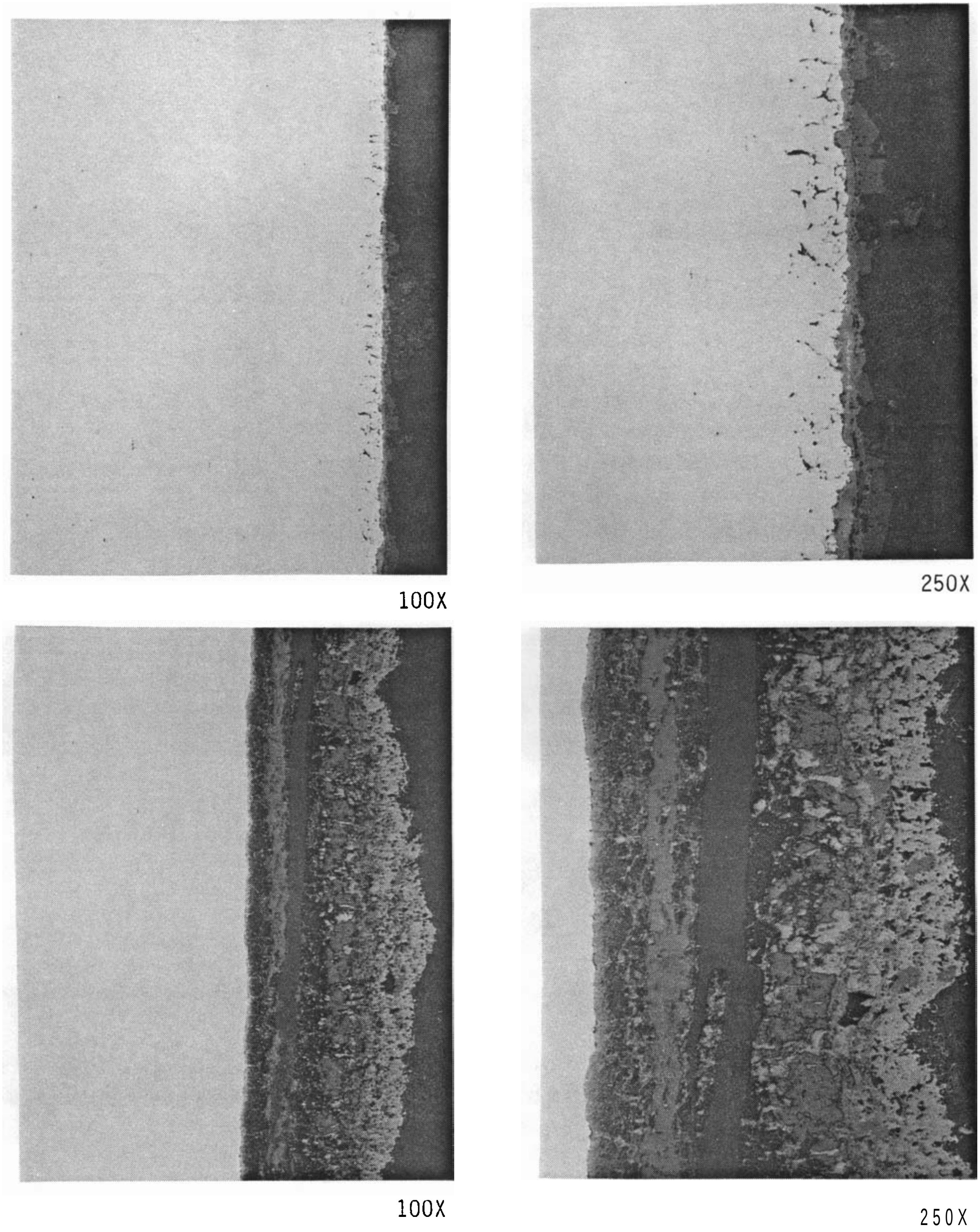

FIGURE A.100. Haynes 188 Sample #1 Under 100X and 250X SEM Magnification

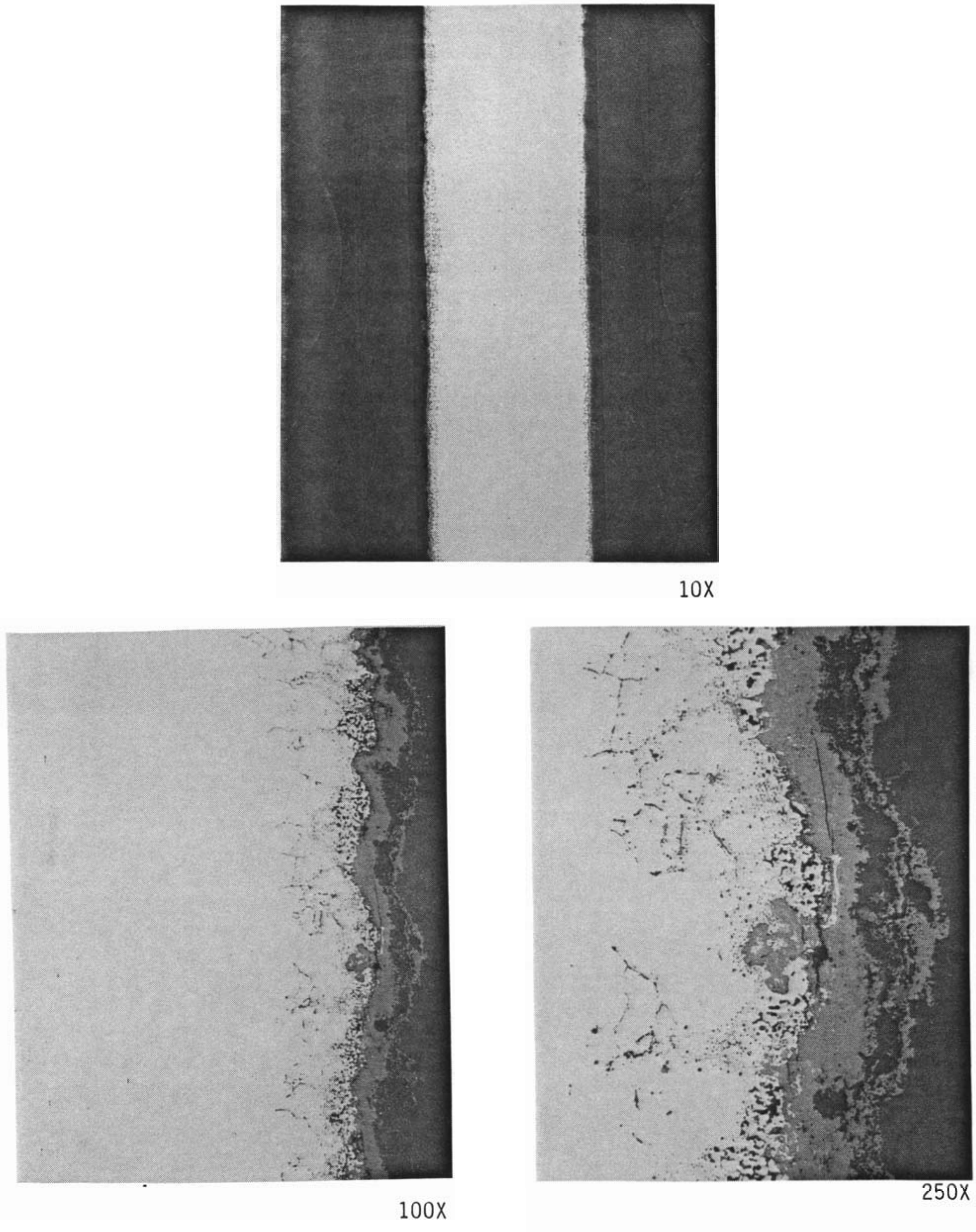

10X

100X

250X

FIGURE A.101. Haynes 188 Sample #2 Under 10X, 100X and 250X SEM Magnification

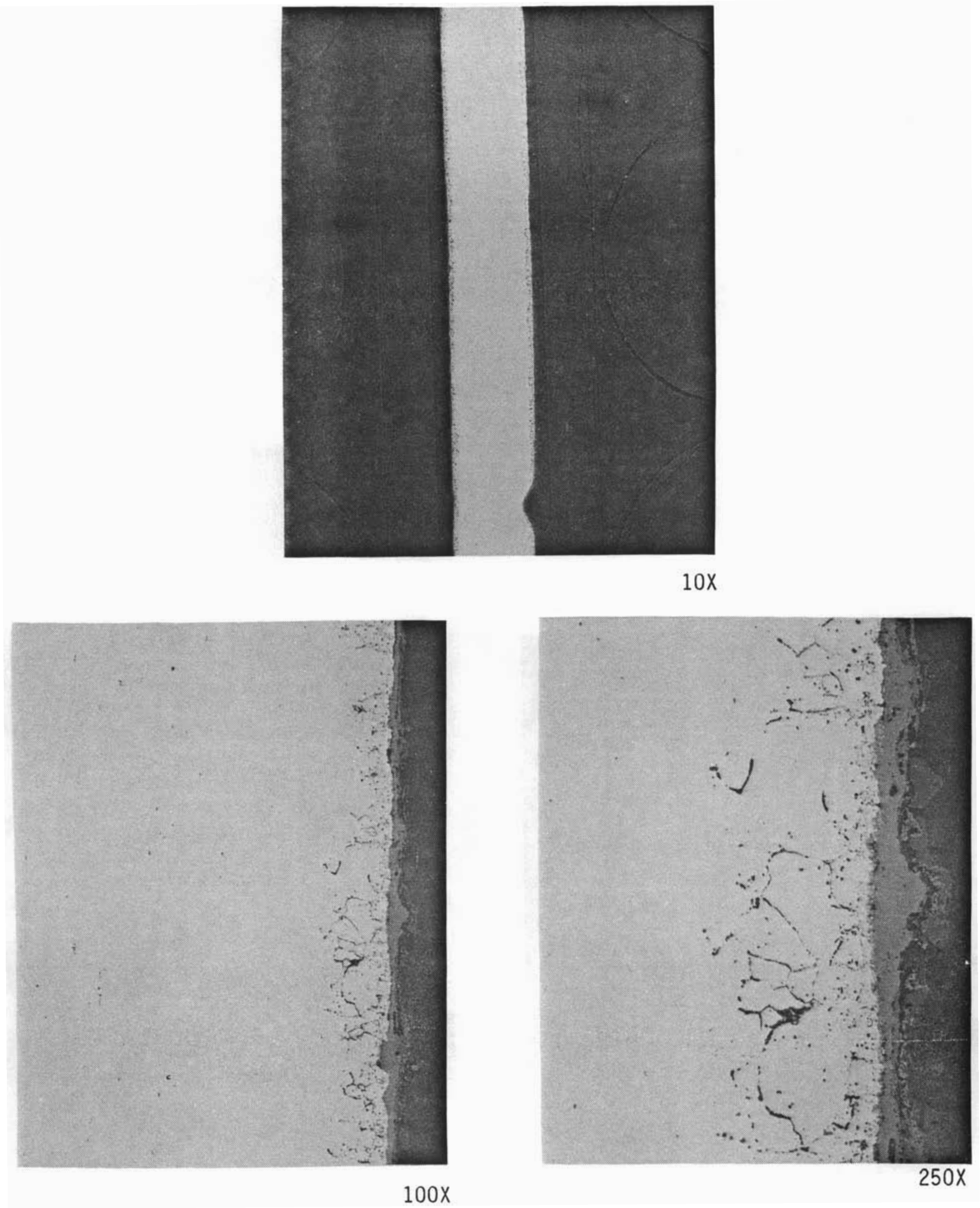

10X

100X

250X

FIGURE A.102. Haynes 25 Sample Under 10X, 100X and 250X SEM Magnification

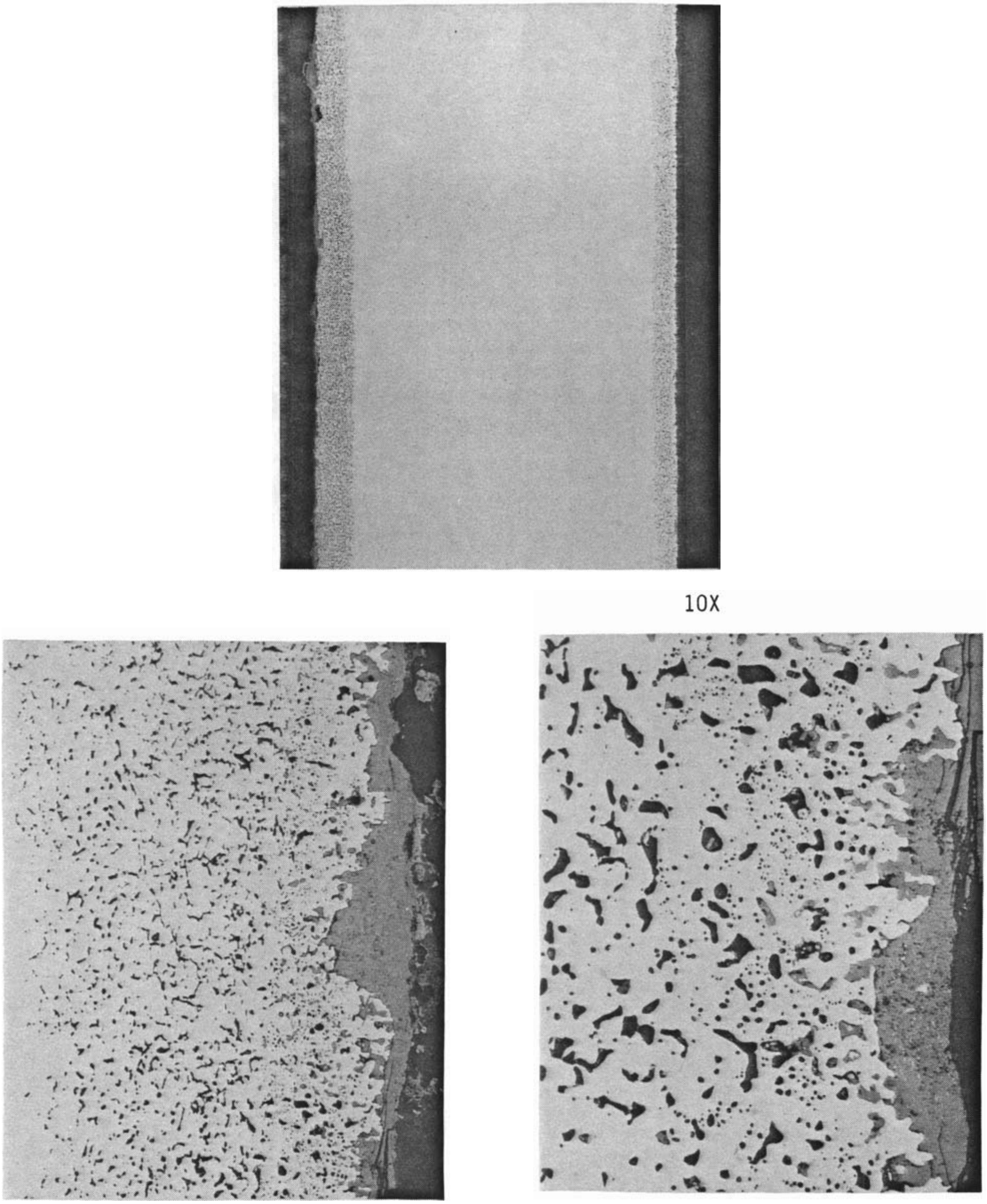

10X

100X

250X

<u>FIGURE A.103.</u> Inconel-690 Sample Under 10X, 100X and 250X SEM Magnification

TABLE A.91. Summary of Alloy Micrographs

Alloy	Exposure Time, h	Void Penetration, μm	Thickness Oxide Layer, μm
Inconel-625 #1	1850	300	40-50
Inconel-615 #2	2100	290	30
Hastelloy X	330	100	5-20
Haynes 25	920	180	10-20
Haynes 188 #1	330	80	300 by pit
Haynes 188 #2	1850	260	40-80
Inconel-690	2100	700	30-150

Figure A.99 & A.100 - Haynes 188 #1

The top two micrographs in Figure A.100 show a Cr-enriched layer on top of the metal substrate with voids. The bottom micrographs show a pitted area. The pitted area has a Cr-depleted surface, with significant amounts of Si and S. Other groups near the surface are enriched in W or Mo, with very little Cr. Below this mixture of groups is a Cr layer with less than half the original Co and Ni. At the reaction interface there is a Cr-enriched layer.

Figure A.101 - Haynes 188 #2

The sample has a surface and substrate depleted in Cr with a Cr_2O_3 layer in the middle. The Cr_2O_3 layer contains almost 100% Cr_2O_3. Some Te was found underneath the Cr_2O_3. The W was also depleted on the surface.

Figure A.102 - Haynes 25

The 10X micrograph shows a small pit developing. The general surface contains many cube-like crystals of Cr, Co, Fe, Ni, which are more enriched in Cr than the base alloy. The largest layer on top of the base metal is essentially all Cr_2O_3.

Figure A.103 - Inconel-690

The sample surface had a Cr_2O_3 layer on top of a metal matrix of Cr-depleted Inconel-690, voids, and islands of Cr and S.

PSCM

The PSCM off-gas port was cleaned of deposits after nine months of operation, and severe pitting was observed. The off-gas port was Inconel-690 pipe, plasma spray coated with 80% Ni/20% Cr. This coating did not protect the pipe and appears to have spalled off. The Inconel viewports were also plasma spray coated, one with Cr_2O_3 and the other with $ZrO-Y_2O_3$. Both these coatings appeared to have spalled, offering little protection to the metal viewports.

The Inconel-690 electrodes were removed from the melter and any adhering glass was chipped away so the electrodes could be inspected. Electrode surfaces normally below the glass surface showed no signs of corrosion. The portion of the electrodes exposed to the plenum vapors was spalling and contained some large pits. The corroded areas were magnetic with the pits being the most magnetic. The pits were found underneath large deposits of partially vitrified glass. These deposits are enriched in Cl and S in previous experiments, and the present deposits are similar. These types of deposits could be causing "hot corrosion," a thin-film salt corrosion process which is not well understood.

The plenum heater thimbles (Inconel-600, -601 and -690) showed the same pitting corrosion as the electrode, except that the Inconel-690 was not badly attacked. The Inconel-600 and -601 thimbles were attacked severely. One of the Inconel-600 thimbles was completely perforated after only 20 days of melter operation. The pits and surrounding areas were magnetic, indicating a loss of Cr from the alloy surface. The thimbles were also discolored where they were exposed to the plenum gases. The thimbles were fabricated from Inconel-600, Inconel-601 or Inconel-690; and only the two Inconel-690 thimbles remained unpitted. Of the five Inconel-600 thimbles used, four were pitted. The unpitted thimble was closest to the melter wall where the gas flow rate was lower. The Inconel-600 thimbles appear to be pitted the most. This can be seen in Figure A.104, where thimbles numbered 2, 3, 7 and 10 are of Inconel-600, and thimble number 8 is made of Inconel-601. Inconel-690 appears the most corrosion resistant of the three alloys used, but more testing is needed to determine resistance over the long term.

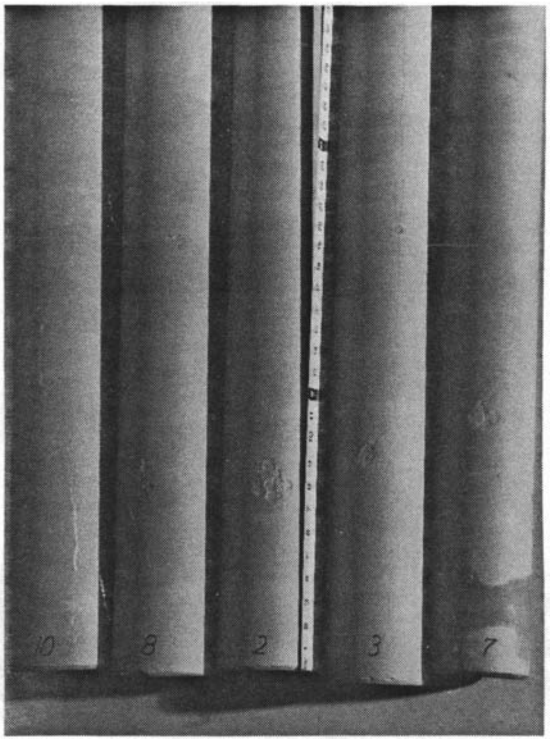

FIGURE A.104. PSCM Plenum Heater Thimbles

SEM micrographs of the plenum heater are shown in Figures A.105 through A.109. The micrographs show the S under the Cr_2O_3 protective layer typical of sulfidation or hot corrosion.

The Inconel-690 plenum thermowell was also pitted excessively after PSCM-8. The original thermowell was 2.5 cm in diameter from top to bottom. Some areas had lost 0.25 cm as shown in Table A.92.

The feed nozzle used for the PSCM melter was closely inspected after PSCM-9, and many small pinholes were observed in the feed nozzle cooling jacket. The cooling jacket was then leak-tested with water at 40 psig, and many of the pinholes leaked. The overall leak rate was <100 ml/h. The outside of the cooling jacket, which is exposed to the melter plenum, was made of stainless steel with an Inconel-690 tip. The holes looked like typical Cl^- pitting corrosion in low pH solutions. This is reasonable since steam from the melter plenum condenses on the cold feed nozzle, and the condensate has a low pH and a Cl^- concentration of about 1000 ppm.

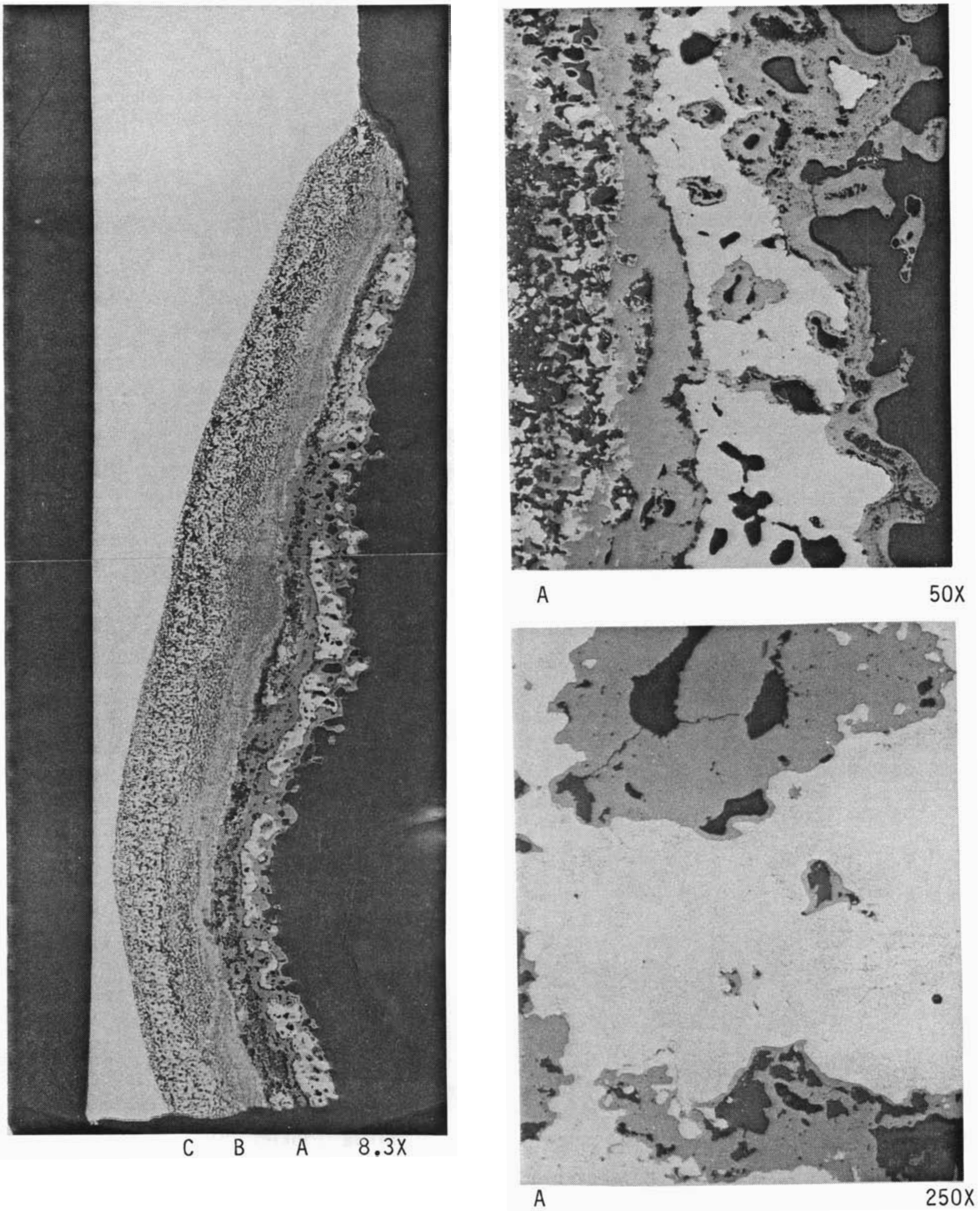

FIGURE A.105. Inconel-600 Thimble 8X SEM Cross Section with 50X and 250X Magnification

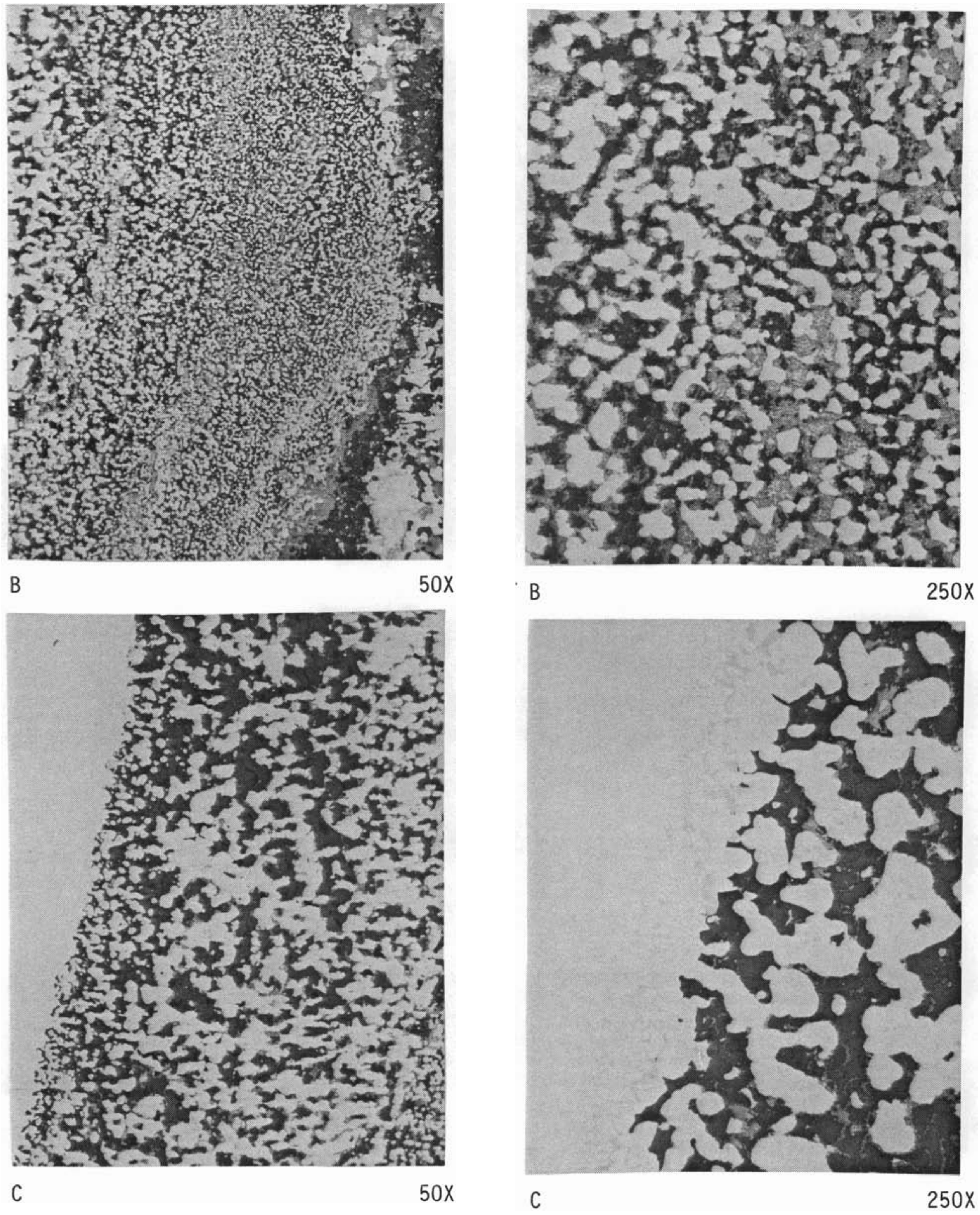

FIGURE A.106. Inconel-600 Thimble Cross Sections of Regions B and C (see Figure 105) Under 50X and 250X Magnifications

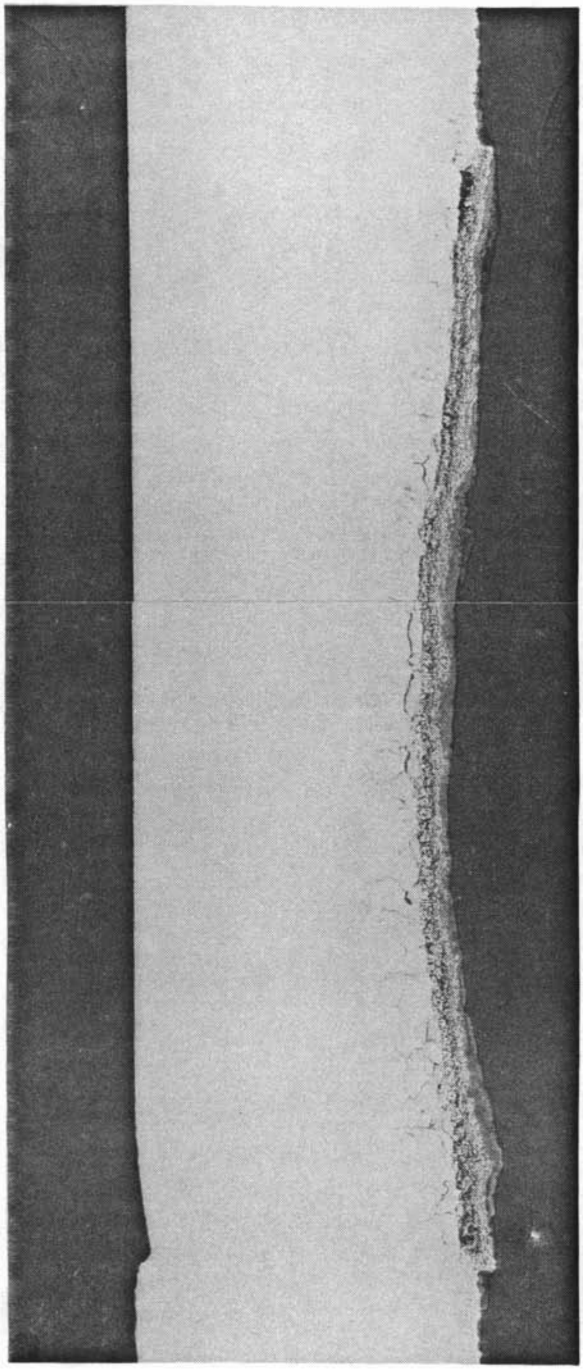

8.3X

FIGURE A.107. Inconel-601 Thimble 8X, SEM Cross Section

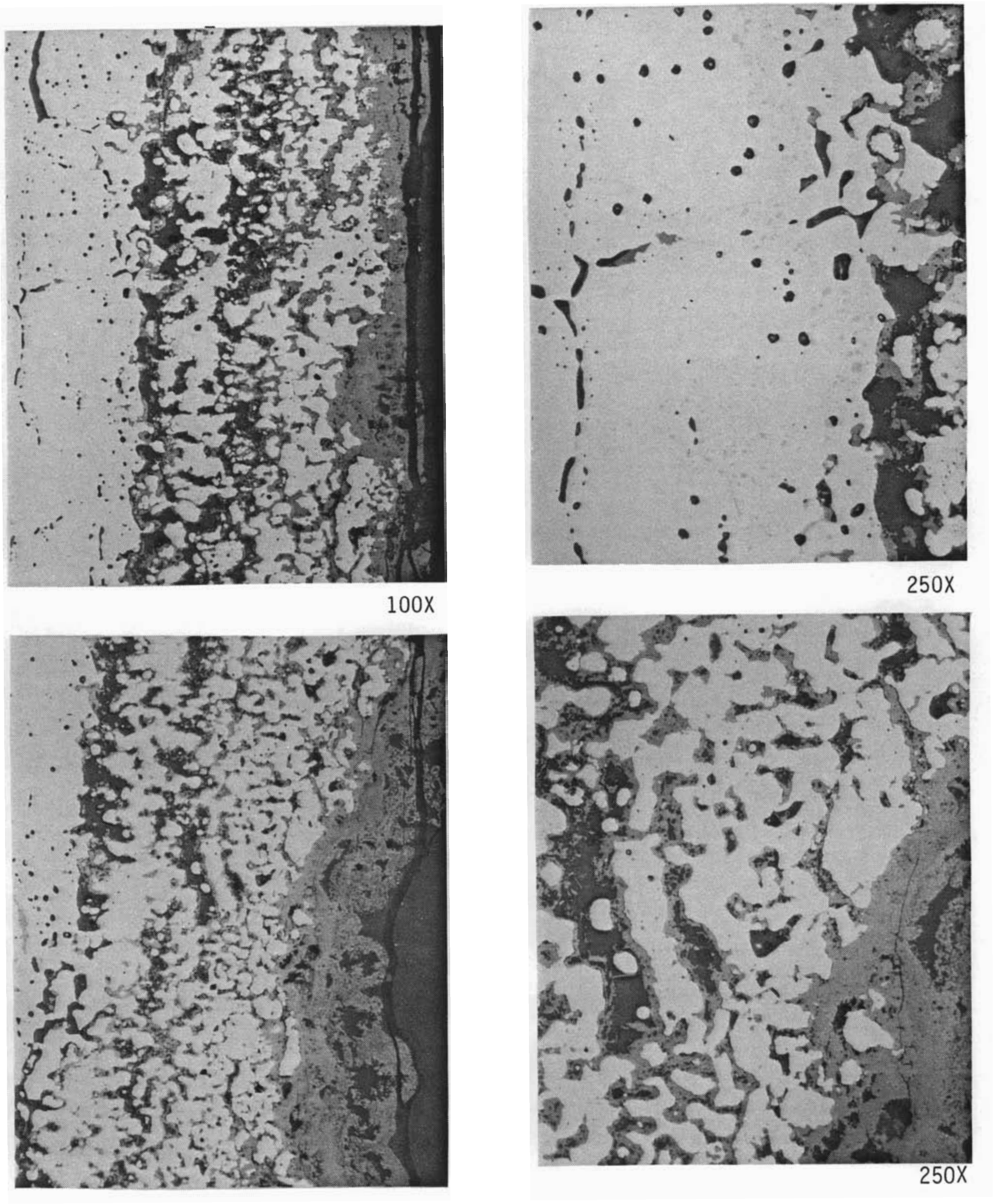

100X

250X

100X

250X

FIGURE A.108. Inconel-601 Cross Section Under 100X and 250X SEM Magnification

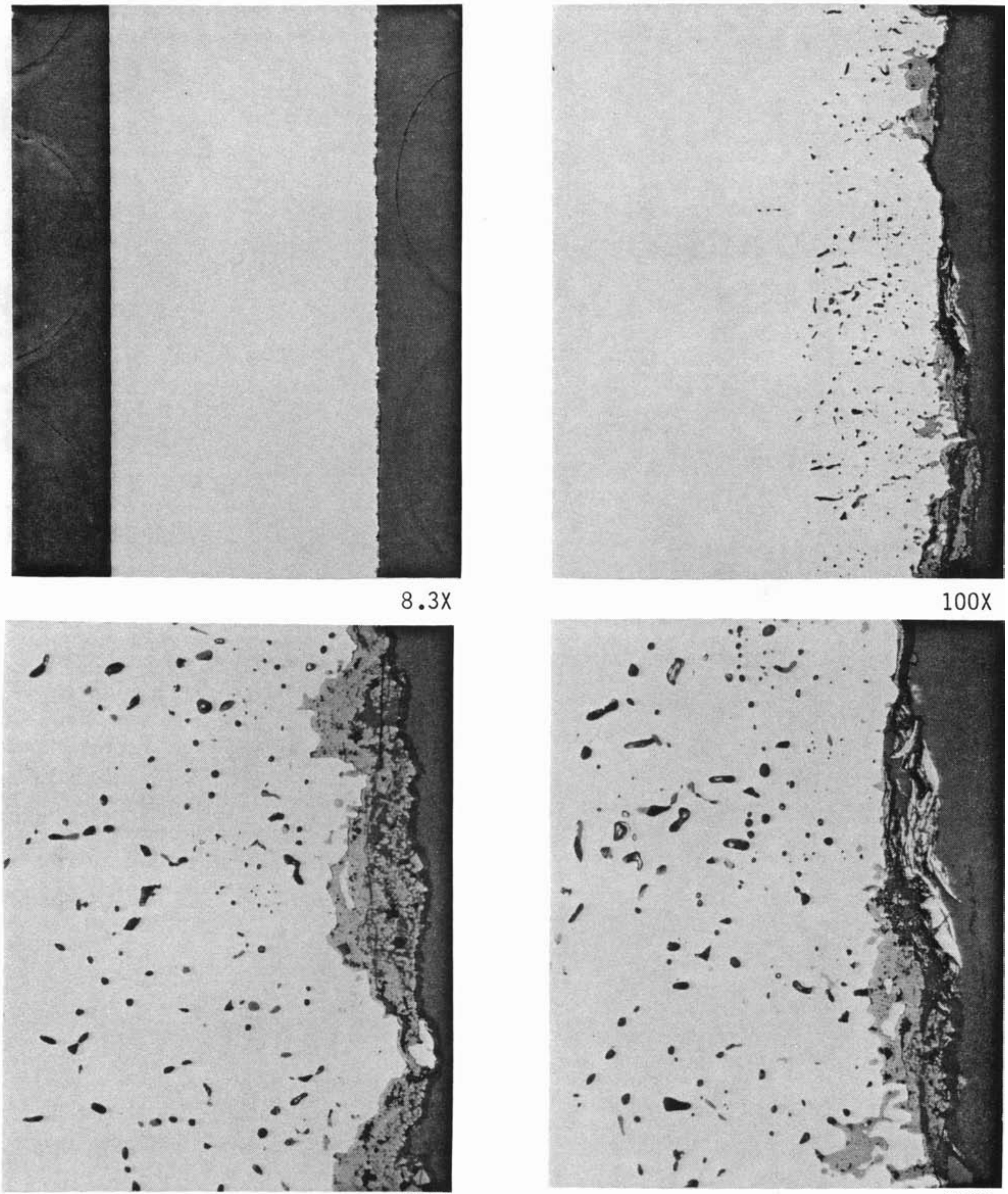

8.3X

100X

250X

250X

FIGURE A.109. Inconel-690 Thimble Cross Section Under 8.3X, 100X and 250X SEM Magnification

TABLE A.92. Plenum Thermowell Measurements

Length From Bottom of Thermowell, cm	Thermowell Diameter, cm
0	2.53
7.6	2.47
15	2.51
23	2.45
27	2.24(a)
30	2.31
38	2.53
46	2.52
53	2.54
61	2.54
69	2.53
76	2.51

(a) Badly pitted.

The feed nozzle weld zones were the most severely attacked. The Inconel-690 tip was also pitted, but had no perforations, except where the Inconel was welded to the stainless steel. Inconel-690 is more resistant to pitting than stainless steel, but it also appears to have a limited service life. A better material for this application would be Inconel-625, Hastelloy C-276 or titanium. However, the Hastelloy C-276 and the titanium would not last long if cooling water was lost to the feed nozzle. Prior plenum corrosion tests of Hastelloy C-4, which is similar to Hastelloy C-276 and titanium, have shown that they fail after a few days without cooling. Inconel-625 would be the best metallic material. Ceramic insulation would also work well if the thermal gradients did not cause it to crack.

OFF-GAS SYSTEM

Throughout the year, crevice and pitting corrosion has occurred in the melter's venturi scrubber system, which consists of a 316 SS venturi and 304L

SS recirculation lines. The majority of the pits are in the heat-affected zones near welds. The corrosion is caused by the off-gas condensate, which contains –1000 ppm Cl and has a pH of 3.

The condensing vapors have also caused some stress corrosion cracking just prior to the venturi entrance. Recirculation lines are pitting because the recirculating solution is equivalent to the off-gas condensate under steady-state conditions. The corrosion process was probably assisted by S, Fe and F ions. Corrosion studies indicate that 316 and 304L SS are very susceptible to chloride attack in acidic solutions. Some consideration should be given to the material used in the initial off-gas quencher for a liquid-fed ceramic melter processing SRL defense waste. High Ni-Cr-Mo alloys are recommended (such as Hastelloy C-276 and Inconel-625) by material manufacturers for wet environments with high Cl concentrations.

OFF-GAS SYSTEM PERFORMANCE

The off-gas system used for the PSCM is shown in Figure A.I10 with some performance characteristics and operating parameters. The system performance up to and including the first venturi scrubber will be discussed under two conditions: boosted and unboosted. The major difference between these modes of operation is the temperature of the off-gas exiting the melter.

Plenum-boosted experiments require a cooling spray nozzle at the off-gas exit to prevent fused deposits from forming in the off-gas line. The cooling spray also reduces corrosion rates of the metal off-gas piping. However, the presence of the cooling spray itself has been responsible for producing off-gas-line blockages. During PSCM-8 an off-gas-line blockage formed as a result of an air-atomized water cooling spray. The nozzle's spray hit the side of the off-gas line, wetting it and causing particulate matter to collect and grow into a plug which eventually caused the off-gas-line blockage shown in Figure A.III.

The off-gas nozzle could be designed not to impinge on the pipe walls or collect water on the tip. During the PSCM-5 experiment, a spray nozzle that did not wet the off-gas pipes worked satisfactorily for the 5 days it was used. However, the spray cooled the plenum and thereby affected melter capacity. The air-atomized water cooling spray could also be replaced with an air-only or steam-cooling spray, but the mass requirements would be much higher.

Melter operation without plenum boosting does not require a cooling spray because the off-gas temperatures are under 400°C (compared to the 600 to 800°C temperatures when boosting is used). The 400°C temperature will not vitrify off-gas line deposits. Idling periods may cause high temperatures, but this can be minimized by keeping the air inleakage low.

Off-gas particulate does collect in the off-gas line, but the deposits are small and easily removed with high velocity air. The deposits are usually less than 118-in. thick in a 5-day run. Most of these deposits collect on protruding thermocouples and sampling nozzles. The elimination of all off-gas-line penetrations would significantly reduce material accumulation. The PSCM off gas line was 6 in. in diameter so the average gas velocity for a nonboosted

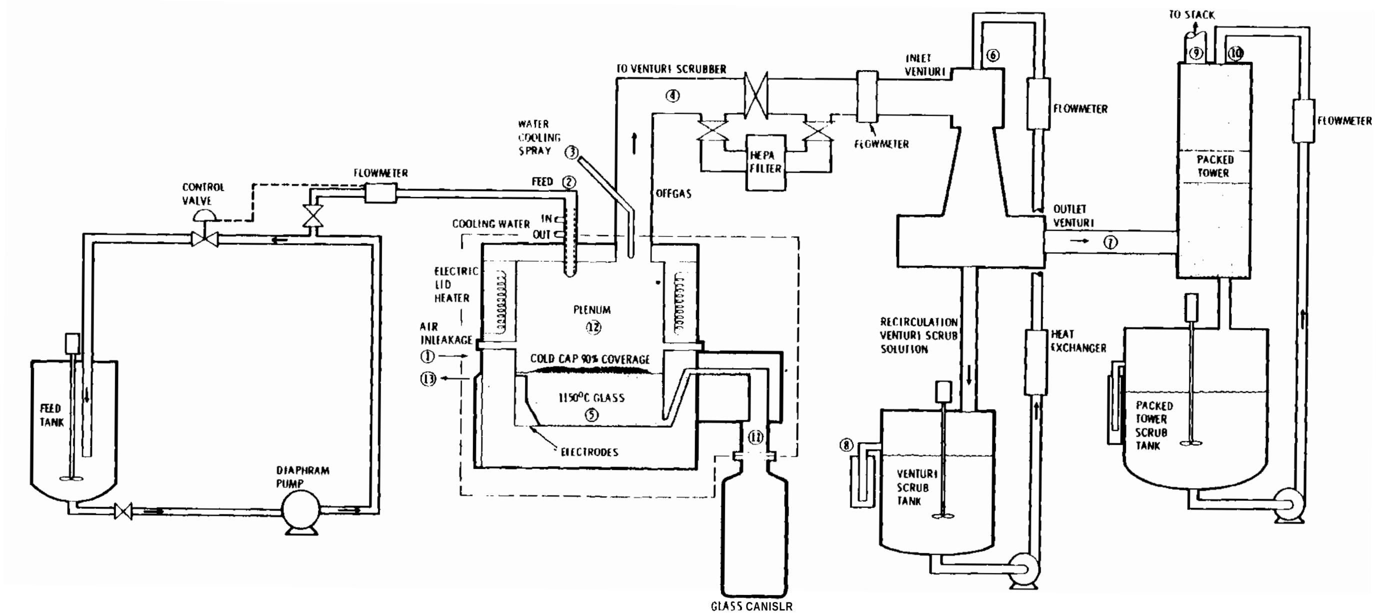

	INLEAKAGE AIR	FEED SLURRY	WATER COOLING SPRAY	OFFGAS TO SCRUBBER	GLASS TANK	VENTURI RECIRCULATING SOL	GAS VENTURI OUTLET	VENTURI SCRUBBER OVERFLOW	PACKED TOWER OUTLET	PACKED TOWER RECIRCULATING SOL	GLASS TO CANISTER	MELTER PLENUM	OTHER HEAT LOSSES *	
	1	2	3	4	5	6	7	8	9	10	11	12	13	
pH	-	11	7	-	-	3	-	3				-	-	
TEMP °C	25	35	20	375	1150	25	25	25		25	1150	600		
PRESS.	-	15 psig	40 psig	-10" H_2O	-	60 psig	-1" H_2O	-	-3" H_2O	6 psig	10" H_2O	10" H_2O		
SP. GR.		1.3	1.0		2.1	1.0		1.0	-	1.0	2.1		-	
TOTAL FLOW ℓ/hr		110	23	-	-	7 x E5	-	119		1600	25			
H_2O FLOW kg/hr		96	23	-	-	7 x E5	-	119		1600	-	-		
SOLID FLOW kg/hr	0	50	0	0.12	-	500	0.07 - 0.01	0.07 0.11	0.01 - 0.06		50			
GAS FLOW STD. L/M	1100	-	-	3700	-	-	1100	-	1100			-	-	
VISCOSITY POISE		100			20						20	-	-	
kW	-			-85	+120		-				-20	+30	-45	
PARTICLE DF Δ				420			2 - 12							

Δ DECONTAMINATION FACTOR
* CONVECTION, CONDUCTION AND RADIATION LOSSES

	FEED COMPOSITION wt%	CONDENSIBLE OFFGAS COMPOSITION wt% EXCLUDING H_2O
Al	2.1	0.8
B	1.2	7.0
Ca	0.9	0.73
Cd	0.007	0.04
Cr	0.01	0.5
Cs	0.05	0.30
Fe	9.9	7.0
La	0.34	0.10
Li	1.9	1.2
Mg	0.84	0.40
Mn	2.6	1.5
Na	10.2	15.0
Ni	1.3	0.01
Ru	0.014	0.09
Sb	0.027	0.04
Si	20	11.0
Sr	0.018	0.016
Te	0.009	0.09
Ti	0.42	0.31
Zn	<0.01	0.20
Zr	0.30	0.01
Cl	0.1	12.0
S	0.045	9.0
F	NEG.	0.5

	OFFGAS COMPOSITION mole% DRY GAS
N_2	79
O_2	20
CO_2	0.6
CO	0.03
NO_x	0.02
SO_2	0.01
H_2	0.1

FIGURE A.110. Off-Gas System

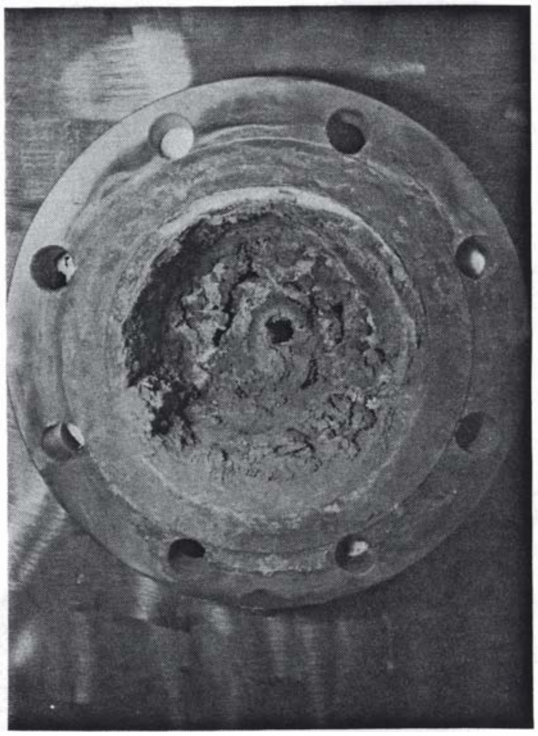

FIGURE A.111. Material Buildup in Melter Plenum Exhaust Port

C

experiment was 10 ft/sec. This relatively slow gas velocity is not effective in sweeping out off-gas particulates. A smaller diameter pipe may be less likely to foul because of the higher gas flow rate. The material deposited in the off-gas line appear to be entrained feed enriched in Cs and other semivolatiles.

The close-coupled venturi scrubber associated with the PSCM was positioned about 5 ft from the melter plenum to minimize the piping which is susceptible to particulate deposits and to allow a straight, unobstructed pipe section to the scrubber. The horizontally mounted venturi scrubber allowed water to collect in the off-gas-line throat of the venturi. A vertically mounted venturi with a separator box had been used previously with less wetting and particulate buildup at its entrance. Consequently, a vertical scrubber configuration appears to be preferred over horizonal mounting. Both venturis effectively condensed all the steam in the off gas, precluding the use of a downstream condenser except as a backup.

MATERIAL BALANCE Te., Se and Ru

The PSCM melter was drained and cleaned, and a new lid was installed in December 1981. Since that time, five experiments have been performed: PSCM-4 throuyh PSCM-8. In each of these experiments, a significant percentage of Se, Te and Ru could not be accounted for by glass production and off-gas system losses. After PSCM-8, the melter was drained and inspected. The inspection revealed a large quantity of metal-like nodules in the position shown in Figure A.112. Each group was analyzed, and the results are shown in Table A.93. The total weight of the nodules collected was 6.16 kg. The average nodule composition was mainly Ni and S, with significant quantities of Te, Se and Ru. Table A.94 is an attempt to account for all the Te, Se and Ru, which could not be accounted for during PSCM-4 through PSCM-8. The nodule samples were not homogeneous, which creates siynificant uncertainty in the calculated total of each element. The off-gas analysis for these elements is also subject to large errors because the concentrations are close to the analytical detection limits. With these limitations in mind, the missing Te and all but 10% of the Se can be accounted for. Much of the Ru is still unaccounted for due in part to the inaccuracy of nodules Ru analysis. Overall, the material balance gives general values on the fate of Te, Se and Ru in a ceramic melter with formic acid feed. The metal nodules accounted for ~40% of the Te, 25% of the Se, and 20% of the Ru fed to the PSCM in formic acid feeds.

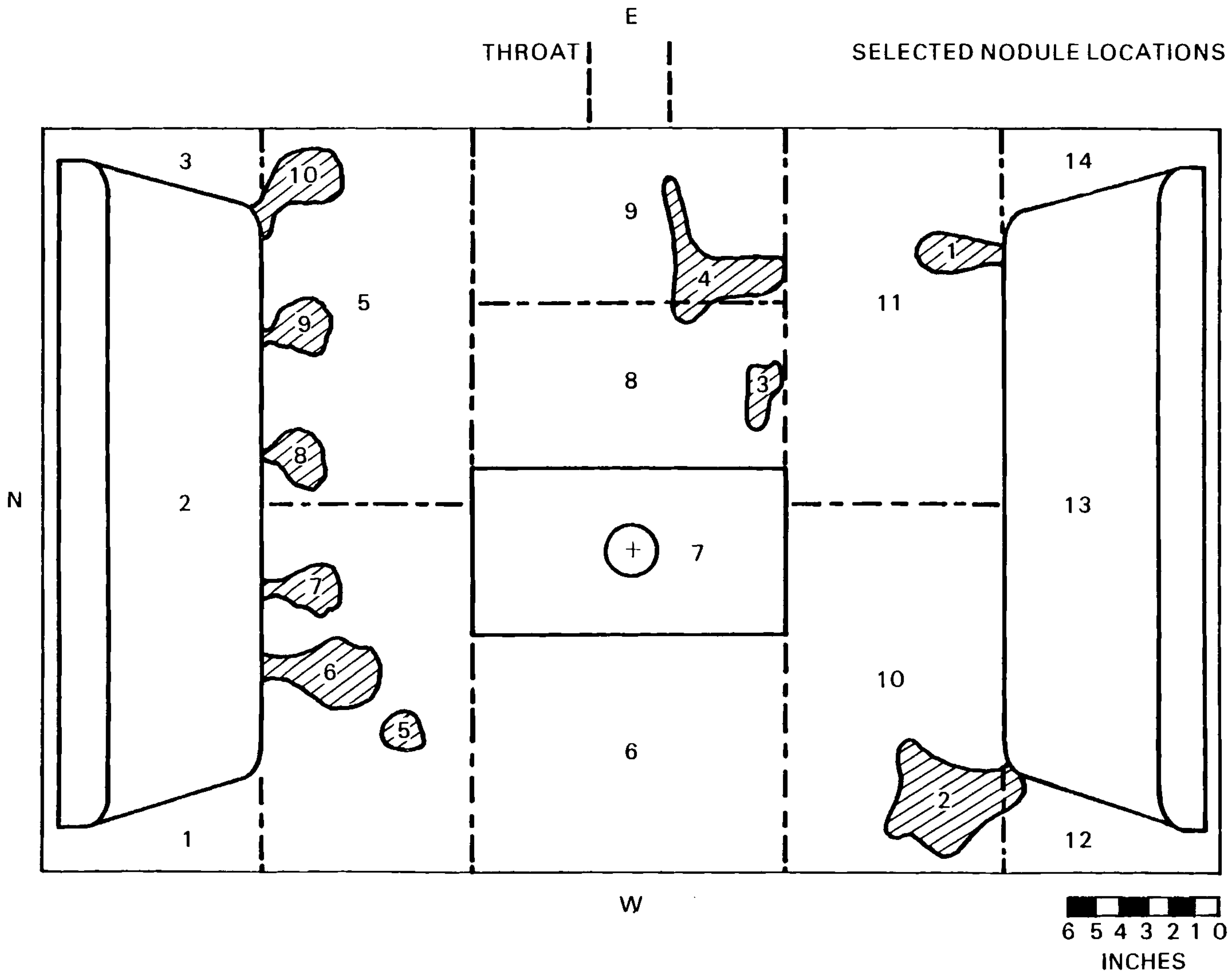

FIGURE A.112. PSCM-8 Melter Floor Survey

TABLE A.93. Metal Found on Melter Floor

Element	Locations Shown on Figure A.l										Blue Ball	Gold Ball	Fine Speckled Ball	Shiny Crystals	Gold Group
	1S	2S	3S	4S	5S	6S	7S	8S	9S	10S					
B	<0.04	<0.04	<0.04	<0.04	<0.04	<0.04	<0.04	<0.04	<0.04	<0.04	<0.04	<0.04	<0.04	<0.04	<0.04
Ca	<0.15	<0.15	<0.15	<0.15	<0.15	<0.15	<0.15	<0.15	<0.15	<0.15	<0.15	<0.15	<0.15	<0.15	<0.15
Cd	<0.01	<0.01	<0.01	<0.01	<0.01	<0.01	<0.01	<0.01	<0.01	<0.01	<0.01	<0.01	<0.01	<0.01	<0.01
Cs	<0.04	<0.04	<0.04	<0.04	<0.04	<0.04	<0.04	<0.04	<0.04	<0.04	<0.04	<0.04	<0.04	<0.04	<0.04
Cu	2.1	2.9	2.6	2.2	1.9	2.0	1.8	1.9	1.9	1.9	1.6	1.5	1.5	2.9	2.0
Fe	<0.10	<0.10	<0.10	<0.10	<0.10	<0.10	<0.10	<0.10	<0.10	<0.10	<0.10	<0.10	<0.10	<0.10	<0.10
Li	<0.02	<0.02	<0.02	<0.02	<0.02	<0.02	<0.02	<0.02	<0.02	<0.02	<0.02	<0.02	<0.02	<0.02	<0.02
Mg	<0.04	<0.04	<0.04	<0.04	<0.04	<0.04	<0.04	<0.04	<0.04	<0.04	<0.04	<0.04	<0.04	<0.04	<0.04
Mn	<0.02	<0.02	<0.02	<0.02	<0.02	<0.02	<0.02	<0.02	<0.02	<0.02	<0.02	<0.02	<0.02	<0.02	<0.02
Na	<0.5	<0.5	<0.5	<0.5	<0.5	<0.5	<0.5	<0.5	<0.5	<0.5	<0.5	<0.5	<0.5	<0.5	<0.5
Ni	56	57	37	53	56	59	58	43	50	57	62	63	51	35	50
Ru	1.6	1.4	9.1	2.3	3.0	1.7	1.7	5.7	4.4	2.2	0.24	0.77	7.8	29.0	1.1
S	18	21	10	17	17	18	19	13	14	15	20	23	12	8	15
Sb	0.21	0.34	0.06	0.16	0.20	0.26	0.21	0.12	0.19	0.25	0.25	0.33	0.16	BD	
Se	2.8	2.3	5.7	3.0	2.5	2.1	2.5	5.1	4.0	2.3	1.5	1.5	3.6	3.3	3.2
Sr	<0.003	<0.003	<0.003	<0.003	<0.003	<0.003	<0.003	<0.003	<0.003	<0.003	<0.003	<0.003	<0.003	<0.003	<0.003
Te	11	9.7	21	11	9.8	8.8	9.9	18	14	9.3	7	6.9	12	10	7.1

TABLE A.94. Te, Se and Ru Material Between PSCM-4 and PSCM-8

Element	Run No. PSCM	Weight in grams Feed	Glass	Off-Gas	Melter Floor Nodules	Unaccounted For
	4	163	80	50		
	5	200	100	60		
Te	6	314	100	100		
	7	468	140	30		
	8	763	150	250		
	Total	1908	570	490	600 - 900	~0
	4	430	<140	70		
	5	390	<170	70		
Se	6	100	<50	20		
	7	80	<30	30		
	8	150	<80	30		
	Total	1150	<470	220	300	150
	4	2240	1220			
	5	400	220			
Ru	6	450	220			
	7	330	180			
	8	0	0			
	Total	3420	1840	~0	200 - 1200	600 - 1600

DISTRIBUTION

No. of
Copies

OFFSITE

27 DOE Technical Information Center

R. D. Smith
Division of Waste Management
Nuclear Regulatory Commission
Washington, DC 20555

W. E. Mott
DOE Division of Environmental Control
Technology
Washington, DC 20545

4 DOE Terminal Waste Disposal and
Remedial Action
GTN
Washington, DC 20545
ATTN: J. E. Baublitz, NE-24
F. E. Coffman, NE-20
J. R. Coleman, NE-23
D. J. McGoff, NE-23

3 DOE Office of Defense Waste and
Byproducts Management
GTN
Washington, DC 20545
ATTN: J. E. Dieckhoner
J. J. Jicha
G. K. Oertel

W. W. Ballard, Jr.
DOE Office of Spent Fuel Management
and Reprocessing Systems
NE-40, GTN
Washington, DC 20545

S. A. Mann
DOE Chicago Operations Office
9800 South Cass Avenue
Argonne, IL 60439

J. O. Neff
DOE National Waste Program Office
505 King Avenue
Columbus, OH 43201

No. of
Copies

J. D. Hamric
DOE Idaho Operations Office
550 2nd Street
Idaho Falls, ID 83401

2 DOE Savannah River Operations
Office
P. O. Box A
Aiken, SC 29801
ATTN: E. S. Goldberg
T. B. Hindman

3 Exxon Nuclear Idaho
P. O. Box 2800
Idaho Falls, ID 83401
ATTN: D. L. Concotta
J. D. Christian
File Copy

3 Battelle Memorial Institute
Office of Nuclear Waste
Isolation
505 King Avenue
Columbus, OH 43201
ATTN: N. E. Carter
S. Goldsmith
B. Rawles

6 E. I. du Pont de Nemours Co.
Savannah River Laboratory
Aiken, SC 29808
ATTN: J. L. Crandall
E. J. Hennelly
H. L. Hull
S. Mirshak
D. Witt
T. Wright

R. Williams
Electric Power Research
Institute
3412 Hillview Avenue
Palo Alto, CA 94304

No. of
Copies

R. Williams
Electric Power Research Institute
3412 Hillview Avenue
Palo Alto, CA 94304

J. L. Knabenschuh
Nuclear Fuels Services, Inc.
P. O. Box 191
West Valley, NY 14171

2 Bechtel National, Inc.
P. O. Box 3965
San Francisco, CA 94119
ATTN: J. L. Jardine
W. A. Freeby

ONSITE

5 DOE Richland Operations Office

H. E. Ransom
O. J. Elgert
R. D. Izatt
J. J. Schreiber (2)

5 Rockwell Hanford Operations

R. N. Gurley
J. W. Patterson
J. H. Roecker
D. D. Wodrich
File Copy

Westinghouse Hanford Company

A. G. Blasewitz

No. of
Copies

41 Pacific Northwest Laboratory

W. J. Bjorklund
W. F. Bonner
L. A. Bray
R. A. Brouns
T. D. Chikalla
R. D. Dierks
L. J. Ethridge
R. W. Goles (10)
M. S. Hanson
F. T. Hara
J. H. Jarrett
D. E. Knowlton
L. T. Lakey
D. E. Larson
J. M. Latkovich
R. C. Liikala
R. P. Marshall/W. R. Wiley/
D. B. Cearlock
J. L. McElroy
J. E. Mendel/M. D. Merz
J. E. Minor
R. E. Nightingale
J. M. Perez, Jr.
A. M. Platt
G. J. Sevigny
H. H. Van Tuyl
Technical Information (5)
Publishing Coordination (2)